(NASA-CR-134861) HAMILTON STANDARD Q-FAN DEMONSTRATOR DYNAMIC PITCH CHANGE TEST PROGRAM, VOLUME 1 Final Report (Hamilton Standard) 200 p HC $7.50 CSCL 21E

N76-29231

Unclas
G3/07 48379

NASA CR134861

HSER 6700

VOLUME 1 OF 2

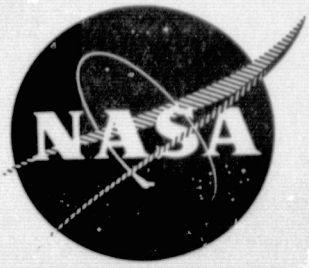

FINAL REPORT

HAMILTON STANDARD Q-FAN^{R} DEMONSTRATOR DYNAMIC PITCH CHANGE TEST PROGRAM

by

W. J. Demers, D. J. Nelson
and H. S. Wainauski

HAMILTON STANDARD
DIVISION OF UNITED TECHNOLOGIES CORPORATION

Prepared for

NATIONAL AERONAUTICS AND SPACE ADMINISTRATION

NASA Lewis Research Center
Contract NAS3-18513

1. Report No.	2. Government Accession No.	3. Recipient's Catalog No.
NASA CR-134861		

4. Title and Subtitle	5. Report Date
HAMILTON STANDARD Q-FAN DEMONSTRATOR DYNAMIC PITCH CHANGE TEST PROGRAM	July, 1975
	6. Performing Organization Code
7. Author(s)	8. Performing Organization Report No.
W.J. DEMERS, D.J. NELSON, H.S. WAINAUSKI	HSER 6700
	10. Work Unit No
9. Performing Organization Name and Address	11. Contract or Grant No.
HAMILTON STANDARD DIVISION DIVISION OF UNITED AIRCRAFT CORP. WINDSOR LOCKS, CONN. 06096	NAS 3-18513
	13. Type of Report and Period Covered
12. Sponsoring Agency Name and Address	CONTRACTOR REPORT
NATIONAL AERONAUTICS AND SPACE ADMINISTRATION WASHINGTON, D. C. 20546	14. Sponsoring Agency Code

15. Supplementary Notes

FINAL REPORT
PROJECT MANAGER - DAVID A. SAGERSER
QCSEE PROJECT OFFICE
NASA LEWIS RESEARCH CENTER
CLEVELAND, OHIO 44135

16. Abstract

Tests of a full scale variable pitch fan engine to obtain data on the structural characteristics, response times, and fan/core engine compatibility during transient changes in blade angle, fan rpm, and engine power is herein reported. Steady state reverse thrust tests with a take-off nozzle configuration were also conducted. The 1.4 meter (4.6 ft.) diameter, 13 bladed controllable pitch fan was driven by a T55-L-11A engine with power and blade angle coordinated by a digital computer. The tests demonstrated an ability to change from full forward thrust (30,359 newtons/6825 pounds) to reverse thrust in less than one (1) second. Reverse thrust was effected through feather and through flat pitch; structural characteristics and engine/fan compatibility were within satisfactory limits.

17. Key Words (Suggested by Author(s))	18. Distribution Statement
AERODYNAMICS AIRCRAFT PROPULSION AND POWER VARIABLE PITCH FAN DYNAMIC PITCH CHANGE TEST	UNLIMITED

19. Security Classif. (of this report)	20. Security Classif. (of this page)	21. No. of Pages	22. Price*
UNCLASSIFIED	UNCLASSIFIED		

*For sale by the National Technical Information Service, Springfield Virginia 22151

TABLE OF CONTENTS

LIST OF TABLES

LIST OF TABLES (continued)

LIST OF FIGURES

LIST OF FIGURES (Continued)

SECTION 1.0

ABSTRACT

Tests of a full scale variable pitch fan engine to obtain data on the structural characteristics, response times, and fan/core engine compatibility during transient changes in blade angle, fan rpm, and engine power is herein reported. Steady state reverse thrust tests with a take-off nozzle configuration were also conducted. The 1.4 meter (4.6 ft.) diameter, 13 bladed controllable pitch fan was driven by a T55-L-11A engine with power and blade angle coordinated by a digital computer. The tests demonstrated an ability to change from full forward thrust (30,359 newtons/6825 pounds) to reverse thrust in less than one (1) second. Reverse thrust was effected through feather and through flat pitch; structural characteristics and engine/fan compatibility were within satisfactory limits.

2.0 SUMMARY

A dynamic pitch change test has been conducted on a full scale variable pitch fan (Q-Fan) powerplant under NASA Contract NAS3-18513. The fan was subjected to extensive testing and successfully completed all phases of each test.

The 1.4 meter diameter, 13 blade fan designed and built by Hamilton Standard to demonstrate the Q-Fan concept, utilized a Lycoming T55-L-11A gas turbine rated at 2794 Kw (3750 HP) as the core engine. With this engine, the fan pressure ratio was 1.14:1 and the bypass ratio was 17:1. The fan was driven through a 4.75:1 reduction gearbox producing a maximum fan speed of 3365 rpm. The fan rotor blades were aluminum spar/fiberglass shell type mounted in a steel disc. The fan duct included a support structure to which seven fan exit guide vanes were attached; the vanes in turn supported the fan/engine mounting ring. A hydraulic pitch change actuator was used for dynamic pitch change transients using a digital computer coordinated control system. The determination of the structural characteristics, response times and fan/core engine compatibility for a variable pitch fan during transient changes in blade angle, rpm, and engine power level were primary objectives of the testing. Steady state reverse thrust tests with a take-off nozzle were also run.

Fan and core engine compatibility were successfully demonstrated for the conditions tested during 137.5 hours of operation on the special Hamilton Standard test rig. Reverse transients were conducted through feather and through flat pitch. This test program verified the basic structural integrity of the fan. More than 200 transients were performed during this test program verifying that changing the fan blade angle is a practical method of obtaining rapid reverse thrust. The fan was successfully operated in reverse with a take-off nozzle.

3.0 INTRODUCTION

Increased interest in STOL aircraft together with the trend toward more restrictive regulations, have combined to highlight the need for an intermediate type propulsor which combines the favorable take-off performance and noise characteristics of the propeller with the good high speed performance and compactness of the low bypass fan. The decided weight advantage and superior thrust response provided additional impetus for the development of this type propulsor.

Since 1968, Hamilton Standard has been working on establishing the technology required to show that the variable pitch fan (Hamilton Standard's Q-Fan®) propulsion system approach provides the desired characteristics. Based on wind tunnel testing of a 0.457 meter (18 inch) model, Hamilton Standard undertook in 1971, the design and fabrication of a full scale Q-Fan propulsion syste (Q-Fan Demonstrator). This system was designed for 1.18 pressure ratio with a 1.402 m (4.6') diameter fan assembly for a projected aircraft application and a growth version of the Lycoming T55 core engine. This testing was conducted using an existing engine rated at 2794 Kw (3750 HP) which limited the fan pressure ratio to 1.14.

As this hardware was being fabricated, Hamilton Standard designed and built a 1.83 m (6'-0") and a 0.508 m (20") Q-Fan model for NASA-Lewis under contract numbers NAS3-16668 and NAS3-16827, respectively. NASA sponsored steady state aero and acoustic testing of the full scale Q-Fan propulsion system was accomplished at Hamilton Standard under NASA contract NAS3-16827 and reported in Reference 1. The model and full scale fans were tested late in 1972 and early in 1973. References 2 and 3 describe the reports which were written for the 0.508 m and 1.83 m Q-Fans, respectively.

This report describes a complete series of transient performance and structural testing of the full scale variable pitch fan powerplant with a hydraulically powered, computer controlled dynamic pitch change system. The object was to accomplish the following on a full scale Q-Fan:

- Obtain structural and performance data during steady state reverse thrust testing with a take-off nozzle.
- Obtain structural and performance data during transient changes in engine power rpm, and blade angle; especially during forward to reverse thrust transitions.
- Evaluate fan/engine compatibility during transient testing.

3.0 INTRODUCTION (Continued)

- Obtain preliminary data to assist NASA Lewis in formulating a test matrix for continued testing to be performed at NASA Lewis under this contract.

- Obtain preliminary data to assist NASA Lewis in their ongoing variable pitch fan studies such as the Quiet Clean Short-haul Experimental Engine (QCSEE) program.

- Confirm the advantages of reversing through feather rather than through flat pitch; i.e., a significantly greater amount of thrust can be generated with reverse pitch effected through feather with negligible structural effect on the propulsion package, especially the fan blades.

- Evaluate the advantages of a modulating forward thrust responsive blade angle system versus the weight and cost advantages of a fixed blade angle system.

4.0 TEST PROGRAM

4.1 Test Hardware

4.1.1 General

The test program described in this report was conducted on a 1.4 meter diameter 13-bladed Hamilton Standard Q-Fan Demonstrator which utilized a Lycoming T55-L-11A 2,794 Kw (3750 HP) gas turbine as the core engine. With this core engine power, the fan had the following characteristics:

Fan pressure ratio	1.14:1
Bypass ratio	17:1
Static thrust rating	32,900 newtons (6825 lbs)

The fan was driven through a 4.75:1 gear reduction with a maximum speed of 3365 rpm; 247 m/s (810 ft/sec) tip speed. The overall configuration of the test hardware is shown on Figures 1, 2, and 3. This hardware was installed and operated on the test rig defined in Section 4.2 of this report.

4.1.2 Fan Rotor

The fan rotor consisted of 13 aluminum spar/fiberglass shell blades mounted in a steel disc. The fan hub and tip solidity was 1.00 and 0.67, respectively, and the airfoil section was NACA series 65. The blades were supported in the hub by an anti-friction retention which consisted of a row of steel balls trapped between a hardened race-way in the disc and hardened split steel races on the blade shank.

Pitch change was accomplished by a hydraulic actuator connected to trunnions on the blades through a scotch yoke arrangement. The blades operated over a range of blade angles from forward thrust to reverse thrust, both through feather and by reindexing the blades, through flat pitch. Figure 4 illustrates the various blade positions and orientations. The actuator fluid was supplied from an external pump and was metered by a servo valve. The valve was controlled either by a thrust setting potentiometer through a computer which coordinated blade angle and the engine fuel control, or by a beta potentiometer which controlled only blade pitch change through an analog controller. The spinner, which was 46% of the fan diameter, was removable to provide access to the rotating instru-mentation, blade retention, and the linear variable differential transformer (LVDT) feedback system. Figure 5 shows the fan assembly with the spinner installed and Figure 6 shows the fan assembly with the spinner removed.

4.1.3 Fan Duct

The fan duct was constructed from four major components:

- A heavy aluminum support structure which mounted on the test rig and to which seven fan exit guide vanes supporting the fan and engine mounting ring were attached. A photograph of this sub-assembly is shown in Figure 7. Low density foam blocks were used between the exit guide vanes to obtain the desired duct contour.

- An aluminum ring attached to the front of the support structure, extended the duct to a point slightly ahead of the fan. This section of the fan duct included a foam rub strip in the plane of the fan, to protect the blades from damage if duct deflection relative to the fan caused contact between the blade tips and the duct.

- A fiberglass covered foam core bellmouth section was attached to the aluminum ring and provided a smooth flow path into the fan. Figure 8 shows the aluminum ring and the bellmouth section installed on the test rig.

- Two fan duct exit nozzles were used. A fiberglass ring, with a takeoff configuration was used for the forward thrust transients and a short series of reverse thrust tests. A laminated wooden bellmouth shape was used during all other transients involving reverse thrust. Both of these nozzles were split into 180^{o} segments for ease in changing from one configuration to the other. Figure 9 is a drawing showing both nozzles.

4.1.4 Mounting

The aluminum support structure in the fan duct was fabricated with a flat plate mounting pad welded and braced to the bottom of the duct. This mounting pad provided a point to attach the fan to a steel post in the test rig, placing the fan centerline 6.1 meters above the ground level.

Seven fan exit guide vanes supported the engine mounting ring in the center of the fan duct aluminum support structure. Four airfoil shaped struts were attached to this ring and passed through the engine inlet duct to support the fan gearbox assembly. The fan bearing housing which contained the bearings supporting the fan assembly, attached directly to the fan gearbox housing.

4.1.5 Gearbox

The fan gearbox provided a 4.75:1 speed reduction between the engine and the fan using a single stage star gear train as shown in Figure 10. The gearing was taken from an existing Hamilton Standard gearbox design and packaged in a new housing designed to interface with the engine and fit the other requirements of the Q-Fan application. External pumps were provided to supply lubricating oil and to scavenge the gearbox. A quill shaft was used to transmit power from the gearbox to the fan.

4.1.6 Engine

The T55-L-11A engine (see Figure 11), rated at 2794 Kw (3750 HP), at 16,000 engine output rpm, was attached to the engine mounting ring using four solid mounts. A sheet metal cowling completely enclosed the engine to provide a suitable surface for the fan exit flow and a dummy pylon was used to simulate a normal installation and to provide a path for routing services and instrumentation into the nacelle.

4.1.7 Control System

The control system consisted of an electronic two channel analog controller, a digital controller or computer, and a teletype unit. Figure 12 is a photograph showing these units. The analog controller is required to close loop control power lever angle (PLA) and Q-Fan blade angle. The analog channels could be independently commanded manually or by the supervisory digital controller.

The digital controller consisted of a console and a teletype which coordinated the analog channel commands as a function of a single input (thrust) as dictated by the digital program. The teletype permitted interactive on-line program changes with hard copy. This system provided the flexibility to change the fan blade pitch change rates, the blade angle range near feather where reduced power was scheduled, the reset power levels, the initial and final blade angles, and the coordinated schedules of fan blade angle, pitch change rate and engine power level.

4.2 Test Rig Description

The Q-Fan Demonstrator dynamic pitch change test program was conducted on a test rig specifically designed for this propulsion unit. The test rig was located at an outdoor test site which will hereafter be referred to as "Hilltop". Figure 13 is a drawing of the test rig and Figures 8 and 14 are photographs of the rig with the Q-Fan installed.

4.2 (Continued)

The control room, located 10 meters west of the rig, was constructed partially below ground level so that 1.5 meters of its total height was above ground level. The rig operator was positioned behind the windows at the control console shown in Figure 15. Figure 16 is a photograph showing the operator's control levers and the auto-manual panel and Figure 17 details the engine control panel and the engine alarm and shutdown panel shown in Figure 15.

The technician was located to the right of the operator. The instrumentation which was used to monitor the important and critical characteristics of the test items are shown in Figures 18 and 19. Figure 20 is a photograph of a typical electronic setup used for the acquisition of structural data and Figure 21 shows the manometer banks monitoring total and static pressures used to evaluate the performance characteristics of the fan.

4.3 Test Procedure

4.3.1 Instrumentation

The instrumentation used in conducting the complete test program is defined in Appendix A, "Test Rig Instrumentation." The individual pieces of instrumentation required for each specific test are defined in Section 4.3.3 (Test Plan) along with the quantity provided for each test:

The following items of instrumentation are common to all testing and these data were recorded on the log sheets.

Ambient Conditions:	Temperature, Pressure, humidity.
Engine Operation:	Turbine inlet temperature Turbine oil temperature, pressure and level Fuel pressure Compressor rpm Power turbine rpm Engine torque (% of 1763 joules) Gearbox oil temperature and pressure Chip detectors (fan and engine) Vibration levels of gas turbine, gearbox, and fan duct

4.3.2 Log Sheets

A log sheet was prepared and filled out each time the rig was operated. Entries were made on the log sheet for each start, for each test condition or at 15 minute intervals and for any unusual occurrence or malfunction as requested by the Test Director. A description and copies of the log sheets are enclosed in Appendix F.

4.3.3 Test Plan

This section defines all of the testing accomplished under this test program. A number was assigned to each test point in order to identify the data. These test numbers are defined in the test plan and include one of the following identifying letter prefixes.

R	Steady state reverse thrust tests with take-off nozzle
TFC	Forward thrust transients
TRC	Reverse through feather transients
TRF	Reverse through flat pitch transients
TRRC	Reverse thrust transients

The test program defined herein was conducted in accordance with 222PT-28A "Installation and Operation Manual - Q-Fan Demonstrator", dated August, 1974. This document is included in Appendix E.

4.3.3.1 Steady State Reverse Thrust Tests With Take-off Nozzle

Performance and Structural Compatibility - This portion of the test program was conducted to establish fan engine compatibility and obtain performance data in reverse thrust with a forward thrust exit nozzle for a full scale Q-Fan. Proper functioning of a variable pitch fan requires that the exit nozzle opens to the correct position to coincide with the request for reverse thrust. This portion of the test program was conducted to examine the nozzle failure case; i.e., the exit nozzle remains closed while the fan is thrusting in reverse. The instrumentation and test procedure described below were used in these tests.

Instrumentation - In addition to the instrumentation defined in paragraph 4.3.1, as common to all testing, the following specific items were installed for this test.

The performance instrumentation employed for reverse thrust steady state testing is defined in Figures 1 through 6 which are included in the Instrumentation Schematic section of Appendix A.

4.3.3.1 (Continued)

Recorded on Magnetic Tape

7 Strain gauges on the blades
89 mm from tip, Vee, Blade 7
127 mm from tip, bending, Blade 7
362 mm from tip, bending, Blades 1, 6, 7 and 12
387 mm from tip, shank L.E., bending, Blade 1

3 Disc gauges
#2 - around circumference of arm number 4; 90° from plane of rotation
#5 - front fillet of arm number 5; 45° from plane of rotation
#6 - fore and aft, centered between arms number 4 and 5

1 Dynamic pressure transducer located at the compressor front face

2 Vane Stresses
Root bending; Vanes 1 and 4

Wind Velocity and Direction
Fan Speed (1F Pip)
Engine Speed (N_2)
Engine Torque
PLA Lever Position
Blade Angle
Time and Run Code
Voice

Displayed on Manometers - Recorded by photographs.

2 Rakes in Fan Duct
Total/Static rake at fan exhaust nozzle
Total Rake in bellmouth behind Fan reverse wake
1 Total pressure rake at front of engine inlet duct
2 Static pressure taps at front of engine inlet duct
8 Total pressure rakes ahead of engine compressor inlet
8 Static pressure taps ahead of engine compressor inlet

Displayed on Temperature Indicator - Recorded by hand

Total temperature in compressor inlet duct

4.3.3.1 (Continued)

Recorded on Visicorder

2 Strain gauges on the blades, 362 mm from tip, bending
1 Dynamic pressure transducer located at the compressor front face
Fan Speed (1F Pip)
Engine Speed (N_2)
PLA Lever Position
Blade Angle

Test Procedure - At each data point, after the engine had stabilized, performance data was recorded; i.e., hand logged data and photo of manometer panels. Data recorded on magnetic tape was obtained at each point at a tape speed of 3.81 meters per second.

Wind Speed - This test program was conducted with a maximum cross wind component of 4.47 m/s (10 mph) and a maximum headwind of 8.94 m/s (20 mph).

4.3.3.1.1 Tabulation of Runs - The following test points were run during the reverse thrust performance/structural steady state testing.

Test No.	Blade Angle	Fan RPM	Tip Speed (m/s)	Engine RPM (N_2) $\left(\frac{(N)}{\sqrt{\theta}}\right)$
R-21	142	2495	183	11850
R-22	142	2907	213	13810
R-24	144	3152	229	14970
R-26	140	2490	183	11830
R-28	142	2128	156	10110
R-29	144	2486	183	11810
R-30	144	2074	152	9850

4.3.3.2 Transient Testing - A dynamic pitch test program was conducted to evaluate fan and core engine compatibility, structural behavior and response characteristics of the fan and engine for transient changes of fan rotor blade angle and engine speed.

Five basic schedules were established for the transient testing and are explained in section 4.3.3.2.2. They are defined as follows:

Schedule 1: Constant blade angle; i.e., full reverse angle between TSL setting of 0 to 20% and fixed forward angle above 20% TSL setting; reverse thru feather mode.

4.3.3.2 (Continued)

Schedule 2: 85% maximum fan speed; reverse through feather mode.

Schedule 3: 100% fan speed; reverse through feather mode.

Schedule 4: Constant blade angle; i.e., full reverse angle between TSL setting of 0 to 35% and fixed forward angle above 35% TSL setting; reverse through Flat Pitch mode.

Schedule 6: 100% fan speed; reverse through Flat Pitch mode.

4.3.3.2.1 Computer Simulation Studies - Early computer simulation of variable pitch fan operation indicated that undesirable torque increases occurred as the fan blade angle approaches feather from the normal forward thrust angle. Figure 22 shows a typical computer simulation which illustrates this phenomena Only by resetting engine power to a reduced level as the blade angle goes thru feather could the torque peak (blip) be reduced to a level where the engine torque limit is not exceeded. Figure 23 shows typical results associated with a power reset. The engine power reset level and the duration of the reset both affected the level and duration of the torque blip as well as the time required to obtain reverse thrust.

Reverse thru flat pitch transients, while not having a torque blip, do however have potential undesirable fan overspeeds. Fortunately, this characteristic was improved in the same manner as the torque blip.

Figure 24 illustrates this overspeed characteristic based on a computer simulation. By resetting the engine power to a low level as the blades moved through flat pitch, and limiting the pitch change rate, the tendency to overspeed was reduced or eliminated as shown in Figure 25.

4.3.3.2.2 Coordinated Control Schedules - The Q-Fan control system coordinates both fan blade angle and engine power with thrust setting (input) lever position. A linear relationship between thrust setting lever and fan thrust from maximum forward to maximum reverse forms the basis for a number of different coordinated steady state schedules. Three schedules for reverse thru feather operation were established. Schedule 1 (Figure 26) is essentially a two blade angle position schedule. A fan blade angle, which produced 100% fan speed at maximum engine power, was used for forward thrust operation with thrust modulation accomplished by changing engine power and accepting the resulting fan speed. A thrust setting lever - TSL - position of 20^{0} was selected as the position where the fan blade angle was commanded to change to the reverse angle. Schedule 2 (Figure 27) maintains an 85% fan speed in the normal forward thrust regime by scheduling fan blade angle with engine power. The 85% fan speed was selected to represent a possible reduced fan speed during

4.3.3.2.2 (continued)

aircraft approach for noise reduction. Fan blade angle varies from +38° low pitch stop -angle to 54° in the forward thrust range. As with schedule 1, at a TSL of 20°, the fan blade angle changed from forward to reverse. Schedule 3 (Figure 28) is similar to schedule 2 with fan speed maintained at 100% in the forward thrust regime to give fast thrust response.

Two coordinated schedules were established for reverse thru flat pitch operation. For this test series, the blades were reindexed with respect to the pitch change actuator, eliminating the low pitch stop angle. Schedule 4 (Figure 29) was similar to schedule 1 and had a forward thrust blade angle of 54° and a reverse thrust blade angle of -33°. Schedule 6 (Figure 30) maintained a steady state fan speed of 100% similar to schedule 3.

4.3.3.2.3 Forward Thrust Transients - Because the coordinated schedules, either thru feather or thru flat pitch were the same in the forward thrust operating regime, the forward thrust transients were run only with thru feather schedules 1, 2 and 3. Forward thrust response characteristics were determined for variations in the following factors:

A. TSL range - degrees
B. TSL rate - deg/sec.
C. Blade Angle Rate - deg/sec.

Eighteen forward thrust transients were performed and are listed in the tabulation of runs, section 4.3.3.2.8.

4.3.3.2.4 Forward to Reverse Thrust Transients - This program was the first test of a full scale variable pitch fan engine where the effects of a large number of control variables on engine-fan compatibility, structural behavior, and response characteristics were being investigated. In addition to the thrust setting lever position at which the transient was initiated and the coordinated schedules, the control variables consisted of the fan blade pitch change rate, the power reset level during the transient, and the blade angle at which the power reset was terminated.

Early in the test planning it was recognized that the classical method of varying one factor at a time while holding other factors constant would result in a slow and time consuming test program consisting of running a few points, looking at the test results, planning the next series of test points and repeating this procedure until the specified number of points were run. There was also

4.3.3.2.4 (continued)

the possibility that significant interactions between the main variables would not be discovered by this method. For these reasons, a series of balanced, full factorial experiments were defined. For each coordinated schedule the main control variables were tested at two levels each in a full test point matrix. This type of experimental design helps insure that extraneous factors not being considered do not effect the analysis of the test results.

The thrust setting lever position selected to start each transient was either 70° or 90°. The 70° TSL corresponds to approximately 60% of the maximum forward thrust condition and represents a normal landing condition. The 90° TSL corresponds to 100% of the maximum forward thrust and represents an aborted take-off condition. The two levels of the other control variables were selected based on engine simulation analysis. The flexibility of the computerized control system allowed the fan blade pitch change rate to be varied during the transient. Previous steady state test results (HS unpublished data) indicated that blade vibratory stresses peaked at 72° blade angle and the stress level was influenced by the engine power level. It was theorized that moving the blades at a slow rate at the start of the transient would allow time to reset the engine power to a low level prior to reaching the peak blade stress blade angle. After reaching 72°, the pitch change rate could be increased to shorten the transient time. For each full factorial experiment the test points were randomized to assure that factors causing variation, other than those under study, had an equal opportunity to affect the results for each test point.

Although each coordinated schedule gives a significantly different mode of operation for steady state forward thrust operation, for transient operation from forward to reverse thrust, the various schedules only change the starting condition in terms of blade angle and fan speed. The test was planned based on the coordinated schedules with schedules 1, 2 and 3 being reversed thru feather and schedules 4 and 6 being reversed thru flat pitch.

Schedule 1 - For schedule 1, twenty-eight reverse thru feather transients were run. The first ten test points were planned as a two-level, three factor (2^3) balanced full factorial experiment. The test point matrix thus becomes:

4.3.3.2.4 (continued)

	b_0		b_1	
	c_0	c_1	c_0	c_1
a_0	(1)	(c)	(b)	(bc)
a_1	(a)	(ac)	(ab)	(abc)

where:

A = Blade Angle Rate below 72^0 - deg/sec.

$a_0 = 50$ $a_1 = 100$

B = PLA Reset Level - deg.

$b_0 = 40$ $b_1 = 75$

C = Blade Angle for completion of PLA reset

$c_0 = 61^0$ $c_1 = 72^0$

The alpha/numeric character in parenthesis indicates the standard statistical notation for treatment combinations and indicates those factors at the high level for the test point.

All schedule 1 transients were initiated from a TSL of 70°. For this starting position, the engine simulation indicated that the blade angle rate above 72° had virtually no effect on the response time over the range of blade angle rates being considered (100 to 150 deg/sec). Accordingly, the plan originally called for running at a blade angle rate of 150 deg/sec above 72°. The first ten schedule 1 test points became:

4.3.3.2.4 (continued)

Experiment Number	Factor A	Factor B	Factor C	Random Test Order	Test Point Number
1	50	40	61	1	TRC1-1
a	100	40	61	9	TRC1-9
b	50	75	61	10	TRC1-10
c	50	40	72	7	TRC1-7
ab	100	75	61	3	TRC1-3
ac	100	40	72	5	TRC1-5
bc	50	75	72	8	TRC1-8
abc	100	75	72	4	TRC1-4
midpoint *	75	57.5	66.5	2	TRC1-2
midpoint	75	57.5	66.5	6	TRC1-6

*Midpoints were included to help estimate experimental error and to determine nonlinear effects of control variables.

The initial ten test points were repeated later in the test program to allow for a better estimate of the experimental error. These test points were:

Treatment Combination	Factor A	Factor B	Factor C	Random Test Order	Test Point Number
1	50	40	61	3	TRC1-13
a	100	40	61	7	TRC1-17
b	50	75	61	1	TRC1-11
c	50	40	72	2	TRC1-12
ab	100	75	61	8	TRC1-18
ac	100	40	72	10	TRC1-20
bc	50	75	72	6	TRC1-16
abc	100	75	72	9	TRC1-19
Midpoint	75	57.5	66.5	4	TRC1-14
Midpoint	75	57.5	66.5	5	TRC1-15

4.3.3.2.4 (continued)

After further consideration of the engine simulation analysis, six additional test points were defined to verify the time response results for changes in blade angle rate above 72°. Factor D (blade angle rate above 72°) was established for this parameter. Two final test points for schedule 1 examined PLA reset to higher values. These test points were identified as TRC1-21 through TRC 1-28.

Starting TSL	Factor A	B	C	D	Test Point Number
70°	50	40	72	100	TRC1-21
↓	50	40	61	100	TRC1-22
	75	57.5	66.5	100	TRC1-23
	100	75	61	100	TRC1-24
	100	75	72	100	TRC1-25
	75	57.5	66.5	100	TRC1-26
	150	80	61	150	TRC1-27
	150	85	61	150	TRC1-28

Schedule 2 - For schedule 2, ten reverse thru feather transients were run. Like schedule 1, this test series was planned as a 2^3 full factorial with the same test point matrix. The two levels of each factor are as follows:

A = Blade Angle Rate Below 72° - deg/sec

$$a_0 = 50 \quad a_1 = 100$$

B = PLA Reset Level - deg

$$b_0 = 40 \quad b_1 = 73$$

C = Blade Angle for Completion of PLA Reset - deg

$$c_0 = 57 \quad c_1 = 72$$

4.3.3.2.4 (continued)

The ten schedule 2 test point became:

Treatment Combination	Factor A	B	C	Random Test Order	Test Point Number
1	50	40	57	5	TRC2-5
a	100	40	57	4	TRC2-4
b	50	73	57	1	TRC2-1
c	50	40	72	7	TRC2-7
ab	100	73	57	6	TRC2-6
ac	100	40	72	8	TRC2-8
bc	50	73	72	9	TRC2-9
abc	100	73	72	2	TRC2-2
Midpoint	75	56.5	64.5	3	TRC2-3
Midpoint	75	56.5	64.5	10	TRC2-10

Schedule 3 - For schedule 3, eighty test points were run. Initially forty test points were defined as a 2^5 full factorial experiment. The test point matrix was:

		b_0				b_1			
		d_0		d_1		d_0		d_1	
		e_0	e_1	e_0	e_1	e_0	e_1	e_0	e_1
a_0	c_0	(1)	(e)	(d)	(de)	(b)	(be)	(bd)	(bdc)
	c_1	(c)	(ce)	(cd)	(cde)	(bc)	(bce)	(bcd)	(bcde)
a_1	c_0	(a)	(ae)	(ad)	(ade)	(ab)	(abe)	(abd)	(abde)
	c_1	(ac)	(ace)	(acd)	(acde)	(abc)	(abce)	(abcd)	(abcde)

4.3.3.2.4 (continued)

A = Blade Angle Rate, Below 72° - deg/sec
a_0 = 50 a_1 = 100

B = PLA Reset Level - deg
b_0 = 40 b_1 - 70

C = Blade Angle for Completion of PLA Reset - deg
c_0 = 51 c_1 = 72

D = Blade Angle Rate, Above 72° - deg/sec
d_0 = 100 d_1 = 150

E = Slow Blade Angle Rate - 20 deg/sec - Below 46°
e_0 = No e_1 = Yes

Factor E, the slow pitch change rate below 46° was added to give the power turbine added time to decelerate at the start of the transient. These test points were all initiated from a starting TSL of 70°. These test points were:

Treatment Combination	Factor A	B	C	D	E	Test Order	Test Point Number
d	50	40	51	100	50	10	TRC3-10
ae	100	40	51	150	20	5	TRC3-5
be	50	70	51	150	20	7	TRC3-7
abd	100	70	51	100	100	9	TRC3-9
cde	50	40	72	100	20	6	TRC3-6
ac	100	40	72	150	100	1	TRC3-1
bc	50	70	72	150	50	4	TRC3-4
abcde	100	70	72	100	20	3	TRC3-3
Midpoint	75	55	61.5	125	10*	2	TRC3-2
Midpoint	75	55	61.5	125	10*	8	TRC3-8
de	50	40	51	150	20	9	TRC3-39
a	100	40	51	100	100	2	TRC3-32
b	50	70	51	100	50	7	TRC3-37
abde	100	70	51	150	20	10	TRC3-40
cd	50	40	72	150	50	3	TRC3-33
ace	100	40	72	100	20	5	TRC3-35
bce	50	70	72	100	20	6	TRC3-36
abcd	100	70	72	150	100	1	TRC3-31
Midpoint	75	55	61.5	125	10*	4	TRC3-34
Midpoint	75	55	61.5	125	10*	8	TRC3-38

*10°/sec for initial testing - changed to 40°/sec on later runs.

4.3.3.2.4 (continued)

Treatment Combination	Factor A	B	C	D	E	Test Order	Test Point Number
1	50	40	51	100	50	8	TRC3-28
ade	100	40	51	150	20	5	TRC3-25
bde	50	70	51	150	20	10	TRC3-30
ab	100	70	51	100	100	9	TRC3-29
ce	50	40	72	100	20	4	TRC3-24
acd	100	40	72	150	100	1	TRC3-21
bcd	50	70	72	150	50	3	TRC3-23
abce	100	70	72	100	20	7	TRC3-27
Midpoint	75	55	61.5	125	40	2	TRC3-22
Midpoint	75	55	61.5	125	40	6	TRC3-26
ad	100	40	51	150	100	1	TRC3-11
e	50	40	51	100	20	4	TRC3-14
abe	100	70	51	100	20	7	TRC3-17
bd	50	70	51	150	50	2	TRC3-12
acde	100	40	72	150	20	5	TRC3-15
c	50	40	72	100	50	3	TRC3-13
abc	100	70	72	100	100	6	TRC3-16
bcde	50	70	72	150	20	8	TRC3-18
Midpoint	75	55	61.5	125	40	9	TRC3-19
Midpoint	75	55	61.5	125	40	10	TRC3-20

As with the schedule 1 and 2 test points, this series was also run in blocks of ten test points. In this design, each block of ten was set up as a 1/4 replicate and could be statistically analyzed as such. During the testing an operating change was made after the first twenty points causing a block effect between the first twenty and last twenty test points. This operating change involved the addition of a "set" mode to the computer sequence. Prior to the addition of this "set" mode, the computer operator's switch from "automatic" to "manual" condition resulted in a slight TSL lever change to the manual lever potentiometer setting which was not precisely coordinated with the computer setting. Ten test points were added to the program which were combined with the last twenty test points for a 2^4 full factorial. These test points were:

4.3.3.2.4 (continued)

Treatment Combination	Factor A	B	C	D	Random Test Order	Test Point Number
a	100	40	51	100	7	TRC3-77
b	50	70	51	100	10	TRC3-80
d	50	40	51	100	4	TRC3-74
ac	100	40	72	150	1	TRC3-71
bc	50	70	72	100	2	TRC3-72
cd	50	40	72	150	8	TRC3-78
abd	100	70	51	150	3	TRC3-73
abcd	100	70	72	150	6	TRC3-76
Midpoint	75	55	61.5	125	5	TRC3-75
Midpoint	75	55	61.5	125	9	TRC3-79

Ten test points from a starting TSL of 90° were planned as a 2^3 experiment. The two levels of each factor are as follows:

A = Blade Angle Rate, below 72° - deg/sec.

$a_0 = 50$ $a_1 = 100$

B = PLA Reset Level - deg

$b_0 = 40$ $b_1 = 80$

C = Blade Angle for Completion of PLA Reset - deg

$c_0 = 60$ $c_1 = 72$

The blade angle rate above 72° was 150 deg/sec. for this series of test points. The ten schedule 3 test points from the high starting TSL position became:

Treatment Combination	Factor A	B	C	Random Test Order	Test Point Number
1	50	40	60	4	TRC3-44
a	100	40	60	6	TRC3-46
b	50	80	60	1	TRC3-41
c	50	40	72	2	TRC3-42
ab	100	80	60	10	TRC3-50
ac	100	40	72	1	TRC3-43
bc	50	80	72	8	TRC3-48
abc	100	80	72	5	TRC3-45
Midpoint	75	60	66	7	TRC3-47
Midpoint	75	60	66	9	TRC3-49

4.3.3.2. 4 (continued)

To simulate a possible operation of the QCSEE engine, a block of ten test points was run with a blade angle rate of 135°/sec during the entire transient from forward to reverse thrust. These test points, all with a starting TSL of 70°, formed another 2^3 experiment. The two levels of each factor were as follows:

A = Blade Angle Rate, below 72° - deg/sec

constant at 135°

B = PLA Reset level - deg

$b_0 = 40$ $b_1 = 70$

C = Blade Angle for Completion of PLA Reset - deg.

$c_0 = 51$ $c_1 = 72$

D = Blade Angle Rate above 72° - deg/sec.

constant at 135°

E = Slow Blade Angle Rate, 20 deg/sec, below 43°

e_0 = Yes e_1 = No

4.3.3.2.4 (continued)

The ten test points for this series were:

Combination	Factor B	Factor C	Factor E	Random Test Order	Test Point No.
1	40	51	20	10	TRC3-60
b	70	51	20	4	TRC3-54
c	40	72	20	2	TRC3-52
e	40	51	135	3	TRC3-53
bc	70	72	20	1	TRC3-51
be	70	51	135	8	TRC3-58
ce	40	72	135	9	TRC3-59
bce	70	72	135	5	TRC3-55
Midpoint	52.5	61.5	40	6	TRC3-56
Midpoint	52.5	61.5	40	7	TRC3-57

The final ten test points for schedule 3 were established to investigate the fastest possible transient times within the operational constraints of the test hardware. These test points were identified as TRC3-61 to TRC3-70 and consisted of the following factors:

Starting TSL	Factor A	Factor B	Factor C	Test Point Number
70	150	75	51	TRC3-61
70	150	80	51	TRC3-62
70	150	85	51	TRC3-63
90	150	75	60	TRC3-64
90	150	80	60	TRC3-65
90	150	85	60	TRC3-66
90	50	40	60	TRC3-67
90	100	40	60	TRC3-68
90	50	80	60	TRC3-69
90	100	80	60	TRC3-70

4.3.3.2. 4 (continued)

Schedule 4 - A total of ten schedule 4 test points were run. These tests were run in the same manner as the transients thru feather. The starting TSL position for all these was 70°. The break point for the blade angle rate was +10° blade angle. These test points as well as the schedule 6 test points were not set up in a full factorial matrix. The factors being tested were:

A = Blade Angle Rate, Above 10° - deg/sec.

B = PLA Reset, deg.

C = Blade Angle for Completion of PLA Reset - deg.

D - Blade Angle Rate, below 10° - deg/sec.

The test points became:

Factor				Test Point
A	B	C	D	Number
150	60	-10	150	TRF 4-1
100	40	-10	100	TRF 4-2
150	40	+10	150	TRF 4-3
100	60	+10	100	TRF 4-4
150	40	-10	150	TRF 4-5
100	40	+10	100	TRF 4-6
100	40	-10	100	TRF 4-7
100	60	-10	100	TRF 4-8
150	40	-10	150	TRF 4-9
150	60	+10	150	TRF 4-10

Schedule 6 - A total of twenty schedule six test points were run with the same factors as the schedule 4 test points. These test points started from a TSL position of 70° or 90° as noted. The schedule 6 test points were:

4.3.3.2.4 (continued)

Starting TSL	Factor A	Factor B	Factor C	Factor D	Test Point Number
70	50	60	-10	150	TRF6-1
70	50	40	+10	150	TRF6-2
70	100	40	+10	150	TRF6-3
70	50	40	-10	150	TRF6-4
70	100	60	+10	150	TRF6-5
70	100	40	-10	150	TRF6-6
70	50	40	+10	150	TRF6-7
70	50	55	+10	150	TRF6-8
70	100	55	-10	150	TRF6-9
70	100	55	+10	100	TRF6-10
70	100	40	-10	100	TRF6-11
70	100	55	+10	100	TRF6-12
70	100	55	-10	100	TRF6-13
70	100	40	+10	100	TRF6-14
90	150	40	+10	150	TRF6-15
90	150	40	-10	150	TRF6-16
90	100	40	-10	100	TRF6-17
90	100	40	-10	100	TRF6-18
70	100	55	+10	150	TRF6-19
70	50	55	-10	150	TRF6-20

4.3.3.2.5 Reverse to Reverse Thrust Transients - Since the reverse thrust operating regime design span was in the reverse through feather mode, the reverse thrust transients were run only in the thru feather schedule number 3. Reverse thrust response characteristics were determined for variations in the following factor:

B.TSL Rate - degrees/second

Four reverse thrust transients were performed and are listed in the tabulation of runs, section 4.3.3.2.8.

4.3.3.2.6 Instrumentation - In addition to the instrumentation defined in paragraph 4.3.1 as common to all testing, the following specific items were installed for the transient testing.

Recorded on Magnetic Tape - Same as paragraph 4.3.3.1 except for the addition of:

N_1 Compressor Speed

Recorded on Visicorder

2 Strain gauges on the blades, 362 mm from tip, bending
1 Dynamic pressure transducer located at the compressor front face
Engine Speed (N_2)
PLA Lever Position
Blade Angle
Fuel Flow
TT_7 Turbine Temperature
Thrust Setting Lever Position
N_1 Compressor Speed

4.3.3.2.7 Test Procedure - For the transient tests, a remotely located digital logic control system was utilized. This system coordinated engine power level and fan blade pitch.

Flexibility was provided in the control system to change the fan blade pitch change rates, the initial and final blade angles, and the coordinated schedules of fan blade angle and engine power level.

For each transient test point, data was recorded on magnetic tape continuously at 3.81 meters per second tape speed from 5 to 10 seconds before starting the transient to 5 to 10 seconds after the transient was completed and all parameters stabilized.

At 15 minute intervals and after each start, data as specified in Section 4.3.2 was hand logged.

Visicorder data was obtained for each transient and the data was reviewed prior to proceeding with the next test point.

4.3.3.2.8 Tabulation of Runs

The following forward thrust transients were performed:

Test No.	Schedule	TSL Range (degrees)	TSL Rate (deg/sec.)	Blade Angle Rate (deg/sec.)
TFC1-1	1	55 to 90	step	-
TFC1-2	1	65 to 95	step	-
TFC1-3	1	80 to 95	step	-
TFC1-4	1	80 to 95	15	-
TFC2-1	2	55 to 95	step	20
TFC2-2	2	55 to 95	step	50
TFC2-3	2	80 to 95	step	50
TFC3-1	3	55 to 95	step	20
TFC3-2	3	80 to 95	step	20
TFC3-3	3	55 to 95	step	50
TFC3-4	3	80 to 95	step	50
TFC3-5	3	80 to 95	15	50
TFC3-6	3	55 to 95	step	100
TFC3-7	3	65 to 95	step	100
TFC3-8	3	80 to 95	step	100
TFC3-9	3	65 to 95	30	50
TFC3-10	3	65 to 95	60	50
TFC3-11	3	65 to 95	150	50

The following reverse through feather transients were performed all with TSL step changes. PLA reset was initiated immediately at call for reverse thrust. The parenthesized portion of the test no. refers to the full factorial experimental design methodology previously discussed in Section 4.3.3.2.2.2.

Test No.	Schedule	TSL Range (degrees)	Blade Angle Rate (deg/sec.) Below 72°	Blade Angle Rate (deg/sec.) Above 72°	PLA Reset (deg.)	Blade Angle (deg.) At Compl. of PLA Reset
TRC1-1 (1)	1	70 to 0	50	150	40	61
TRC1-2 (Mid)	1	70 to 0	75	150	57.5	66.5
TRC1-3 (ab)	1	70 to 0	50	150	40	72
TRC1-4 (abc)	1	70 to 0	100	150	75	72
TRC1-5 (ac)	1	70 to 0	100	150	40	72
TRC1-6 (Mid)	1	70 to 0	75	150	57.5	66.5
TRC1-7 (c)	1	70 to 0	100	150	75	61
TRC1-8 (bc)	1	70 to 0	50	150	75	72
TRC1-9 (a)	1	70 to 0	100	150	40	61
TRC1-10(b)	1	70 to 0	50	150	75	61
TRC1-11(b)	1	70 to 0	50	150	75	61

4.3.3.2.8 (Continued)

Test No.	Schedule	TSL Range (degrees)	Blade Angle Rate (deg/sec.) Below 72°	Blade Angle Rate (deg/sec.) Above 72°	PLA Reset (deg.)	Blade Angle (deg.) At Compl. of PLA Reset
TRC1-12(ab)	1	70 to 0	50	150	40	72
TRC1-13(1)	1	70 to 0	50	150	40	61
TRC1-14(Mid)	1	70 to 0	75	150	57.5	66.5
TRC1-15(Mid)	1	70 to 0	75	150	57.5	66.5
TRC1-16(bc)	1	70 to 0	50	150	75	72
TRC1-17(a)	1	70 to 0	100	150	40	61
TRC1-18(c)	1	70 to 0	100	150	75	61
TRC1-19(abc)	1	70 to 0	100	150	75	72
TRC1-20(ac)	1	70 to 0	100	150	40	72
TRC1-21	1	70 to 0	50	100	40	72
TRC1-22	1	70 to 0	50	100	40	61
TRC1-23	1	70 to 0	75	100	57.5	66.5
TRC1-24	1	70 to 0	100	100	75	61
TRC1-25	1	70 to 0	100	100	75	72
TRC1-26	1	70 to 0	75	100	57.5	66.5
TRC1-27	1	70 to 0	150	150	80	61
TRC1-28	1	70 to 0	150	150	85	61
TRC2-1 (b)	2	70 to 0	50	150	73	57
TRC2-2 (abc)	2	70 to 0	100	150	73	72
TRC2-3 (Mid)	2	70 to 0	75	150	56.5	64.5
TRC2-4 (a)	2	70 to 0	100	150	40	57
TRC2-5 (1)	2	70 to 0	50	150	40	57
TRC2-6 (ab)	2	70 to 0	100	150	73	57
TRC2-7 (c)	2	70 to 0	50	150	40	72
TRC2-8 (ad)	2	70 to 0	100	150	40	72
TRC2-9 (bc)	2	70 to 0	50	150	73	72
TRC2-10(Mid)	2	70 to 0	75	150	56.5	64.5

Test No.	Schedule	TSL Range (degrees)	Blade Angle Rate (deg/sec.) Below 46°	Blade Angle Rate (deg/sec.) 46° - 72°	Blade Angle Rate (deg/sec.) Above 72°	PLA Reset (deg.)	Blade Angle (deg.) At Compl. of PLA Reset
TRC3-1	3	70 to 0	100	100	100	40	72
TRC3-2	3	70 to 0	10	75	125	55	61.5
TRC3-3	3	70 to 0	20	100	150	70	72
TRC3-4	3	70 to 0	50	50	100	70	72
TRC3-5	3	70 to 0	20	100	100	40	51
TRC3-6	3	70 to 0	20	50	150	40	72
TRC3-7	3	70 to 0	20	50	100	70	51
TRC3-8	3	70 to 0	10	75	125	55	61.5
TRC3-9	3	70 to 0	100	100	150	70	51
TRC3-10	3	70 to 0	50	50	150	40	51

4.3.3.2.8 (Continued)

Test No.	Schedule	TSL Range (degrees)	Blade Angle Rate (deg/sec.) Below 43°	43° - 72°	Above 72°	PLA Reset (deg.)	Blade Angle (deg.) At Compl. of PLA Reset
TRC3-11 (ad)	3	70 to 0	100	100	150	40	51
TRC3-12 (bd)	3	70 to 0	50	50	150	70	51
TRC3-13 (c)	3	70 to 0	50	50	100	40	72
TRC3-14	3	70 to 0	20	50	100	40	51
TRC3-15	3	70 to 0	20	100	150	40	72
TRC3-16 (abc)	3	70 to 0	100	100	100	70	72
TRC3-17	3	70 to 0	20	100	100	70	51
TRC3-18	3	70 to 0	20	50	150	70	72
TRC3-19 (Mid)	3	70 to 0	40	75	125	55	61.5
TRC3-20 (Mid)	3	70 to 0	40	75	125	55	61.5
TRC3-21 (acd)	3	70 to 0	100	100	150	40	72
TRC3-22 (Mid)	3	70 to 0	40	75	125	55	61.5
TRC3-23 (bcd)	3	70 to 0	50	50	150	70	72
TRC3-24	3	70 to 0	20	50	100	40	72
TRC3-25	3	70 to 0	20	100	150	40	51
TRC3-26 (Mid)	3	70 to 0	40	75	125	55	61.5
TRC3-27	3	70 to 0	20	100	100	70	72
TRC3-28 (1)	3	70 to 0	50	50	100	40	51
TRC3-29 (ab)	3	70 to 0	100	100	100	70	51
TRC3-30	3	70 to 0	20	50	150	70	51
			Below 46°	46° - 72°	Above 72°		
TRC3-31	3	70 to 0	100	100	150	70	72
TRC3-32	3	70 to 0	100	100	100	40	51
TRC3-33	3	70 to 0	50	50	150	40	72
TRC3-34	3	70 to 0	10	75	125	55	61.5
TRC3-35	3	70 to 0	20	100	100	40	72
TRC3-36	3	70 to 0	20	50	100	70	72
TRC3-37	3	70 to 0	50	50	100	70	51
TRC3-38	3	70 to 0	10	75	125	55	61.5
TRC3-39	3	70 to 0	20	50	150	40	51
TRC3-40	3	70 to 0	20	100	150	70	51
			Below 72°		Above 72°		
TRC3-41 (b)	3	90 to 0	50		150	80	60
TRC3-42 (c)	3	90 to 0	50		150	40	72
TRC3-43 (ac)	3	90 to 0	100		150	40	72
TRC3-44 (1)	3	90 to 0	50		150	40	60
TRC3-45 (abc)	3	90 to 0	100		150	80	72

4.3.3.2.8 (Continued)

Test No.	Schedule	TSL Range (degrees)	Blade Angle Rate (deg/sec.) Below 72°	Above 72°	PLA Reset (deg.)	Blade Angle (deg.) At Compl. of PLA Reset
TRC3-46 (a)	3	90 to 0	100	150	40	60
TRC3-47 (Mid)	3	90 to 0	75	150	60	66
TRC3-48 (bc)	3	90 to 0	50	150	80	72
TRC3-49 (Mid)	3	90 to 0	75	150	60	66
TRC3-50 (ab)	3	90 to 0	100	150	80	60
			Below 43°	43° - 72°	Above 72°	
TRC3-51 (bc)	3	70 to 0	20	125	135	70	72
TRC3-52 (c)	3	70 to 0	20	135	135	40	72
TRC3-53 (e)	3	70 to 0	135	135	135	40	51
TRC3-54 (b)	3	70 to 0	20	135	135	70	51
TRC3-55 (bce)	3	70 to 0	135	135	135	70	72
TRC3-56 (Mid)	3	70 to 0	40	135	135	55	61.5
TRC3-57 (Mid)	3	70 to 0	40	135	135	55	61.5
TRC3-58 (be)	3	70 to 0	135	135	135	70	51
TRC3-59 (ce)	3	70 to 0	135	135	135	40	72
TRC3-60 (1)	3	70 to 0	20	135	135	40	51
			Below 72°	Above 72°		
TRC3-61	3	70 to 0	150	150	75	51
TRC3-62	3	70 to 0	150	150	80	51
TRC3-63	3	70 to 0	150	150	85	51
TRC3-64	3	90 to 0	150	150	75	60
TRC3-65	3	90 to 0	150	150	80	60
TRC3-66	3	90 to 0	150	150	85	60
TRC3-67	3	90 to 0	50	150	40	60
TRC3-68	3	90 to 0	100	150	40	60
TRC3-69	3	90 to 0	50	150	80	60
TRC3-70	3	90 to 0	100	150	80	60
TRC3-71 (ac)	3	70 to 0	100	100	40	72
TRC3-72 (bc)	3	70 to 0	50	100	70	72
TRC3-73 (abd)	3	70 to 0	100	150	70	51
TRC3-74 (d)	3	70 to 0	50	150	40	51
TRC3-75 (Mid)	3	70 to 0	75	125	55	61.5
TRC3-76 (abcd)	3	70 to 0	100	150	70	72
TRC3-77 (a)	3	70 to 0	100	100	40	51
TRC3-78 (cd)	3	70 to 0	50	150	40	72
TRC3-79 (Mid)	3	70 to 0	75	125	55	61.5
TRC3-80 (b)	3	70 to 0	50	100	70	51

4.3.3.2.8 (Continued)

The following reverse through flat pitch transients were performed all with TSL step changes and PLA reset was initiated immediately at call for reverse thrust.

Test No.	Schedule	TSL Range (degrees)	Blade Angle Rate (deg/sec.) Above 10°	Blade Angle Rate (deg/sec.) Below 10°	PLA Reset (deg.)	Blade Angle (deg.) At Compl. of PLA Reset
TRF4-1	4	70 to 0	150	150	60	-10
TRF4-2	4	70 to 0	100	100	40	-10
TRF4-3	4	70 to 0	150	150	40	+10
TRF4-4	4	70 to 0	100	100	60	+10
TRF4-5	4	70 to 0	150	150	40	-10
TRF4-6	4	70 to 0	100	100	40	+10
TRF4-7	4	70 to 0	100	100	40	-10
TRF4-8	4	70 to 0	100	100	60	-10
TRF4-9	4	70 to 0	150	150	40	-10
TRF4-10	4	70 to 0	150	150	60	+10
TRF6-1	6	70 to 0	50	150	55	-10
TRF6-2	6	70 to 0	50	150	40	+10
TRF6-3	6	70 to 0	100	150	40	+10
TRF6-4	6	70 to 0	50	150	40	-10
TRF6-5	6	70 to 0	100	150	60	+10
TRF6-6	6	70 to 0	100	150	40	-10
TRF6-7	6	70 to 0	50	150	40	+10
TRF6-8	6	70 to 0	50	150	55	+10
TRF6-9	6	70 to 0	100	150	55	-10
TRF6-10	6	70 to 0	100	100	55	+10
TRF6-11	6	70 to 0	100	100	40	-10
TRF6-12	6	70 to 0	100	100	55	+10
TRF6-13	6	70 to 0	100	100	55	-10
TRF6-14	6	70 to 0	100	100	40	+10
TRF6-15	6	90 to 0	150	150	40	+10
TRF6-16	6	90 to 0	150	150	40	-10
TRF6-17	6	90 to 0	100	100	40	-10
TRF6-18	6	90 to 0	100	100	40	-10
TRF6-19	6	70 to 0	100	150	55	+10
TRF6-20	6	70 to 0	50	150	55	-10

The following reverse thrust transients were performed:

Test No.	Schedule	TSL Range (degrees)	TSL Rate (deg/sec)	Blade Angle (deg.)
TRRC3-1	3	19 to 0	Step	144
TRRC3-2	3	19 to 0	20	144
TRRC3-3	3	19 to 0	100	144
TRRC3-4	3	19 to 0	100	144

4.4 Data Reduction Procedure

4.4.1 Q-Fan/Engine Performance

The following technique was employed in reducing and analyzing test data for evaluating Q-Fan/engine performance.

4.4.1.1 Raw Data Acquisition - The guidelines below applied in obtaining raw test data:

All manometer photographs were read to the nearest 0.25 cm of ABR4.

Manometer raw data were tabulated by tube number to define origin of measurement.

Engine raw data were recorded on test run log sheets.

4.4.1.2 Steady State Reverse Thrust with Take-off Nozzle

4.4.1.2.1 Engine Torque - The engine torque was reduced using a calibration curve supplied by the engine manufacturer. The torque data were converted to horsepower, corrected to local ambient atmospheric conditions, and plotted against corrected speed at a constant blade angle setting.

4.4.1.2.2 Pressure Ratio at Compressor Inlet - The total pressure at the engine compressor inlet was determined from an average of the total pressures sensed by the Kiel probes at the engine compressor inlet as shown in Figure 2 of Appendix A. This value was ratioed to local barometric pressure to obtain the pressure ratio.

4.4.1.2.3 Engine Weight Flow - The average Mach number at the engine inlet was used to determine the engine weight flow. The Mach number was determined from the engine inlet rake shown in Figure 4 of Appendix A and static taps #91 and #92 of Figure 1 in Appendix A. These data were corrected to local atmospheric conditions and compared to those values specified for the engine.

4.4.1.2.4 Engine Thrust - This was derived from a curve of engine thrust versus corrected power supplied by the engine manufacturer.

4.4.1.2.5 Engine Exit Velocity - These values were derived by combining the engine air and fuel flows and then combining the exit velocities from the equation, $V_e = \frac{T \times g}{W}$ where V_e = exit

4.4.1.2.5 (Continued)

velocity in m/s, T = engine thrust in newtons, w = weight flow in kilograms/second (air plus fuel), and g = 9.80 m/sec^2. These values were plotted against corrected speed for lines of constant blade angle setting.

4.4.1.2.6 Compressor Inlet Distortion - An average of all the total pressures measured at the compressor inlet from the rakes shown in View B-B of Figure 1 in Appendix A were employed to determine distortion. The degree of distortion was calculated by dividing the difference between the maximum and minimum total pressure, regardless of azimuthal or radial position by the average total pressure at the compressor inlet. Sanborn traces of dynamic response instrumentation were provided to show the amplitude of the pressure variation at the pickup location.

4.4.1.2.7 Fan Weight Flow - The average Mach number at the fan duct exit (inlet during reverse thrust operation) was used to determine the total flow into the fan/duct. The Mach number was determined from the rake located in the duct exit as shown in Figure 5 of Appendix A. For the reverse thrust condition, the inlet rake was oriented in the proper direction to measure the weight flow. For a representative test point, the rake readings were integrated to verify that the use of the average Mach number leads to an acceptable value of weight flow, i.e., the integrated and averaged flows must agree within ± 5%. Otherwise, the flows were determined by subtracting the engine flow from the total average flow.

4.4.1.2.8 Fan Pressure Ratio - An area averaged pressure ratio was determined from the measurements on the rake located behind the fan.

4.4.1.2.9 Fan Exit Velocity - Assuming exhaust to ambient conditions, the average Mach number at the fan exhaust was determined from the area averaged fan pressure ratio. The average exit velocity was determined from the Mach number.

4.4.1.2.10 Fan Thrust - The fan thrust was determined from the fan weight flow and exit velocity using the relationship, $T = \frac{1117}{g} w [P_R^{2/7} - 1]5]7/2$ where w = weight flow from fan, P_R = fan pressure ratio and g = 9.8 m/sec^2.

4.4.1.3 Forward and Reverse Thrust Transients

Dynamic Pressure Variation at Compressor Inlet - Comparisons of pressure variation with time were made for selected test conditions. These dynamic measurements were compared to steady measurements made on the same rake.

4.4.2 Steady State and Transient Structural Data Reduction and Analysis

4.4.2.1 General - All of the strain gage signals drove voltage - controlled oscillators whose outputs were mixed and recorded on magnetic tape. The method of converting these FM multiplexed recordings into engineering data summaries is described in the following paragraphs. While only the stress data is discussed specifically, the procedures described for vibratory stress data are also applicable to the vibratory motion data.

4.4.2.2 First Stage Reduction - In the first stage of data reduction, the tape is played back on an Ampex Model FR1900 reproduce transport. Total strain signals are recovered from the recordings by a set of EMR Model 210B discriminators and then led through Hamilton Standard system correctors for adjustment of gain.

4.4.2.3 Calibration - Calibration of the data reduction system is accomplished by means of standardization signals generated within the magnetic tape recorder and recorded prior to testing. These signals, representing known signal levels from the transducers, are used to adjust the sensitivity of the playback equipment.

4.4.2.4 Vibratory Stress Data - For vibratory information, the total stress signals are processed by Hamilton Standard data modifiers whose function is to produce a signal equal to half the peak-to-peak amplitude of the input voltage. This signal, representing vibratory stress amplitude, is then recorded on a Sanborn Model 150 direct-writing recorder that accommodates eight data channels plus time and coding pips. One of the Sanborn channels is usually allocated to an analog rpm signal obtained by processing the one-per-rev (IF) pulse through a shaper, multiplier, and frequency-to-voltage converter. When appropriate, Sanborn channels were also allocated to the wind speed and direction signals.

4.4.2.5 Sanborn Charts - The Sanborn charts are time plots of steady or peak vibratory stress recorded during accelerations and steady state operation of the Q-Fan. Due to the decay characteristics of the peak stress converters used in the data reduction process, the characteristic of stress versus time from the charts is distorted. However, if desired, this trend can be accurately established from the oscillograph records described in the following paragraph. From the Sanborn charts, peak stress and the general trend of stress versus time can be established. Portions of the data can then be corrected plots of stress versus rpm.

4.4.2.6 Oscillograph Records - The output of up to twelve (12) system correctors were recorded on the Honeywell Model 1612 Visicorder Oscillograph. These records of total stress provide information on the phase relationships between the various measurements as well as the general frequency content of the signals.

4.4.2.7 Frequency Content - To determine the frequency content in detail, however, the system corrector outputs are analyzed on a Spectral Dynamics Model SD301B Real Time Analyzer. This analyzer, coupled with a Model SD302B Ensemble Averager, is used to perform a spectrum analysis from 0 to 1000 Hz with an effective bandwidth of 3 Hz. The data sample used for this analysis varies from four (4) to sixteen (16) seconds. The outputs of the analyzer are plotted on a Hewlett-Packard Model 7030AR X-Y recorder.

A block diagram of the equipment used for the reduction of the Q-Fan test data is shown in Figure 31.

5.0 Discussion of Results

5.1 Performance

5.1.1 Steady State Reverse Thrust with Take-Off Nozzle - Prior to the start of the transient testing, a series of steady-state reverse blade angle runs were made with the take-off nozzle used in place of the normal reverse exit. The objective of this testing was to determine the effect that a closed nozzle would have on reverse thrust. This section will present the results of that testing.

5.1.1.1 Instrumentation - The instrumentation used in this test is described in detail in Section 7.0, Appendix A, and is the same as that used in developing the data in Ref. 1. This instrumentation consists of a fixed rake located at the fan duct exit, one behind the rotor, one at the compressor duct entrance and eight at the compressor face, as shown in Figure 1 of Appendix A.

In order to aid in the interpretation of the data from the rake behind the rotor, flow visualization during reverse thrust operation tests utilizing a smoke generator were made prior to the start of the steady state testing. These tests were directed primarily at determining the directions of the flow leaving the bellmouth inlet near the spinner surface. It had been found during the previous reverse thrust testing that the inboard readings on the rake downstream of the rotor were below ambient total pressure leading to questions concerning the validity of all the readings on the rake. Hence, the smoke tests were undertaken to determine the existance of flow angularity in the center of the annulus and whether this angularity exceeded the rake measurement limit.

The results show a disturbed region of flow extending from the spinner surface to approximately the mid-blade radius under reverse thrust conditions. Flow in this disturbed region is erratic, fluctuating both up and downstream with no consistent pattern or regularity as shown in Figure 32. On the other hand, flow outboard of this region is consistently directed axially along the duct. It would thus appear that the inboard rake readings are of questionable accuracy because of the random nature of the flow.

Due to mounting constraints, the weight flow rake located near the duct exit was positioned in a field with a strong radial velocity gradient as shown in Figure 33. Because of this gradient, static and total pressures measured at the rake must be adjusted for pitch angle.

Bryer and Pankhurst corrections, Ref. 4, were applied to some of these data and the results will be discussed later in the appropriate sections.

5.1.1.2 Results - The engine power data are not affected by any of the flow problems mentioned above, as they are derived from a direct reading of the torquemeter and engine speed. The torquemeter calibration curve used to reduce the data is shown in Figure 34. The corrected powers and speeds for each of the test points is given in Table 1.

The variation of power with blade angle and corrected speed is shown in Figure 35. As noted in the previous testing, the power closely follows a cubic variation with corrected speed. As reference, the power data for the same blade angles from the previous testing with the reverse nozzle as reported in Ref. 1 are shown on the curve. It is immediately obvious that the fan did not absorb the same power at the same blade angle and corrected speed with the take-off nozzle. These low values of horsepower are verified by an observed reduction in fan weight flow. Using the relationship:

$$HP = \frac{W\ C_p\ J\ \Delta T}{550}$$

Then the ratio of horsepowers should be:

$$\frac{HP_1}{HP_2} = \frac{W_1\ C_p\ J\ \Delta T}{W_2\ C_p\ J\ \Delta T}$$

or

$$\frac{HP_1}{HP_2} = \frac{W_1\ \Delta T_1}{W_2\ \Delta T_2}$$

It is assumed that the changes in ΔT are small, then the horsepowers should be in the ratio of the weight flows or:

$$\frac{HP_1}{HP_2} = \frac{320}{165.5} = \frac{W_1 \text{ flow with reverse exit}}{W_2 \text{ flow with takeoff nozzle}}$$

where 145 kg/sec (320 #/sec.) was measured with the reverse exit and 75 kg/sec (165.5 #/sec.) was measured with the take-off nozzle of the present test. Reducing and rearranging gives:

$$HP_1 = 1.93345\ HP_2 \text{ (Test point R-24)}$$

5.1.1.2 (continued)

The actual ratio of powers for this test point was 1.5938, indicating a change in ΔT as well as flow. Nevertheless, there would appear to be a consistency between the observed low measured horsepower and flows.

The above results also imply a change in the duct reverse operating load line. Such a change could be caused by larger inlet losses with the take-off rather than the reverse thrust nozzle. This is not an unexpected result as the flow with the take-off nozzle is drawn over sharp edges whereas a relatively smooth bellmouth inlet is effected by the reverse thrust nozzle. Such losses have been noted and reported by NASA in Ref. 5.

The variation of engine weight flow with power is shown in Figure 36. These values are based on the engine duct inlet rake measurements. Since static tap #92 on the inboard end of this rake was not operative, the static pressure sensed at tap #91 was assumed to act at tap #92 in deriving the flows. In view of this and the fact that the points are within 0.226 kg/sec (1/2 lb./sec.) of the original curve from Ref. 1 as shown in Figure 36, the original curve was used in the subsequent data analysis.

Knowing the corrected power, the fuel flow and engine thrust were obtained from the Lycoming specification for this T55-L-11 engine. Using the relationship $T = W \times V_e$, the engine exit velocities were computed assuming that W is the total flow including both fuel and air. These values are presented in Table 2.

As previously mentioned, because of mounting constraints, the weight flow rake had to be located in a region with strong radial flow. Accordingly, corrections must be made to both the static and total pressure readings. Both of these readings were adjusted by the corrections for flow angle contained in Ref. 4.

The magnitude of the corrections to the total head readings is shown in Figure 37. Taps 67 and 71 are simple pitot tubes located on the inlet rake approximately 76 and 178 mm (three and seven inches) respectively above the inner cowl surface. The uncorrected readings indicate a loss in total head of from 1 to 1 1/2 percent before the reverse inlet is even reached. Adjusting these readings for flow angle results in the corrections shown in Figure 37 leading to indicated total head losses at the rake of less than 1/2%. This is not an unmeasurable value and therefore these small losses were subsequently used in calculating the axial velocities.

5.1.1.2 (continued)

Results of adjusting the static and total pressures for angularity on the integrated weight flow are shown in Figure 38. With no correction applied to either the static or total pressures, the integrated weight flow was 49.7 kg/sec (109.5 #/sec). Adjusting only the static pressure measurements resulted in a flow of 53.8 kg/sec (118.5 #/sec) while correcting both static and total pressures gives 64.2 kg/sec (141.5 #/sec). All of these values were obtained by integrating only to the outer radius of the take-off exit. Assuming a larger "capture area" at the rake, out to the 760 mm (30") radius would result in a weight flow of 75.1 kg/sec (165.5 #/sec). Subtracting the engine weight flow from this value results in a flow through the fan rotor of 64.9 kg/sec (143.2 #/sec). Utilizing the total head measurements from the rake located behind the fan (downstream reverse thrust conditions), a flow of 71.2 kg/sec (157.03 #/sec) may be deduced. This implies that the "capture area" should be even larger than assumed for the 75 kg/sec (165.5 #/sec) value. However, this does show reasonable agreement between the two sets of independent measurements.

The total head rake located downstream of the fan under reverse thrust conditions, both in the previous testing (Ref. 1) and the current test, has indicated total head readings below ambient over the inner 40-50% of the rake radius as shown in Figure 39. However, the radial distribution of total pressure is different for the two tests, the reverse exit nozzle producing a higher total pressure rise than the take-off nozzle of the present test for reasons previously given. The inboard readings are not accurate and should be ignored since the flow was too unstable and erratic in this region and not measurable with fixed instrumentation. The outboard readings were reliable and were used in the data analysis. The radial distribution of total pressure for the various test points is shown in Figures 40, 41 and 42 as a function of the radius squared. These curves were integrated by the technique of Ref. 1 to obtain the thrust values indicated on these figures. The integration of ΔP_T versus R^2 is an indication of the circulation and therefore the thrust of the blade. In addition, by assuming a pressure ratio of one over the inboard end of the rake where the data are questionable, an area averaged pressure ratio was calculated for each test point and plotted on Figure 43. These pressure ratios, as well as the associated flows and exit velocities, are presented in Table 3. For convenience, the calculated thrust for each test point, as explained below, is also given.

5.1.1.2 (continued)

Using the area averaged pressure ratio and assuming flow only through the outer annulus as defined by the total pressure distribution from the downstream rake as shown in Figures 40, 41 and 42, fan duct thrust was calculated for the take-off nozzle and is shown as solid symbols on Figure 44. These compare to the open symbols on the same curves which are the thrust values from Figures 40, 41, and 42. The agreement between these two different calculation methods is good and confirms the low levels of thrust indicated. Also shown on this figure is the level of thrust observed during the previous testing with the reverse nozzle. As can be seen, with the take-off nozzle, less than 1/3 of the reverse thrust previously obtained was realized. Although it would appear that some further gain in thrust might be obtained by going to still larger angles as indicated in Figure 45, it is clear that the use of a take-off nozzle during reverse operation, results in a significant reduction in reverse thrust.

In addition to the reduction in reverse thrust, an increase in compressor face distortion is also experienced as shown in Figure 46. The distortion levels are more than double those measured with the reverse nozzle. However, it should be pointed out that even with this increased level, no difficulty was encountered in operating the engine.

A high response dynamic pressure transducer (Kulite) was installed on one of the compressor inlet total head rakes. The output of this one Kulite is compared to steady state values in the same rake in Figure 47 for test point R-24, the maximum reverse thrust point. The following comments may be made on the Kulite data:

1. The Kulite pressures indicate a variation of $\pm$ 5.5 KN/M^2 ($\pm$0.8 psi) from a mean value of the Kulite output.

2. Visicorder pressure traces of the Kulite output show a 13 spike variation per revolution indicating that each blade passage is sensed by the Kulite.

These data indicate that the "dynamic" distortion is higher than the steady state distortion.

5.1.1.2 (continued)

The pressure rise at the core engine compressor face was also computed for these test points. As previously experienced, there is a loss in total head at the compressor face during reverse operation. Here again, there was no problem in running the engine at these lower levels of total head. These data are presented in Table 4 as the ratio, Ptcore = Pt/Ho. Comparing these values with the same test points using the reverse nozzle exlet shows less loss with the take-off nozzle. For example: the equivalent of point R-24, i.e., β = 144° and 229 m/s (750 ft/sec.) tip speed, has a ratio P_{T}core/Ho = 0.890 with the reverse exlet; but, as can be seen from Figure 35, almost twice as much power could be applied with the reverse nozzle exlet and, therefore, the engine weight flows and attendant losses would be expected to be larger.

5.1.2 Transients

5.1.2.1 Introduction - A total of 213 transient test runs were made during the course of the test program. This included forward, reverse, and forward to reverse transients as well as repeat runs. The more significant transients were analyzed and the results of this examination are discussed below.

5.1.2.2 Variation of Fan/Engine Parameters with Time; Aerodynamic Analysis - The variation of horsepower, blade angle, fan speed, PLA and compressor face total pressure are shown in Figures 48, 49 and 50 as a function of elapsed time for the faster transients TRC 3-71, TRC 3-43 and TRC 3-66. Of these, TRC 3-66 is of the most interest since it represents the case with the maximum power input to the fan and the smallest fan speed decrease during the transient.

Examination of Figure 48 shows small power peaks at a blade angle of 70° and a minimum power near a blade angle of 130°. This is in general agreement with previous steady state testing. These characteristics persisted even though very different PLA schedules were used during the transients as shown in Figure 49. The small power increase in transient TRC 3-71 occurred when the PLA was at its minimum, while the minimum powers occurred after the PLA had been reset to a higher level. These powers, along with the corresponding fan rpms. from Figure 49 when converted to power coefficient, are shown in Figure 51 along with a transient in the reverse through flat pitch direction. Also shown on this figure is the steady state data from previous testing as reported in Ref. 1.

5.1.2.2 (continued)

Obviously a difference exists in the reverse through feather mode between the steady state and the transient data. Particularly noteworthy, is the lack of large power coefficient peaks at blade angles of 70 and 140 degrees. In fact, by scheduling a slight decrease in the blade angle before advancing to the feather direction, as shown in transient TRC 3-43, Figure 48, power coefficient can be made to decrease before increasing again to the reverse thrust value. Unless the blade angle rate during the transient is very low, steady state data do not accurately represent transient variations.

The variation of compressor face total pressure with blade angle is shown in Figure 50. Unlike the power variations, there is a significant increase, then a very large decrease in total pressure as the blade angle is increased. The increase in total pressure implies an increase in thrust while the lower than ambient total pressures are an indication of reverse or negative flow. An indication of the aerodynamic lag in the system can be observed by noting that even though the root airfoil angle has advanced beyond 90°, the compressor face pressure which is most affected by the performance of this airfoil shows little or no change.

In order to better interpret the variation of total pressure, analytical calculations were used to determine an approximate variation of total pressure with blade radius. The increase or decrease above the nominal rotor pressure ratio is shown in Figure 52 as a function of rotor radius for two different operating conditions. This plot was then integrated to determine what ΔP_R was required at the root to have a net ΔP_R equal to zero over the entire radius which corresponds to a zero duct thrust. This value, when converted to pressure, results in a total pressure increment of 9100 n/m^2 (-1.32 psi), a value which correlates reasonably with the minimums shown in Figure 50. Thus, from the pressure trace of Figure 49, the sequence of events during a transient is that the pressure first increases when going through stall and falls rapidly when going to the zero thrust point, increases and then falls again as the reverse thrust is built up.

This sequence of events is in general substantiated by an observation of the blade steady bending stresses for these runs. If it is assumed that the maximum steady stress occurs near the stall point and that zero fan thrust occurs when the blade steady stress has a value of zero, then the comparison of the times required for each event as determined from Sanborn traces of the compressor face total pressure measurements and blade steady bending stresses may be depicted as shown in Figure 53. In view of the assumptions made, the agreement within 0.1 second is especially noteworthy. Blade stresses should respond before a change in the compressor face

5.1.2.2 (continued)

total pressure is noted and TRC 3-66 was a higher power, faster transient than TRC 3-71. Thus it would appear that based on Sanborn records, rotor stall can be reached 0.25 seconds after the transient is initiated and zero thrust 0.4 seconds after. If the time to maximum reverse thrust is arbitrarily defined as the point where the stresses on the 362 mm gages return to a nominal value, then the Sanborn traces indicate that approximately 1.3 seconds are required to complete the transient. However, because of the characteristics of the signal conditioners used in developing the Sanborn data, the time interval on these traces tends to be longer than that actually required. A much more sensitive time indicator is a Visicorder trace of the same transient. This is shown in Figure 54 where a Sanborn and Visicorder trace are compared side by side for transient TRC 3-66. The Visicorder trace indicates that the transient can be completed in 0.9 seconds or less. A much better indicator of the response time is the time required for thrust reversal as measured on a thrust meter. This will be performed in subsequent NASA testing.

A comparison of transient TRC 3-66 with a computer simulation of the same transient is shown in Figure 55. A difference is noted between the simulated and actual torques. As will be recalled, the simulation data were based on steady state performance testing and modified for rotor/engine inertia effects. A better simulation can now be effected by using an average of the transient variations shown in Figure 51.

However, since more extensive and accurate data will be obtained during the NASA testing of this engine, it is not deemed worthwhile at this time to compare other transients or re-do the simulation study.

5.1.2.3 Time Response for Forward to Reverse Transients; Statistical Analysis - The effect of the various control variables both individually and in combination and their statistical significance on the time to go from forward to reverse thrust has been determined using Analysis of Variance Techniques. The statistical technique used to analyze the results of each designed experiment in this test program is called the "Analysis of Variance" - ANOVA. This technique consists of analysis of the variation of the main factors, interactions and experimental error as approximated by the mean square deviation from the average for each. The standard F-test is applied to each mean square value to determine the significance of each source of variation. Variables with larger F-ratios can be thought of as having a larger effect on the test results than those with smaller F-ratios. The test results used in all of the statistical analyses are tabulated in Table 5.

5.1.2.3 (continued)

The following tabulation indicates the time, in seconds, to go from forward to reverse thrust for the entire 2^3 schedule 1, full factorial experiment which was repeated once. The response time is defined as the period from transient initiation to a point where the stresses on the 362 min gages return to a nominal value.

	b_0		b_1	
	c_0	c_1	c_0	c_1
a_0	1.30 1.25	2.05 1.85	1.30 1.20	1.40 1.30
a_1	1.20 1.10	1.70 1.40	1.20 1.00	1.05 1.10

where: $a_0 = 50$ $b_0 = 40$ $c_0 = 61$

$a_1 = 100$ $b_1 = 75$ $c_1 = 72$

where: A = Blade angle rate, below 72° - degrees/second
B = PLA reset level - degrees
C = Blade angle for completion of PLA reset - degrees
TSL range = 70° to 0°

For the range of variables tested the average response time was 1.34 seconds. An "Analysis of Variance", Table 6, indicates that all three main variables have a statistically significant effect on the test results. This is found by comparing the "F" ratios for each source of variation. If an F-ratio for the variable exceeds the value found in an "F" Distribution Table for 95% certainty (approximately 6.0) this would indicate a 95% certainty that the effect was due to the variable and only a 5% chance that it was due to chance. Additionally there is a significant interaction between Factors B and C. Figure 56 shows the average result for each treatment combination in graphical form. When C was at its low level, the response was independent of B, whereas, when C was at its high level, there was a large response to variations in Factor B.

5.1.2.3 (continued)

The average effects of the significant variables are:

A = -0.24 seconds (increasing variable decreases response time)

B = -0.29 seconds (increasing variable decreases response time)

C = +0.29 seconds (increasing variable increases response time)

BC = -0.25 seconds (increasing variable decreases response time)

The fastest test point combination was a_1, b_1, c_0; that is a high pitch change rate below 72°, a small reset in power level and a short duration of power reset. The average expected response for this treatment combination is 1.05 seconds.

For the 2^3, Schedule 2, full factorial experiment, the time, in seconds, to go from forward to reverse thrust is tabulated below:

	b_0		b_1	
	c_0	c_1	c_0	c_1
a_0	1.60	2.10	1.30	1.50
a_1	1.20	1.45	1.25	1.10

Where: $a_0 = 50$ $b_0 = 40$ $c_0 = 57$

$a_1 = 100$ $b_1 = 73$ $c_1 = 72$

For the range of variables tested the average response time was 1.44 seconds. Analysis of variance, Table 7, indicates that as with the schedule 1 data, all three main variables have a significant effect on the test results. Interaction effects are weak and not statistically significant, as shown in Figure 57.

5.1.2.3 (continued)

The average effects of the significant variables are:

A = -0.38 seconds (increasing variable decreases response time)

B = -0.30 seconds (increasing variable decreases response time)

C = +0.20 seconds (increasing variable increases response time)

The fastest test point combination was a_1, b_1, c_0 (the same as schedule 1) with an average expected response of 1.09 seconds.

The schedule 3 test from a starting TSL of 70° was planned as a 2^5 full factorial experiment. As noted earlier, an operating procedure change was introduced after the first half of this series was run. Additional test points were run (TRC 3-71 to TRC 3-80) which when combined with the second half of the test series completed a 2^4 full factorial experiment. With the fourth test variable, factor D, the blade angle rate above 72°. The response times for this experiment were as follows:

		b_0		b_1	
		d_0	d_1	d_0	d_1
a_0	c_0	1.6	1.5	1.6	1.4
	c_1	2.5	2.2	1.6	1.5
a_1	c_0	1.3	1.1	1.3	1.1
	c_1	1.4	1.6	1.3	1.1

where:

a_0 = 50

a_1 = 100

b_0 = 40

b_1 = 70

c_0 = 51

c_1 = 72

d_0 = 100

d_1 = 150

The average response time for the schedule 3 experiment was 1.51 seconds. The new test variable, factor D, was statistically insignificant over the range tested, whereas the other three main effects plus the interaction between factors B and C had a significant effect on the test results. This is essentially the same result as obtained with schedules 1 and 2.

5.1.2.3 (continued)

The average effects of the significant variables are:

A = -0.46 seconds (increasing variable decreases response time)

B = -0.29 seconds (increasing variable decreases response time)

C = +0.29 seconds (increasing variable increases response time)

BC = -0.26 seconds (increasing variable decreases response time)

The fastest test point combination was a_1, b_1, c_0 (the same as schedules 1 and 2) with an average expected response of 1.07 seconds. Table 8 shows the Analysis of Variance and Figure 58 illustrates the interaction effects for this case.

The effect of the operating procedure change can be determined by comparing the average results of the same test points before and after the change. These points are:

Treatment Combination	Before Change		After Change	
	Test Point	Time Response	Test Point	Time Response
a	TRC 3-32	1.40	TRC 3-77	1.30
b	TRC 3-37	1.75	TRC 3-80	1.60
d	TRC 3-10	1.65	TRC 3-74	1.50
ac	TRC 3-1	2.00	TRC 3-71	1.40
bc	TRC 3-4	1.70	TRC 3-72	1.60
cd	TRC 3-33	3.10	TRC 3-78	2.20
abd	TRC 3-9	2.00	TRC 3-73	1.10
abcd	TRC 3-31	1.25	TRC 3-76	1.10
	Total	14.85		11.8
	Average	1.86		1.48

As expected the average response time is less after the operating procedure change. By an average of approximately 0.4 seconds.

5.1.2.3 (continued)

Another Schedule 3 experiment, this time with a high starting forward thrust(TSL = 90°), was run with the three main factors, A, B and C. The response times for this experiment were:

	b_0		b_1	
	c_0	c_1	c_0	c_1
a_0	1.40	1.90	1.35	1.50
a_1	1.20	1.25	1.20	1.10

where: $a_0 = 50$ $b_0 = 40$ $c_0 = 60$

$a_1 = 100$ $b_1 = 80$ $c_1 = 72$

The average response time for this test series was 1.36 seconds. Unlike the previous test, only Factor A had a statistically significant effect on the time response (Figure 59) with an average effect of +0.35 seconds. See Table 9 for the Analysis of Variance.

5.2 Structural - During the transient testing, several strain measurements were made on the blades, barrel and exit guide vanes while vibratory motion pickups were monitored at various locations on the nonrotating structure. The objective of these measurements was to provide information on the structural behavior of a full-scale variable pitch fan.

The most significant of the data obtained is that from the blade strain gages. These data are discussed in detail in the following sections.

5.2.1 Steady State Reverse Thrust with Take-off Nozzle Blade Stress - Blade stresses recorded during the reverse thrust testing with the take-off nozzle are summarized in Table 10. As expected, the highest readings among the various gage positions on the blades were from the flatwise bending gage pairs located 362 mm from the blade tip. The edgewise bending gage pairs at 387 mm from the tip gave much lower outputs as did the tip bending gage at 127 mm from the tip. The "vee" gage at 89 mm from the tip, installed to show blade torsional response, always indicated low stress levels.

5.2.1 (continued)

The vibratory stress levels listed in Table 10 are the maximum stress levels recorded during the entire run. Both Visicorder and Sanborn records were made of these runs with acceptable correlation noted between the two types of records. The maximum stress recorded was 89.4 mn/m^2 ($\pm$ 13000 psi) during run R24 at 3150 fan rpm which also corresponds to the maximum reverse thrust point shown on Figure 44.

This value is considerably greater than those observed during the testing with the reverse nozzle exlet. In that test, the maximum recorded stress at the 362 mm from tip station was $\pm$ 51 MN/M^2 (7400 psi). Thus, the use of the take-off nozzle in reverse thrust aggravates the blade stress.

The response of the blades to various P orders as determined from spectral plots is summarized in Table 11. A "P" order is defined as an integral order of the fan rotational frequency. A sample spectral plot is shown in Figure 60. The primary response is at or near the frequency corresponding to the first flatwise blade bending mode as shown in Figure 61. Stress responses at frequencies other than the first flatwise are also present but never with substantial levels. A dash in Table 11 indicates negligible or no response. The response of the blades to non-integer P orders is clearly present in the spectral plots.

Examination of Visicorder traces of all the R runs shows that the variations in vibratory stress level of the two instrumented blades do not follow the same time-history. The blades appear to be responding independently rather than as part of a synchronous dynamic system.

5.2.2 Transient Testing; Aerodynamic Analysis - Blade Stress - Prior to the reduction of all the data, eight of the faster transients in both forward and reverse thrust were selected for examination. Peak vibratory and steady stresses as well as stresses observed during the start and end of each of these initial transients are summarized in Tables 12 and 13. A complete tabulation of the transient schedules is contained in Section 4.3. As noted previously in the R runs, maximum response occurs at the flatwise bending gage pairs located 362 mm from the blade tip.

Maximum vibratory stress occurred during the reverse through feather (TRC) transients with significantly lower levels observed during the reverse through flat pitch (TRF) and forward thrust (TFC) transients. Vibratory stresses at the start and end of a transient are in all cases lower than those observed during the transient.

The steady stresses of Table 13 reflect the changes in thrust during a transient. For example, the steady stress for the 362 mm gage on the #12 blade increases during a forward thrust transient while it decreases and even changes sign during a reverse thrust transient as a result of a change in the thrust direction.

After these initial transients were reduced, all of the other transient data were reduced. The results of the forward thrust transients are summarized in Table 14, the reverse through feather transients in Table 15, the reverse through flat pitch transients in Table 16, and the reverse thrust transients in Table 17. In each of these tables, 362 mm refers to the gage 362 mm from the blade tip on blade 1, 6 or 12; BBL #3 refers to blade barrel gage #3; stator #1 refers to stator gage #1. The exact location of each of these gages is contained in Appendix A of Section 7.0. Examination of these tables shows that the maximum blade vibratory stress was 24.1 mn/m^2 ($\pm$ 3500 psi) for the forward thrust transients 99.8 mn/m^2 ($\pm$ 14,500 psi) for the reverse through feather transients, 41.98 mn/m^2 ($\pm$ 6100 psi) for the reverse through flat pitch transients and 61.9 mn/m^2 ($\pm$ 9000 psi) for the reverse thrust transients. The Sanborn records for each of these fan transients where the maximum stresses reduced is shown in Figures 62 through 65. The records for other transients are contained in Section 7, Appendix F. Care must be taken in interpreting these traces as there are occasional break-ups of the signals as may be noted by the "spikes" in Figure 62. These breaks should not be interpreted as high stress levels but rather as instrumentation abnormalities. The blade angle calibration curve presented in Figure 66 must be used with these Sanborn records in order to determine the proper blade angle.

5.2.2 (continued)

During the reverse thrust transient testing, the infinite life allowable blade stress levels of ± 38 mn/m^2 (± 5500 psi) was exceeded while operating near the feather blade angle. Based on Miner's rule which relates actual to allowable stress cycles at any stress level, the structural life used to date for all of the testing based on a sigma (n/N) of 0.5 is 8.5%. None of the transients performed would appear to present any serious structural problems for a fan rotor designed to current spar shell blade design standards.

5.2.3 Transient Testing; Statistical Analysis - Blade Stress - The statistical technique used to analyze the results at each designed experiment in this test program is discussed in Section 5.1.2.3.

Earlier tests at HS have indicated that the blade vibratory stress during a forward to reverse thrust transient would momentarily exceed the allowable stress. Because it is desireable to keep the magnitude of blade overstressing to a minimum, ANOVA techniques were used to analyze the effects of the various control variables on blade vibratory stress. During the transient from forward to reverse thrust through feather, two distinct blade vibratory stress peaks occur. The first of these peaks occurs as the blades go through feather and the second peak occurs when the blades reach the reverse pitch angle but prior to the build up of reverse thrust. Although these stress peaks appear similar in character, the average peak stress at reverse is substantially higher than the peak near feather. For instance, for the schedule 1 test points, the average peak near feather is 35.78 mn/m^2 (5200 psi) while the peak at reverse is approximately 40% higher at 50.22 mn/m^2 (7300 psi).

For the schedule 1 test points, the blade peak vibratory stress, in + mn/m^2 (+ psi), which occurs as the blades go through feather is tabulated below for the entire full factorial experiment. This data was obtained in pairs from two different blades at the same blade station as shown in Table 15. The schedule 1 test points were each run twice, a total of four readings for each test point, to obtain an estimate of the variability in stress due to factors not included in the controlled experiment.

5.2.3 (continued)

	b_0		b_1	
	c_0	c_1	c_0	c_1
a_0	27.5(4000) 41.3(6000)	37.8(5500) 27.5(4000)	41.3(6000) 37.8(5500)	58.5(8500) 27.5(4000)
	20.6(3000) 34.4(5000)	17.2(2500) 24.1(3500)	58.5(8500) 72.2(10500)	34.4(5000) 48.2(7000)
a_1	24.1(3500) 27.5(4000)	20.6(3000) 31.0(4500)	27.5(4000) 27.5(4000)	34.4(5000) 34.4(5000)
	34.4(5000) 27.5(4000)	24.1(3500) 27.5(4000)	51.6(7500) 51.6(7500)	48.2(7000) 51.6(7500)

$a_0 = 50$
$a_1 = 100$

$b_0 = 40$
$b_1 = 75$

$c_0 = 61$
$c_1 = 72$

where:

A = Blade Angle Rate, Below 72° = deg/sec.

B = PLA Reset Angle - deg.

C = Blade Angle for Completion of PLA Reset - deg.

The average variability in blade stress from blade to blade is 8.26 mn/m^2 (1200 psi). This was determined by first calculating the difference between each pair of results and then calculating the average of these differences. Repeating the test points resulted in a variability in blade stress from run to run of 14.45 mn/m^2 (2100 psi). Even with these large variabilities from blade to blade and for repeat runs, an ANOVA, Table 18, indicates that factor B, the reset in engine power at the start of the transient, has a statistically significant effect on the test results. With factor B at its low level, equivalent to resetting engine power to flight idle, the average peak stress was $\pm$ 28.2 mn/m^2 ($\pm$ 4100 psi). With factor B at its high level, equivalent to a slight reduction in engine power at the start of the transient, the average peak stress was $\pm$ 44.0 mn/m^2 ($\pm$ 6400 psi). No other controlled factors either by themselves or in combination had a statistically significant effect on the peak stress near feather for schedule 1. In Figure 67 the average stress for each test point is shown versus each main factor.

5.2.3 (continued)

To verify the validity of using the peak stress for this analysis, a study was made using the average vibratory stress for the thirty stress cycles just after the feather blade angle was reached. For this study the test results from the on-line visicorder traces were used. The stress level for each cycle was read from these recordings and then the average vibratory stress was computed. The average stresses in mn/m^2 ($\pm$ psi) are tabulated below and are shown in Figure 68.

	b_0		b_1		
	c_0	c_1	c_0	c_1	$a_0 = 50$ $a_1 = 100$
a_0	10.6(1545) 18.6(2710)	9.5(1375) 15.5(2260)	73.6(3425) 20.3(2955)	19.4(2825) 33.0(4800)	$b_0 = 40$ $b_1 = 75$
a_1	15.9(2315) 12.3(1785)	15.4(2235) 13.2(1915)	26.5(3855) 24.3(3525)	19.6(2850) 17.1(2485)	$c_0 = 61$ $c_1 = 72$

The ANOVA of this data, Table 19, indicates that factor B is the only statistically significant factor of those considered, the same result obtained using the peak stress data. Resetting the engine power to flight idle decreases the average vibratory stress by 40% compared with a reduction in peak vibratory stress of 36%.

5.2.3 (continued)

The schedule 2 test results are very nearly the same as the schedule 1 results. The average peak vibratory stress near feather is ± 36.46 mn/m² (± 5300 psi). The following tabulation indicates the peak stress near feather for the full factorial, schedule 2 experiment.

		b_0		b_1	
		c_0	c_1	c_0	c_1
a_0		37.8(5500)	24.1(3500)	37.8(5500)	48.2(7000)
		34.4(5000)	17.2(2500)	48.2(7000)	48.2(7000)
a_1		37.8(5500)	24.1(3500)	34.4(5000)	37.8(5500)
		34.4(5000)	24.1(3500)	41.3(6000)	31.9(4500)

$a_0 = 50$
$a_1 = 100$

$b_0 = 40$
$b_1 = 73$

$c_0 = 57$
$c_1 = 72$

In addition to factor B, the ANOVA (Table 20) indicates that there is also a significant interaction between factors B and C. This interaction can be seen in Figure 69.

For the schedule 3 test series, from a starting TSL of 70%, a fourth variable - Factor D - the pitch change rate above 72° was introduced. The results of this 2^4 full factorial experiment are:

			b_0		b_1	
			d_0	d_1	d_0	d_1
a_0	c_0		37.8(5500)	44.7(6500)	61.9(9000)	68.8(10000)
			58.5(8500)	48.2(7000)	65.4(9500)	58.5(8500)
	c_1		41.3(6000)	34.4(5000)	79.1(11500)	55.0(8000)
			34.4(5000)	27.5(4000)	72.2(10500)	31.0(4500)
a_1	c_0		37.8(5500)	41.3(6000)	41.3(6000)	51.6(7500)
			37.8(5500)	50.0(7273)	41.3(6000)	72.2(10500)
	c_1		58.5(8500)	44.7(6500)	31.0(4500)	75.7(11000)
			37.8(5500)	37.8(5500)	51.6(7500)	82.6(12000)

$a_0 = 50$
$a_1 = 100$

$b_0 = 40$
$b_1 = 70$

$c_0 = 51$
$c_1 = 72$

$d_0 = 100$
$d_1 = 150$

The average peak vibratory stress near feather for this test series was ± 50.22 mn/m^2 (± 7300 psi) which is substantially higher than the schedule 1 and 2 results. Since the ANOVA for this series indicates that the main effect of factor D is not statistically significant, this increase must be associated with the schedule itself. The AD interaction, although statistically significant, could not account for the large variation between schedules. Besides the AD interaction, factor B also has a significant result on these results. Figure 70 shows the average results plotted for each main variable.

A short test series (2^3) with a starting TSL of 90° had the following results:

	b_0		b_1	
	c_0	c_1	c_0	c_1
a_0	4500 5500	3500 4000	7500 3500	7000 7500
a_1	5500 6000	3500 8000	3500 4000	5500 9500

The ANOVA for this test series, Table 22, indicates that none of the variables have a statistically significant effect on the test results. The results are plotted in Figure 71.

The second blade vibratory stress peak which occurs as the blades reach the reverse blade angle but prior to the build-up of thrust was analyzed using the same procedure as the first stress peak. For the schedule 1 test data, the average blade vibratory stress was ± 50.22 mn/m^2 (± 7200 psi) at the second peak; approximately 40% higher than the first peak near feather. The average variability in blade stress from blade to blade was 8.81 mn/m^2 (1280 psi) and the variability in blade stress from run to run was 13.55 mn/m^2 (1970 psi) which are nearly the same as the comparable variabilities of the stress peak near feather.

5.2.3 (continued)

Tabulated below are the test results for the schedule 1 test points in mn/m^2 (psi).

	b_0		b_1	
	c_0	c_1	c_0	c_1
a_0	55.0(8000) 55.0(8000) 37.8(5500) 37.8(5500)	41.3(6000) 31.0(4500) 37.8(5500) 27.5(4000)	55.0(8000) 55.0(8000) 48.2(7000) 51.6(7500)	61.9(9000) 65.4(9500) 48.2(7000) 72.2(10500)
a_1	41.3(6000) 44.7(6500) 65.4(9500) 68.8(10000)	31.0(4500) 34.4(5000) 48.2(7000) 51.6(7500)	41.3(6000) 68.8(10000) 58.5(8500) 41.3(6000)	68.8(10000) 44.7(6500) 61.9(9000) 55.0(8000)

$a_0 = 50$
$a_1 = 100$

$b_0 = 40$
$b_1 = 75$

$c_0 = 61$
$c_1 = 72$

The average results for each test point are:

	b_0		b_1	
	c_0	c_1	c_0	c_1
a_0	46.4 (6750)	34.4 (5000)	52.5 (7625)	61.9 (9000)
a_1	55.1 (8000)	41.3 (6000)	52.5 (7625)	57.6 (8375)

These results are plotted in Figure 72. Inspection of this Figure indicates a strong BC interaction. The ANOVA, Table 23, for this test series, indicates that both the PLA reset level, Factor B, and the interaction of the PLA reset level with the blade angle for completion of the PLA reset, the BC interaction, are satistically significant.

5.2.3 (continued)

The stress peak near reverse for the schedule 2 test points has an average vibratory stress of ± 53.66 mn/m^2 (± 7800 psi); approximately 47% higher than the corresponding peak near feather. Tabulated below are the test results in mn/m^2 (psi) for the complete 2^3 full factorial experiment.

	b_0		b_1	
	c_0	c_1	c_0	c_1
a_0	55.0(8000) 61.9(9000)	41.3(6000) 55.0(8000)	31.0(4500) 44.7(6500)	82.6(12000) 75.7(11000)
a_1	51.6(7500) 44.7(6500)	37.8(5500) 51.6(7500)	55.0(8000) 51.6(7500)	68.8(10000) 51.6(7500)

$a_0 = 50$
$a_1 = 100$
$b_0 = 40$
$b_1 = 73$
$c_0 = 57$
$c_1 = 72$

For this test series the analysis of variance, Table 23, indicates that only the BC interaction is statistically significant. The average result for the three main variables is shown in Figure 73.

5.2.3 (continued)

The stress peak near reverse results in mn/m^2 (psi) of the schedule 3 test series are:

		b_0		b_1	
		d_0	d_1	d_0	d_1
a_0	c_0	68.8(10000) 86.0(12500)	48.2(7000) 65.4(9500)	65.4(9500) 68.8(10000)	51.6(7500) 61.9(9000)
	c_1	24.1(3500) 34.4(5000)	44.7(6500) 31.0(4500)	61.9(9000) 44.7(6500)	51.6(7500) 68.8(10000)
a_1	c_0	51.6(7500) 65.4(9500)	61.9(9000) 55.0(8000)	75.7(11000) 55.0(8000)	65.4(9500) 72.2(10500)
	c_1	41.3(6000) 44.7(65-0)	79.8(11600) 61.9(9000)	48.2(7000) 55.0(8000)	75.7(11000) 65.4(9500)

Where:

$a_0 = 50$
$a_1 = 100$

$b_0 = 40$
$b_1 = 70$

$c_0 = 51$
$c_1 = 72$

$d_0 = 100$
$d_1 = 150$

The average peak stress near reverse for this test series was $\pm$ 57.79 mn/m^2 ($\pm$ 8400 psi); approximately 16% higher than the peak at feather. The ANOVA for these test points, Table 25, indicates that two main effects, factors B and C, as well as three interactions, AB, AD and CD have a statistically significant effect on the stress peak near reverse. These test results are illustrated in Figure 74.

5.2.3 (continued)

A short test series (2^3) with a starting TSL of 90° had the following results:

	b_0		b_1	
	c_0	c_1	c_0	c_1
a_0	61.9(9000) 41.3(6000)	65.4(9500) 58.5(8500)	55.0(8000) 75.7(11000)	68.8(10000) 72.2(10500)
a_1	51.6(7500) 72.2(10500)	58.5(8500) 68.8(10000)	68.8(10000) 61.9(9000)	58.5(8500) 58.5(8500)

The ANOVA for this test series, Table 26, indicates that none of the factors have a significant effect on the stress peak near reverse when the transient is started from a high TSL. Figure 75 illustrates the average results for the variables with a high starting TSL.

5.2.4 Barrel Stress - Barrel vibratory stresses during forward thrust transients were low averaging ± 11.6 mn/m^2 (1700 psi). A peak vibratory stress of ± 46.8 mn/m^2 (± 6800) was observed for one test transient but, in general, no consistent trends were noted. Stresses were higher during the reverse through feather transients, averaging 28.7 mn/m^2 (4200 psi). Again no consistent trends were observed with a peak stress of ± 44 mn/m^2 (± 6400 psi) measured. Barrel stresses were not measured during the reverse through flat pitch transients. The average stress measured during the reverse thrust transients was 16.9 mn/m^2 (2425 psi) with a peak stress of ± 17.5 mn/m^2 (± 2500 psi) recorded. In very general terms, barrel stresses were the lowest during forward thrust transients, slightly higher during the reverse thrust transients and the highest during reverse through feather transients.

5.2.5 Exit Guide Vane Stress - In general, the stresses on the exit guide vanes were low during all of the transient testing. The average stresses were lowest for the forward thrust transients, ± 2.9 mn/m^2 (± 417 psi); higher for the reverse thrust transients, ± 3.9 mn/m^2 (± 550 psi); next highest for transients through flat pitch, ± 4.6 mn/m^2 (± 650 psi); and the highest for the transients through feather, ± 7.1 mn/m^2 (± 1009 psi). For only one reverse through feather transient, the vibratory stresses reached a level of 34.2 mn/m^2 (± 5000 psi) which is equal to the infinite life

5.2.5 (continued)

stress limits established for the vane material. It should be emphasized that this occured for only one point and it is believed that this is an erroneous data point since similar transients did not reflect this stress level.

5.26 Velocity Pickup Data - The velocity pickups on the rig were continually monitored to insure satisfactory operation of the unit. Although the limits as specified in Appendix E were momentarily exceeded on several occasions, the unit continued to operate satisfactorily during all phases of testing. A review of the data indicates no specific trends. The maximum recorded vertical velocity was 8.1 cm/sec (3.2 ips) on the gearbox and 22.1 cm/sed (8.7 ips) on the bellmouth.

TABLE 1. CORRECTED POWERS AND SPEEDS

Test Point	N2 RPM	% Torque	β Degrees	Tamb °F	Ambient Total Pressure		$\delta = \frac{H_O}{P_O}$	$\sqrt{\frac{T}{T_O}} = \sqrt{\theta}$	$\delta \div \sqrt{\theta}$	Fan Tip Speed	
					N/M^2	in.Hg				m/s	ft/sec
R-21	11850	32	142	78	101069	29.93	1.0003	1.0181	1.0184	183.2	600.9
R-22	13810	39	142	77	101069	29.93	1.0003	1.0171	1.0175	213.4	700.2
R-24	14970	56	144	79	101069	29.93	1.0003	1.0190	1.0194	231.4	759.1
R-26	11830	33	140	79	101069	29.93	1.0003	1.0190	1.0194	182.8	599.9
R-28	10110	23	142	79	101069	29.93	1.0003	1.0190	1.0194	156.2	512.6
R-29	11810	38	144	79	101069	29.93	1.0003	1.0190	1.0194	182.5	598.8
R-30	9850	29	144	81	101069	29.93	1.0003	1.0209	1.0213	152.2	499.5

Test Point	Corrected Fan Tip Speed		Torque		Power		Corrected Power	
	m/s	ft/sec	M-N	in-lb	KW	HP	KW	HP
R-21	179.9	590.2	446	3950	554	743	545	731
R-22	209.9	688.5	559	4950	808	1084	794	1065
R-24	227.1	744.9	797	7050	1245	1670	1221	1638
R-26	179.4	588.7	463	4100	575	771	564	756
R-28	153.3	503.1	311	2750	329	441	323	433
R-29	179.1	587.7	542	4800	670	899	658	882
R-30	149.1	489.2	401	3550	413	554	404	542

TABLE 2. ENGINE EXIT VELOCITIES

Test Point	Corrected Fan Tip Speed		β	Corrected Power		Engine Fuel Flow			
	m/s	ft/sec	Degrees	KW	HP	kg/hr	lb/hr	kg/sec	lb/sec
R-21	179.9	590.2	142	545	731	327	720	0.0907	0.2000
R-22	209.9	688.5	142	794	1065	386	850	0.1071	0.2361
R-28	153.3	503.1	142	323	433	249	550	0.0693	0.1528
R-24	227.1	744.9	144	1221	1638	481	1060	0.1335	0.2944
R-29	179.1	587.7	144	658	882	354	780	0.0983	0.2167
R-30	149.1	489.2	144	404	542	286	630	0.0794	0.1750
R-26	179.4	588.7	140	564	756	331	730	0.0920	0.2028

Test Point	Engine Air Flow		Weight Flow		Engine Thrust		Engine Exit Velocity	
	kg/sec	lb/sec	kg/sec	lb/sec	N	lb	m/s	ft/min
R-21	8.3	18.2	8.346	18.400	378	85	0.756	148.75
R-22	9.1	20.0	9.179	20.236	480	108	0.873	171.85
R-28	7.4	16.4	7.508	16.553	267	60	0.593	116.72
R-24	10.1	22.3	10.248	22.594	645	145	1.050	206.65
R-29	8.7	19.1	8.762	19.317	423	95	0.804	158.36
R-30	7.8	17.3	7.927	17.475	311	70	0.655	128.98
R-26	8.4	18.5	8.484	18.703	378	85	0.743	146.34

TABLE 3. TOTAL HEAD RAKE DATA

Test Point	Corrected Fan Tip Speed m/s	Corrected Fan Tip Speed ft/sec	β Degrees	Pressure Ratio P_R	$1/P_R$	Mach. No.	Corrected Flow/A kg/sec m^2	Corrected Flow/A lb/sec ft^2	Corrected Flow kg/sec	Corrected Flow lb/sec	Corrected Power KW	Corrected Power HP
R-21	179.9	590.2	142	1.0163	0.98396	0.152	62.5	12.803	35.57	78.429	545	731
R-22	209.9	688.5	142	1.0224	0.97809	0.179	73.2	14.996	43.17	95.167	794	1065
R-28	153.3	503.1	142	1.0115	0.98863	0.130	53.7	10.990	30.54	67.327	323	433
R-24	227.1	744.9	144	1.0364	0.96488	0.226	91.4	18.721	71.23	157.03	1221	1638
R-29	179.1	587.7	144	1.0214	0.97905	0.175	71.6	14.674	55.83	123.08	658	882
R-30	149.1	489.2	144	1.0144	0.98580	0.142	58.5	11.981	45.59	100.498	404	542
R-26	179.4	588.7	140	1.0177	0.98261	0.160	65.7	13.456	35.47	78.207	564	756

Test Point	Weight Flow kg/sec	Weight Flow lb/sec	Tamb °F	$\sqrt{\text{Tamb}}$ °R	Speed of Sound m/s	Speed of Sound ft/sec	Exit Velocity m/s	Exit Velocity ft/sec	Thrust N	Thrust lb
R-21	34.95	77.058	78	23.195	347	1137.01	52.7	172.83	1840	413.6
R-22	42.45	93.595	77	23.173	346	1135.94	62.0	203.33	2629	591 01
R-28	29.98	66.091	79	23.216	347	1138.07	45.1	147.95	1351	303.69
R-24	69.92	154.150	79	23.216	347	1138.07	78.4	257.20	5477	1231.29
R-29	54.80	120.820	79	23.216	347	1138.07	60.7	199.16	3324	747.29
R-30	44.67	98.470	81	23.259	348	1140.18	49.4	161.91	2202	495.12
R-26	34.82	76.772	79	23.216	347	1138.07	55.5	182.09	1931	434.14

TABLE 4. CORE ENGINE FACE PRESSURE RATIO AND DISTORTION

Test Point	Tube No.	Max. Total Pressure		Min. Total Pressure		Ave. Total Pressure		Ambient Total Pressure		Δ Total Pressure		
		N/m^2	in.ABr_4	N/m^2	in.ABr_4	N/m^2	in.ABr_4	N/m^2	in.Hg	N/m^2	in.ABr_4	in.Hg
R-21	33	-3297	-4.5	-6448	-8.8	-5206	-7.106	101069	29.93	-2418	-3.3	-0.716
R-22	33	-3737	-5.1	-8060	-11.0	-6417	-8.758	101069	29.93	-7986	-10.9	-2.365
R-24	34	-6374	-8.7	-14068	-19.2	-8891	-12.135	101069	29.93	-7693	-10.5	-2.278
R-26	33	-3004	-4.1	-6521	-8.9	-5278	-7.203	101069	29.93	-3517	-4.8	-1.041
R-28	33	-1978	-2.7	-4909	-6.7	-3792	-5.176	101069	29.93	-2931	-4.0	-0.868
R-29	34	-3297	-4.5	-9305	-12.7	-5747	-7.844	101069	29.93	-6008	-8.2	-1.779
R-30	34	-2345	-3.2	-6228	-8.5	-4275	-5.835	101069	29.93	-3883	-5.3	-1.150

Test Point	Distor-tion	Δ Total Pressure Core				Total Pressure Core/Ho
		N/m^2	in.Hg	N/m^2	in.Hg	
R-21	0.0252	-5207	-1.542	95862	28.388	0.948
R-22	0.0844	-6419	-1.901	94650	28.029	0.938
R-24	0.0834	-8898	-2.635	92171	27.295	0.913
R-26	0.0367	-5285	-1.565	95784	28.365	0.948
R-28	0.0301	-3789	-1.122	97280	28.808	0.964
R-29	0.0630	-5747	-1.702	95322	28.228	0.943
R-30	0.0401	-4282	-1.268	96787	28.662	0.958

TABLE 5 - REVERSE THRU FEATHER TRANSIENTS

SCHEDULE 1 and 2 - TEST RESULTS

Test Point Number	Time to Reverse (sec.)	Blade Vibratory Bending Stress - 362MM from Tip							
		Blade #1				Blade #6			
		@ Feather		@ Reverse		@ Feather		@ Reverse	
		MN/M^2	(PSI)	MN/M^2	(PSI)	MN/M^2	(PSI)	MN/M^2	(PSI)
TRC1-1	1.3	27.5	(4000)	55.0	(8000)	41.3	(6000)	55.0	(8000)
2	1.2	34.4	(5000)	44.7	(6500)	24.1	(3500)	34.4	(5000)
3	2.05	37.8	(5500)	41.3	(6000)	27.5	(4000)	31.0	(4500)
4	1.05	34.4	(5000)	68.8	(10000)	34.4	(5000)	44.7	(6500)
5	1.7	20.6	(3000)	31.0	(4500)	31.0	(4500)	34.4	(5000)
6	1.3	24.1	(3500)	65.4	(9500)	27.5	(4000)	48.1	(7000)
7	1.2	27.5	(4000)	41.3	(6000)	27.5	(4000)	20.6	(3000)
8	1.4	58.5	(8500)	61.9	(9000)	27.5	(4000)	65.4	(9500)
9	1.2	24.1	(3500)	41.3	(6000)	27.5	(4000)	44.7	(6500)
10	1.3	41.3	(6000)	55.0	(8000)	37.8	(5500)	55.0	(8000)
11	1.2	58.5	(8500)	48.2	(7000)	72.2	(10500)	51.6	(7500)
12	1.85	17.2	(2500)	37.8	(5500)	24.1	(3500)	27.4	(4000)
13	1.25	20.6	(3000)	37.8	(5500)	34.4	(5000)	37.8	(5500)
14	1.1	37.8	(5500)	65.4	(9500)	37.8	(5500)	64.5	(9500)
15	1.1	17.2	(2500)	41.3	(6000)	37.8	(5500)	41.3	(6000)
16	1.3	34.4	(5000)	48.2	(7000)	48.2	(7000)	72.2	(10500)
17	1.1	34.4	(5000)	65.4	(9500)	27.5	(4000)	68.8	(10000)
18	1.0	51.6	(7500)	58.5	(8500)	51.6	(7500)	55.0	(8000)
19	1.1	48.2	(7000)	61.9	(9000)	51.6	(7500)	55.0	(8000)
20	1.4	24.1	(3500)	48.2	(7000)	27.5	(4000)	51.6	(7500)
21	1.6	55.0	(8000)	31.0	(4500)	41.3	(5000)	48.1	(7000)
22	1.3	37.8	(5500)	31.0	(4500)	61.9	(9000)	58.5	(8500)
23	1.3	27.5	(4000)	55.0	(8000)	58.5	(8500)	75.7	(11000)
24	1.15	48.2	(7000)	61.9	(9000)	37.8	(5500)	79.1	(11500)
25	1.2	48.2	(7000)	44.7	(6500)	41.3	(6000)	41.3	(6000)
26	1.3	34.4	(5000)	44.7	(6500)	86.0	(12500)	37.8	(5500)
27	0.9	55.0	(8000)	55.0	(8000)	51.6	(7500)	61.9	(9000)
28	0.9	37.8	(5500)	34.4	(5000)	34.4	(5000)	34.4	(5000)
TRC2-1	1.3	37.8	(5500)	31.0	(4500)	48.2	(7000)	55.0	(8000)
2	1.1	58.5	(8500)	68.8	(10000)	31.0	(4500)	75.7	(11000)
3	1.35	27.5	(4000)	51.6	(7500)	31.0	(4500)	51.6	(7500)
4	1.2	37.8	(5500)	51.6	(7500)	34.4	(5000)	44.7	(6500)
5	1.6	37.8	(5500)	55.0	(8000)	34.4	(5000)	61.9	(9000)
6	1.25	34.4	(5000)	55.0	(8000)	41.3	(6000)	51.6	(7500)
7	2.1	24.1	(3500)	41.3	(6000)	17.2	(2500)	55.0	(8000)
8	1.45	24.1	(3500)	37.8	(5500)	24.1	(3500)	51.6	(7500)
9	1.5	48.2	(7000)	82.6	(12000)	48.2	(7000)	75.7	(11000)
10	1.3	34.4	(5000)	41.3	(6000)	27.5	(4000)	44.7	(6500)

TABLE 5 (Continued)

REVERSE THRU FEATHER TRANSIENTS

SCHEDULE 3 - TEST RESULTS

Test Point Number	Time to Reverse (sec.)	Blade Vibratory Bending Stress - 362MM from Tip							
		Blade #1				Blade #6			
		@ Feather		@ Reverse		@ Feather		@ Reverse	
		MN/M^2	(PSI)	MN/M^2	(PSI)	MN/M^2	(PSI)	MN/M^2	(PSI)
TRC3-1	2.0	37.8	(5500)	41.3	(6000)	65.4	(9500)	61.9	(9000)
2	2.0	68.8	(10000)	31.0	(4500)	34.4	(5000)	48.2	(7000)
3	1.5	44.7	(6500)	68.8	(10000)	44.7	(6500)	48.2	(7000)
4	1.7	58.5	(8500)	68.8	(10000)	48.2	(7000)	68.8	(10000)
5	2.4	41.3	(6000)	41.3	(6000)	31.0	(4500)	37.8	(5500)
6	3.7	13.8	(2000)	20.6	(3000)	13.8	(2000)	31.0	(4500)
7	2.1	58.5	(8500)	92.9	(13500)	65.4	(9500)	58.5	(8500)
8	2.2	24.1	(3500)	44.7	(6500)	31.0	(4500)	41.3	(6000)
9	1.2	34.4	(5000)	68.8	(10000)	65.4	(9500)	61.9	(9000)
10	1.65	24.1	(3500)	58.5	(8500)	31.0	(4500)	44.7	(6500)
11	1.1	41.3	(6000)	61.9	(9000)	34.4	(5000)	55.0	(8000)
12	1.4	68.8	(10000)	51.6	(7500)	58.5	(8500)	75.7	(11000)
13	2.5	41.3	(6000)	24.1	(3500)	34.4	(5000)	34.4	(5000)
14	1.9	51.6	(7500)	61.9	(9000)	65.4	(9500)	51.6	(7500)
15	2.1	24.1	(3500)	48.2	(7000)	44.7	(6500)	48.2	(7000)
16	1.3	31.0	(4500)	48.2	(7000)	51.6	(7500)	55.0	(8000)
17	1.5	55.0	(8000)	44.7	(6500)	55.0	(8000)	86.0	(12500)
18	1.65	48.2	(7000)	51.6	(7500)	37.8	(5500)	75.7	(11000)
19	1.45	44.7	(6500)	58.5	(8500)	41.3	(6000)	44.7	(6500)
20	1.4	44.7	(6500)	61.9	(9000)	34.4	(5000)	68.8	(10000)
21	1.6	44.7	(6500)	79.1	(11500)	37.8	(5500)	61.9	(9000)
22	1.4	48.2	(7000)	51.6	(7500)	48.2	(7000)	48.2	(7000)
23	1.5	55.0	(8000)	51.6	(7500)	31.0	(4500)	68.8	(10000)
24	2.8	27.5	(4000)	37.8	(5500)	27.6	(4000)	34.4	(5000)
25	1.6	31.8	(4500)	44.7	(6500)	31.0	(4500)	55.0	(8000)
26	1.45	48.2	(7000)	55.0	(8000)	37.8	(5500)	48.2	(7000)
27	1.55	41.3	(6000)	68.8	(10000)	65.4	(9500)	51.6	(7500)
28	1.6	37.8	(5500)	68.8	(10000)	58.5	(8500)	86.0	(12500)
29	1.3	41.3	(6000)	75.7	(11000)	41.3	(6000)	55.0	(8000)
30	1.6	48.2	(7000)	61.9	(9000)	55.0	(8000)	41.3	(6000)
31	1.25	34.4	(5000)	41.3	(6000)	51.6	(7500)	75.7	(11000)
32	1.4	48.2	(7000)	48.2	(7000)	41.3	(6000)	51.6	(7500)
33	3.1	20.6	(3000)	48.2	(7000)	27.6	(4000)	27.5	(4000)
34	2.1	37.8	(5500)	51.6	(7500)	24.1	(3500)	55.0	(8000)
35	3.2	31.0	(4500)	31.0	(4500)	51.6	(7500)	48.2	(7000)
36	2.1	68.8	(10000)	44.7	(6500)	51.6	(7500)	44.7	(6500)

TABLE 5 (Continued)

REVERSE THRU FEATHER TRANSIENTS

SCHEDULE 3 - TEST RESULTS

Test Point Number	Time to Reverse (sec.)	Blade Vibratory Bending Stress - 362MM from Tip							
		Blade #1				Blade #6			
		@ Feather		@ Reverse		@ Feather		@ Reverse	
		MN/M^2	(PSI)	MN/M^2	(PSI)	MN/M^2	(PSI)	MN/M^2	(PSI)
TRC3-37	1.75	89.4	(13000)	72.2	(10500)	61.9	(9000)	79.1	(11500)
38	2.2	58.5	(8500)	51.6	(7500)	44.7	(6500)	61.9	(9000)
39	2.0	24.1	(3500)	44.7	(6500)	24.1	(3500)	51.6	(7500)
40	1.55	55.0	(8000)	65.4	(9500)	65.4	(9500)	65.4	(9500)
41	1.35	51.6	(7500)	55.0	(8000)	65.4	(9500)	75.7	(11000)
42	1.9	24.1	(3500)	65.4	(9500)	27.5	(4000)	58.5	(8500)
43	1.25	24.1	(3500)	58.5	(8500)	55.0	(8000)	68.8	(10000)
44	1.4	31.0	(4500)	61.9	(9000)	37.8	(5500)	41.3	(6000)
45	1.1	37.8	(5500)	58.5	(8500)	65.4	(9500)	58.5	(8500)
46	1.2	37.8	(5500)	51.6	(7500)	41.3	(6000)	72.2	(10500)
47	1.35	37.8	(5500)	51.6	(7500)	31.0	(4500)	72.2	(10500)
48	1.5	48.2	(7000)	68.8	(10000)	51.6	(7500)	72.2	(10500)
49	1.3	27.5	(4000)	61.9	(9000)	27.5	(4000)	55.0	(8000)
50	1.2	24.1	(3500)	68.8	(10000)	27.5	(4000)	61.9	(9000)
51	1.4	61.9	(9000)	61.9	(9000)	48.2	(7000)	61.9	(9000)
52	2.0	55.0	(8000)	51.6	(7500)	41.3	(6000)	37.8	(5500)
53	1.15	34.4	(5000)	41.3	(6000)	31.0	(4500)	75.7	(11000)
54	1.3	65.4	(9500)	37.8	(5500)	41.3	(6000)	65.4	(9500)
55	1.1	58.5	(8500)	61.9	(9000)	51.6	(7500)	58.5	(8500)
56	1.3	48.2	(7000)	55.0	(8000)	41.3	(6000)	44.7	(6500)
57	1.2	55.0	(8000)	48.2	(7000)	44.7	(6500)	68.8	(10000)
58	1.0	55.0	(8000)	61.9	(9000)	41.3	(6000)	61.9	(9000)
59	1.4	48.2	(7000)	44.7	(6500)	48.2	(7000)	51.6	(7500)
60	1.3	41.3	(6000)	41.3	(6000)	34.4	(5000)	58.5	(8500)
61	0.95	41.3	(6000)	44.7	(6500)	55.0	(8000)	55.0	(8000)
62	0.9	72.2	(10500)	55.0	(8000)	48.2	(7000)	61.9	(9000)
63	0.9	48.2	(7000)	5815	(8500)	55.0	(8000)	51.6	(7500)
64	0.95	51.6	(7500)	48.7	(7000)	61.9	(9000)	68.8	(10000)
65	0.9	37.8	(5500)	55.0	(8000)	44.7	(6500)	75.7	(11000)
66	0.9	51.6	(7500)	68.8	(10000)	55.0	(8000)	72.2	(10500)
67	1.25	65.4	(9500)	51.6	(7500)	48.2	(7000)	65.4	(9500)
68	1.0	44.7	(6500)	55.0	(8000)	51.6	(7500)	65.4	(9500)
69	1.3	37.8	(5500)	82.6	(12000)	41.3	(6000)	61.9	(9000)
70	1.0	68.8	(10000)	55.0	(8000)	79.1	(11500)	75.7	(11000)
71	1.4	58.5	(8500)	41.3	(6000)	37.8	(5500)	44.7	(6500)
72	1.6	79.1	(11500)	61.9	(9000)	72.2	(10500)	44.7	(6500)
73	1.1	51.6	(7500)	65.4	(9500)	72.2	(10500)	72.2	(10500)

TABLE 5 (Continued)

REVERSE THRU FEATHER TRANSIENTS

SCHEDULE 3 - TEST RESULTS

Test Point Number	Time to Reverse (sec.)	Blade Vibratory Bending Stress - 362MM from Tip							
		Blade #1				Blade #6			
		@ Feather		@ Reverse		@ Feather		@ Reverse	
		MN/M^2	(PSI)	MN/M^2	(PSI)	MN/M^2	(PSI)	MN/M^2	(PSI)
TRC3-74	1.5	44.7	(6500)	48.2	(7000)	48.2	(7000)	65.4	(9500)
75	1.4	61.9	(9000)	51.6	(7500)	37.8	(5500)	44.7	(6500)
76	1.1	75.7	(11000)	75.7	(11000)	86.0	(12500)	65.4	(9500)
77	1.3	37.8	(5500)	51.6	(7500)	37.8	(5500)	65.4	(9500)
78	2.2	34.4	(5000)	14.7	(6500)	27.5	(4000)	31.0	(4500)
79	1.35	37.8	(5500)	41.3	(6000)	41.3	(6000)	75.7	(11000)
80	1.6	61.9	(9000)	65.4	(9500)	65.4	(9500)	68.8	(10000)

NOTE: Stresses were obtained from visicorder traces

TABLE 6. ANOVA FOR TIME FROM FORWARD TO REVERSE THRUST-SCHEDULE 1

SOURCE OF VARIATION	DEGREES OF FREEDOM	SUM OF SQUARES	MEAN SQUARES	F-RATIO
MAIN				
A	1	0.23	0.23	18.78
B	1	0.33	0.33	27.52
C	1	0.33	0.33	27.52
INTERACTIONS				
AB	1	0.003	0.003	0.21
AC	1	0.04	0.04	3.33
BC	1	0.25	0.25	20.81
RESIDUAL	9	0.11	0.012	
TOTAL	15	1.29		

Error: $\hat{\sigma} = \sqrt{.012} = 0.11$

TABLE 7. ANOVA FOR TIME FROM FORWARD TO REVERSE THRUST-SCHEDULE 2

SOURCE OF VARIATION	DEGREES OF FREEDOM	SUM OF SQUARES	MEAN SQUARES	F-RATIO
MAIN				
A	1	0.28	0.28	23.44
B	1	0.18	0.18	15.00
C	1	0.08	0.08	6.66
INTERACTIONS				
AB	1	0.05	0.05	3.75
AC	1	0.05	0.05	3.75
BC	1	0.05	0.06	5.10
RESIDUAL	1	0.001	0.001	
TOTAL	7	0.70		

Error: $\hat{\sigma}$ = 0.11 from Schedule 1

TABLE 8. ANOVA FOR TIME FROM
FORWARD TO REVERSE THRUST-SCHEDULE 3 (TSL 70° to 0°)

SOURCE OF VARIATION	DEGREES OF FREEDOM	SUM OF SQUARES	MEAN SQUARES	F-RATIO
MAIN				
A	1	0.86	0.86	53.75
B	1	0.33	0.33	20.63
C	1	0.33	0.33	20.63
D	1	0.08	0.08	5.00
INTERACTIONS				
AB	1	0.08	0.08	5.00
AC	1	0.08	0.08	5.00
AD	1	0.01	0.01	0.63
BC	1	0.28	0.28	17.50
BD	1	0.01	0.01	0.63
CD	1	0.01	0.01	0.63
RESIDUAL	5	0.08	0.016	
TOTAL	15	2.15		

Error: $\hat{\sigma} = \sqrt{.016} = 0.13$

TABLE 9. ANOVA FOR TIME FROM
FORWARD TO REVERSE THRUST-SCHEDULE 3 (TSL 90° to 0°)

SOURCE OF VARIATION	DEGREES OF FREEDOM	SUM OF SQUARES	MEAN SQUARES	F-RATIO
MAIN				
A	1	0.25	0.25	20.42
B	1	0.05	0.05	3.75
C	1	0.05	0.05	3.75
INTERACTIONS				
AB	1	0.01	0.01	0.94
AC	1	0.06	0.06	5.10
BC	1	0.03	0.03	2.60
RESIDUAL	1	0.005	0.005	
TOTAL	7	0.44		

Error: $\hat{\sigma}$ = 0.11 from Schedule 1

TABLE 10

BLADE STRESS - REVERSE THRUST WITH TAKE-OFF NOZZLE

PARAMETER	LOCATION	RUN 21	RUN 22	RUN 24	RUN 26	RUN 28	RUN 29	RUN 30
BLADE ANGLE, β DEG		142.°	142.°	144.°	140.°	142.°	141.°	144.°
FAN SPEED, RPM		2500	2900	3150	2490	2130	2490	2070
				VISICORDER RECORDS				
VIBRATORY STRESS ±MN/M^2 (±PSI)	387MM FT BL #1	11.7 (1700)	12.0 (1750)	16.2 (2350)	12.0 (1750)	7.9 (1150)	12.0 (1750)	8.9 (1300)
	362MM FT BL #1	54.0 (7850)	57.5 (8360)	48.3 (7020)	52.5 (7630)	32.7 (4760)	55.8 (8110)	36.9 (5370)
	362MM FT BL #6	46.2 (676)	79.1(11500)	81.9(11900)	51.6 (7500)	32.7 (4760)	50.4 (7320)	36.1 (5250)
	127MM FT BL #7	17.5 (2550)	24.3 (3530)	28.0 (4070)	15.8 (2300)	14.9 (2160)	21.3 (3090)	16.5 (2400)
	89MM FT V BL #7	4.3 (620)	8.4 (1220)	4.8 (700)	3.8 (550)	3.1 (450)	4.8 (700)	3.8 (550)
				SANBORN RECORDS				
VIBRATORY STRESS ±MN/M^2 (±PSI)	387MM FT EB BL #1	12.4 (1800)	13.8 (2000)	18.6 (2700)	9.6 (1400)	6.2 (900)	11.0 (1000)	7.6 (1100)
	362MM FT BL #1	49.5 (720)	61.9 (9000)	79.1(11500)	44.7 (6500)	30.9 (4500)	48.2 (7000)	34.4 (5000)
	362MM FT BL #6	51.6 (7500)	67.4 (9800)	89.4(13000)	51.6 (7500)	32.7 (4750)	53.3 (7750)	44.7 (6500)
	127MM FT BL #7	19.9 (2900)	27.5 (4000)	30.3 (4400)	15.8 (2300)	12.4 (1800)	23.4 (3400)	16.5 (2400)
	89MM FT V BL #7	3.1 (450)	8.9 (1300)	8.3 (1250)	2.9 (420)	1.7 (250)	5.5 (800)	4.1 (600)
	BBL #2	4.1 (600)	---	---	---	---	---	---
	BBL #3	5.5 (800)	6.9 (1000)	6.9 (1000)	5.5 (800)	1.4 (200)	4.1 (600)	2.8 (400)
	BBL #4	5.5 (800)	6.9 (1000)	8.3 (1200)	13.8 (200)	4.1 (600)	5.5 (800)	4.1 (600)

TABLE 11

STRESS DATA FROM SPECTRAL PLOTS, ± MN/M^2, (±PSI)

Gage No. / P-ORDER	RUN R21 3-1	5-1	3-4	3-3	R22 3-1	5-1	3-4	3-3	R24 3-1	5-1	3-4	3-3	R28 3-1	5-1	3-4	3-3
0<P<1	-	-	-	-	-	-	-	-	2.3 (340)	15.8(2305)	5.7(830)	3.(435)	-	-	-	-
1.	-	-	-	-	-	-	-	-	-	4.8(700)	2.1(310)	0.5(75)	-	-	-	-
1<P<2	-	-	-	-	-	-	-	-	-	-	1.1(160)	0.3(45)	-	-	-	-
2.	-	-	-	-	-	-	-	-	-	-	1.4(210)	-	-	-	-	-
2<P<3	-	-	-	-	3.5(510)	25.1(3650)	5.6(810)	0.9(125)	3.5(210)	17.2(2500)	5.8(850)	0.9(135)	-	-	-	-
3.	2.1(310)	12.5(1820)	3.5(510)	0.6(80)	-	-	-	-	-	-	1.2(170)	0.5(75)	1.9(270)	11.6(1680)	3.1(450)	0.4(65)
3<P<4	-	-	-	-	-	-	-	-	1.7(240)	-	-	-	-	-	-	-
4.	1.0(150)	-	-	-	0.6(90)	-	-	-	-	-	-	-	0.3(50)	-	-	-
4<P<5	-	-	-	-	-	-	-	-	1.0(140)	-	0.6(90)	-	-	-	-	-
5.	-	-	-	-	-	-	-	-	-	-	-	0.6(90)	-	-	-	-
5<P<6	-	-	-	-	-	-	-	-	-	-	-	-	-	-	-	-
6.	-	-	-	0.2(35)	-	-	1.4(210)	2.0(295)	-	-	-	-	-	-	-	-
6<P<7	-	-	-	-	-	-	-	-	-	-	-	-	-	-	-	-
7.	-	-	-	-	-	-	-	-	-	-	0.6(90)	0.4(65)	-	-	-	-
7<P<8	-	-	-	-	-	-	-	-	-	-	1.9(280)	0.5(72)	-	-	-	-
8.	-	-	-	-	-	-	-	-	0.8(120)	-	6.3(910)	0.5(72)	-	-	-	-
8<P<9	-	-	-	-	-	-	1.4(210)	-	-	-	1.2(170)	0.4(65)	-	-	-	-
9.	-	-	-	-	-	-	-	-	-	-	-	-	-	-	-	-
9<P<10	-	-	-	-	-	-	0.6(90)	-	-	-	-	-	-	-	-	-
10.	-	-	0.6(90)	-	-	-	-	-	-	-	-	-	-	-	-	-
10<P<11	-	-	-	-	-	-	-	-	-	-	-	-	-	-	-	-
11.	-	-	-	-	-	-	-	-	-	-	-	-	-	-	0.6(90)	-
11<P<12	-	-	-	-	-	-	-	-	-	-	-	-	-	-	-	-
12.	-	-	-	-	-	-	-	-	-	-	-	-	-	-	-	-
12<P<13	-	-	-	-	-	-	-	-	-	-	-	-	-	-	-	-
13.	-	-	-	-	-	-	-	0.5(70)	-	-	-	-	-	-	-	-
13<P<14	-	-	-	-	-	-	-	-	-	-	-	-	-	-	-	-

Gage No.	LOCATION
3-1	387MM FT EB BL #1
5-4	362MM FT BL #6
3-4	127MM FT BL #7
3-3	89MM FT V BL #7

NOTE: Dashed Lines indicate no measureable response.

TABLE 12

PEAK VIBRATORY STRESS DURING TRANSIENTS ± MN/M^2, (±PSI)

TRANSIENT	387MM FT EB BL #1	362MM FT BL #12	362MM FT BL #6	127MM FT BL #7	89MM FT VBL #7	BBL #2	BBL #3	BBL #4
TFC 3-3.3	5.8 (850)	9.6 (1400)	11.7 (1700)	4.1 (600)	1.4 (200)	35.8 (5200)	16.5 (2400)	1.4 (200)
TFC 3-4.3	4.8 (700)	9.3 (1350)	11.0 (1600)	4.8 (700)	1.0 (150)	8.3 (1200)	11.0 (1600)	1.4 (200)
TFC 1-1.2	12.4 (1800)	15.1 (2200)	12.9 (2600)	10.3 (1500)	3.0 (550)	8.3 (1200)	8.3 (1200)	---
TFC 1-3.2	11.0 (1600)	13.8 (2000)	14.4 (2100)	8.3 (1200)	3.4 (500)	8.3 (1200)	17.9 (2600)	2.8 (400)
TFC 3-43	10.3 (1500)	55.7 (8100)	68.8 (10000)	26.8 (3900)	6.2 (900)	57.8 (8400)	41.3 (6000)	19.3 (2800)
TRC 3-71	8.9 (1300)	61.9 (9000)	41.9 (6100)	19.9 (2900)	8.3 (1200)	79.8 (11600)	44.0 (6400)	16.5 (2400)
TRC 3-66	17.9 (2600)	68.8 (10000)	57.8 (8400)	26.8 (3900)	11.0 (1600)	52.2 (7600)	32.0 (4800)	13.8 (2000)
TRF 6-6	34.4 (5000)	19.9 (2900)	21.3 (3100)	13.8 (2000)	7.9 (1150)	110.0 (16000)	16.5 (2400)	5.5 (800)

VIBRATORY STRESS AT START AND END OF TRANSIENT ± MN/M^2, (±PSI)

TRANSIENT	387MM FT EB BL #1	362MM FT BL #12	362MM FT BL #6	127MM FT BL #7	89MM FT VBL #7	BBL #2	BBL #3	BBL #4
TFC 3-3.3	Start 2.8 (400)	4.8 (700)	4.5 (650)	2.1 (300)	0.3 (50)	16.5 (2400)	8.3 (1200)	1.4 (200)
	End 5.8 (850)	9.6 (1400)	11.7 (1700)	4.1 (600)	1.4 (200)	1.4 (200)	11.0 (1600)	1.4 (200)
TFC 3-4.3	Start 4.8 (700)	6.5 (950)	6.2 (900)	4.8 (700)	0.7 (100)	8.3 (1200)	11.0 (1600)	1.4 (200)
	End 4.1 (600)	9.3 (1350)	7.6 (1100)	3.8 (550)	1.0 (150)	1.4 (200)	8.3 (1200)	1.4 (200)
TFC 1-1.2	Start 2.1 (300)	6.5 (950)	4.8 (700)	1.0 (150)	0.3 (50)	8.3 (1200)	1.4 (200)	---
	End 12.4 (1800)	10.3 (1500)	11.7 (1700)	6.2 (900)	2.1 (300)	2.8 (400)	1.4 (2000)	---
TFC 1-3.2	Start 2.1 (300)	6.2 (900)	3.4 (500)	2.8 (400)	1.0 (150)	17.9 (2600)	2.8 (400)	1.4 (200)
	End 4.1 (600)	8.9 (1300)	9.6 (1400)	6.2 (900)	2.1 (300)	4.1 (600)	17.9 (2600)	1.4 (200)
TRC 3-43	Start 4.8 (700)	6.2 (900)	6.2 (900)	2.8 (400)	0.7 (100)	19.3 (2800)	11.0 (1600)	5.5 (800)
	End 3.1 (450)	12.4 (1800)	12.4 (1800)	11.7 (1700)	3.1 (450)	1.4 (200)	13.8 (2000)	1.4 (200)
TRC 3-71	Start 3.4 (500)	4.1 (600)	4.8 (700)	2.8 (400)	0.3 (50)	8.3 (1200)	8.3 (1200)	1.4 (200)
	End 2.8 (400)	12.4 (1800)	17.9 (2600)	11.0 (1600)	2.8 (400)	5.5 (800)	11.0 (1600)	1.4 (200)
TRC 3-66	Start 4.1 (600)	6.9 (1000)	8.3 (1200)	4.8 (700)	1.0 (150)	1.4 (200)	8.3 (1200)	1.4 (200)
	End 4.1 (600)	10.3 (1500)	11.0 (1600)	11.0 (1600)	3.4 (500)	2.8 (400)	8.3 (1200)	1.4 (200)
TRFC-6	Start 1.4 (200)	4.8 (700)	6.2 (900)	1.4 (200)	0.7 (100)	24.8 (3600)	5.5 (800)	2.8 (400)
	End 12.4 (1800)	22.0 (3200)	22.0 (3200)	22.0 (3200)	5.5 (800)	6.9 (1000)	8.3 (1200)	2.8 (400)

NOTE: The numeric following a decimal point; for example TFC1-3.2; indicates that this transient was performed a number of times, in this case twice.

TABLE 13

PEAK STEADY STRESS DURING TRANSIENTS MN/M^2, (PSI)

TRANSIENT	387MM FT EB BL #1	362MM FT BL #12	362MM FT BL #6	127MM FT BL #7	89MM FT V BL #7
TFC 3-3.3	13.1 (1900)	31.6 (4600)	55.0 (8600)	17.9 (2600)	4.1 (600)
TFC 3-4.3	13.8 (2000)	31.6 (4600)	55.0 (8000)	20.6 (3000)	5.5 (800)
TFC 1-1.2	12.4 (1800)	30.2 (4400)	49.5 (7200)	23.4 (3400)	---
TFC 1-3.2	11.7 (1700)	33.0 (4800)	52.2 (7600)	30.2 (4400)	---
TRC 3-43	17.9 (2600)	34.4 (5000)	52.2 (7600)	8.9 (1300)	17.2 (2500)
TRC 3-71	19.3 (2800)	33.0 (4800)	52.2 (7600)	48.8 (7100)	18.6 (2700)
TRC 3-66	22.7 (3300)	38.5 (5600)	---	42.7 (6200)	21.3 (3100)
TRF 6-6	116.9 (17000)	57.8 (8400)	44.0 (-6400)	37.2 (5400)	15.1 (2200)

STEADY STRESS AT START AND END OF TRANSIENTS MN/M^2, (PSI)

TRANSIENT		387MM FT EB BL #1	362 MM FT BL #12	362MM FT BL #6	127MM FT BL #7	89MM FT V BL #7
TFC 3-3.3	Start	8.9 (1300)	9.6 (1400)	30.3 (4400)	5.5 (800)	4.1 (600)
	End	13.1 (1900)	31.6 (4600)	55.0 (8000)	17.9 (2600)	1.4 (200)
TFC 3-4.3	Start	13.1 (1900)	20.6 (3000)	41.3 (6000)	14.4 (2100)	5.5 (800)
	End	13.8 (2000)	31.6 (4600)	55.0 (8000)	20.6 (3000)	2.8 (400)
TFC 1-1.2	Start	1.4 (200)	8.3 (1200)	19.3 (2800)	7.6 (1100)	---
	End	12.4 (1800)	30.3 (4400)	49.5 (7200)	23.4 (3400)	---
TFC 1-3.2	Start	8.9 (1300)	23.4 (3400)	39.9 (5800)	19.3 (2800)	---
	End	11.7 (1700)	33.0 (4800)	52.3 (7600)	30.3 (4400)	---
TRC 3-43	Start	15.8 (2300)	34.4 (5000)	52.3 (7600)	2.8 (400)	-2.1 (-300)
	End	17.9 (2600)	15.1 (2200)	19.3 (2800)	8.9 (1300)	17.2 (2500)
TRC 3-71	Start	16.5 (2400)	-12.4 (1800)	37.2 (5400)	27.5 (4000)	-4.1 (-600)
	End	19.3 (2800)	5.5 (800)	22.0 (3200)	46.8 (6800)	18.6 (2700)
TRC 3-66	Start	15.8 (2300)	30.9 (4500)	---	34.4 (5000)	2.1 (300)
	End	20.6 (3000)	6.9 (1000)	---	42.7 (6200)	18.6 (2700)
TRF 6-6	Start	27.5 (4000)	-13.8 (-2000)	-44.0 (-6400)	37.2 (5400)	-2.8 (-400)
	End	116.9 (17000)	57.8 (8400)	35.8 (5200)	26.8 (3900)	15.1 (2200)

TABLE 14

PEAK VIBRATORY STRESS DURING FORWARD THRUST TRANSIENTS; ± MN/M^2 (±PSI)

PARA/TEST PT	TFC1-1	TFC1-2	TFC1-4	TFC1-4	TFC2-1	TFC2-2	TCF1-1.1	TFC1-2.1	TFC3.1	TFC1-4.1	TFC2-1.1	TFC2-2.1	TFC2-3.1	TFC3-1.2
β DEG	53°	53°	54.5°	54.5°	59°	59°	54.5°	54.5°	53°	53°	53°	59°	59°	53°
362MM-1 (14 1/4")	12.4 (1800)	9.8 (1400)	2.8 (400)	5.4 (800)	5.4 (800)	5.4 (800)	6.9 (1000)	9.8 (1400)	16.5 (2400)	6.3 (900)	11.8 (1700)	5.4 (800)	6.9 (1000)	9.8 (1400)
362MM-6 (14 1/4")	13.8 (2000)	12.4 (1800)	1.4 (2000)	5.4 (800)	6.1 (900)	5.4 (800)	8.1 (1200)	10.3 (1500)	18.5 (2700)	8.1 (1200)	11.8 (1700)	7.5 (1100)	6.0 (900)	11.8 (1700)
RPM	3120	3120	1320	3120	2720	2720	3360	3360	3400	3360	2880	2920	2920	3280
BBL #3	4.1 (600)	5.4 (800)	5.4 (800)	5.4 (800)	5.4 (800)	19.5 (2800)	5.4 (800)	9.8 (1400)	8.3 (1200)	8.3 (1200)	4.1 (600)	5.4 (800)	6.9 (1000)	8.3 (1200)
STATOR #1	1.4 (200)	2.5 (300)	1.4 (200)	1.4 (200)	2.5 (300)	2.5 (300)	2.5 (300)	2.5 (300)	2.5 (300)	2.8 (400)	2.8 (400)	1.4 (200)	1.4 (200)	3.5 (500)
PARA/TEST PT	TFC3-2.2	TFC3-3.2	TFC3-4.2	TFC3-5.2	TFC3-6.2	TFC3-7.2	TFC3-8.2	TFC3-9.2	TFC3-10.2	TFC3-11.2	TFC3-1.3	TFC3-1.3	TFC3-2.3	TFC3-1.3
β DEG	53°	53°	53°	53°	53°	53°	53°	53°	53°	53°	41°	53°	53°	53°
362MM-1 (14 1/4")	11.8 (1700)	11.8 (1700)	8.8 (1300)	8.8 (1300)	8.8 (1300)	8.1 (1200)	15.8 (2300)	9.8 (1400)	8.1 (1200)	9.8 (1400)	6.9 (1000)	8.5 (1250)	13.8 (2000)	6.9 (1000)
362MM-6 (14 1/4")	13.0 (1900)	11.8 (1700)	9.8 (1400)	6.9 (1000)	8.8 (1300)	9.8 (1400)	16.5 (2400)	15.0 (2200)	8.1 (1200)	8.1 (1200)	6.9 (1000)	6.9 (1000)	12.0 (1750)	3.5 (500)
RPM	3280	3280	3360	3280	3280	3240	3360	3280	3280	3240	2560	3320	3360	3280
BBL #3	6.9 (1000)	6.9 (1000)	6.9 (1000)	5.4 (800)	11.0 (1600)	11.6 (1600)	11.6 (1600)	6.9 (1000)	13.8 (2000)	5.4 (800)	46.8 (6800)	8.2 (1200)	13.8 (2000)	11.6 (1600)
STATOR #1	3.5 (500)	2.8 (400)	4.1 (600)	3.5 (500)	2.8 (400)	3.5 (500)	2.8 (400)	3.5 (500)	3.5 (500)	2.8 (400)	2.5 (300)	4.1 (600)	5.6 (800)	2.5 (300)
PARA/TEST PT	TFC3-3.3	TFC3-23	TFC3-4.3	TFC3-5.3	TFC3-6.3	TFC3-7.3	TFC3-8.3	TFC3-9.3	TFC3-10.3	TFC3-11.3	TFC1-12	TFC1-2.2	TFC1-3.2	TFC1-4.2
β DEG	53°	53°	53°	53°	53°	53°	53°	53°	53°	53°	55.4°	55.4°	55.4°	55.4°
362MM-1 (14 1/4")	10.5 (1500)	12.0 (1750)	10.5 (1500)	24.0 (3500)	17.3 (2500)	19.0 (2750)	20.8 (3000)	10.4 (1500)	13.8 (2000)	12.0 (1750)	17.3 (2500)	13.8 (2000)	13.8 (2000)	13.8 (2000)
362MM-6 (14 1/4")	10.5 (1500)	12.0 (1750)	10.5 (1500)	20.5 (3000)	17.3 (2500)	17.3 (2500)	20.8 (3000)	10.4 (1800)	13.8 (2000)	12.0 (1750)	17.3 (2500)	13.8 (2000)	13.8 (2000)	13.8 (2000)
RPM	3320	3360	3320	3260	3320	3400	3320	3320	3320	3260	3120	3200	3040	3200
BBL #3	16.5 (2400)	13.8 (2000)	13.8 (2000)	13.8 (2000)	16.5 (2400)	30.2 (4400)	16.5 (2400)	19.3 (2800)	13.8 (2000)	16.5 (2400)	13.8 (2000)	16.5 (2400)	13.8 (2000)	13.8 (2000)
STATOR #1	2.8 (400)	2.8 (400)	3.5 (500)	3.5 (500)	2.8 (400)	2.8 (400)	5.0 (600)	5.0 (600)	2.8 (400)	2.8 (400)	2.8 (400)	2.8 (400)	2.8 (400)	2.8 (400)

TABLE 15

PEAK VIBRATORY STRESS DURING REVERSE THROUGH FEATHER TRANSIENTS ; ± MN/M^2 (±PSI)

PARA/TEST PT	TRC1-1	TRC1-1A	TRC1-2	TRC1-3	TRC1-4	TRC1-5	TRC1-6	TRC1-7	TRC1-8	TRC1-9	TRC1-10	TRC2-1	TRC2-2	TRC2-3
β DEG	144.5°	144.5°	144.5°	146.0°	146.0°	144.5°	144.5°	144.5°	144.5°	144.5°	143.0°	144.5°	144.5°	144.5°
362MM-12 (14 1/4")	79 (11500)	58.5 (8500)	48.0 (7000)	41.5 (6000)	68.8 (10000)	32.5 (4750)	68.8 (10000)	20.5 (3000)	68.8 (10000)	41.5 (6000)	55.0 (8000)	34.4 (5000)	65.5 (9500)	55.5 (8500)
362MM-6 (14 1/4")	55 (8000)	55.0 (8000)	39.5 (5750)	31.0 (4500)	48.0 (7000)	37.8 (5500)	55.0 (8000)	20.5 (3000)	68.8 (10000)	48.0 (7000)	58.5 (8500)	55.0 (8000)	75.5 (11000)	55.0 (8000)
RPM	2650	2640	2560	2400	2840	2400	2480	1700	3040	2640	2560	3120	3040	2880
BBL #3	19.5 (2800)	22.0 (3200)	22.0 (3200)	16.5 (2400)	19.5 (2800)	22.0 (3200)	22.0 (3200)	13.5 (2000)	16.5 (2400)	24.5 (3600)	19.5 (2800)	16.5 (2400)	30.5 (4400)	30.5 (4400)
STATOR #1	2.8 (400)	5.0 (600)	3.5 (500)	2.8 (400)	2.8 (400)	2.8 (400)	2.8 (400)	2.8 (400)	2.5 (300)	8.5 (1200)	2.8 (400)	2.8 (400)	2.8 (400)	9.0 (1300)
PARA/TEST PT	TRC2-4	TRC2-5	TRC2-6	TRC2-7	TRC2-8	TRC2-9	TRC2-10	TRC3-1	TRC3-1R	TRC3-6	TRC3-3	TRC3-4	TRC3-5	TRC3-5
β DEG	144.5°	144.5°	144.5°	144.5°	144.5°	144.5°	144.5°	143.0°	143.0°	143.0°	143.0°	143.0°	143.0°	143.0°
362MM-12 (14 1/4")	51.5 (7500)	61.5 (9000)	55.0 (8000)	38.0 (5500)	34.4 (5000)	99.5 (14500)	4.8 (7000)	37.5 (5500)	37.5 (5500)	65.5 (9500)	61.5 (9000)	65.5 (9500)	31.0 (4500)	17.5 (2500)
362MM-6 (14 1/4")	48.0 (7000)	65.5 (9500)	48.0 (7000)	4.5 (9000)	51.5 (7500)	82.5 (1200)	48.0 (7000)	58.5 (8500)	61.5 (9000)	48.0 (7000)	51.5 (7500)	65.5 (9500)	37.5 (5000)	31.0 (4500)
RPM	2880	2960	3040	2240	2569	3120	2880	2480	2560	2880	3040	2960	2720	1840
BBL #3	33.0 (4800)	33.0 (4800)	22.0 (3200)	30.5 (4400)	35.5 (5200)	27.5 (4000)	33.0 (4800)	38.5 (5600)	33.0 (4800)	24.5 (3600)	27.5 (4000)	16.5 (2400)	16.5 (2400)	19.5 (2800)
STATOR #1	2.8 (400)	2.8 (400)	2.8 (400)	2.8 (400)	3.5 (500)	2.8 (400)	3.5 (500)	2.8 (400)	2.8 (400)	1.4 (200)	1.4 (200)	1.4 (200)	1.4 (200)	1.4 (200)
PARA/TEST PT	TRC3-7	TRC3-8	TRC3-9	TRC3-10	TRC3-41	TRC3-42	TRC3-43	TRC3-44	TRC3-45	TRC3-46	TRC3-47	TRC3-48	TRC3-49	TRC3-59A
β DEG	143.0°	143.0°	143.0°	143.0°	143.0°	143.0°	143.0°	143.0°	143.0°	143.0°	143.0°	143.0°	143.0°	143.0°
362MM-12 (14 1/4")	99.5 (14500)	44.5 (6500)	55.0 (8000)	55.0 (8000)	55.0 (8000)	58.5 (8500)	48.0 (7000)	51.5 (7000)	55.0 (8000)	82.5 (12000)	51.5 (7500)	72.5 (10500)	55.0 (8000)	68.8 (10000)
362MM-6 (14 1/4")	72.5 (10500)	34.4 (5000)	65.5 (9800)	51.5 (7500)	75.5 (11000)	55.0 (8000)	68.8 (10000)	37.5 (5500)	58.5 (5500)	99.5 (1450)	68.8 (10000)	79.0 (11500)	55.0 (8000)	62.0 (9000)
RPM	3040	2880	3040	2800	3000	2320	2720	2880	3040	2960	2880	3040	2980	2880
BBL #3	22.0 (3300)	27.5 (4000)	30.5 (4400)	33.0 (4800)	19.5 (2800)	24.5 (3600)	33.0 (4800)	24.5 (3600)	27.5 (4000)	38.5 (5600)	33.0 (4800)	24.5 (3600)	27.5 (4000)	27.5 (4000)
STATOR #1	1.4 (200)	1.4 (200)	1.4 (200)	1.4 (200)	5.0 (600)	2.8 (400)	5.6 (8000)	1.4 (200)	1.4 (200)	1.4 (200)	14.0 (2000)	2.8 (400)	2.8 (400)	1.4 (200)

TABLE 15 (Continued)

PARA/TEST PT	TRC3-19	TRC3-20	TRC3-71	TRC3-72	TRC3-73	TRC3-74	TRC3-75	TRC3-76	TRC3-77	TRC3-78	TRC3-79	TRC3-80	TRC3-61	TRC3-62
β DEG	146.0°	146.0°	146.0°	83.0°	146.0°	146.0°	146.0°	146.0°	146.0°	146.0°	146.0°	146.0°	146.0°	146.0
362MM-12 (14 1/4")	55.0 (8000)	62.0 (9000)	55.0 (8000)	82.5 (12000)	68.8 (10000)	48.0 (7000)	62.0 (9000)	85.5 (12500)	75.5 (11000)	44.5 (6500)	44.5 (6800)	62.0 (9000)	44.5 (6500)	75.5 (11000)
362MM-6 (14 1/4")	41.5 (6000)	65.5 (9500)	41.5 (6000)	68.8 (10000)	82.5 (12000)	72.5 (10500)	48.0 (7000)	89.5 (12000)	72.5 (10500)	30.5 (4500)	68.8 (10000)	72.5 (10500)	55.0 (8000)	62.0 (9000)
RPM	3040	2960	2560	2720	3200	3040	2980	3200	3040	2980	3120	3200	3200	3200
BBL #3	35.5 (5200)	38.5 (5600)	38.5 (5600)	30.5 (4400)	30.5 (4400)	41.5 (6000)	38.5 (5600)	38.5 (5600)	41.5 (6000)	38.5 (5600)	41.5 (6000)	35.5 (5200)	27.5 (4000)	30.5 (4400)
STATOR #1	5.0 (600)	16.5 (2400)	5.0 (600)	5.0 (600)	5.0 (600)	15.0 (1800)	5.0 (600)	5.0 (600)	5.0 (600)	5.0 (600)	34.5 (5000)	20.5 (3000)	5.6 (800)	5.0 (600)
PARA/TEST PT	TRC3-63	TRC3-64	TRC3-64A	TRC3-65	TRC3-66	TRC-66A	TRC3-67	TRC3-68	TRC3-69	TRC3-70	TRC1-21	TRC1-22	TRC1-23	TRC1-24
β DEG	146.0°	146.0°	146.0°	146.0°	146.0°	146.0°	146.0°	146.0°	146.0°	146.0°	146.0°	146.0°	146.0°	146.0°
362MM-12 (14 1/4")	62.0 (9000)	62.0 (9000)	55.0 (8000)	55.0 (8000)	72.5 (10500)	72.5 (10500)	68.8 (10000)	55.0 (8000)	85.5 (12500)	75.5 (11000)	55.0	37.5 (5500)	55.0 (8000)	62.0 (9000)
362MM-6 (14 1/4")	51.5 (7500)	127.5 (18500)	68.8 (10000)	75.5 (11000)	62.0 (9000)	68.8 (10000)	62.0 (9000)	62.0 (9000)	62.0 (9000)	85.5 (12500)	41.5 (6000)	62.0 (9000)	75.5 (11000)	85.5 (12500)
RPM	3200	3200	3160	3200	3280	3280	3120	3120	3160	3200	2400	2880	2880	3120
BBL #3	33.0 (4800)	33.0 (4800)	33.6 (4800)	30.5 (4400)	33.6 (4800)	30.5 (4400)	41.5 (6000)	35.5)5200)	30.5 (4400)	35.5 (5200)	16.5 (2400)	24.5 (3600)	22.0 (3200)	16.5 (2400)
STATOR #1	22.0 (3200)	23.5 (2400)	22.0 (3200)	5.6 (800)	16.8 (2400)	5.0 (600)	22.0 (3200)	5.0 (600)	5.6 (800)	5.0 (600)	15.0 (1800)	5.6 (600)	5.0 (600)	5.0 (600)
PARA/TEST PT	TRC1-25	TRC1-26	TRC1-27	TRC1-28	TRC1-11	TRC1-12	TRC1-13	TRC1-14	TRC1-15	TRC1-16	TRC1-17	TRC1-18	TRC1-19	TRC1-20
β DEG	146.0°	146.0°	146.0°	146.0°	146.0°	146.0°	146.0°	146.0°	146.0°	146.0°	146.0°	146.0°	146.0°	146.0°
362MM-12 (14 1/4")	51.5 (7500)	48.5 (7000)	51.5 (7500)	34.5 (5000)	55.0 (8000)	37.5 (5500)	37.5 (5500)	62.0 (9000)	48.5 (7000)	48.5 (7000)	55.0 (8000)	55.0 (8000)	48.5 (200)	48.5 (7000)
362MM-6 (14 1/4")	51.5 (7500)	99.5 (14500)	62.0 (9000)	34.5 (5000)	79.0 (11500)	27.5 (4000)	41.5 (6000)	68.8 (10000)	44.5 (6500)	72.5 (10500)	51.5 (7500)	55.0 (8000)	55.0 (8000)	55.0 (8000)
RPM	3120	2640	3040	3040	2640	2240	2640	2800	2800	3040	2800	3040	3040	2560
BBL #3	16.5 (2400)	19.5 (2800)	13.8 (2000)	16.5 (2400)	16.5 (2400)	16.5 (2400)	22.0 (3200)	22.0 (3200)	22.0 (3200)	16.5 (2400)	22.0 (3200)	16.5 (2400)	16.5 (2400)	22.0 (3200)
STATOR #1	5.0 (600)	29.5 (4400)	23.5 (3400)	5.0 (600)	5.0 (600)	5.0 (600)	5.0 (600)	16.5 (2400)	5.0 (600)	18.5 (2700)	18.5 (2700)	23.5 (3400)	14.5 (2100)	17.5 (2600)

TABLE 15 (Continued)

PARA/TEST PT	TRC3-49B	TRC3-50	TRC3-46A	TRC3-31	TRC3-32	TRC3-33	TRC3-34	TRC3-35	TRC3-36	TRC3-37	TRC3-35	TRC3-39	TRC3-40	TRC3-52
β DEG	143.0°	143.0°	143.0°	146.0°	146.0°	146.0	146.0°	146.0°	146.0°	146.0°	146.0	146.0°	146.0°	146.0°
362MM-12 (14 1/4")	51.5 (7500)	18.8 (10000)	55.0 (8000)	37.5 (5500)	51.5 (7500)	44.5 (6500)	38.5 (5600)	27.5 (4000)	61.5 (9000)	92.5 (13500)	55.0 (8000)	37.5 (5500)	65.5 (9500)	65.5 (9500)
362MM-6 (14 1/4")	58.5 (8500)	55 (8000)	75.5 (11000)	68.8 (10000)	48.0 (7000)	24.5 (3500)	58.5 (8500)	41.5 (6000)	51.5 (7500)	72.5 (10500)	58.5 (8500)	48.0 (7000)	65.5 (9500)	37.5 (5500)
RPM	2880	3040	3040	2980	2880	2080	2880	2080	2640	3120	2980	2800	3120	3120
BBL #3	33 (4800)	27.5 (4000)	33.0 (4800)	30.5 (4400)	38.5 (5600)	33.0 (4800)	24.5 (3000)	19.5 (2800)	24.5 (3600)	27.5 (4000)	22.0 (3200)	22.0 (3200)	24.5 (3600)	38.5 (5000)
STATOR #1	14.0 (2000)	1.4 (200)	1.4 (200)	2.8 (400)	2.8 (400)	3.5 (500)	2.8 (400)	.5 (500)	3.5 (500)	2.8 (400)	3.8 (500)	3.5 (500)	3.5 (500)	5.0 (600)
PARA/TEST PT	TRC3-56	TRC3-53	TRC3-54	TRC3-55	TRC3-56	TRC3-57	TRC3-58	TRC3-59	TRC3-60	TRC3-21	TRC3-22	TRC3-23	TRC3-24	TRC3-25
β DEG	146.0°	146.0°	146.0°	146.0°	146.0°	146.0°	146.0°	146.0°	146.0°	146.0°	146.0°	146.0°	146.0°	146.0°
362MM-12 (14 1/4")	51.5 (7500)	48.0 (7000)	68.8 (10000)	58,5 (8500)	55.0 (8000)	55.0 (8000)	62.0 (9000)	48.0 (7000)	41.5 (6000)	75.5 (11000)	51.5 (7500)	55.0 (6800)	37.5 (5500)	41.5 (6000)
362MM-6 (14 1/4")	37.5 (5500)	93.0 (12000)	68.8 (10000)	62.0 (9000)	48.0 (7000)	72.5 (10500)	62.0 (9000)	51.5 (7500)	62.0 (9000)	62.0 (9000)	51.5 (7500)	75.5 (11000)	31.0 (4500)	55.0 (8000)
RPM	2480	2980	3160	3160	2880	2880	3120	2980	2800	2640	2880	3120	2160	2720
BBL #3	41.5 (6000)	44.0 (6400)	35.5 (5200)	35.5 (5200)	41.5 (6000)	35.5 (5200)	33.0 (4800)	41.5 (6000)	28.8 (4200)	41.5 (6000)	35.5 (5200)	30.5 (4400)	30.5 (4400)	35.5 (5200)
STATOR #1	12.5 (1800)	5.0 (600)	5.0 (600)	19.5 (2800)	15.8 (2300)	5.0 (600)	5.0 (600)	24.0 (3500)	5.0 (600)	5.0 (600)	9.5 (1400)	5.0 (600)	3.5 (500)	3.5 (500)
PARA/TEST PT	TRC3-26	TRC3-27	TRC3-28	TRC3-29	TRC3-30	TRC3-11	TRC3-12	TRC3-13	TRC3-14	TRC3-15	TRC3-16	TRC3-17	TRC3-17A	TRC3-18
β DEG	146.0°	146.0°	146.0°	146.0°	146.0°	146.0°	146.0°	146.0°	146.0°	146.0°	146.0°	146.0°	146.0°	146.0°
362MM-12 (14 1/4")	55.0 (8000)	68.8 (10000)	68.8 (10000)	68.8 (10000)	58.5 (8500)	62.0 (9000)	68.8 (1000)	41.5 (6000)	62.0 (9000)	48.0 (7000)	48.0 (7000)	58.5 (8500)	55.0 (8000)	41.5 (6000)
362MM-6 (14 1/4")	48.0 (7000)	68.8 (10000)	86.0 (12500)	51.5 (7500)	62.0 (9000)	62.0 (9000)	75.5 (11000)	34.5 (5000)	68.8 (10000)	48.0 (7000)	51.5 (7500)	62.0 (9000)	85.5 (12500)	75.5 (11000)
RPM	2960	3150	3040	3200	3120	2880	3160	2080	2880	2400	3120	3200	3200	3120
BBL #3	41.5 (6000)	33.0 (4800)	41.5 (6000)	35.5 (520)	30.5 (4400)	35.5 (5200)	27.5 (4000)	35.5 (5200)	23.0 (4800)	38.5 (5600)	41.5 (6000)	24.5 (3600)	35.5 (5200)	27.5 (4000)
STATOR #1	3.5 (500)	5.0 (600)	5.0 (600)	10.5 (1500)	5.0 (600)	5.6 (800)	6.9 (1000)	5.0 (600)	5.0 (600)	18.5 (2700)	22.0 (1500)	13.8 (2000)	23.5 (3400)	5.0 (600)

TABLE 16 PEAK VIBRATORY STRESS DURING REVERSE THROUGH FLAT PITCH TRANSIENTS ; ± MN/M^2 (±PSI)

PARA/TEST PT	TRF6-1	TRF6-2	TRF6-2R	TRF6-2RR	TRF62RRR	TRF6-3	TRF6-4	TRF6-4R	TRF6-5	TRF6-5R	TRF6-19	TRF6-6
β DEG	-28.°	-29.5°	-29.5°	-31.0°	-31.0°	-31.0°	-31.0°	-31.0°	-31.0°	-31.0°	-31.0°	-31.0°
362MM-12 (14 1/4")	16.2 (2400)	23.5 (3400)	26.0 (3000)	28.8 (4200)	22.8 (3300)	37.8 (5500)	28.8 (4200)	40.0 (5800)	26.0 (3800)	30.5 (4400)	20.0 (2900)	26.8 (3900)
362MM-6 (14 1/4")	18.5 (2700)	24.5 (3000)	34.5 (3000)	32.8 (5000)	32.8 (4800)	41.8 (6100)	31.0 (4500)	27.5 (4000)	32.4 (4800)	27.5 (4000)	23.5 (3400)	28.3 (4100)
RPM	3280	3280	3280	3280	3280	3280	3280	3280	3280	3360	3360	3320
STATOR #1	2.8 (400)	5.0 (600)	5.0 (600)	3.5 (500)	3.5 (500)	23.5 (3400)	3.5 (500)	5.0 (600)	23.5 (3400)	2.8 (400)	3.5 (500)	3.5 (500)
PARA/TEST PT	TRF6-7	TRF6-8	TRF6-9	TRF6-20	TRF6-10	TRF6-11	TRF6-12	TRF6-13	TRF6-14	TRF6-15	TRF6-15R	TRF6-16
β DEG	-31.0°	-31.0°	-31.0°	-31.0°	-31.0°	-31.0°	-31.0°	-31.0°	-31.0°	-31.0°	-31.0°	-31.0°
362MM-12 (14 1/4")	27.5 (4000)	33.6 (4900)	26.8 (3900)	22.0 (3200)	20.0 (2900)	28.8 (4200)	26.8 (3900)	27.5 (4000)	26.8 (3900)	27.5 (4000)	22.0 (3200)	22.0 (3200)
362MM-6 (14 1/4")	30.5 (4400)	24.0 (3500)	32.5 (4700)	25.5 (3700)	20.0 (2900)	26.2 (3800)	29.5 (4300)	24.5 (3600)	23.5 (3400)	24.0 (3500)	24.0 (3500)	22.0 (3200)
RPM	3280	3440	3320	3320	3040	3320	3360	3320	3320	3360	3400	2840
STATOR #1	3.5 (500)	3.5 (500)	2.8 (400)	3.5 (500)	2.8 (400)	3.5 (500)	2.8 (400)	3.5 (500)	5.0 (600)	5.0 (600)	2.8 (400)	1.4 (200)
PARA/TEST PT	TRF6-16R	TRF6-17	TRF6-18	TRF4-1	TRF4-2	TRF4-3	TRF4-4	TRF4-5	TRF4-7	TRF4-8	TRF4-9	TRF4-10
β DEG	-31.0°	-31.0°	-31.0°	-31.0°	-31.0°	-31.0°	-31.0°	-31.0°	-31.0°	-31.0°	-31.0°	-31.0°
362MM-12 (14 1/4")	19.8 (2800)	28.5 (4200)	25.5 (3700)	22.0 (3200)	28.5 (4200)	31.5 (4000)	24.0 (3500)	29.5 (4000)	26.2 (3800)	27.5 (4000)	26.2 (3800)	24.0 (3500)
362MM-6 (14 1/4")	18.5 (2700)	30.5 (4400)	30.5 (3700)	26.5 (3700)	26.6 (3800)	28.2 (4100)	27.5 (4000)	24.4 (3600)	26.2 (3800)	30.5 (4400)	33.5 (4900)	29.5 (4300)
RPM	3200	3360	3360	3200	3200	3200	3280	3280	3240	3280	3200	3280
STATOR #1	2.8 (400)	5.0 (500)	5.0 (600)	3.5 (500)	2.8 (400)	2.8 (400)	3.5 (500)	5.0 (600)	2.8 (400)	5.0 (600)	3.5 (500)	5.0 (600)

TABLE 17

PEAK VIBRATORY STRESS DURING REVERSE THRUST TRANSIENTS
± MN/M^2 (±PSI)

TEST PT PARA	TRRC 3-1	TRRC 3-2	TRRC 3-3	TRRC 3-4
β DEG	146.°	146.°	146.°	146.°
362MM-1 (14 1/4")	48.5 (7000)	48.5 (7000)	61.8 (9000)	10.5 (1500)
362MM-6	61.8 (9000)	37.8 (5500)	41.5 (6000)	10.5 (1500)
RPM	1600.	1600.	1600.	2400.
BBL #3	16.5 (2400)	16.5 (2400)	16.5 (2400)	17.5 (2500)
STATOR #1	5.0 (600)	5.0 (600)	5.0 (600)	2.8 (400)

TABLE 18. ANOVA FOR BLADE VIBRATORY STRESS PEAK NEAR FEATHER - SCHEDULE 1

SOURCE OF VARIATION	DEGREES OF FREEDOM	SUM OF SQUARES	MEAN SQUARES	F-RATIO
MAIN				
A	1	2.82	2.82	1.19
B	1	43.95	43.95	18.54
C	1	2.26	2.26	0.95
INTERACTIONS				
AB	1	0.95	0.95	0.40
AC	1	2.26	2.26	0.95
BC	1	0.01	0.01	0.00
RESIDUAL	25	59.25	2.37	
TOTAL	31	111.50		

Estimate of Standard Error: $\hat{\sigma} = \sqrt{2.37} = 1.54$

TABLE 19. ANOVA FOR AVERAGE BLADE VIBRATORY STRESS NEAR FEATHER - SCHEDULE 1

SOURCE OF VARIATION	DEGREES OF FREEDOM	SUM OF SQUARES	MEAN SQUARES	F-RATIO
MAIN				
A	1	0.05	0.05	0.10
B	1	7.04	7.04	14.08
C	1	0.12	0.12	0.24
INTERACTIONS				
AB	1	0.18	0.18	0.36
AC	1	0.41	0.41	0.82
BC	1	0.002	0.002	0.00
RESIDUAL	9	4.51	0.50	
TOTAL	15	12.312		

Estimate of Standard Error: $\hat{\sigma} = \sqrt{0.5} = 0.22$

TABLE 20. ANOVA FOR BLADE VIBRATORY STRESS PEAK NEAR FEATHER - SCHEDULE 2

SOURCE OF VARIATION	DEGREES OF FREEDOM	SUM OF SQUARES	MEAN SQUARES	F-RATIO
MAIN				
A	1	0.14	0.14	0.12
B	1	17.02	17.02	14.80
C	1	1.27	1.27	1.10
INTERACTIONS				
AB	1	0.77	0.77	0.67
AC	1	0.14	0.14	0.12
BC	1	8.27	8.27	7.19
RESIDUAL	9	10.37	1.15	
TOTAL	15	37.98		

Estimate of Standard Error: $\hat{\sigma} = \sqrt{1.15} = 1.07$

TABLE 21. ANOVA FOR BLADE VIBRATORY STRESS
PEAK NEAR FEATHER - SCHEDULE 3 (TSL 70° to 0°)

SOURCE OF VARIATION	DEGREES OF FREEDOM	SUM OF SQUARES	MEAN SQUARES	F-RATIO
MAIN				
A	1	0.95	0.95	0.30
B	1	53.82	53.82	17.03
C	1	0.01	0.01	0.00
D	1	0.38	0.38	0.12
INTERACTIONS				
AB	1	1.32	1.32	0.42
AC	1	11.89	11.89	3.76
AD	1	23.64	23.64	7.48
BC	1	1.32	1.32	0.42
BD	1	4.89	4.89	1.55
CD	1	1.76	1.76	0.56
RESIDUAL	21	66.44	3.16	
TOTAL	31	166.00		

Estimate of Standard Error: $\hat{\sigma} = \sqrt{3.16} = 1.78$

TABLE 22. ANOVA FOR BLADE VIBRATORY STRESS
PEAK NEAR FEATHER - SCHEDULE 3 (TSL 90° to 0°)

SOURCE OF VARIATION	DEGREES OF FREEDOM	SUM OF SQUARES	MEAN SQUARES	F-RATIO
MAIN				
A	1	0.77	0.77	0.28
B	1	11.39	11.39	4.16
C	1	0.39	0.39	0.14
INTERACTIONS				
AB	1	13.14	13.14	4.80
AC	1	9.77	9.77	3.57
BC	1	3.52	3.52	1.28
RESIDUAL	9	24.63	2.74	
TOTAL	15	63.61		

Estimate of Standard Error: $\hat{\sigma} = \sqrt{2.74} = 1.66$

TABLE 23. ANOVA FOR BLADE VIBRATORY STRESS
PEAK NEAR REVERSE - SCHEDULE 1

SOURCE OF VARIATION	DEGREES OF FREEDOM	SUM OF SQUARES	MEAN SQUARES	F-RATIO
MAIN				
A	1	1.32	1.32	0.62
B	1	23.63	23.63	11.09
C	1	1.32	1.32	0.62
INTERACTIONS				
AB	1	4.13	4.13	1.94
AC	1	0.38	0.38	0.18
BC	1	17.26	17.26	8.10
RESIDUAL	25	53.21	2.13	
TOTAL	31	101.25		

Estimate of Standard Error: $\hat{\sigma} = \sqrt{2.13} = 1.46$

C-2

TABLE 24. ANOVA FOR BLADE VIBRATORY STRESS PEAK NEAR REVERSE-SCHEDULE 2

SOURCE OF VARIATION	DEGREES OF FREEDOM	SUM OF SQUARES	MEAN SQUARES	F-RATIO
MAIN				
A	1	1.56	1.56	1.09
B	1	5.06	5.06	3.56
C	1	6.25	6.25	4.40
INTERACTIONS				
AB	1	0.56	0.56	0.39
AC	1	4.00	4.00	2.82
BC	1	20.25	20.25	14.26
RESIDUAL	9	12.76	1.42	
TOTAL	15	50.44		

Estimate of Standard Error: $\hat{\sigma} = \sqrt{1.42} = 1.19$

TABLE 25. ANOVA FOR BLADE VIBRATORY STRESS
PEAK NEAR REVERSE - SCHEDULE 3 (TSL 70° to 0°)

SOURCE OF VARIATION	DEGREES OF FREEDOM	SUM OF SQUARES	MEAN SQUARES	F-RATIO
MAIN				
A	1	6.12	6.12	3.06
B	1	10.12	10.12	5.06
C	1	22.78	22.78	11.39
D	1	3.12	3.12	1.51
INTERACTIONS				
AB	1	0.28	0.28	0.14
AC	1	10.12	10.12	5.06
AD	1	11.28	11.28	5.64
BC	1	7.03	7.03	3.51
BD	1	0.03	0.03	0.01
CD	1	21.12	21.12	10.56
RESIDUAL	21	42.00	2.00	
TOTAL	31	134.00		

Estimate of Standard Error: $\hat{\sigma} = \sqrt{2.0} = 1.414$

TABLE 26. ANOVA FOR BLADE VIBRATORY STRESS
PEAK NEAR REVERSE - SCHEDULE 3 (TSL 90° to 0°)

SOURCE OF VARIATION	DEGREES OF FREEDOM	SUM OF SQUARES	MEAN SQUARES	F-RATIO
MAIN				
A	1	0.00	0.00	0.00
B	1	2.25	2.25	1.28
C	1	0.56	0.56	0.32
INTERACTIONS				
AB	1	3.06	3.06	1.74
AC	1	2.25	2.25	1.28
BC	1	1.00	1.00	0.57
RESIDUAL	9	15.88	1.76	
TOTAL	15	25.00		

Estimate of Standard Error: $\hat{\sigma} = \sqrt{1.76} = 1.33$

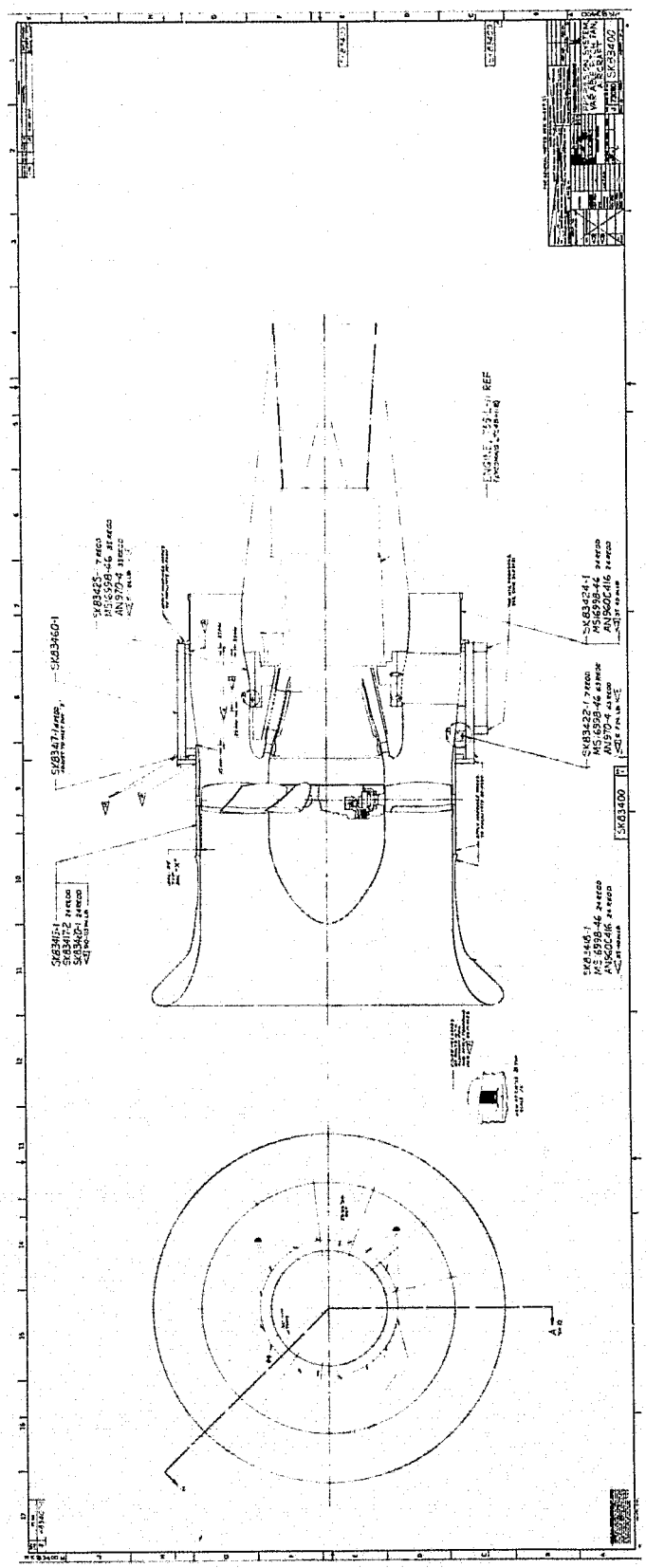

FIGURE 1. Q-FAN ASSEMBLY - SHEET 1

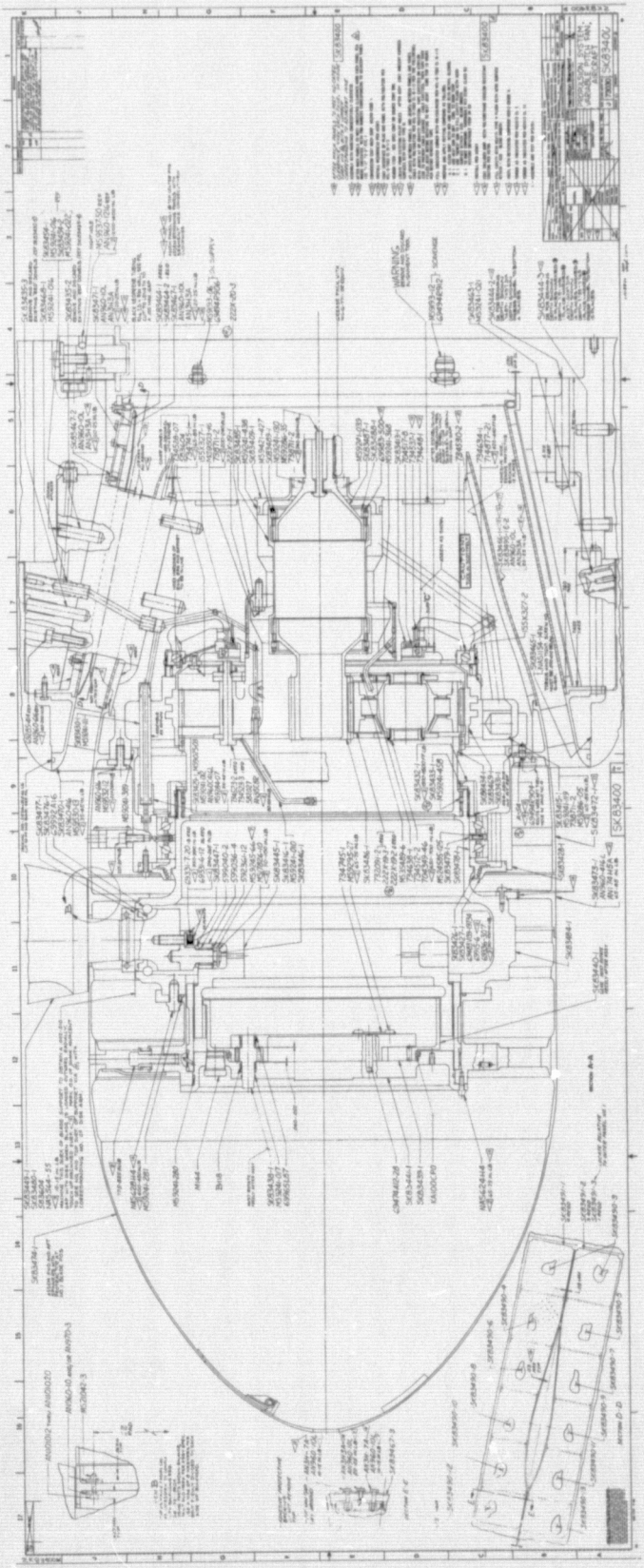

FIGURE 2. Q-FAN ASSEMBLY - SHEET 2

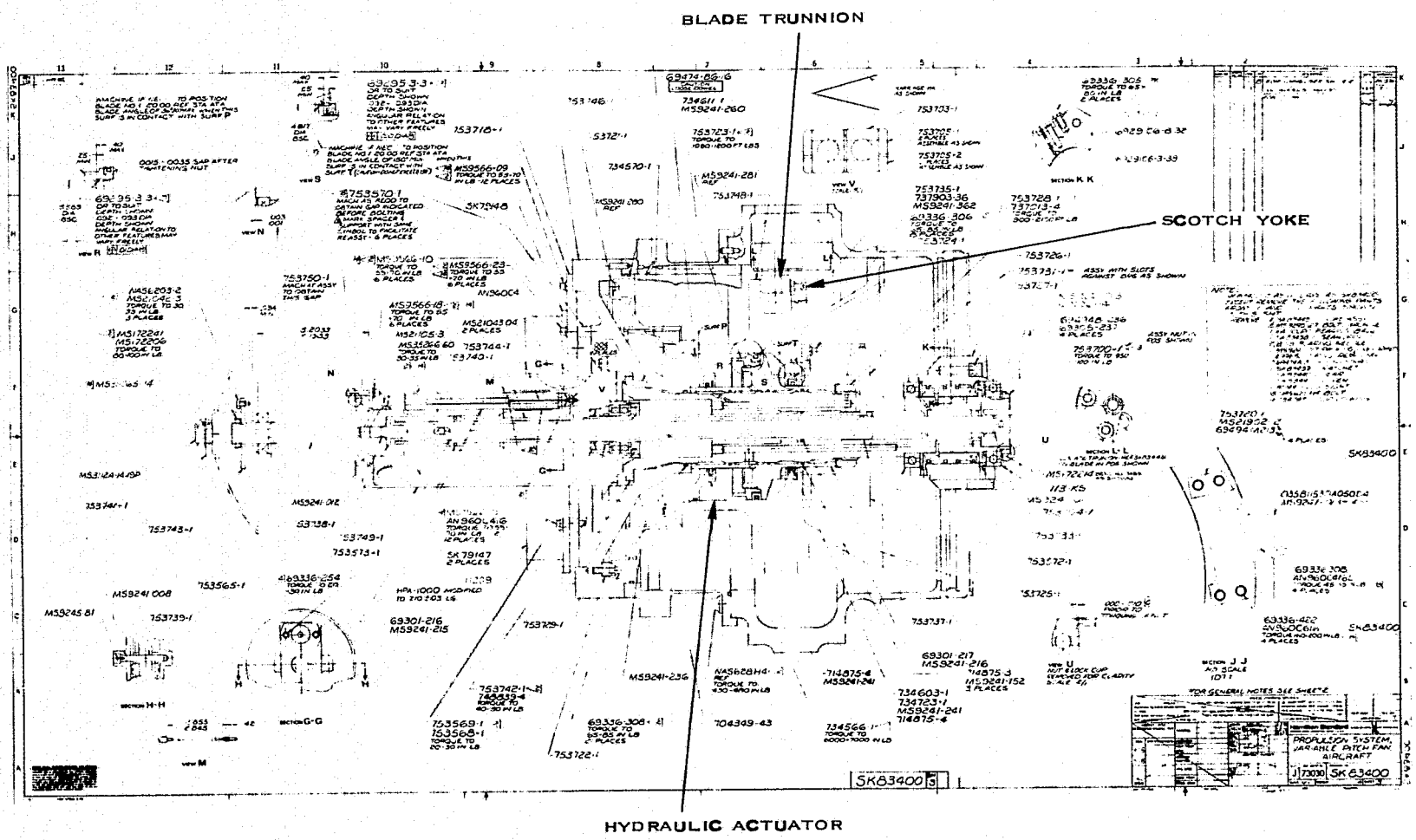

FIGURE 3. Q-FAN ASSEMBLY-SHEET 3

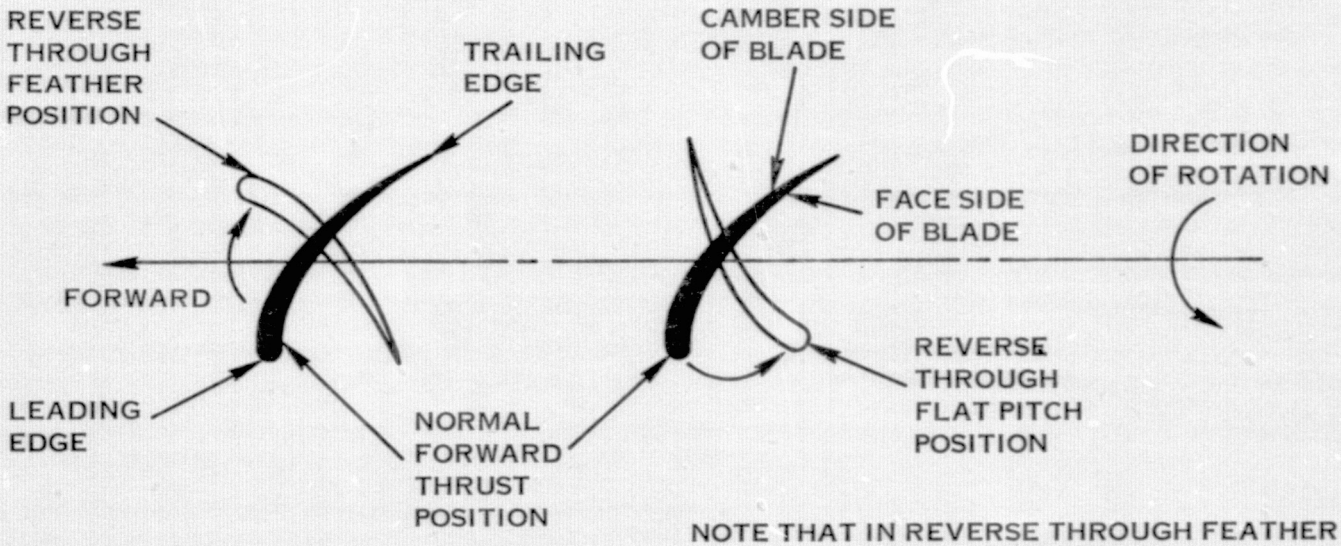

NOTE THAT IN REVERSE THROUGH FEATHER CONFIGURATION, THE BLADE IS RUNNING TRAILING EDGE FIRST (IN REVERSE THRUST MODE) BUT THE FACE SIDE OF THE BLADE IS ORIENTED PROPERLY ON THE THRUSTING SIDE; WHILE IN THE REVERSE THROUGH FLAT PITCH CONFIGURATION, THE LEADING EDGE IS PROPERLY ORIENTED BUT THE CAMBER SIDE OF THE BLADE IS NOW THE THRUSTING SIDE.

FIGURE 4. DIAGRAM SHOWING BLADE INDEXING POSITIONS THROUGH FEATHER AND THROUGH FLAT PITCH

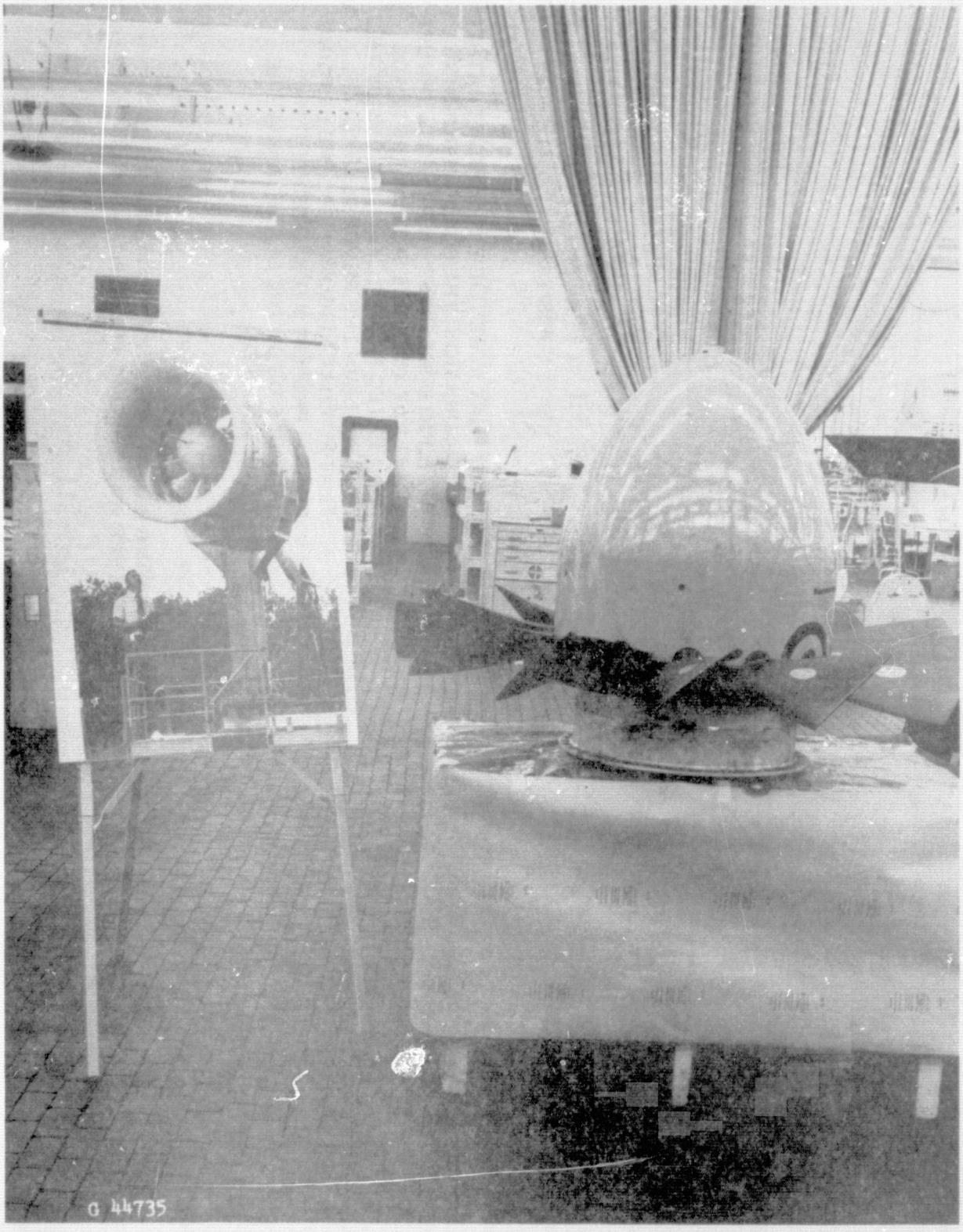

FIGURE 5. FAN ASSEMBLY WITH SPINNER INSTALLED

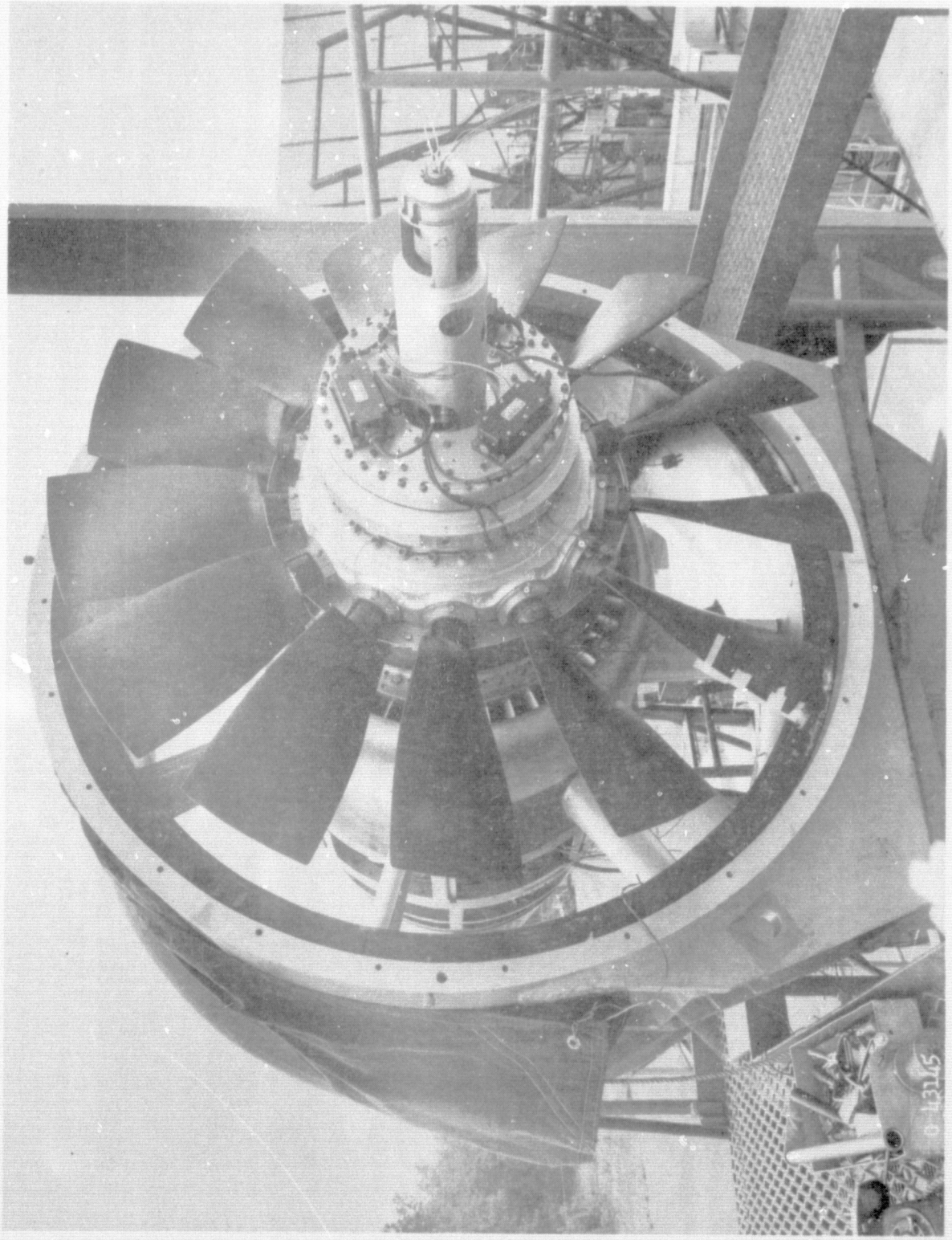

FIGURE 6. FAN ASSEMBLY WITH SPINNER REMOVED

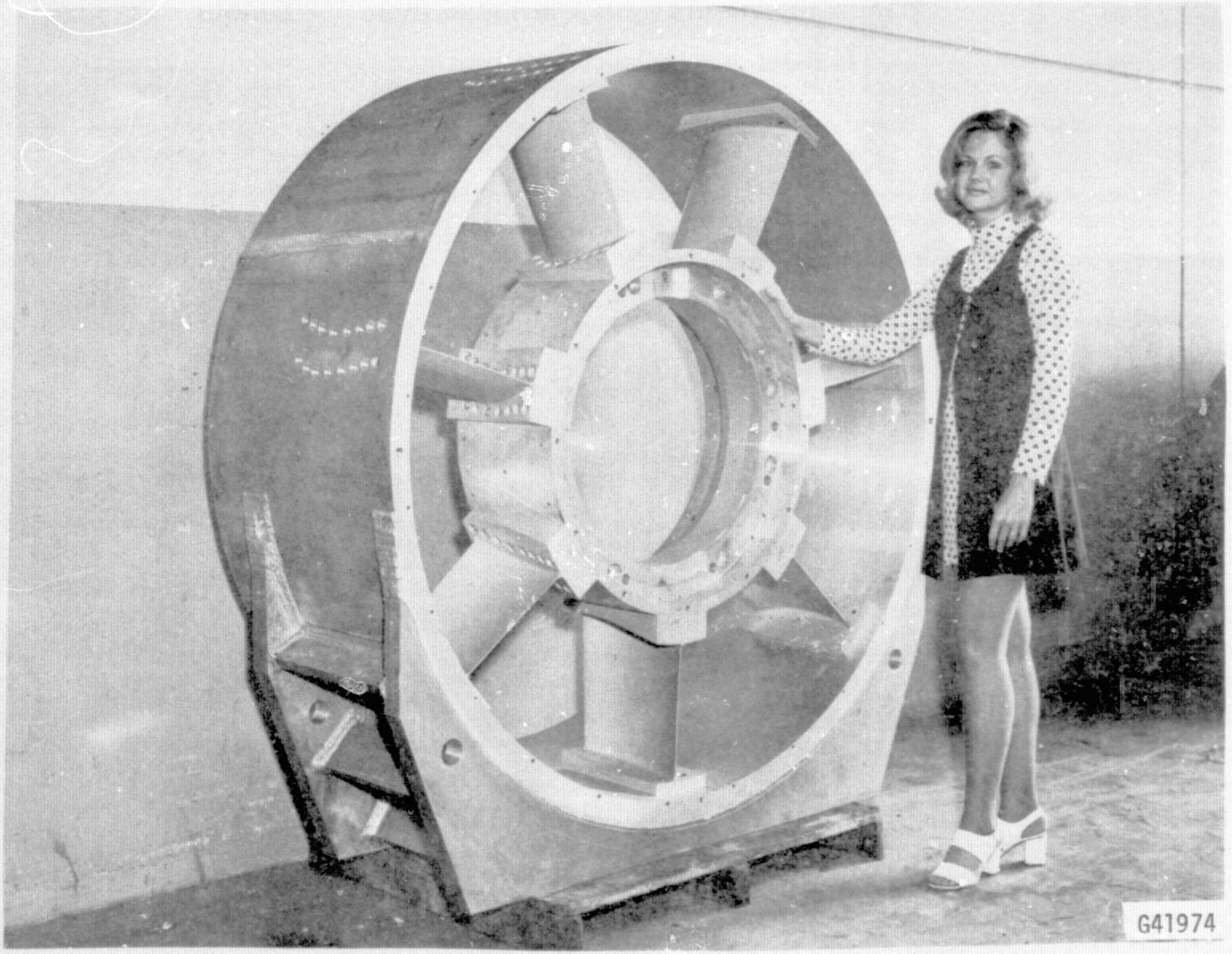

FIGURE 7. SUPPORT STRUCTURE AND EXIT VANES SUBASSEMBLY WITH GEARBOX HOUSING INSTALLED

FIGURE 8. Q-FAN ASSEMBLY - FRONT VIEW

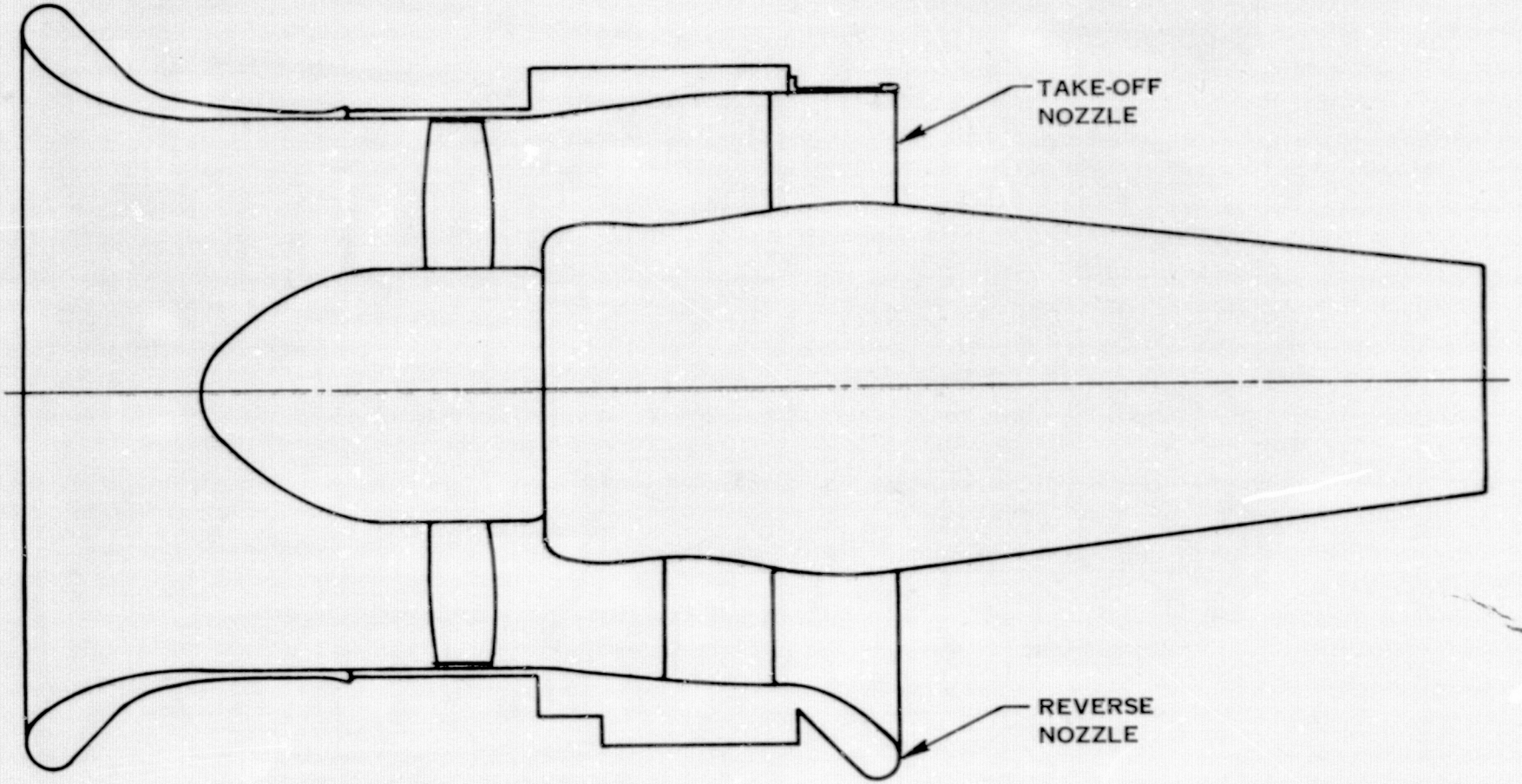

FIGURE 9. DRAWING-EXIT NOZZLE CONFIGURATIONS

FIGURE 10. Q-FAN GEARBOX ASSEMBLY - FRONT VIEW WITH DUCTS INSTALLED

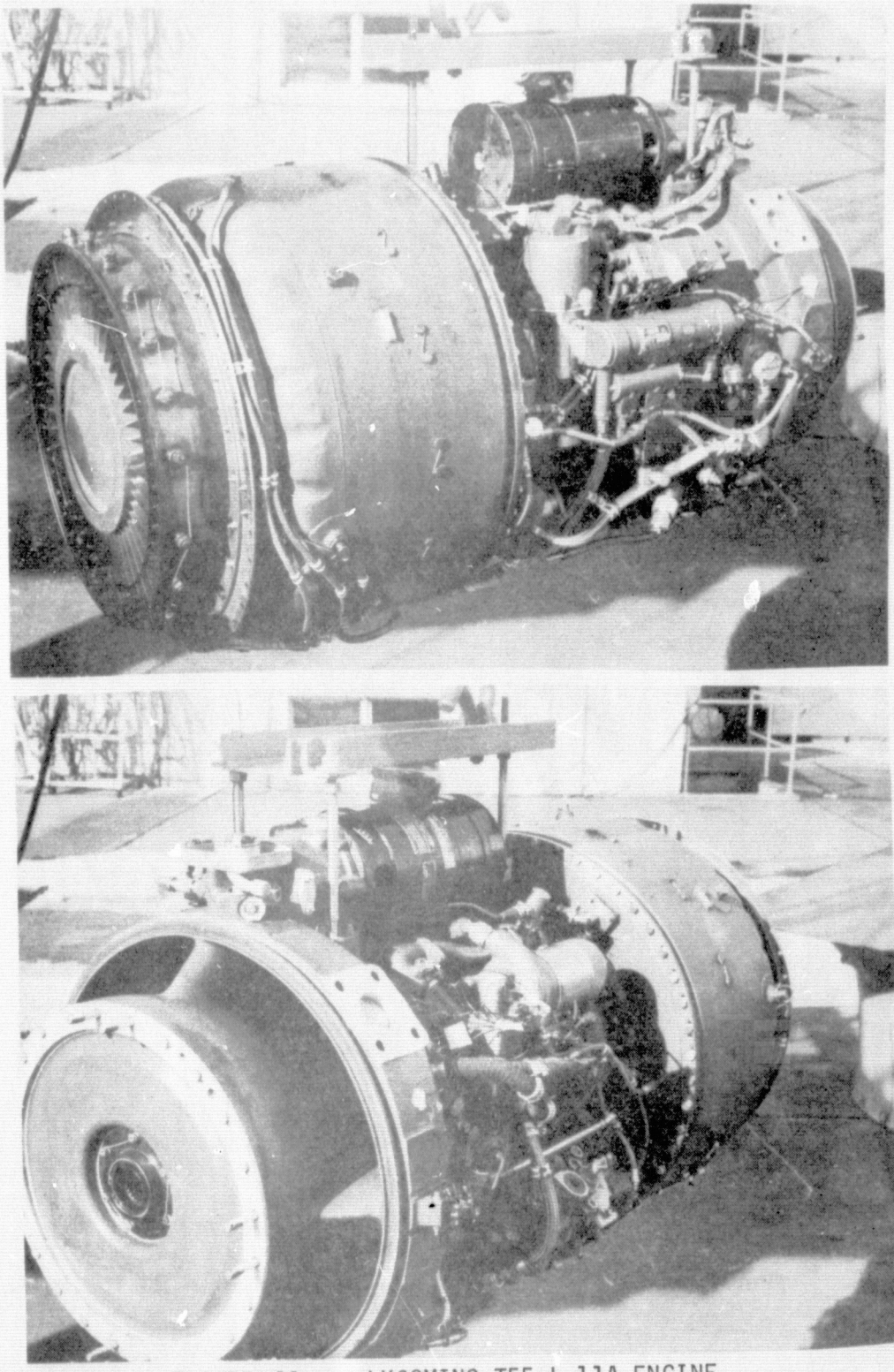

G 42675 FIGURE 11. LYCOMING T55-L-11A ENGINE

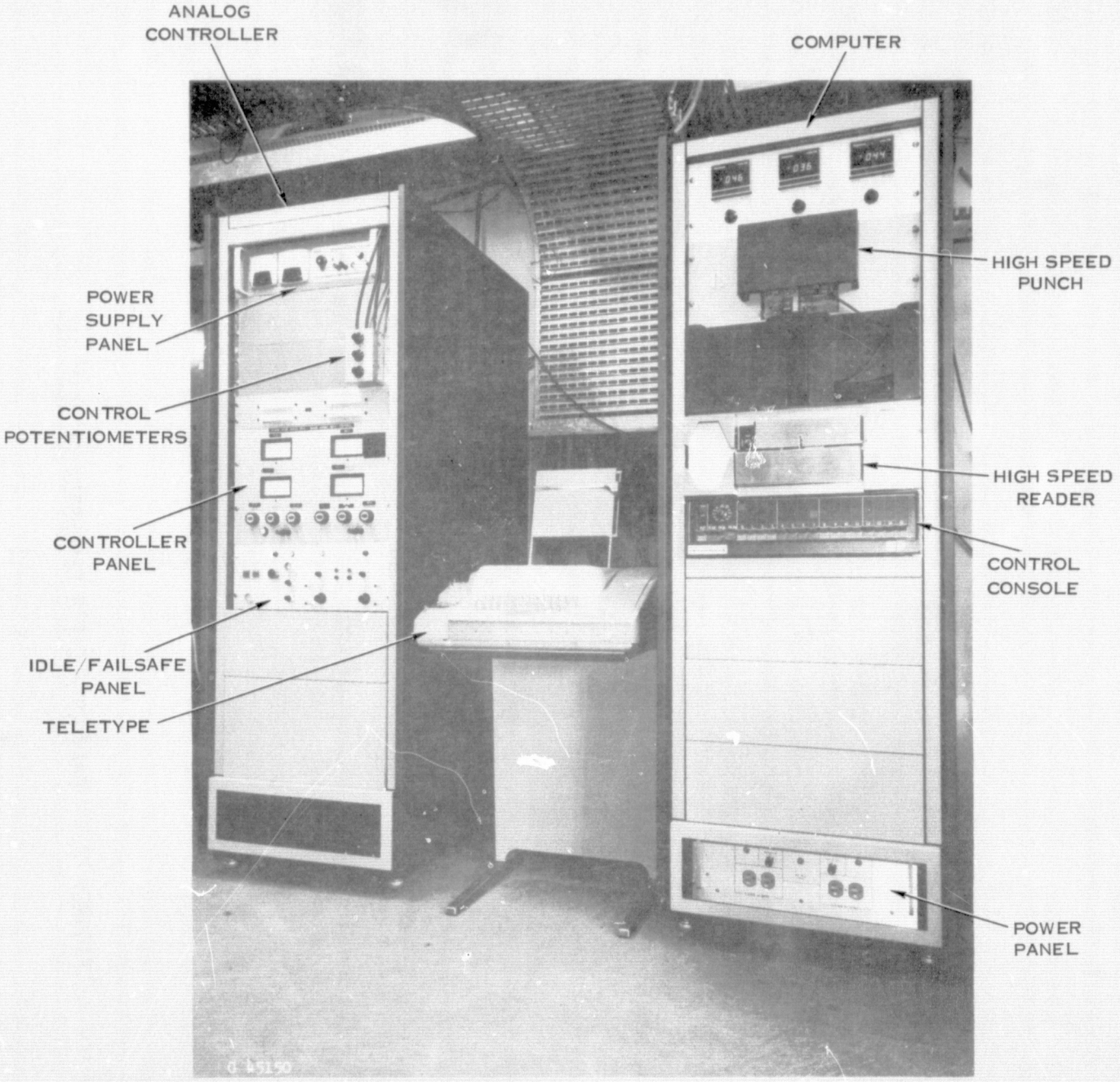

FIGURE 12. Q-FAN CONTROL SYSTEM

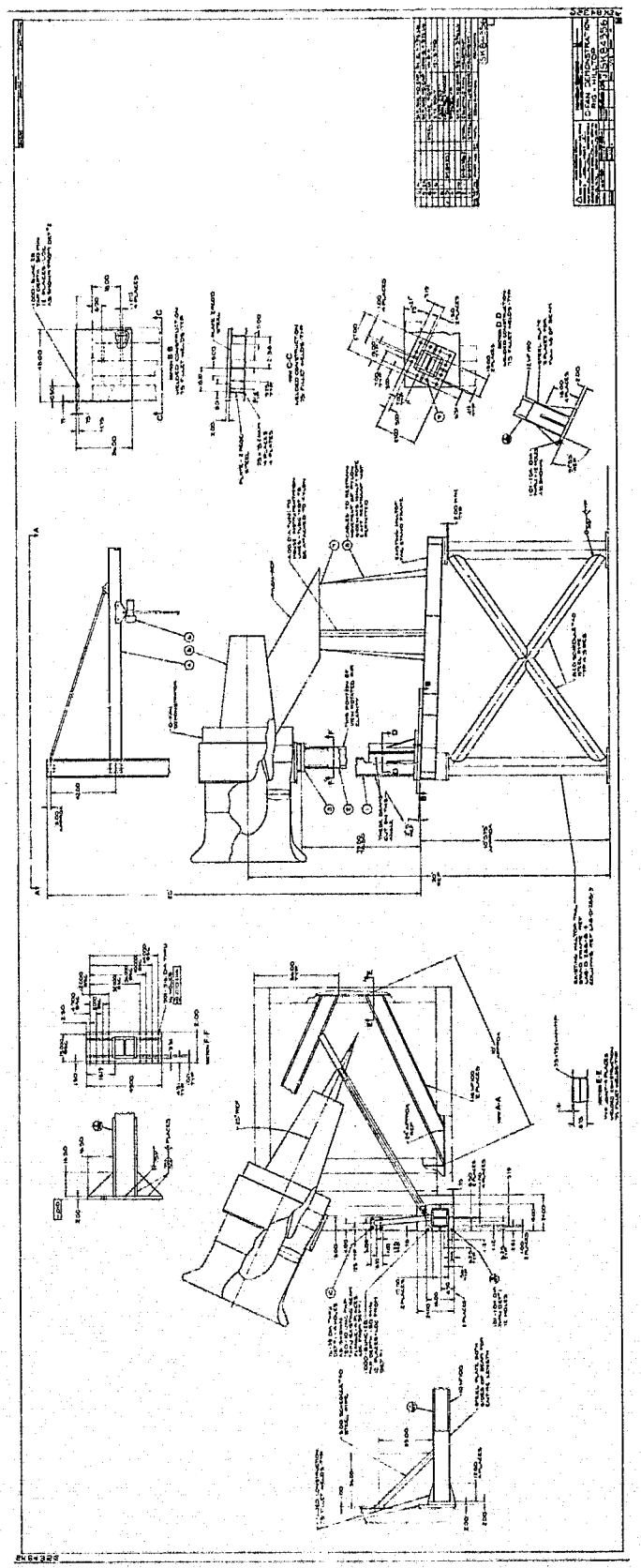

FIGURE 13. DRAWING - Q-FAN DEMONSTRATOR TEST RIG

FIGURE 14. TEST RIG WITH Q-FAN INSTALLED - FRONT OBLIQUE VIEW

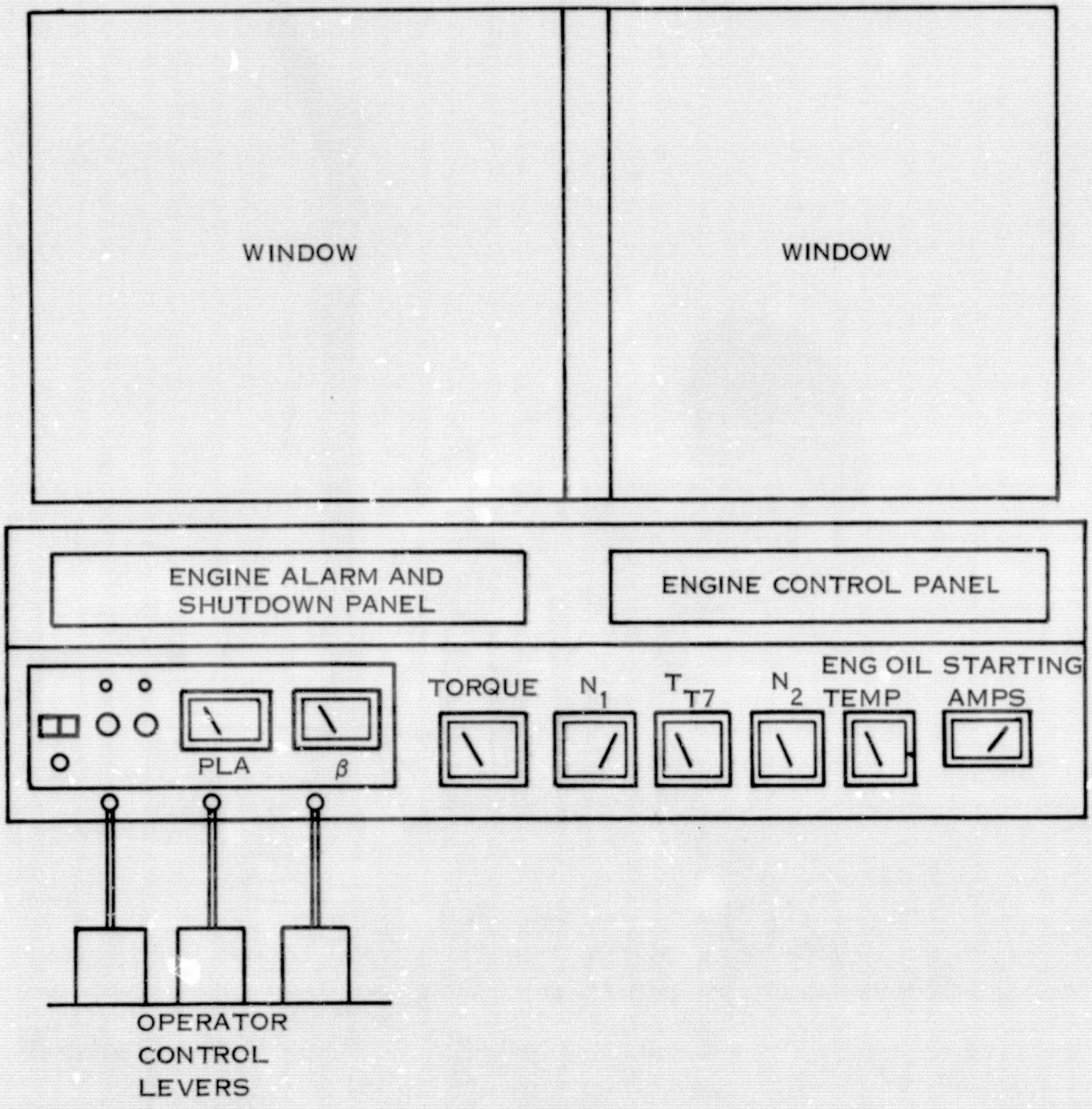

FIGURE 15. RIG OPERATORS CONSOLE

FIGURE 16. RIG OPERATORS CONTROL STATION

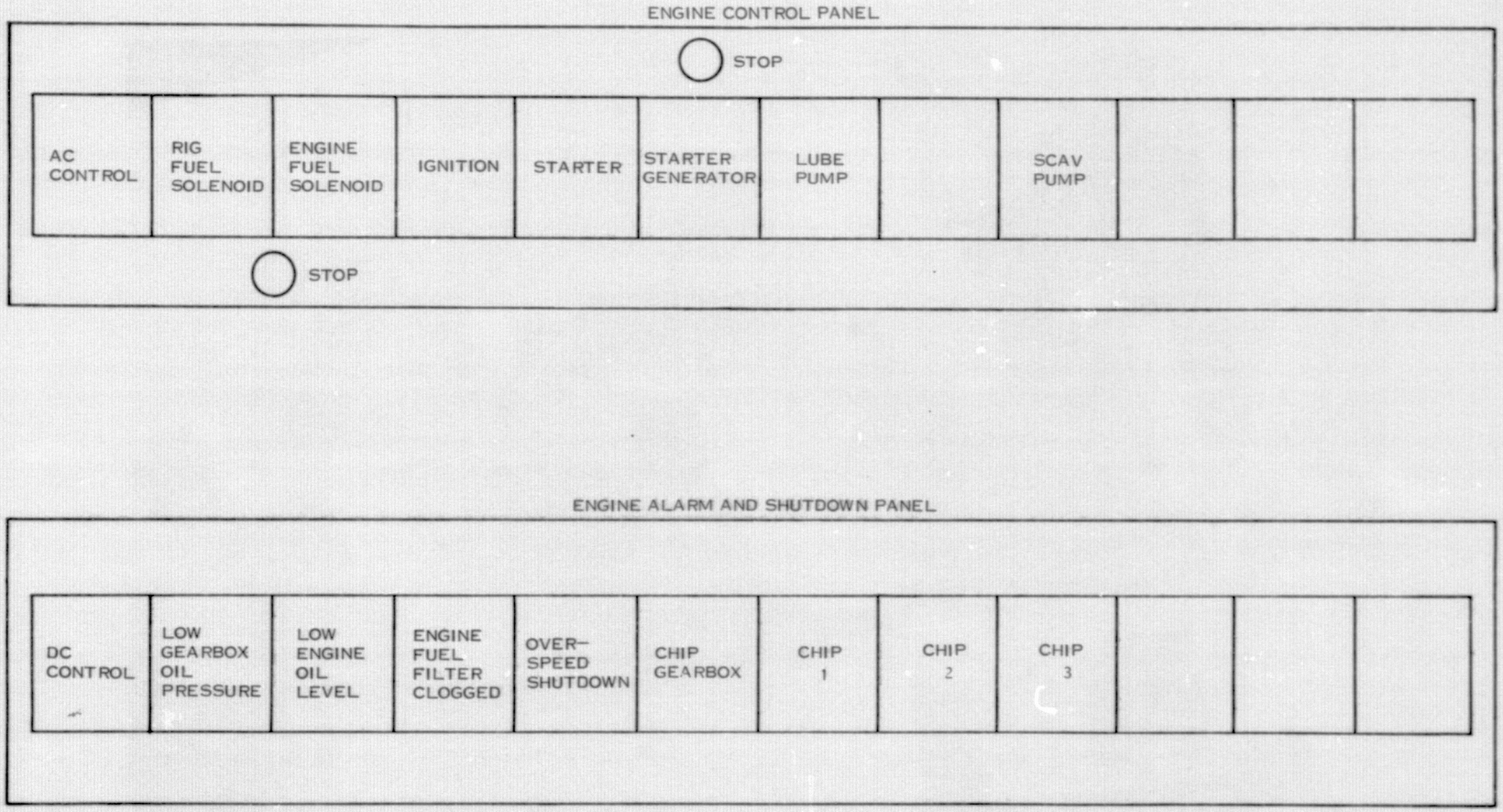

FIGURE 17. OPERATOR CONTROL PANEL

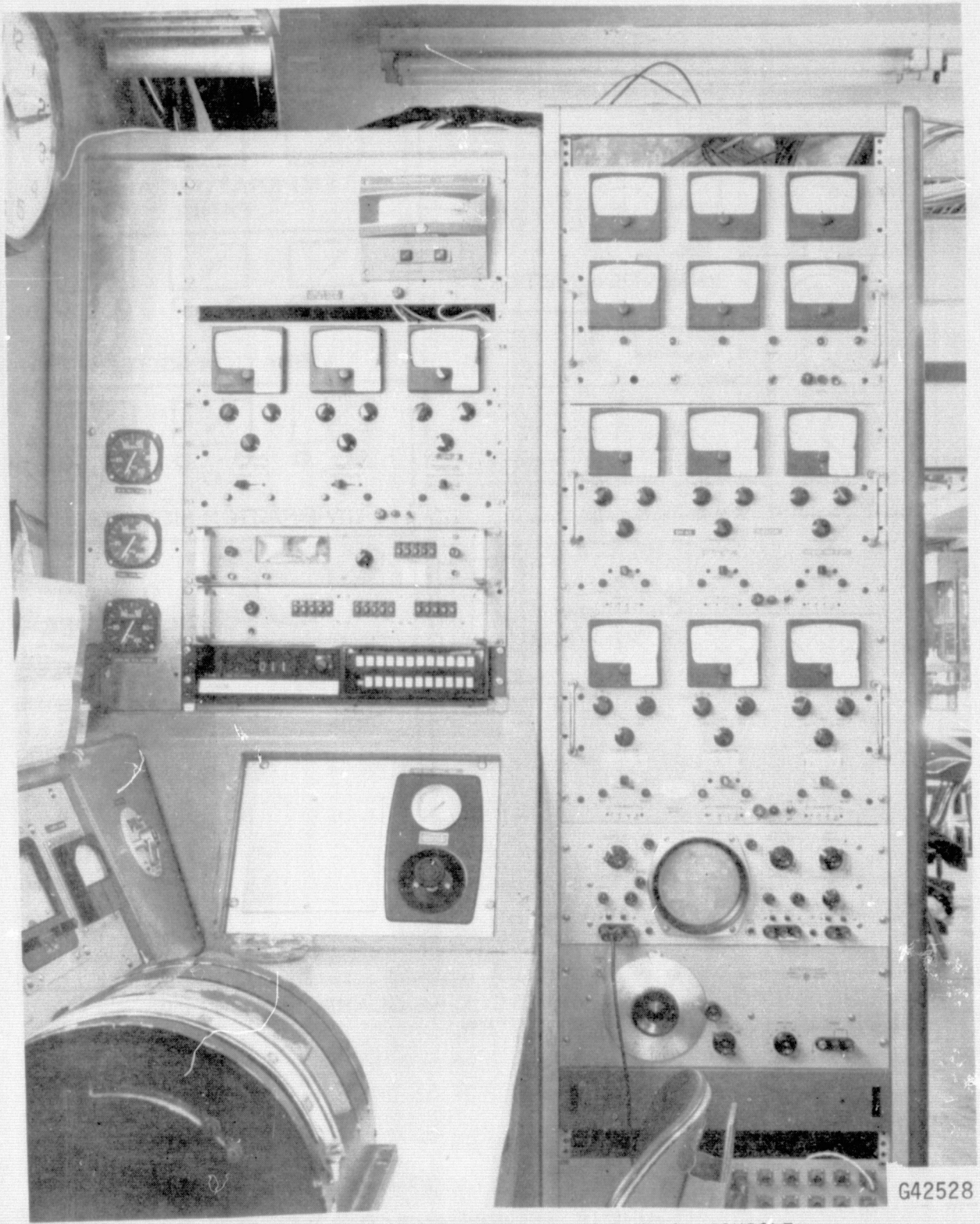

G42528

FIGURE 18. CONTROL ROOM - TECHNICIAN'S CONSOLE

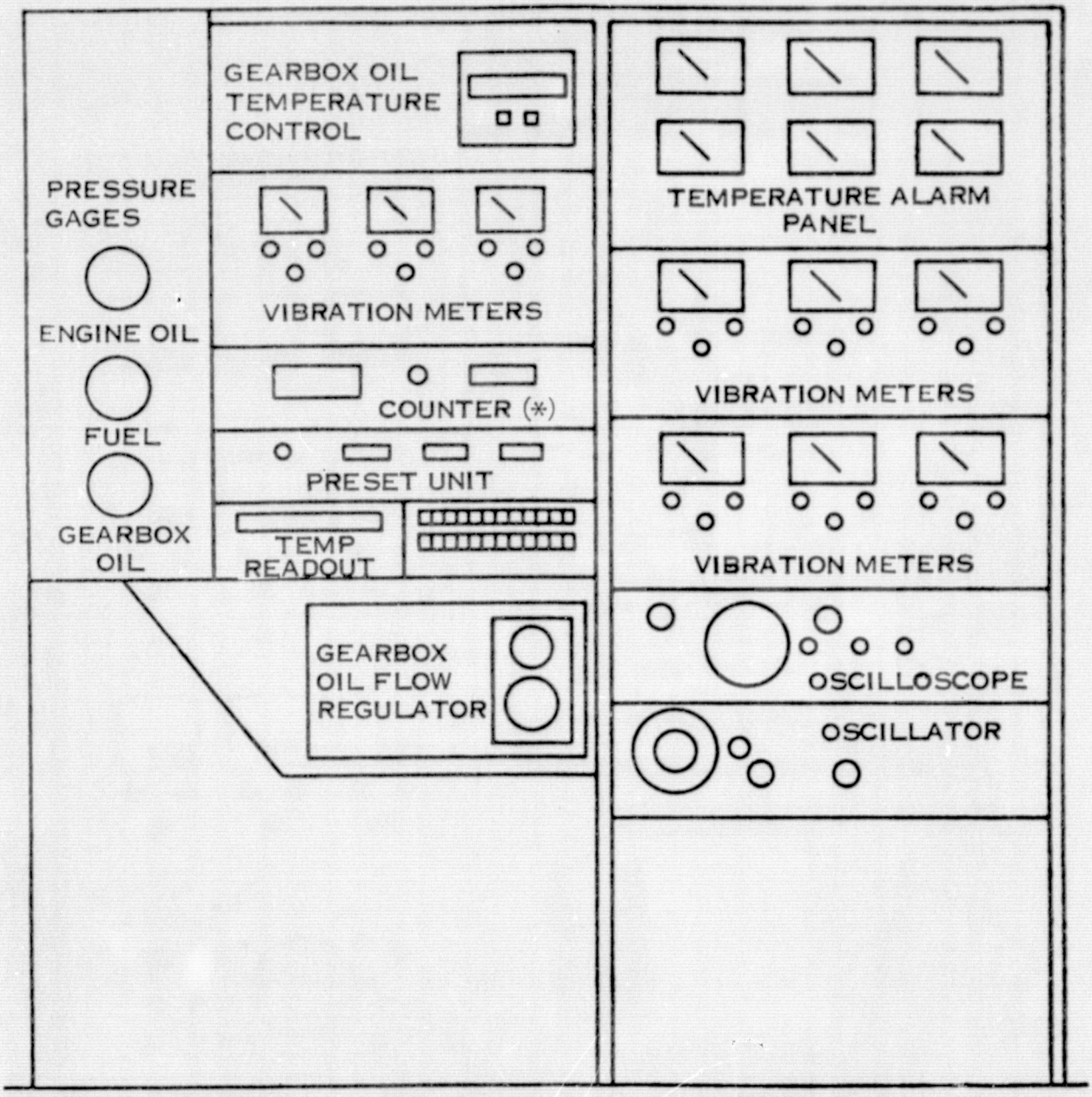

* ENGINE SPEEDS N_1 AND N_2 AS WELL AS GEARBOX OIL FLOW WERE MONITORED ON THE COUNTER.

FIGURE 19. TECHNICIAN'S CONSOLE

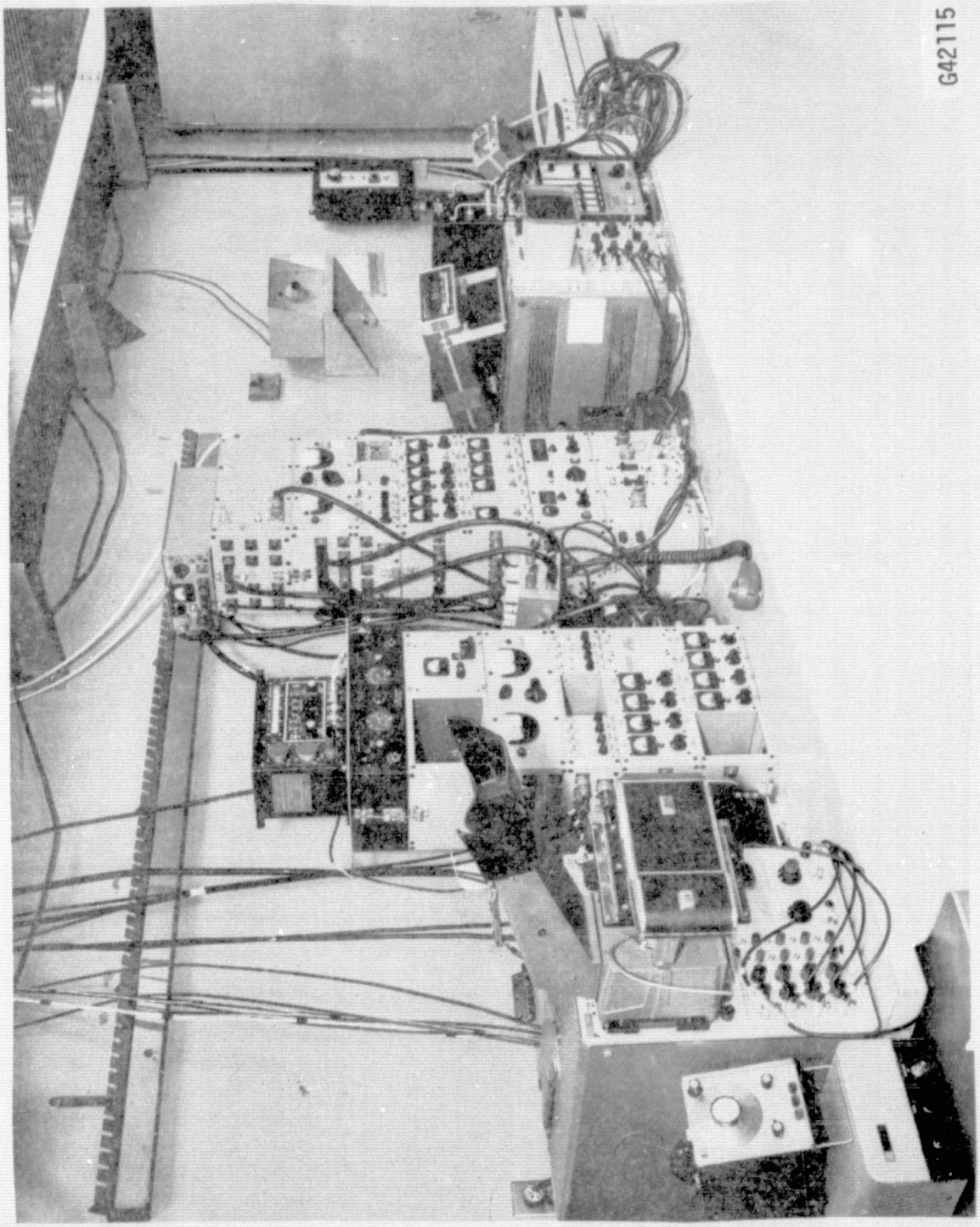

G42115

FIGURE 20. TYPICAL ELECTRONIC SETUP DURING PERFORMANCE TESTING

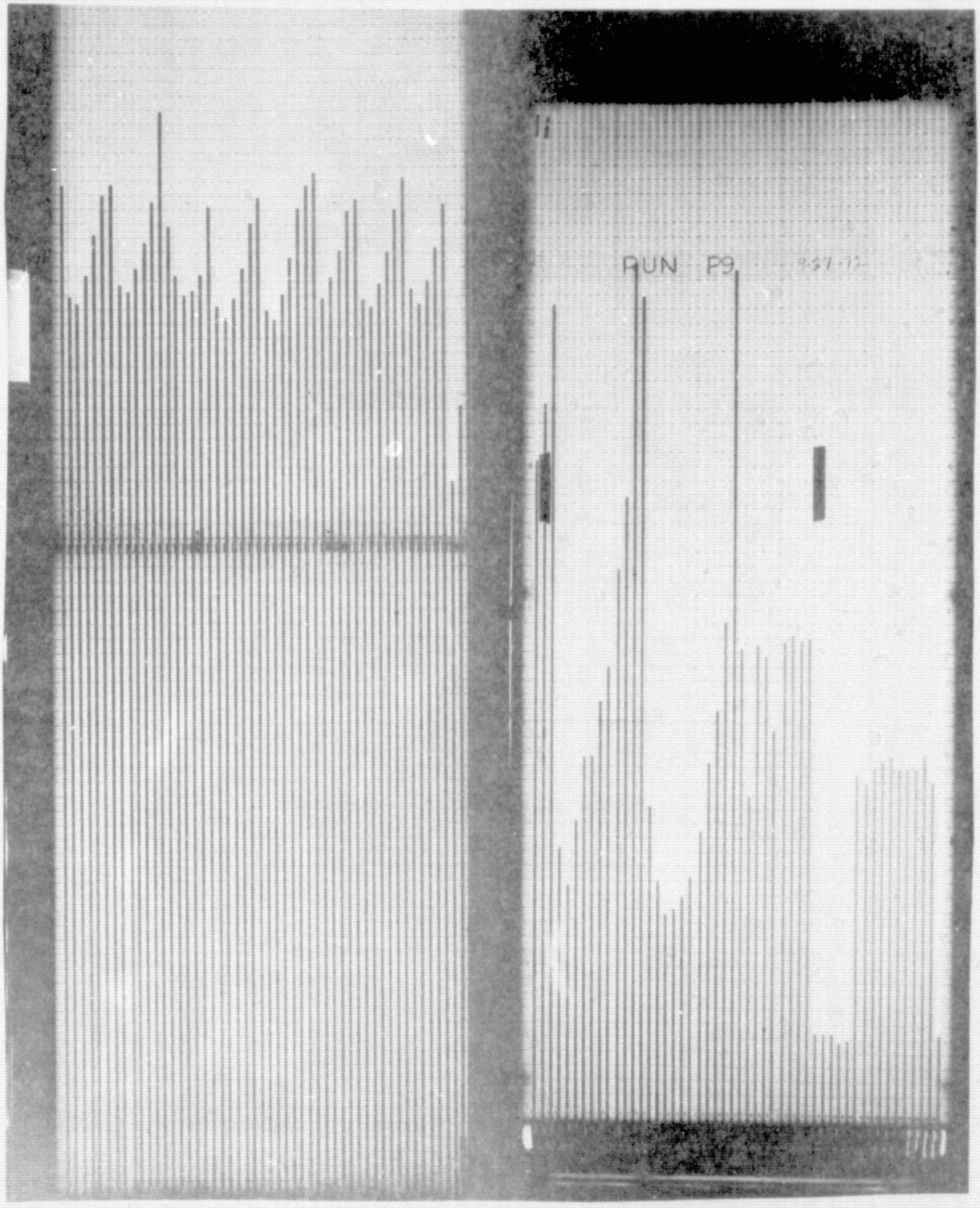

FIGURE 21. MANOMETER BANKS

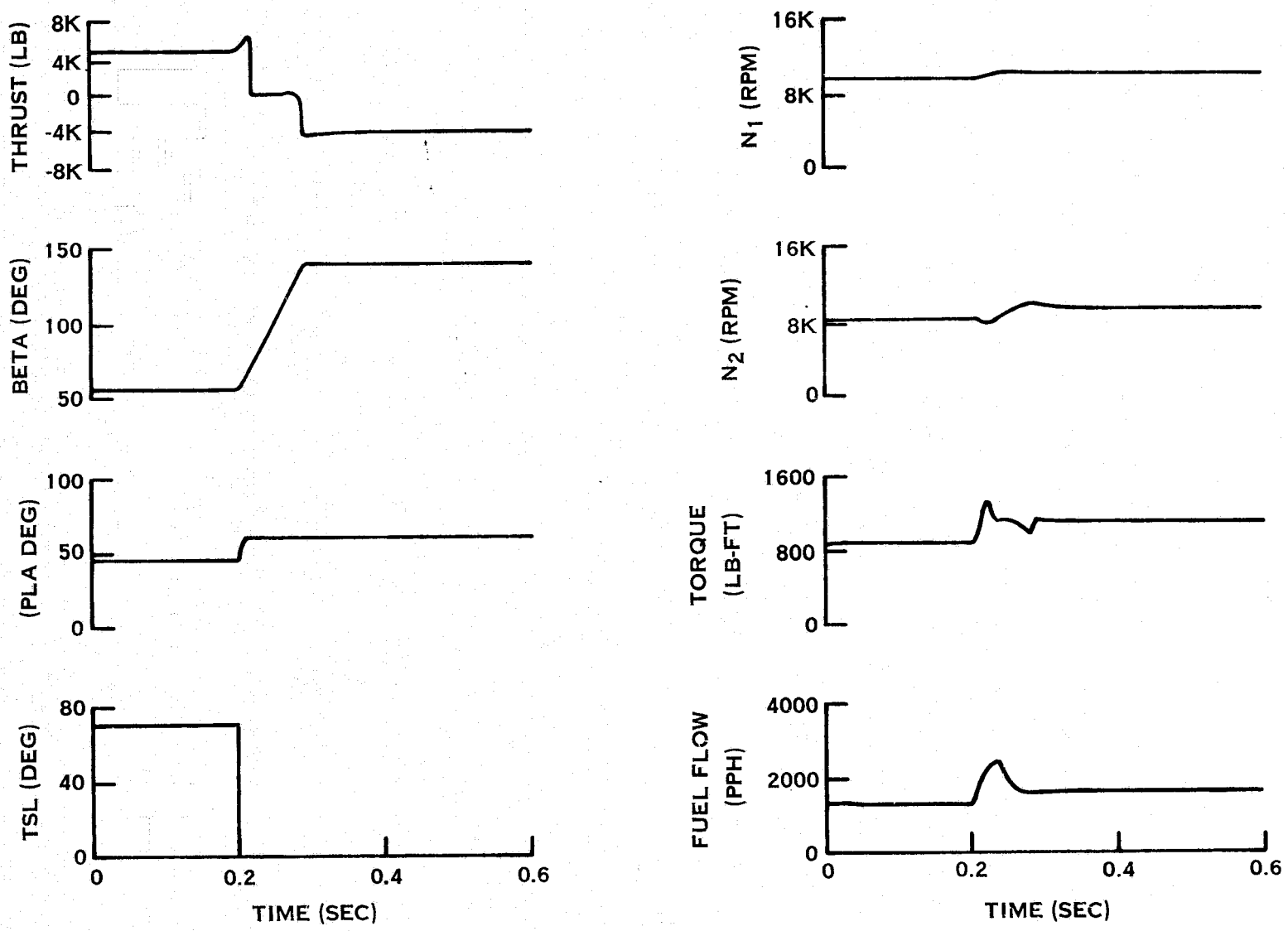

FIGURE 22. Q-FAN DEMONSTRATOR COMPUTER SIMULATION, FORWARD TO REVERSE THRUST TRANSIENT (THROUGH FEATHER) WITH NO PLA RESET

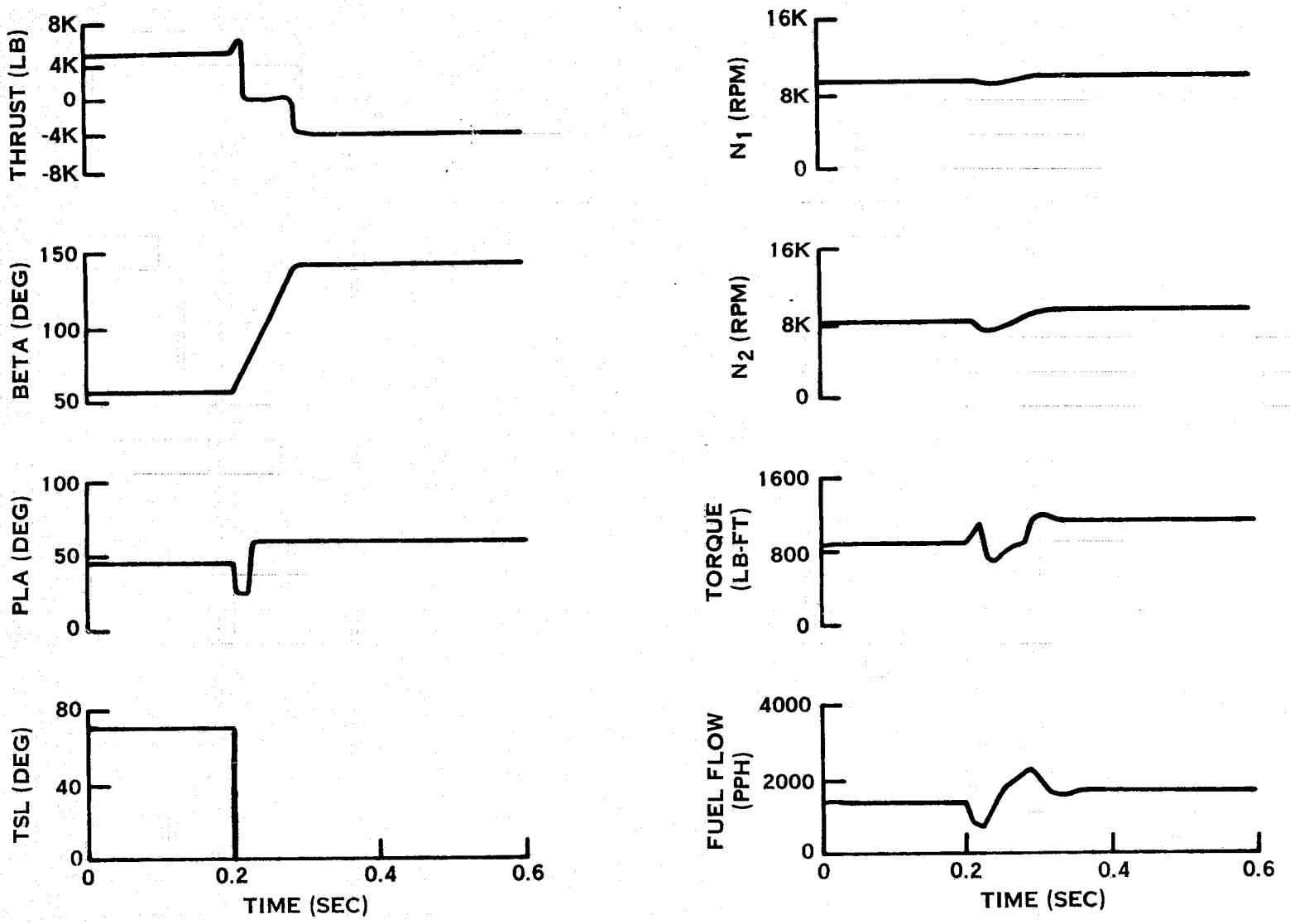

FIGURE 23. Q-FAN DEMONSTRATOR COMPUTER SIMULATION, FORWARD TO REVERSE THRUST TRANSIENT (THROUGH FEATHER) WITH PLA RESET

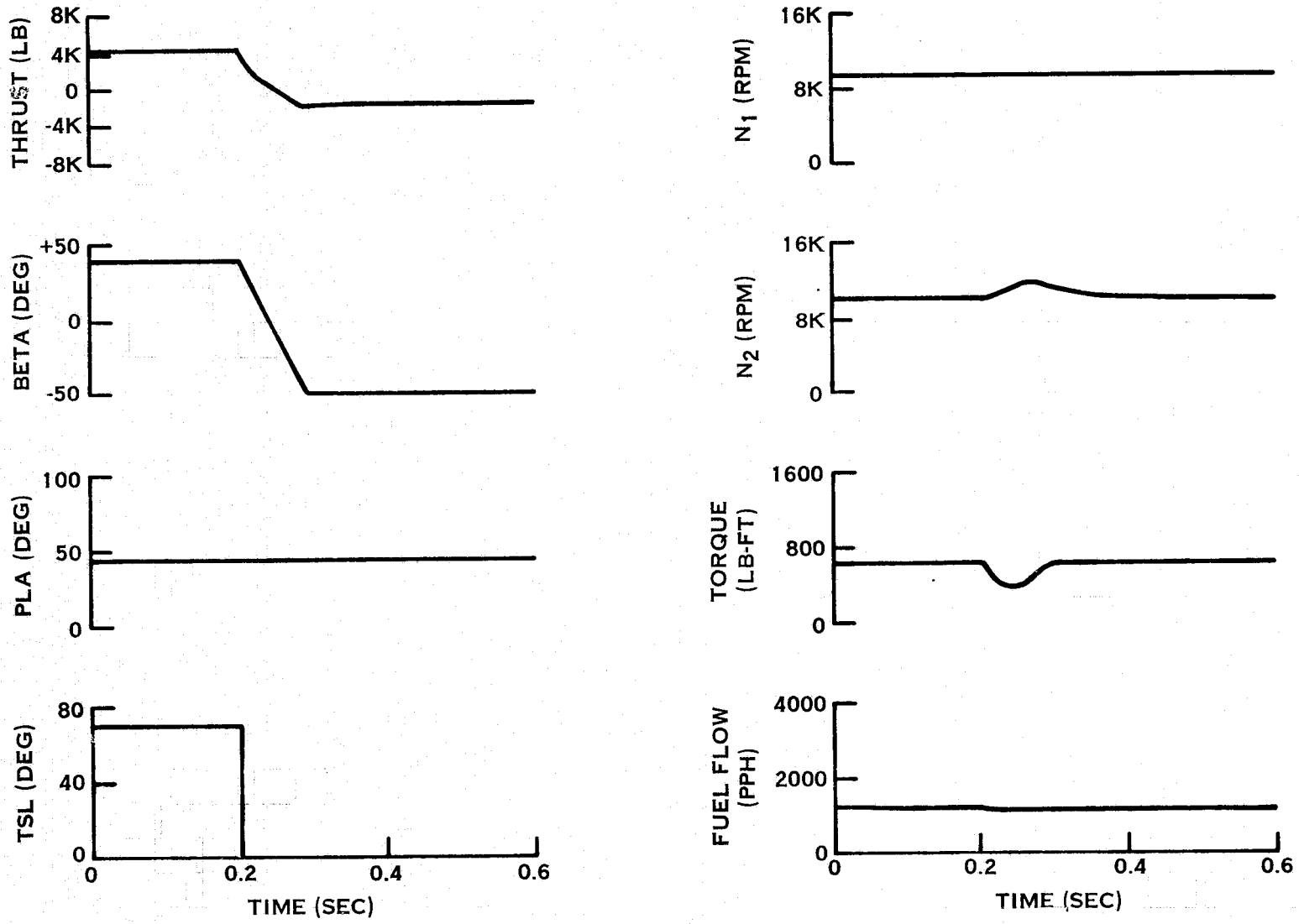

FIGURE 24. Q-FAN DEMONSTRATOR COMPUTER SIMULATION, FORWARD TO REVERSE THRUST TRANSIENT (THROUGH FLAT PITCH) WITH NO PLA RESET

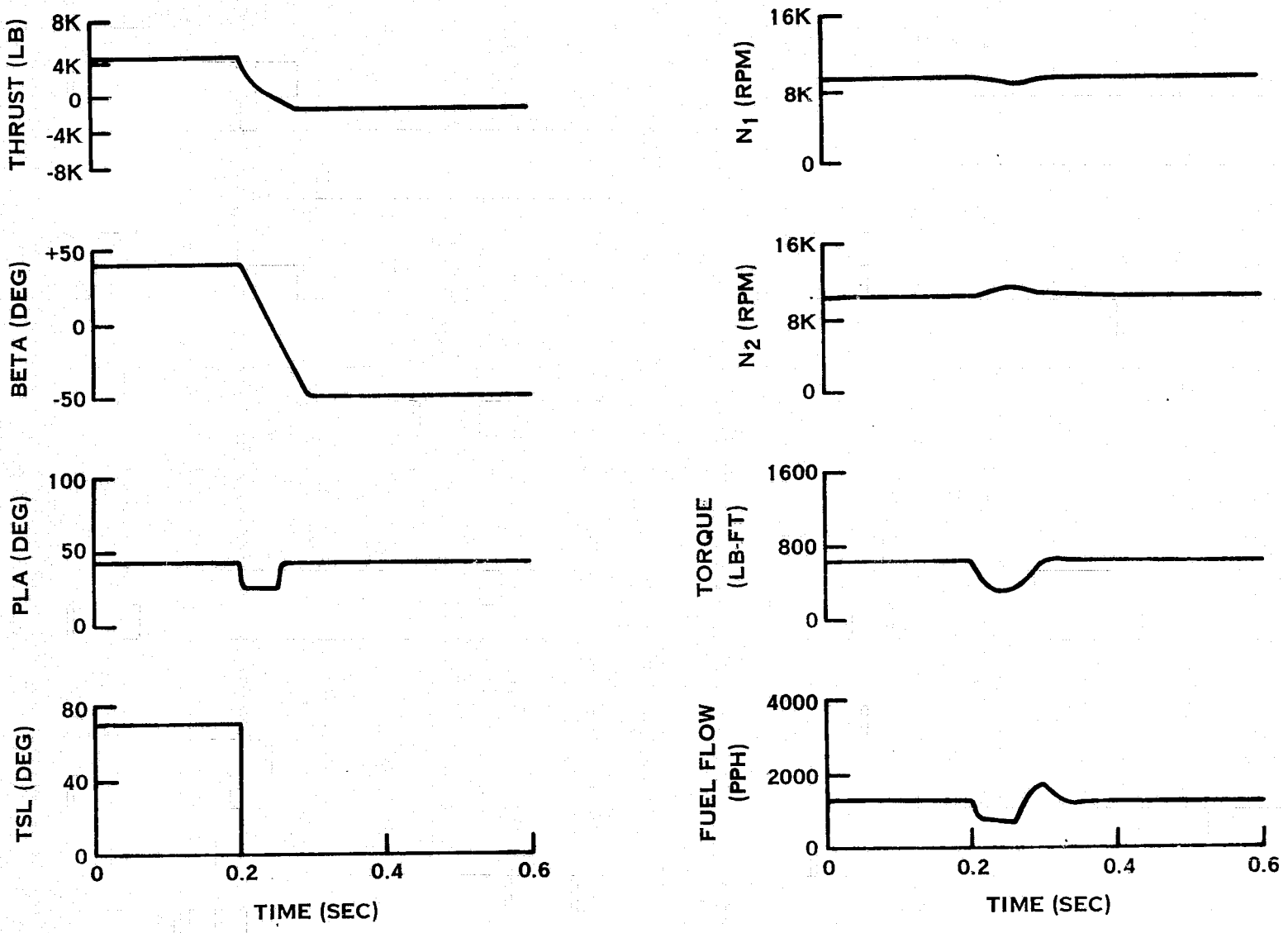

FIGURE 25. Q-FAN DEMONSTRATOR COMPUTER SIMULATION, FORWARD TO REVERSE THRUST TRANSIENT (THROUGH FLAT PITCH) WITH NO PLA RESET

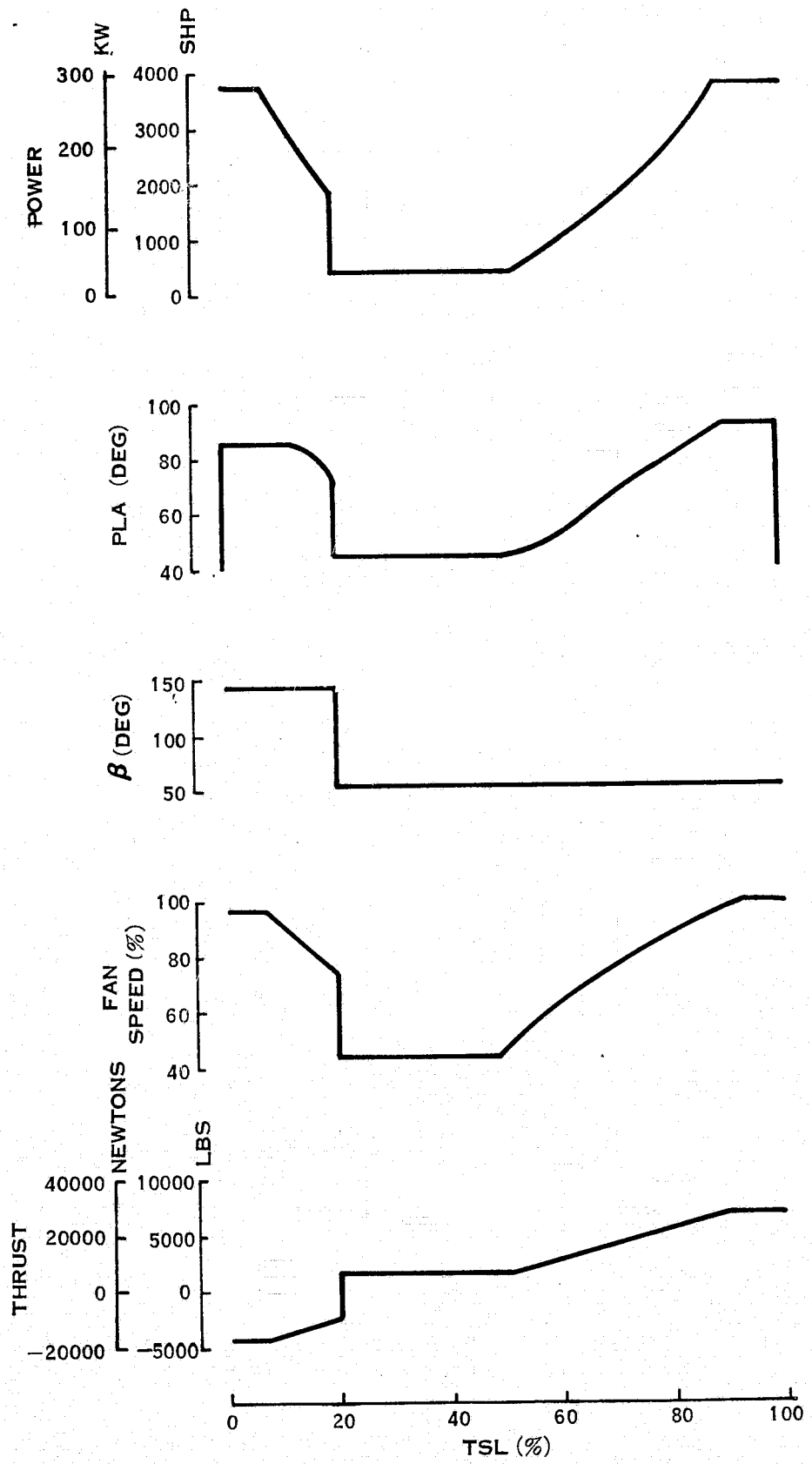

FIGURE 26. COORDINATED CONTROL SCHEDULE NUMBER 1.

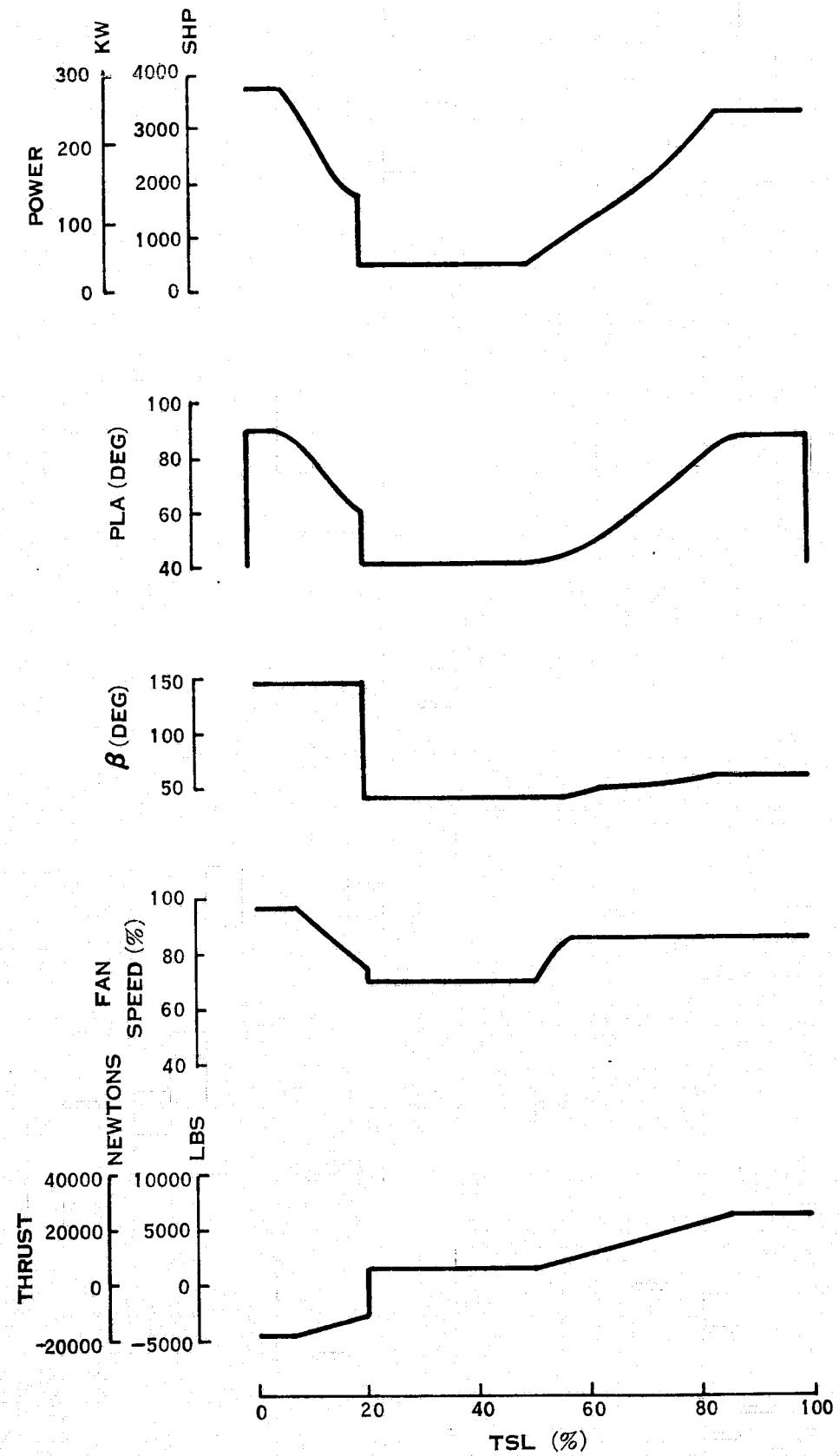

FIGURE 27. COORDINATED CONTROL SCHEDULE NUMBER 2.

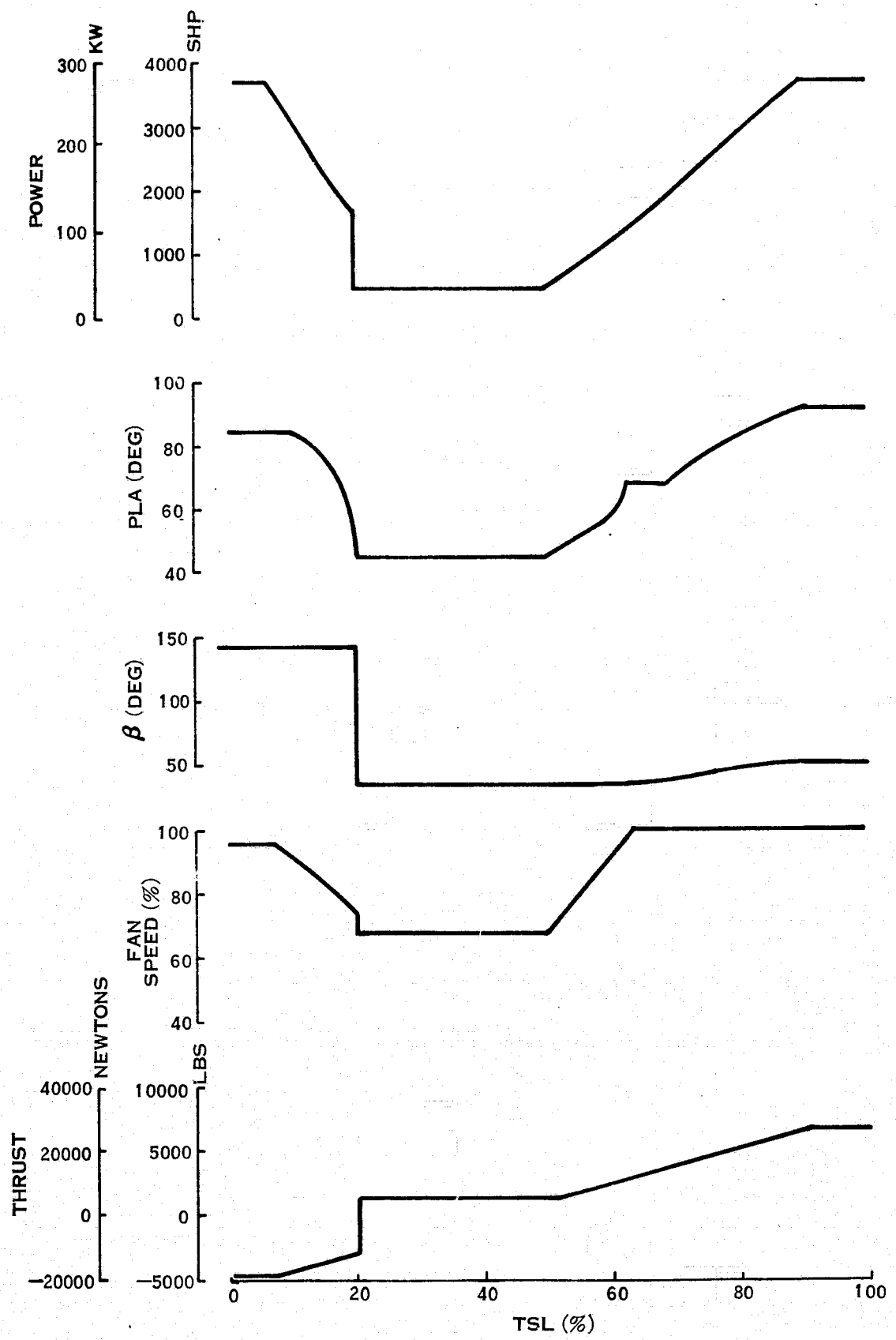

FIGURE 28. COORDINATED CONTROL SCHEDULE NUMBER 3.

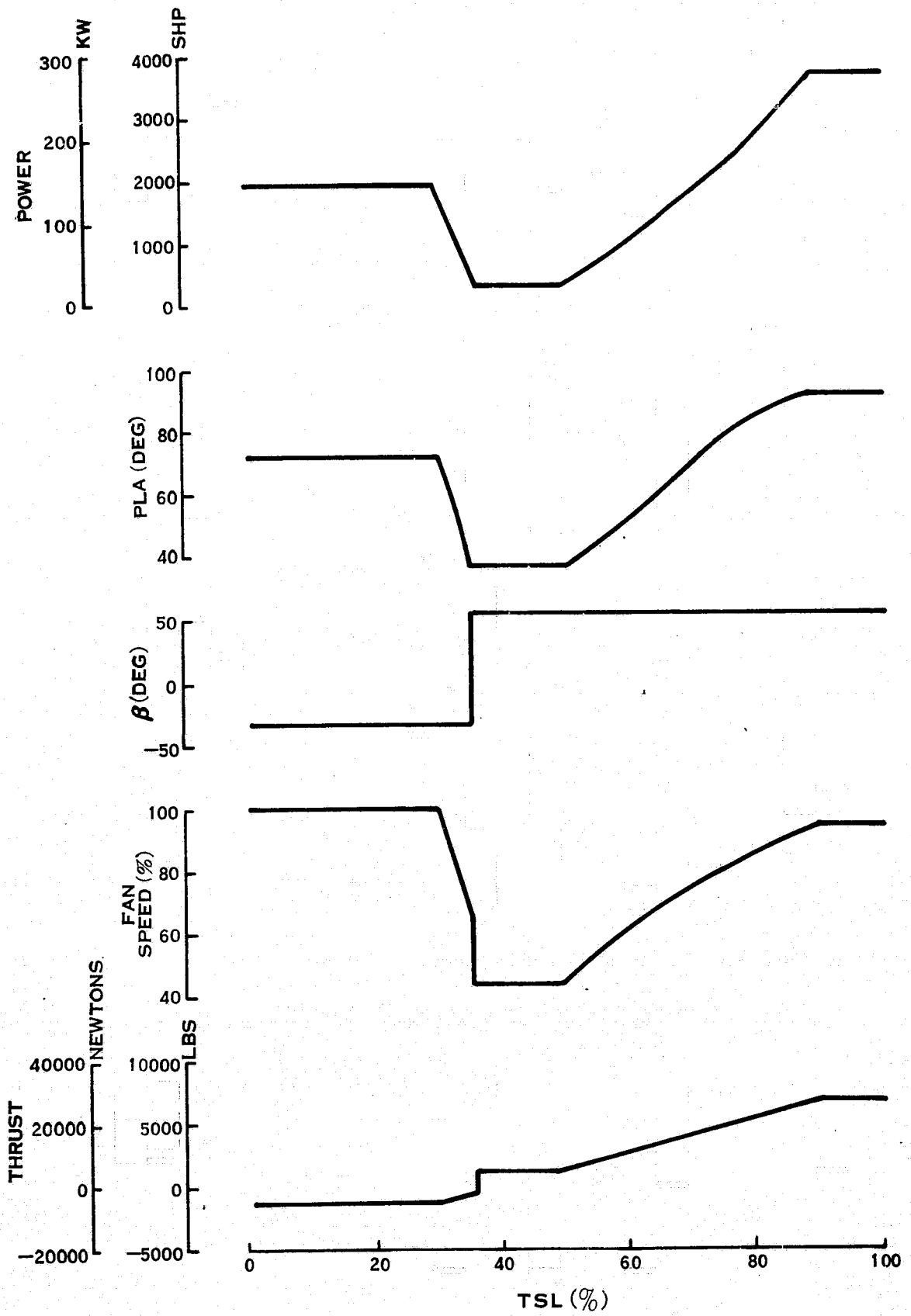

FIGURE 29. COORDINATED CONTROL SCHEDULE NUMBER 4.

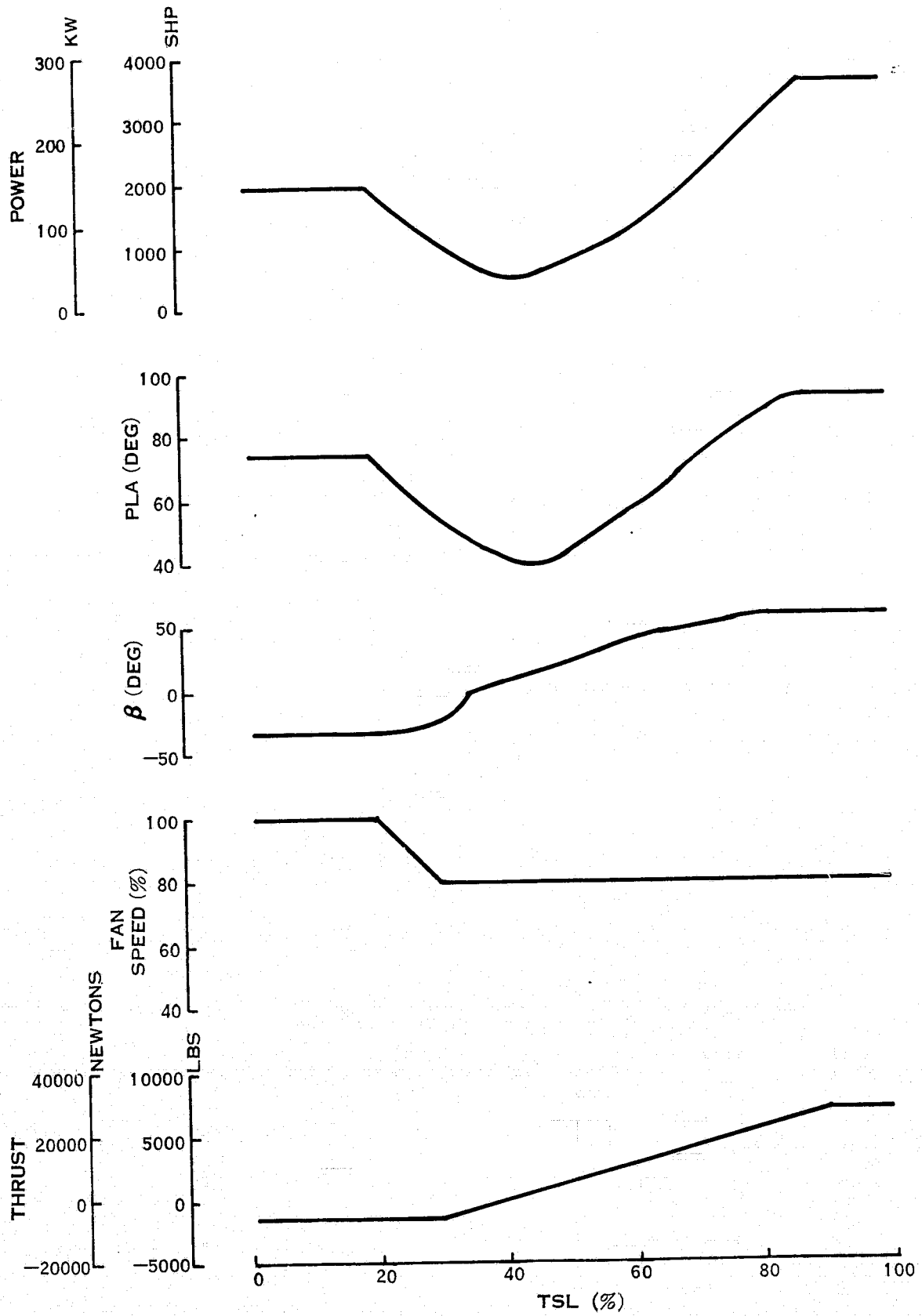

FIGURE 30. COORDINATED CONTROL SCHEDULE NUMBER 6.

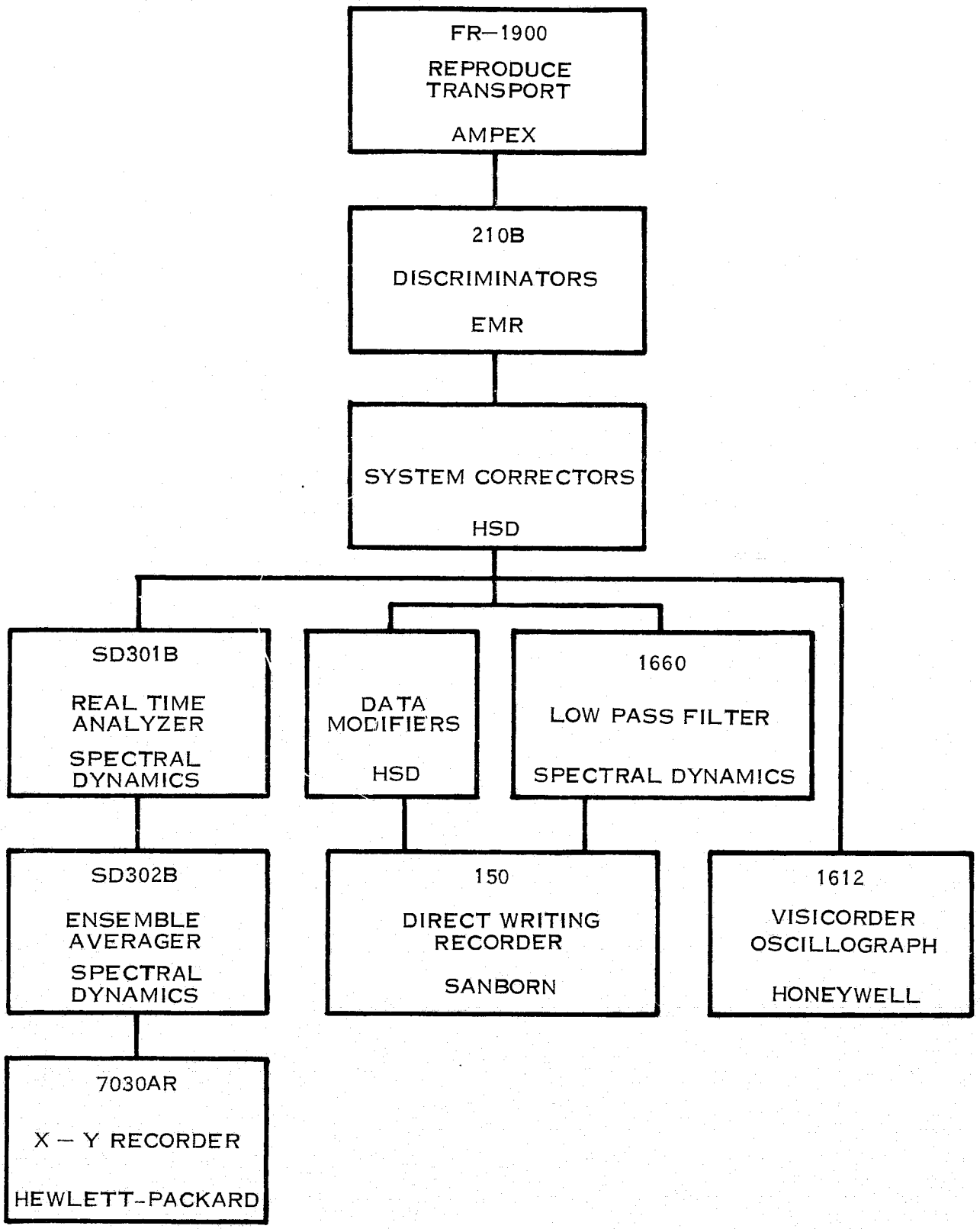

FIGURE 31. BLOCK DIAGRAM - STRUCTURAL DATA ANALYSIS

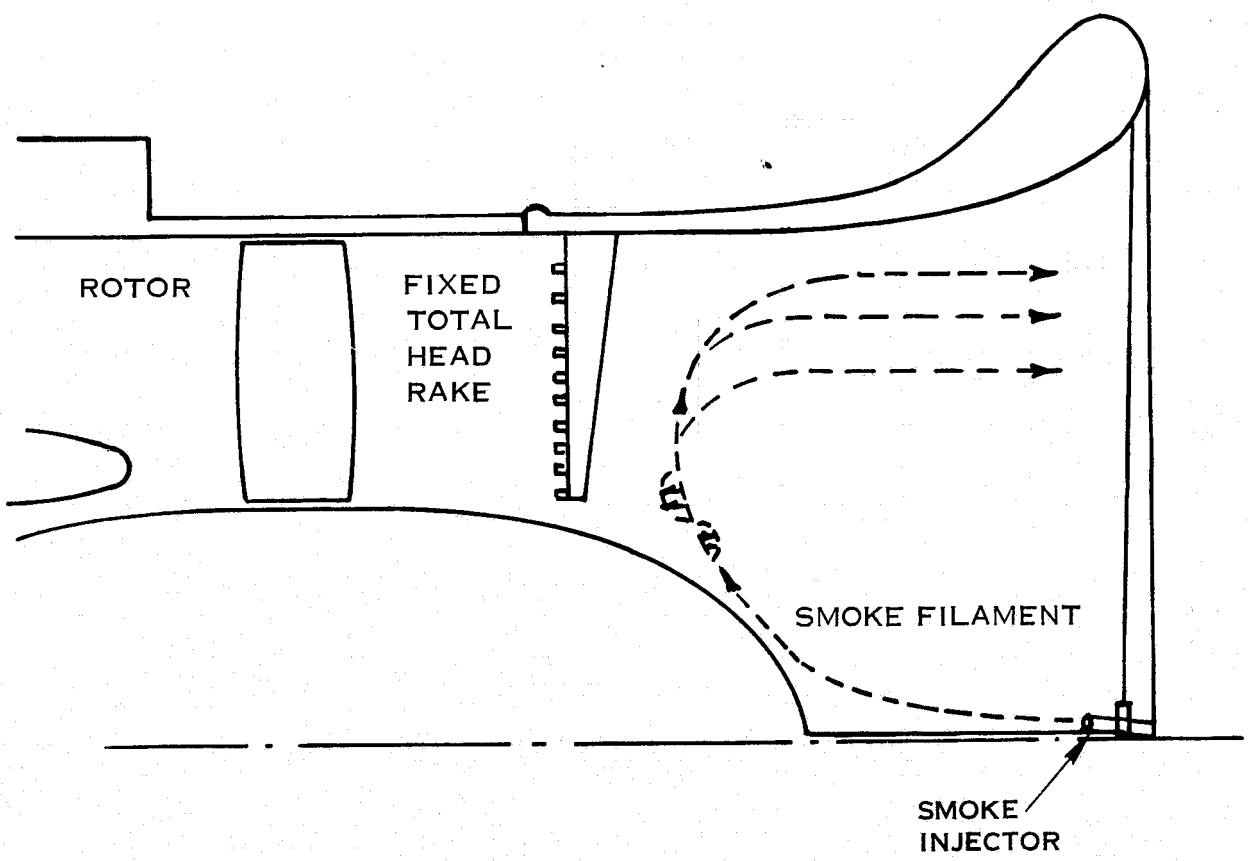

FIGURE 32. Q-FAN DEMONSTRATOR REVERSE FLOW PATTERN

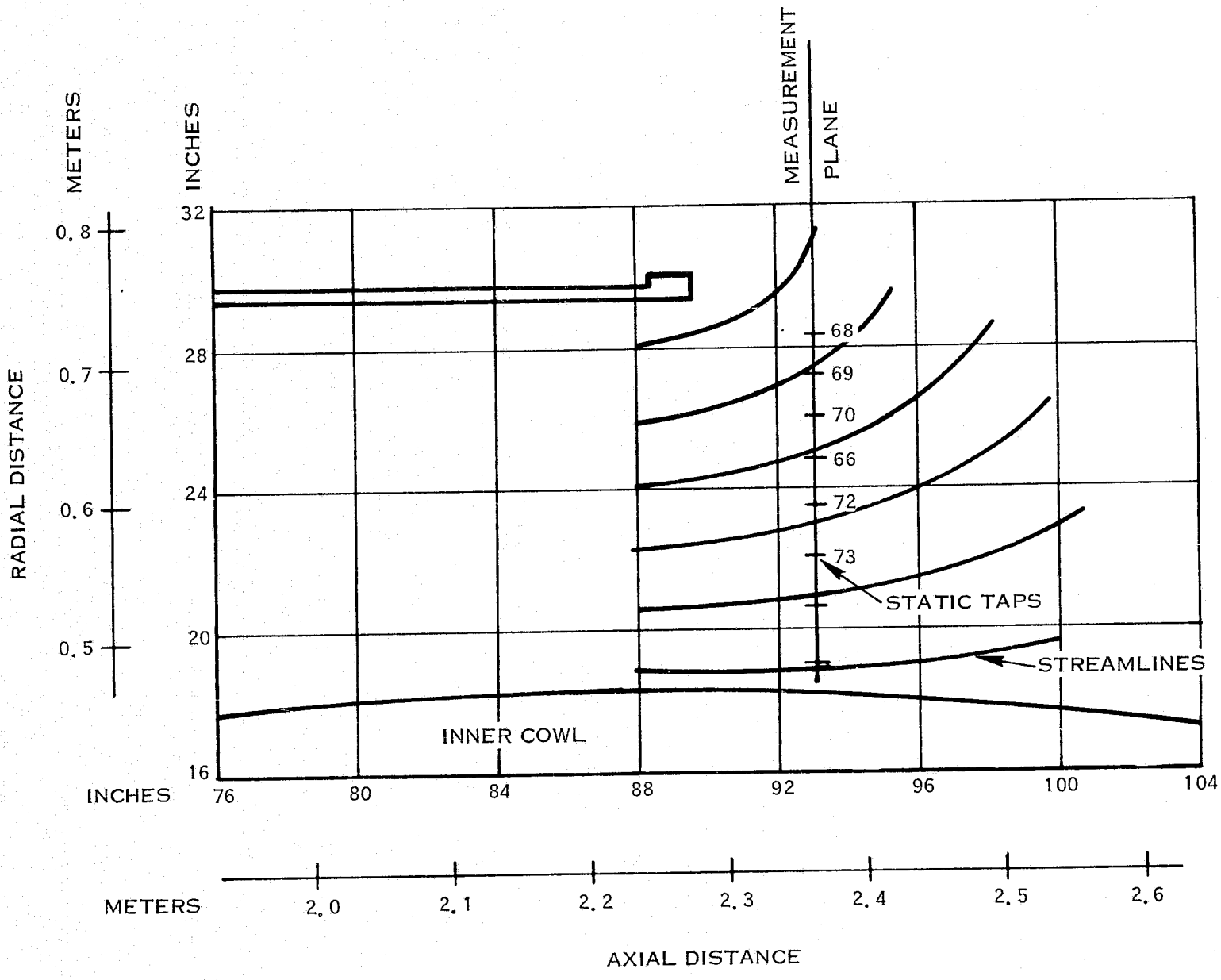

FIGURE 33. Q-FAN DEMONSTRATOR REVERSE FLOW FIELD

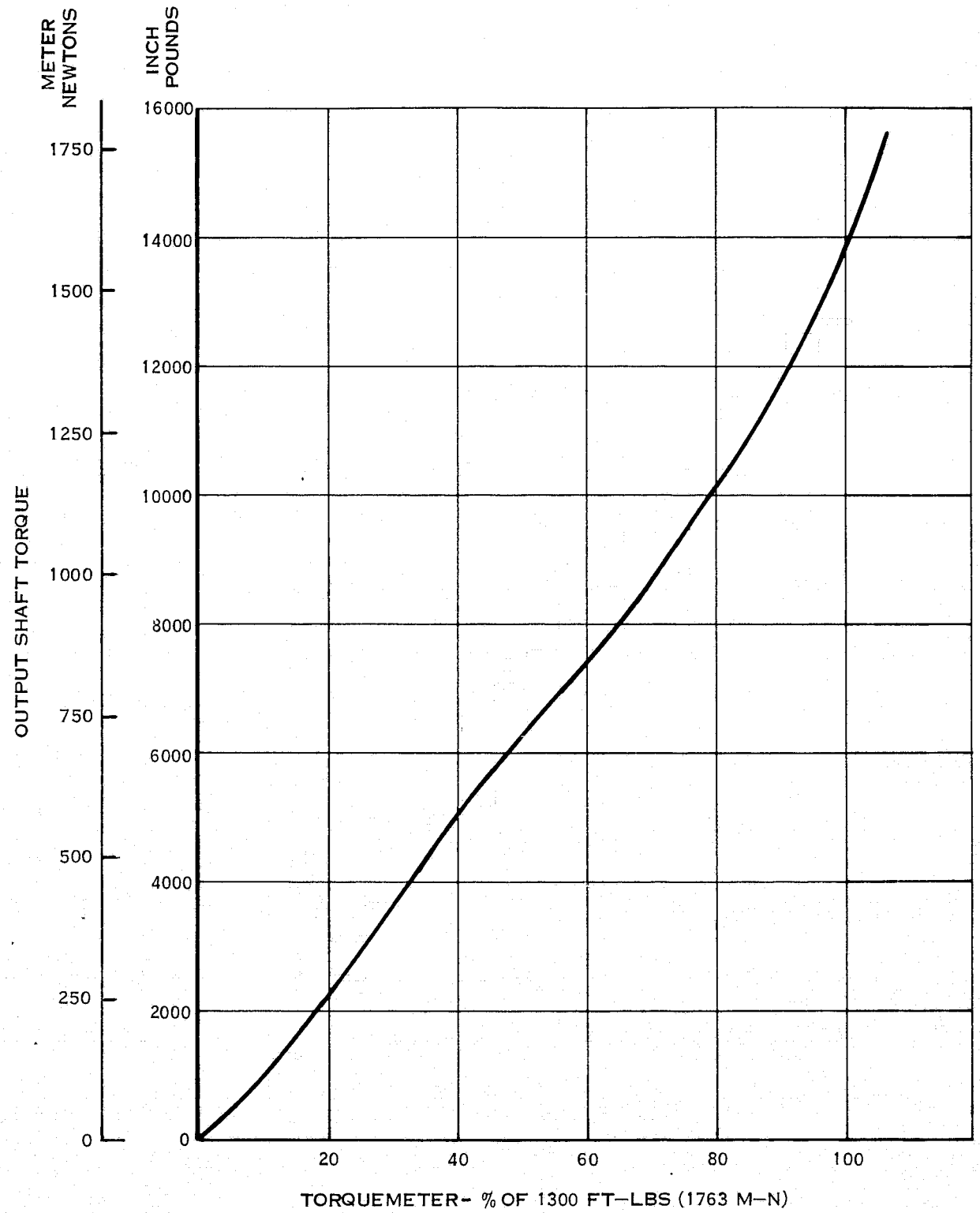

FIGURE 34. Q-FAN DEMONSTRATOR TORQUEMETER CALIBRATION CURVE

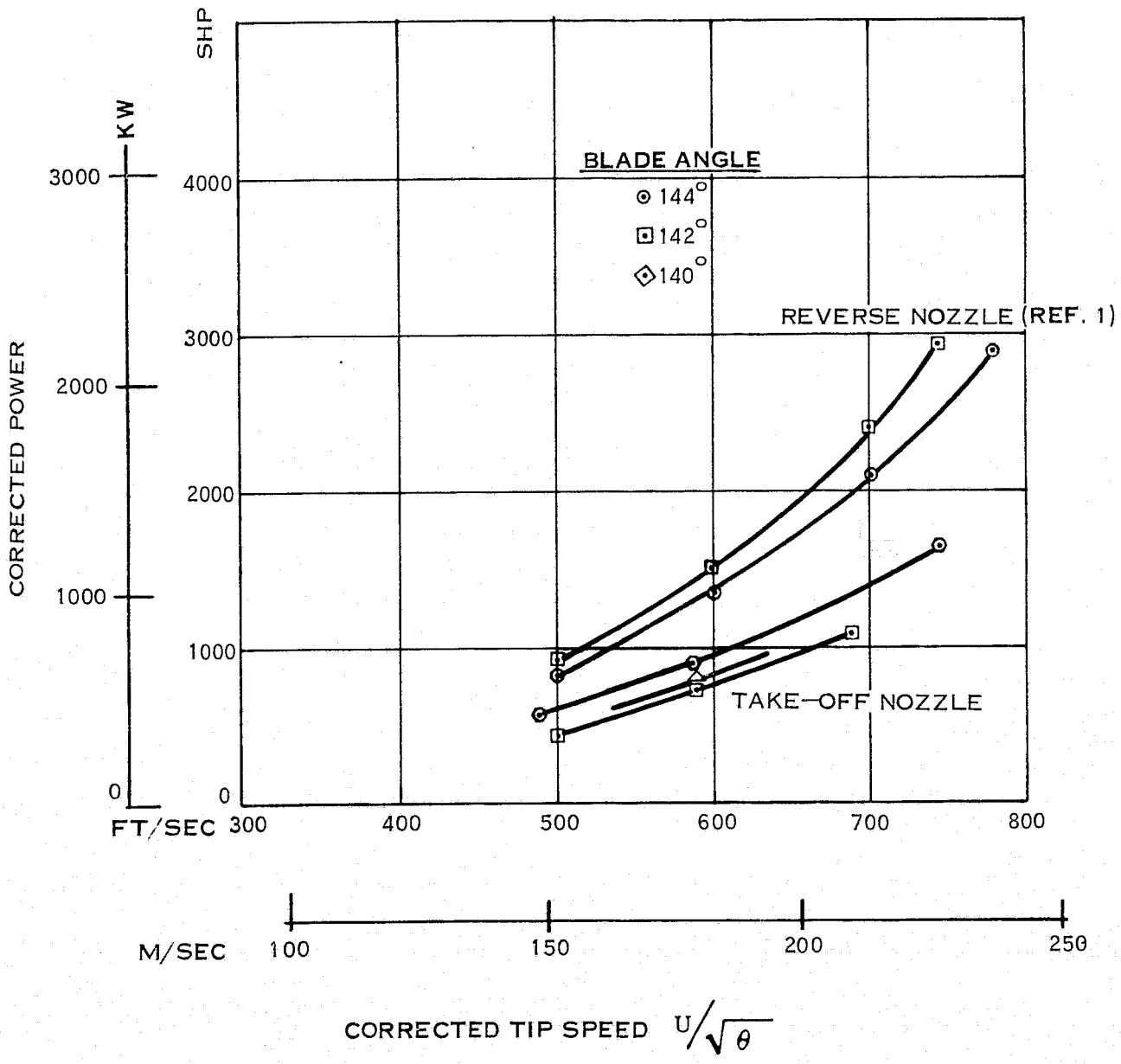

FIGURE 35. Q-FAN DEMONSTRATOR –
VARIATION OF POWER WITH BLADE ANGLE AND SPEED

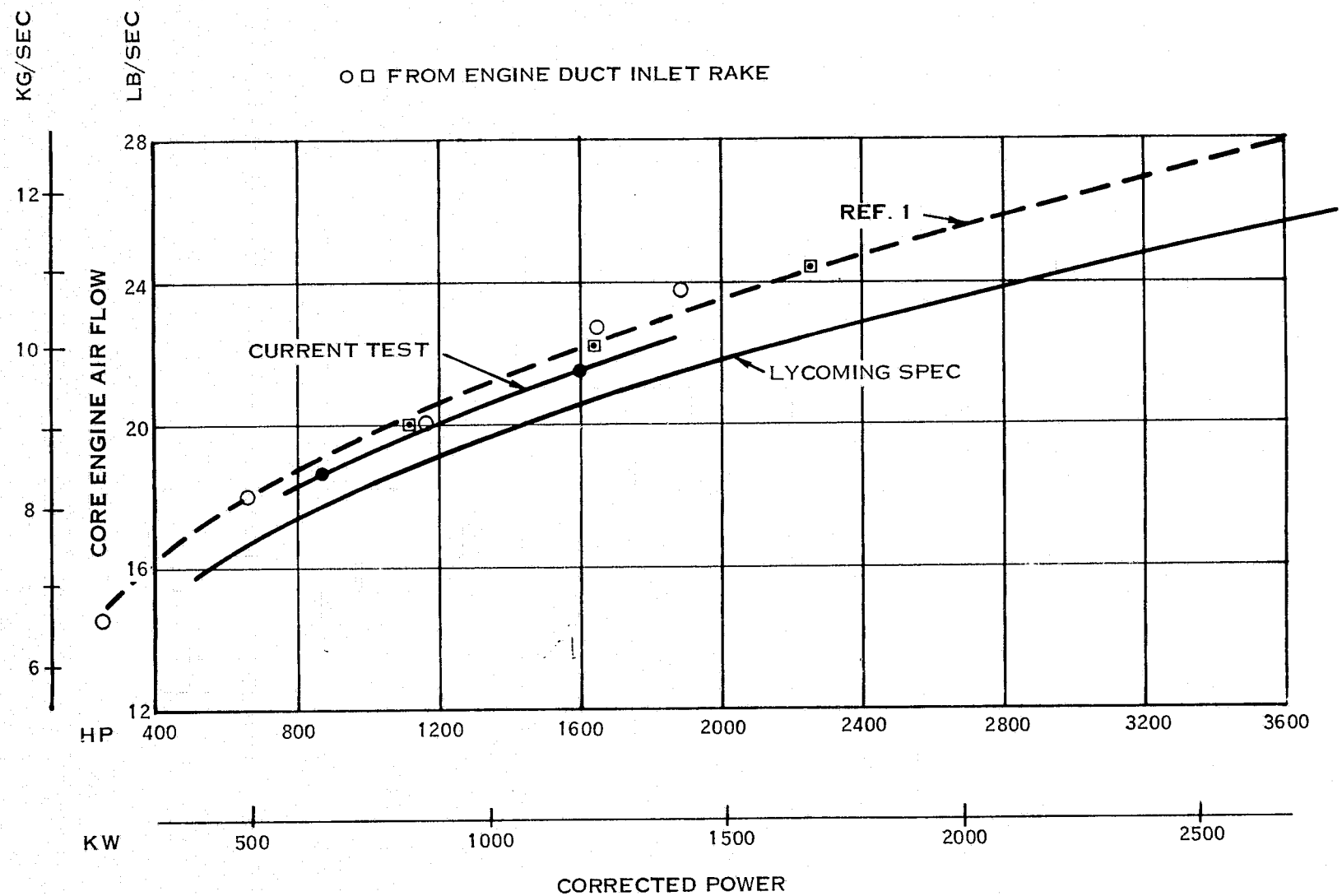

FIGURE 36. Q-FAN DEMONSTRATOR ENGINE AIR FLOW VERSUS CORRECTED POWER

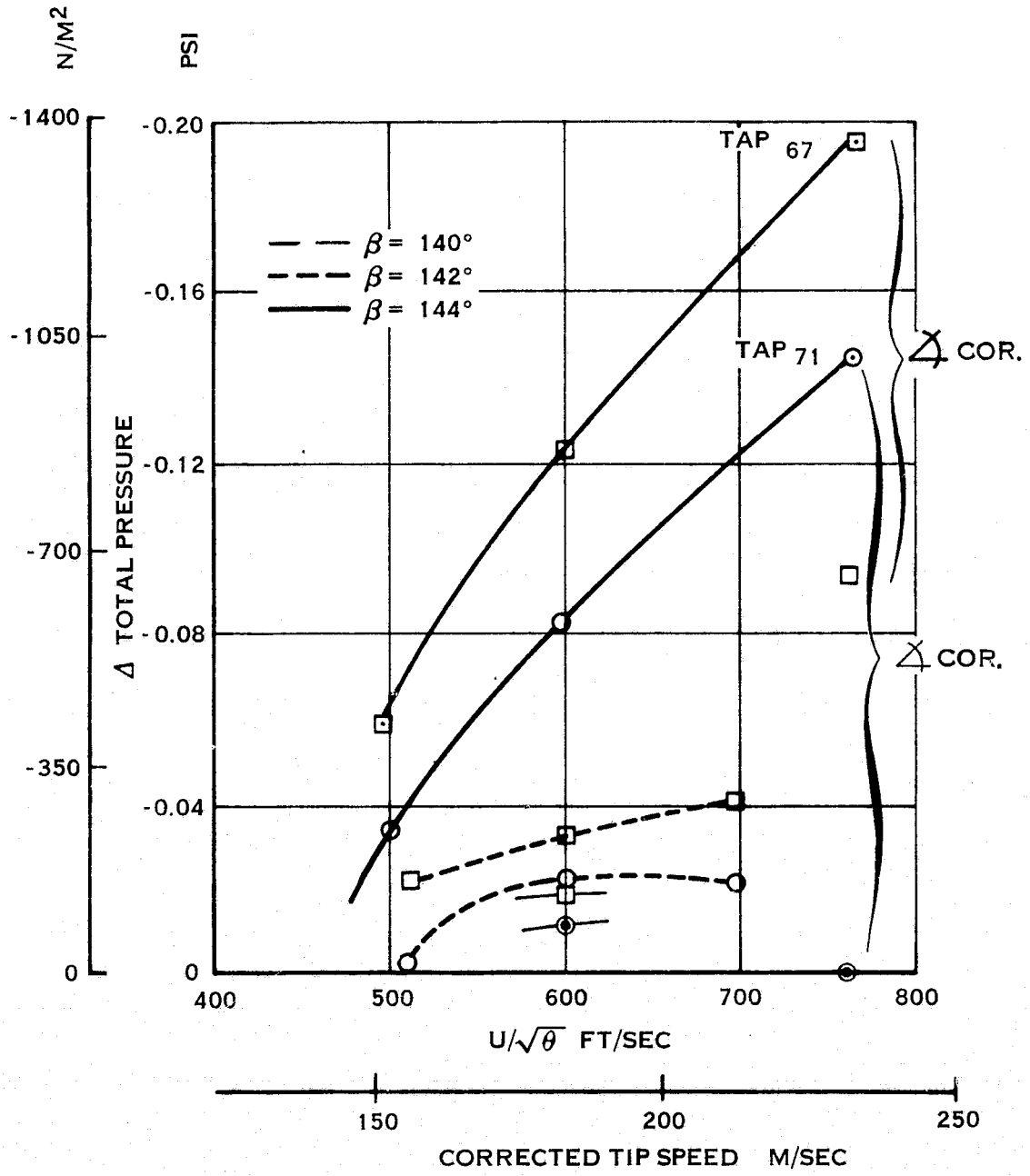

FIGURE 37. Q-FAN DEMONSTRATOR – TOTAL PRESSURE READINGS AT REVERSE INLET RAKE

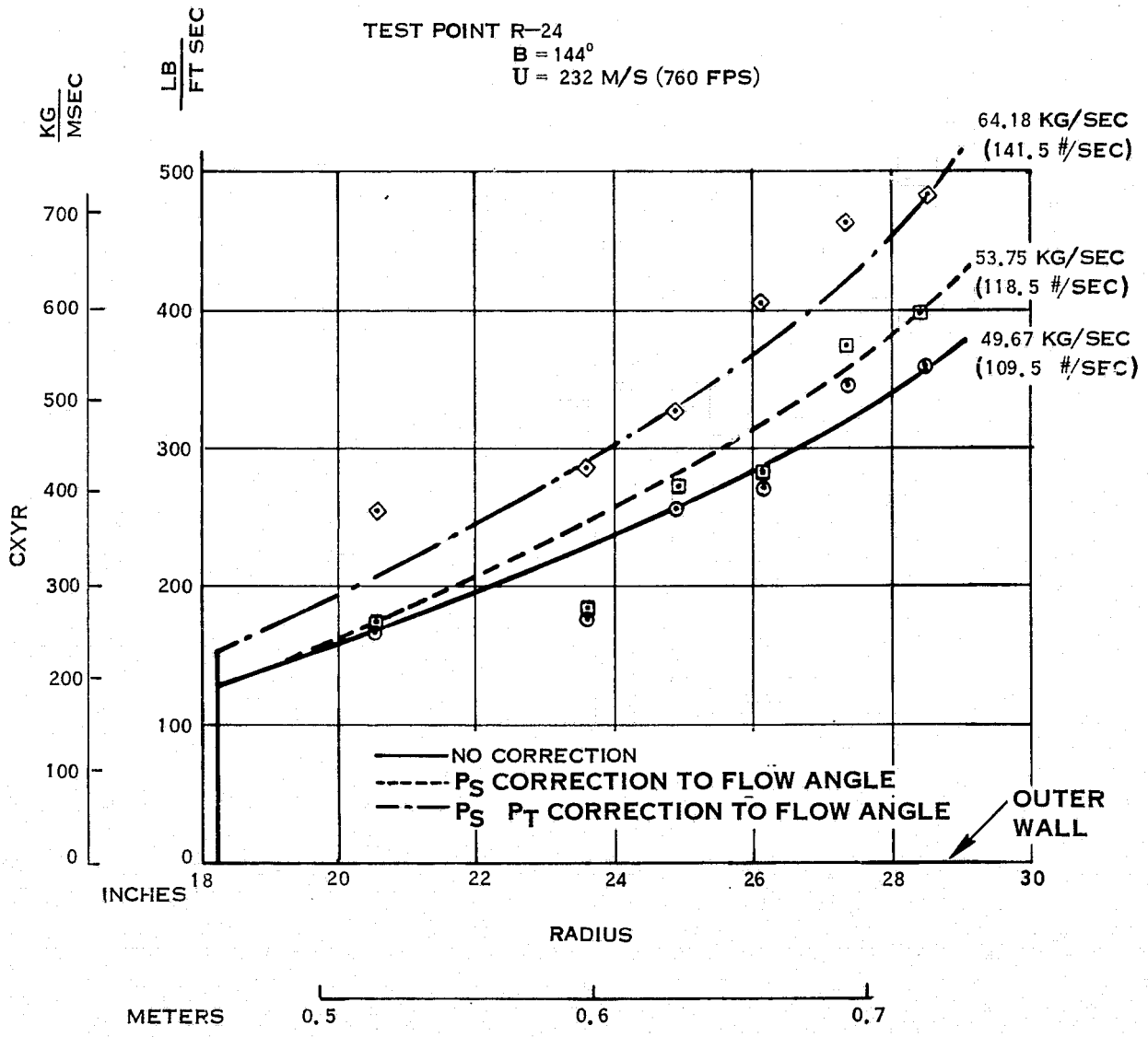

FIGURE 38. Q—FAN DEMONSTRATOR
INLET WEIGHT FLOWS WITH REVERSE INLET RAKE

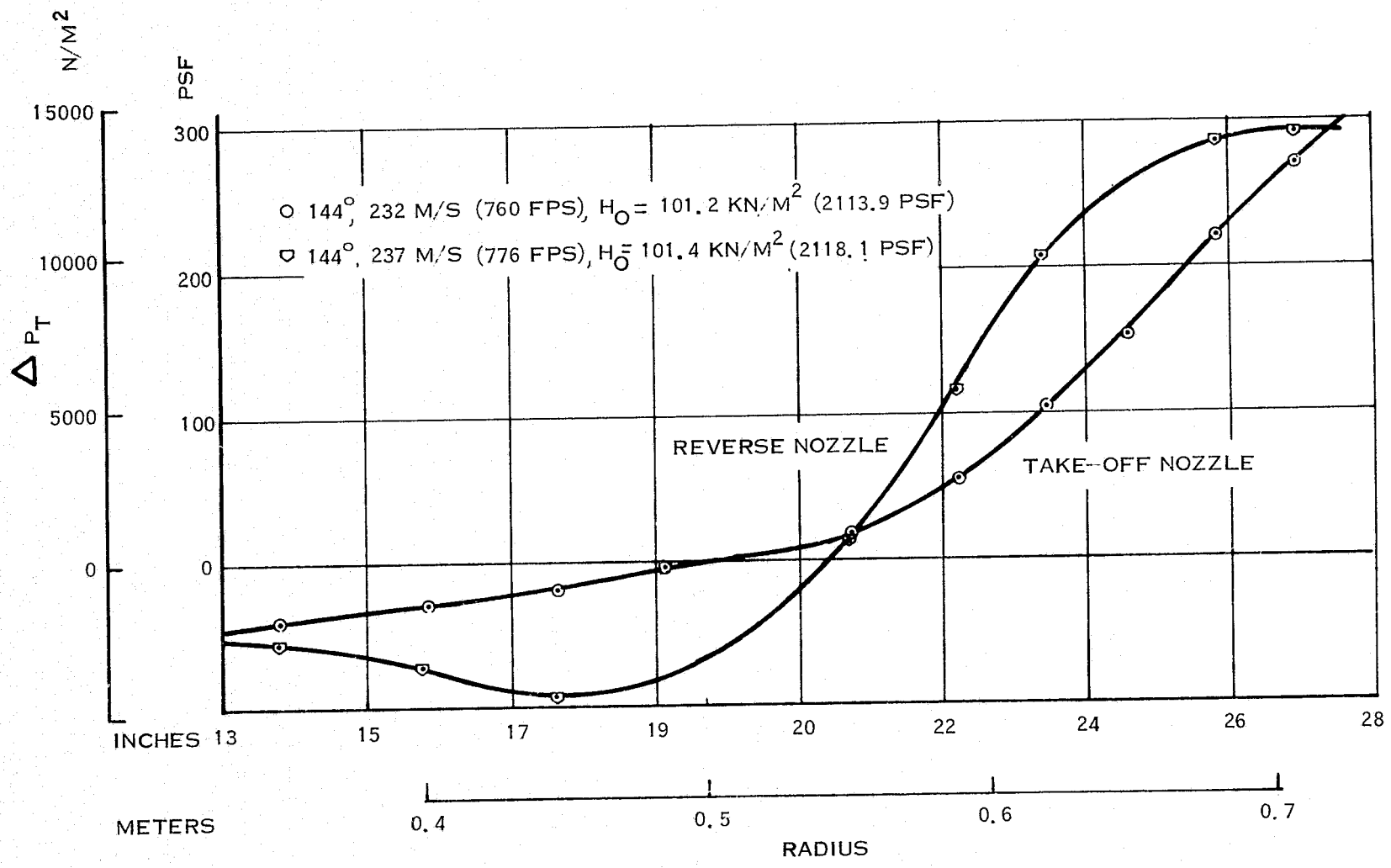

FIGURE 39. Q-FAN DEMONSTRATOR—TOTAL PRESSURE RISE BEHIND ROTOR, REVERSE NOZZLE VS TAKEOFF NOZZLE

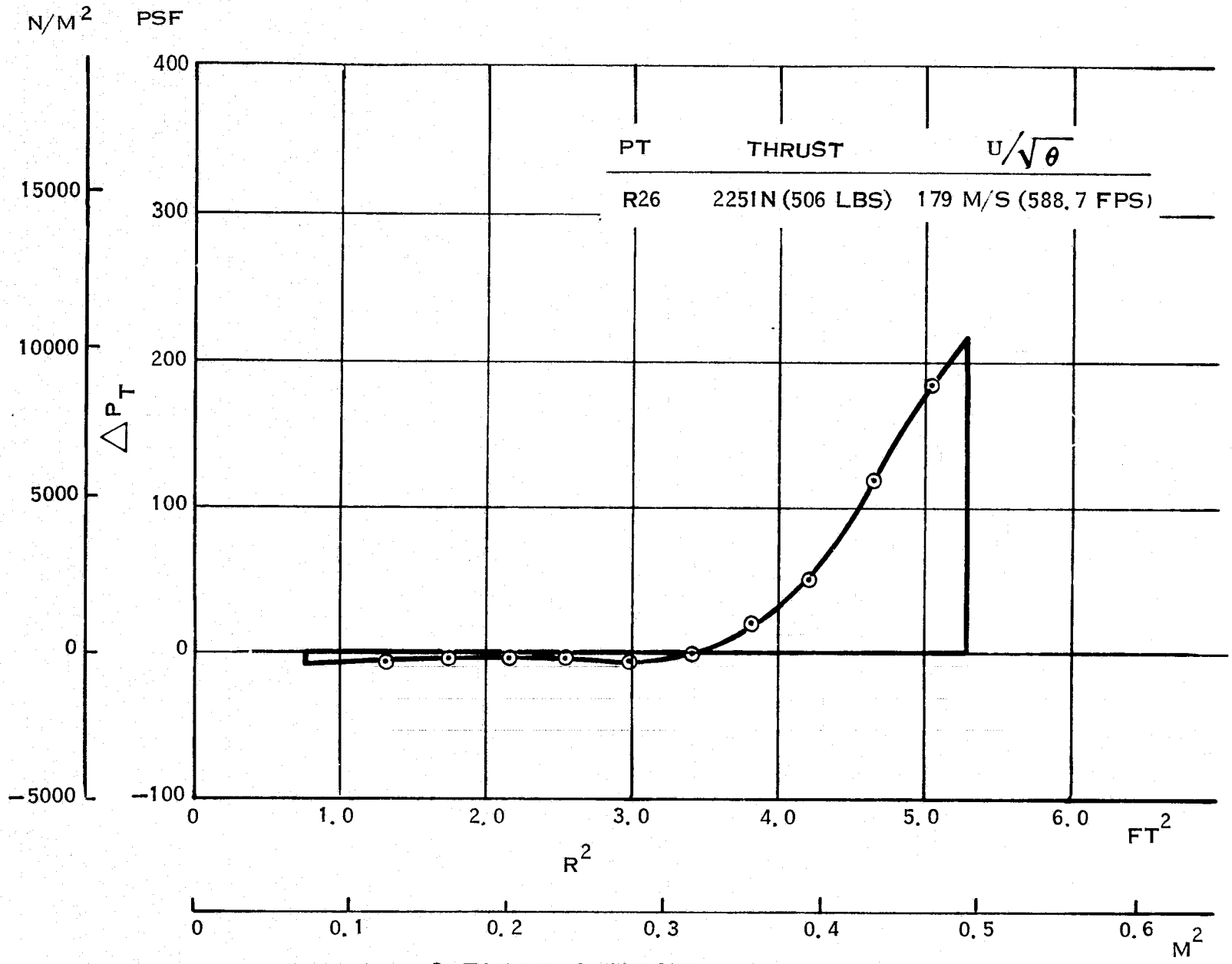

FIGURE 40. Q-FAN DEMONSTRATOR – TOTAL PRESSURE RISE BEHIND ROTOR $\beta = 140^{\circ}$

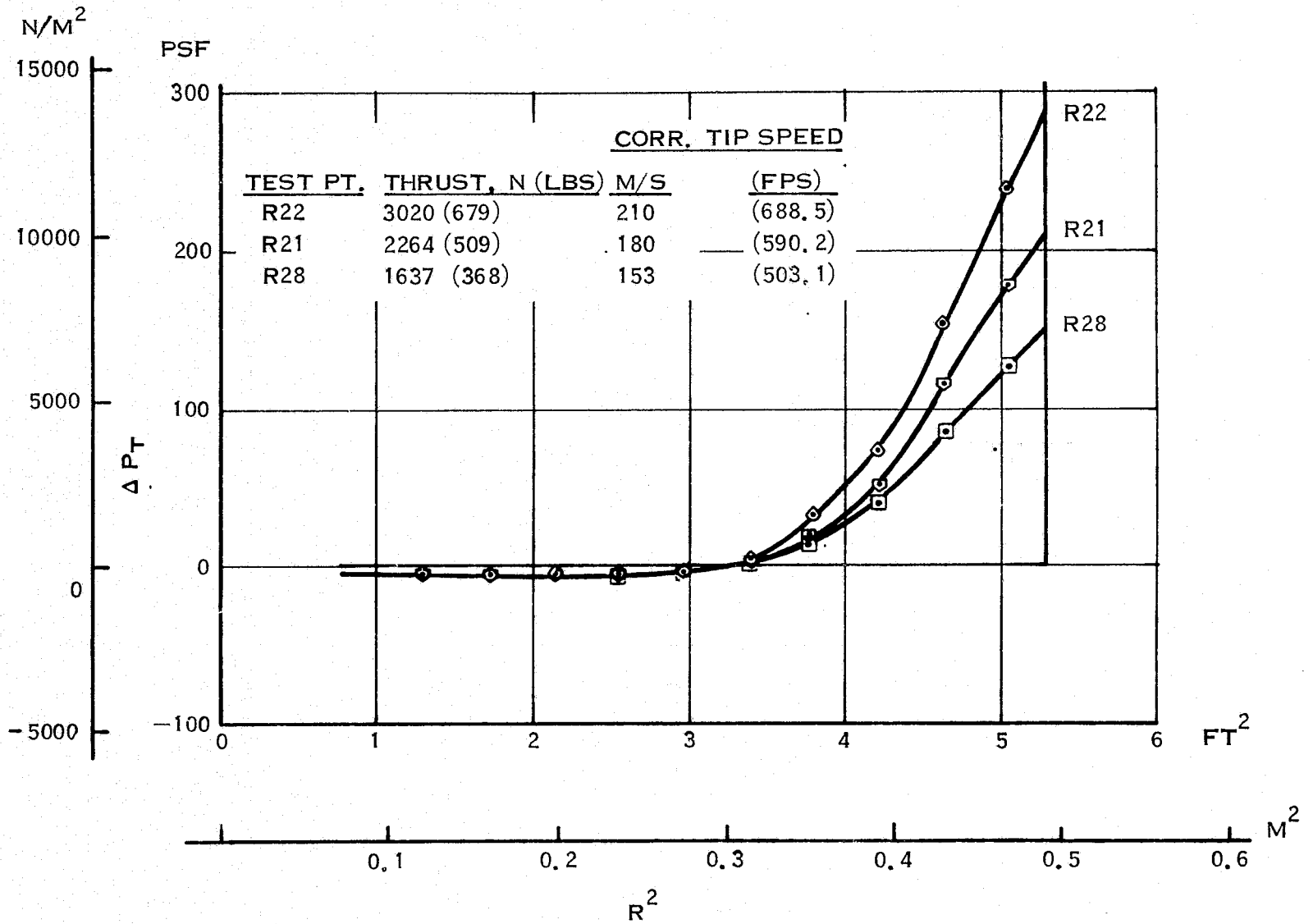

FIGURE 41. Q-FAN DEMONSTRATOR – TOTAL PRESSURE RISE BEHIND ROTOR $\beta = 142^{\circ}$

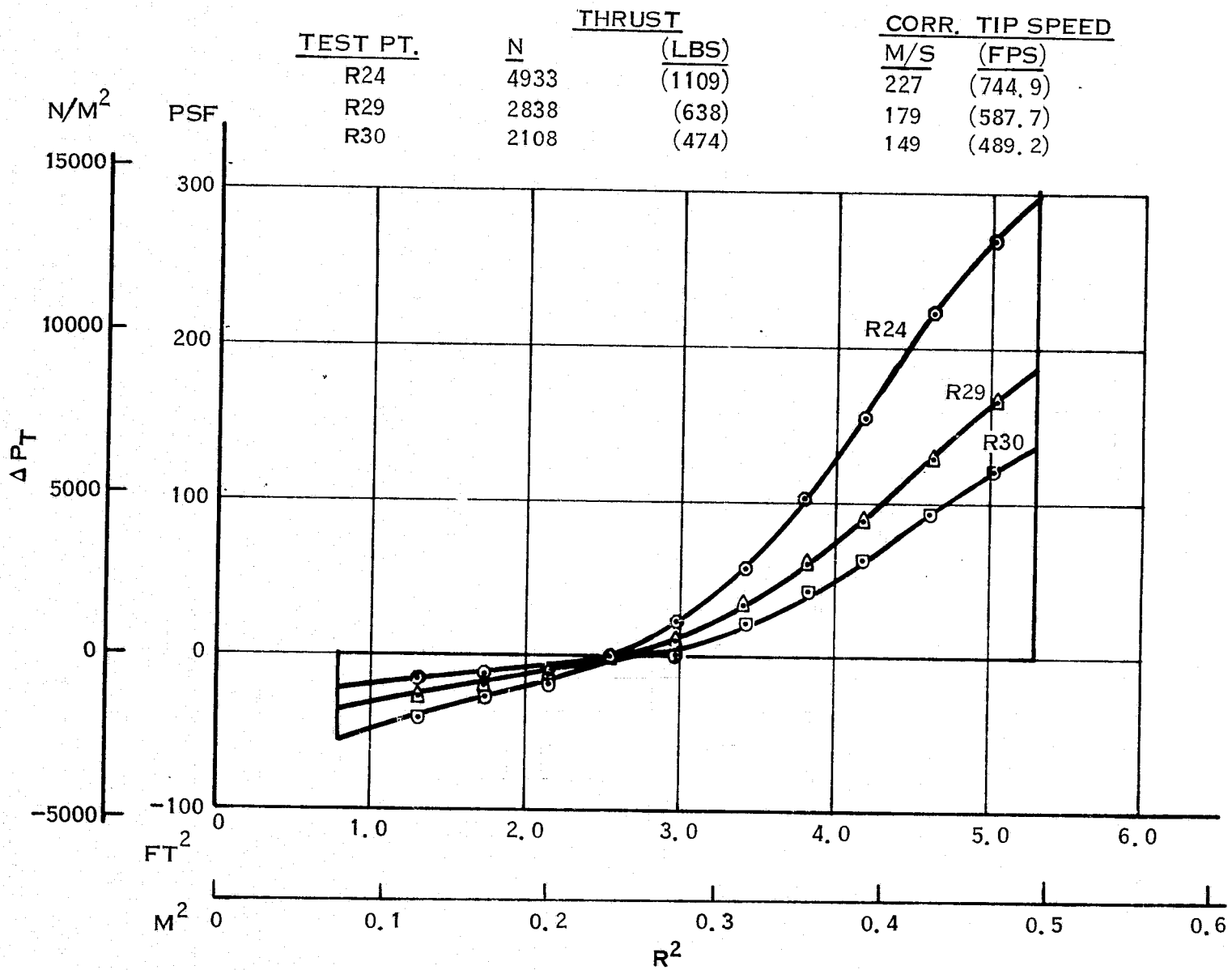

FIGURE 42. Q-FAN DEMONSTRATOR – TOTAL PRESSURE RISE BEHIND ROTOR β = 144°

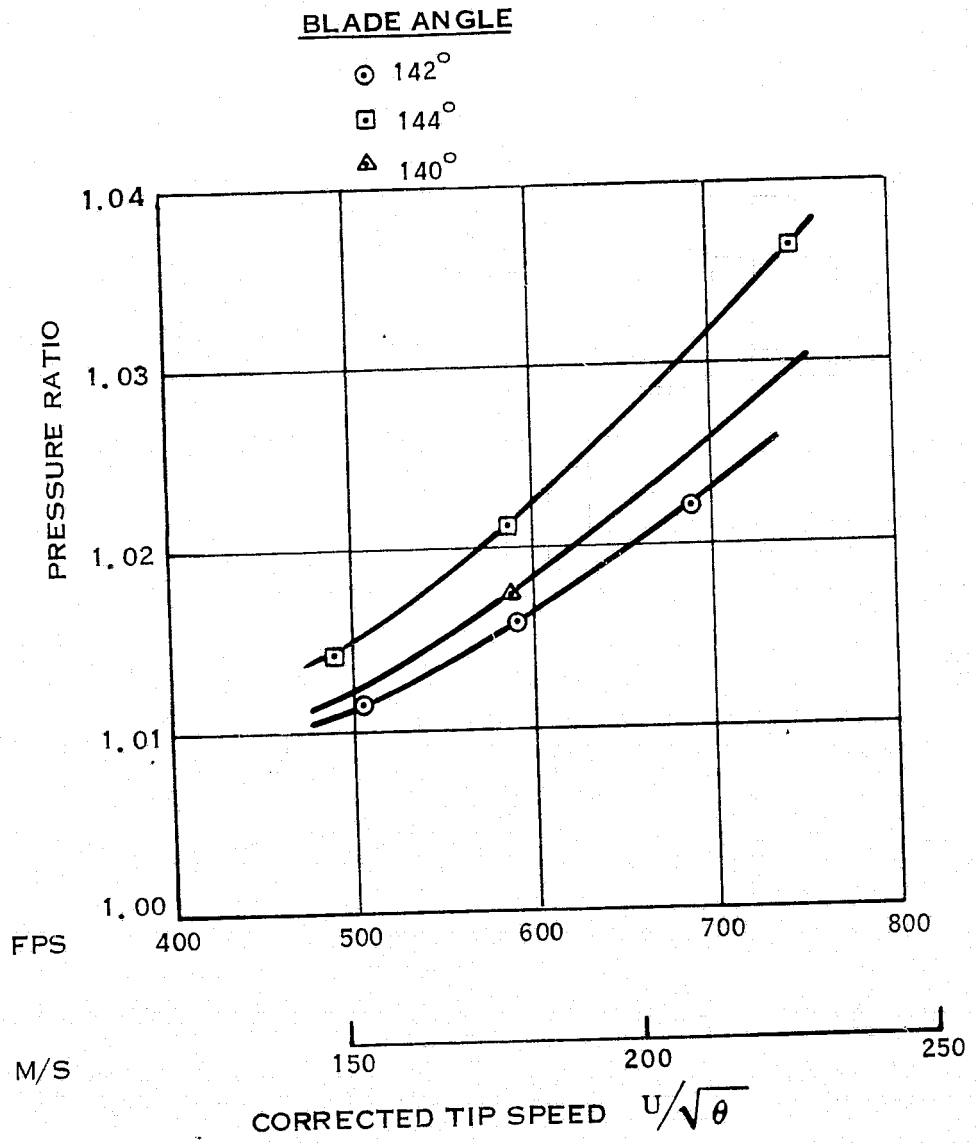

FIGURE 43. Q-FAN DEMONSTRATOR-VARIATION OF PRESSURE RATIO WITH CORRECTED TIP SPEED

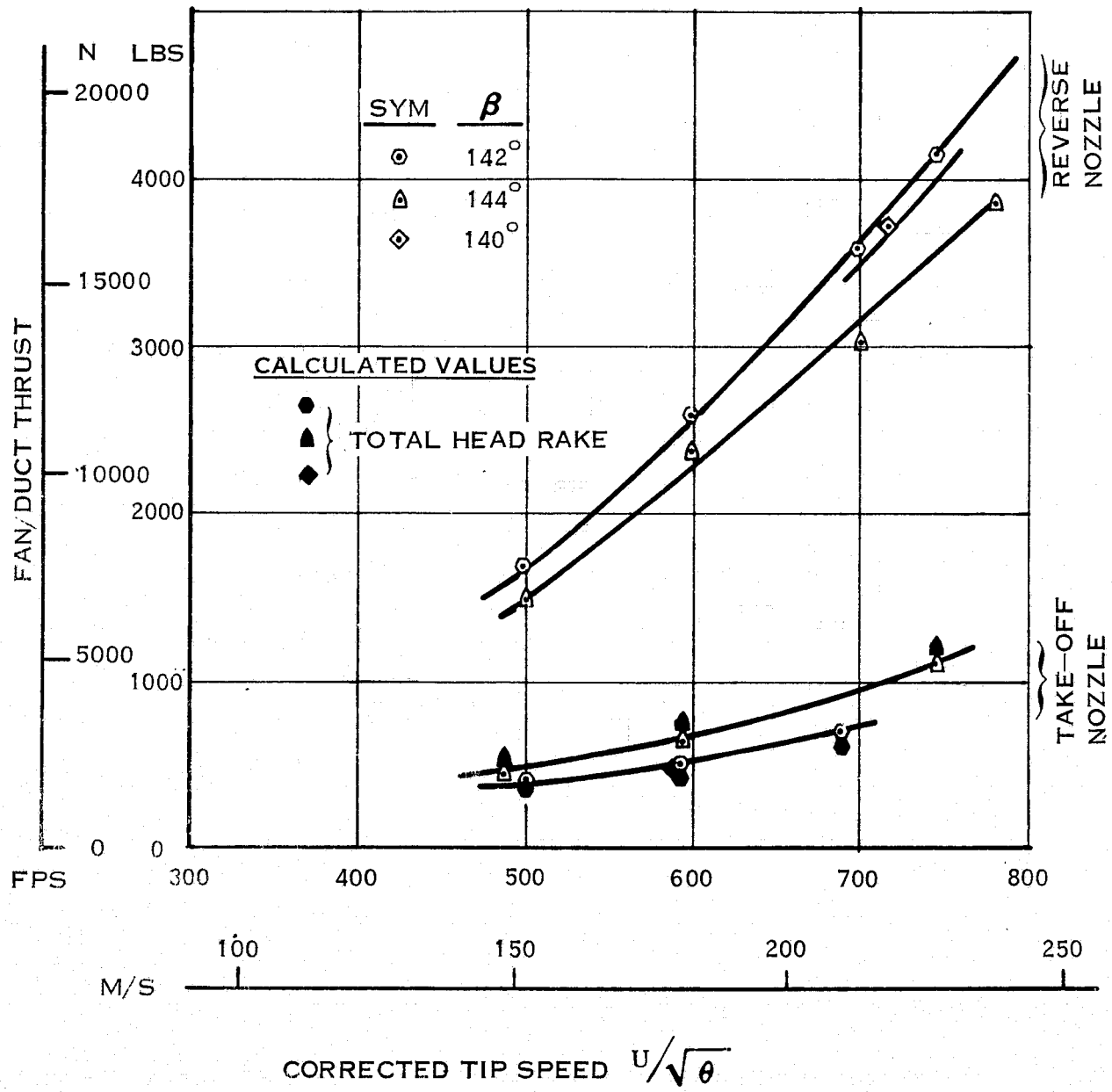

FIGURE 44. Q-FAN DEMONSTRATOR VARIATION OF THRUST WITH CORRECTED TIP SPEED

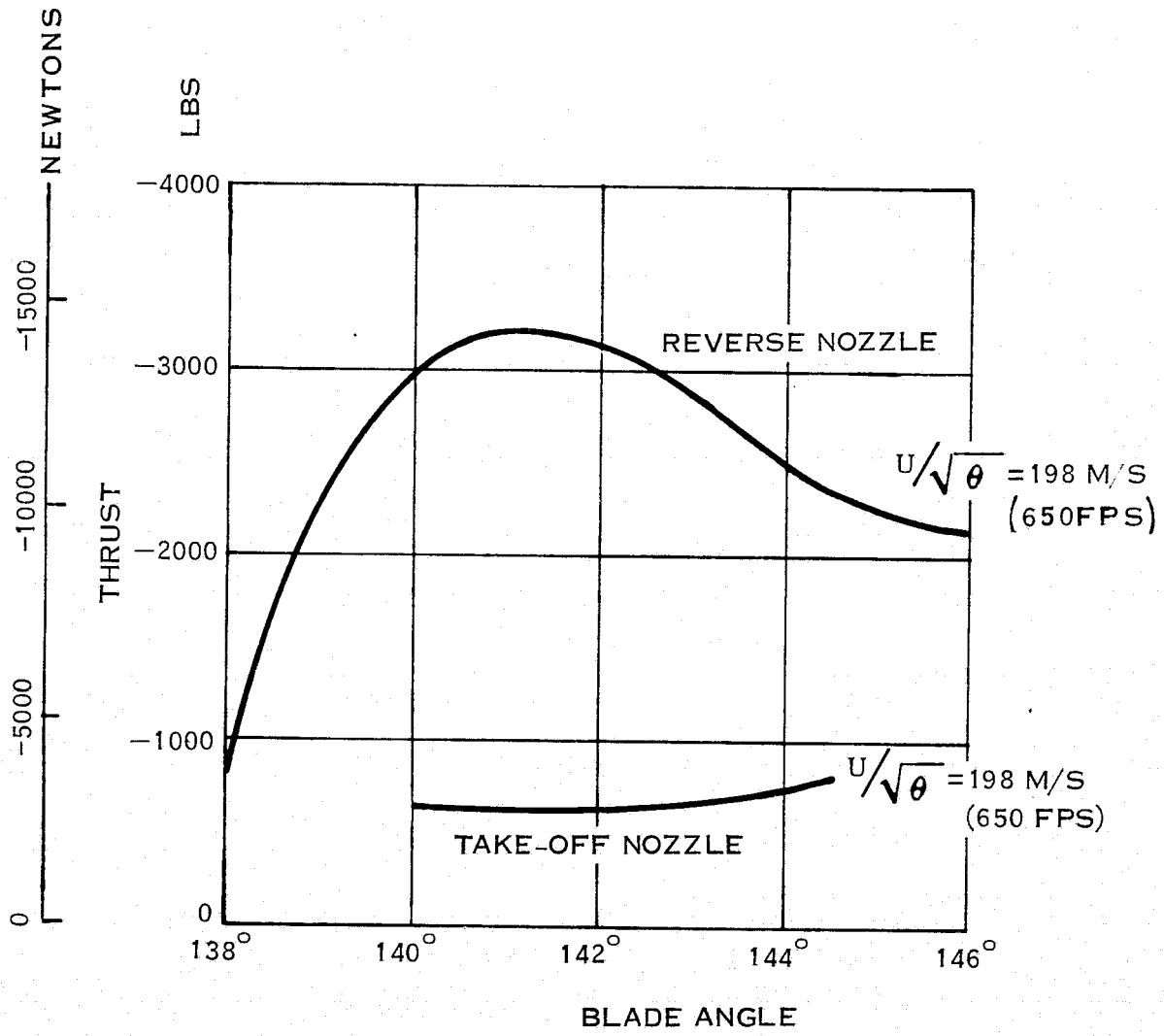

FIGURE 45. Q-FAN DEMONSTRATOR
VARIATION OF REVERSE THRUST WITH BLADE ANGLE

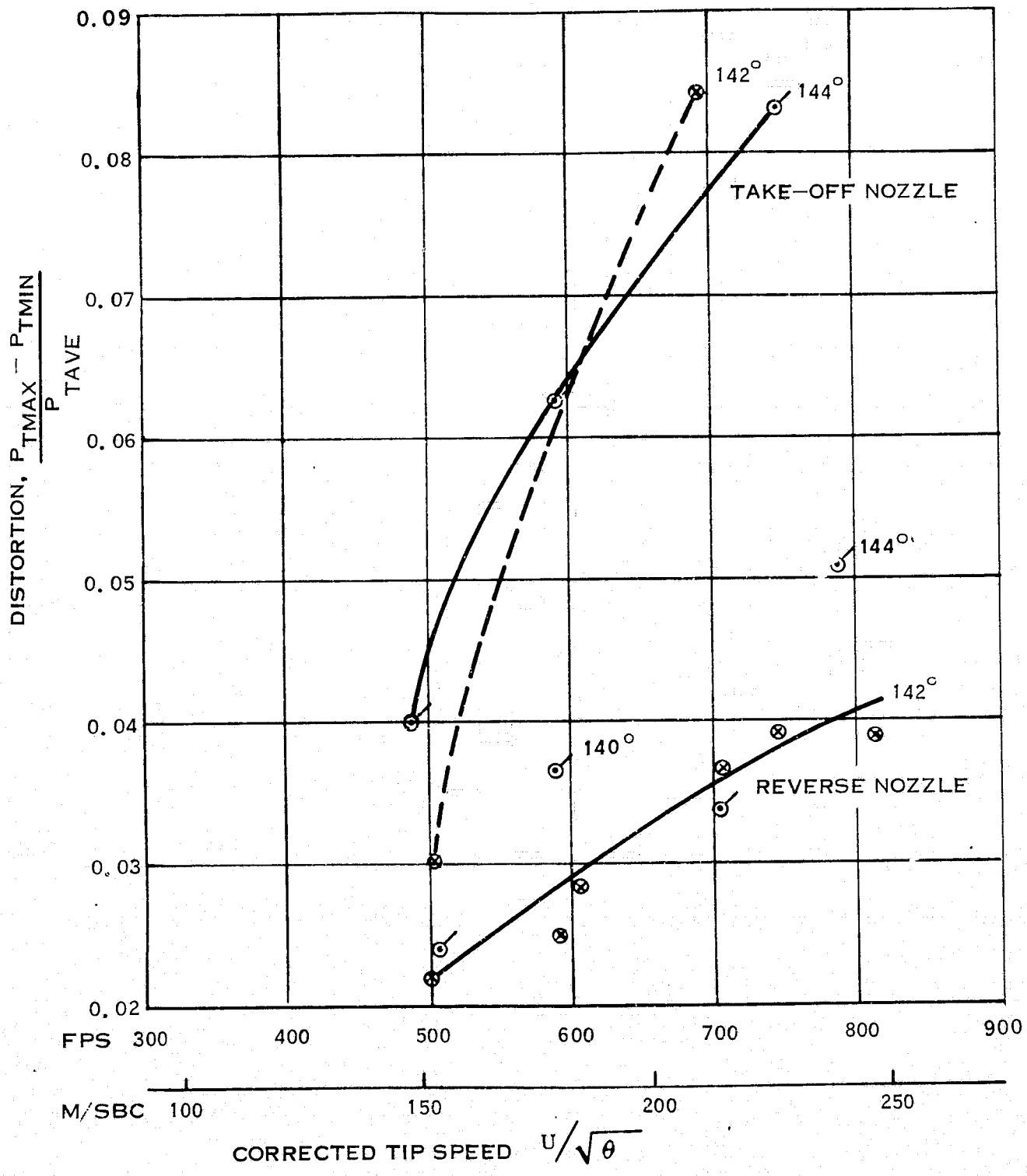

FIGURE 46. Q-FAN DEMONSTRATOR-COMPRESSOR FACE DISTORTION

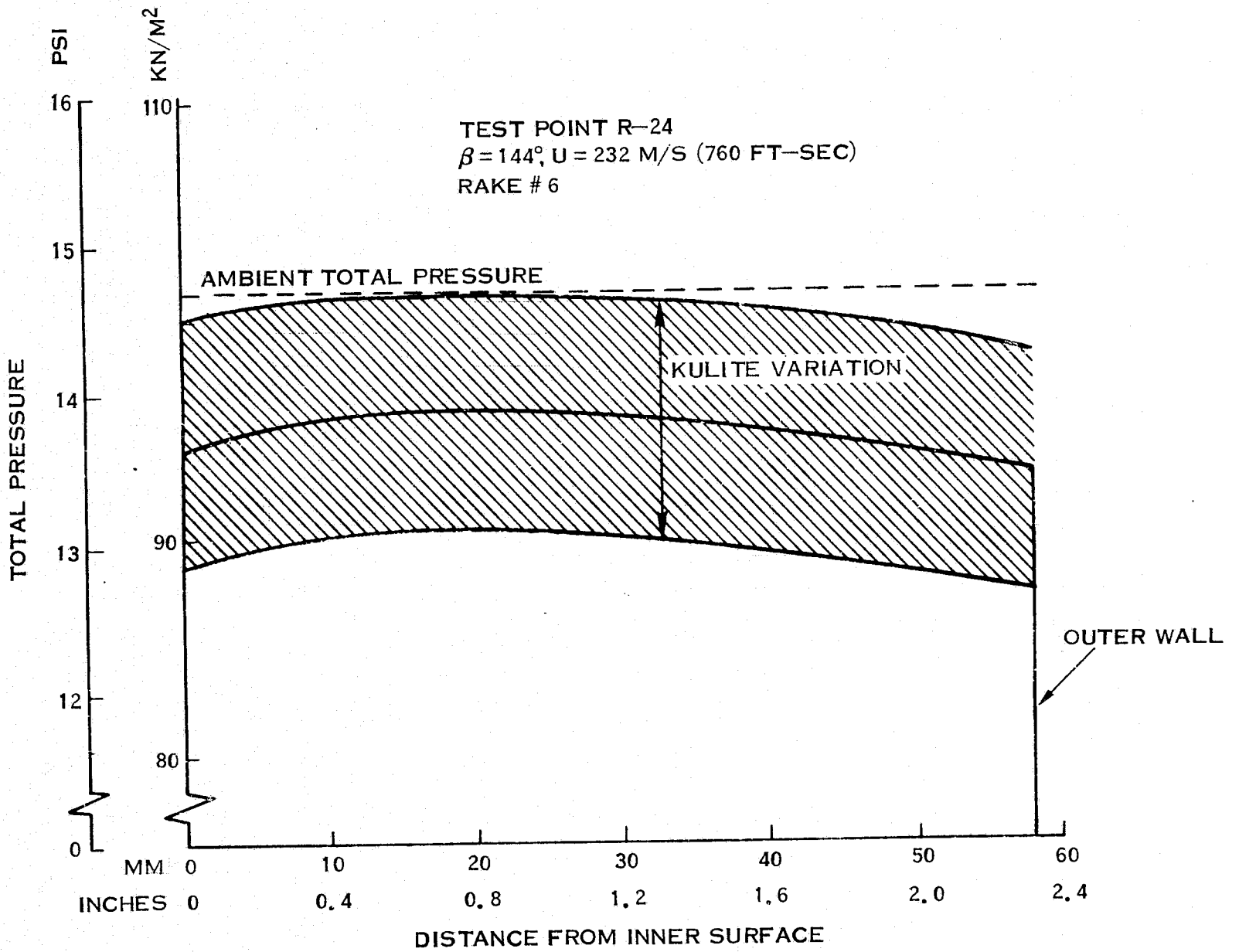

FIGURE 47. Q–FAN DEMONSTRATOR, TEST POINT R–24 INSTANTANEOUS TOTAL PRESSURE VARIATION

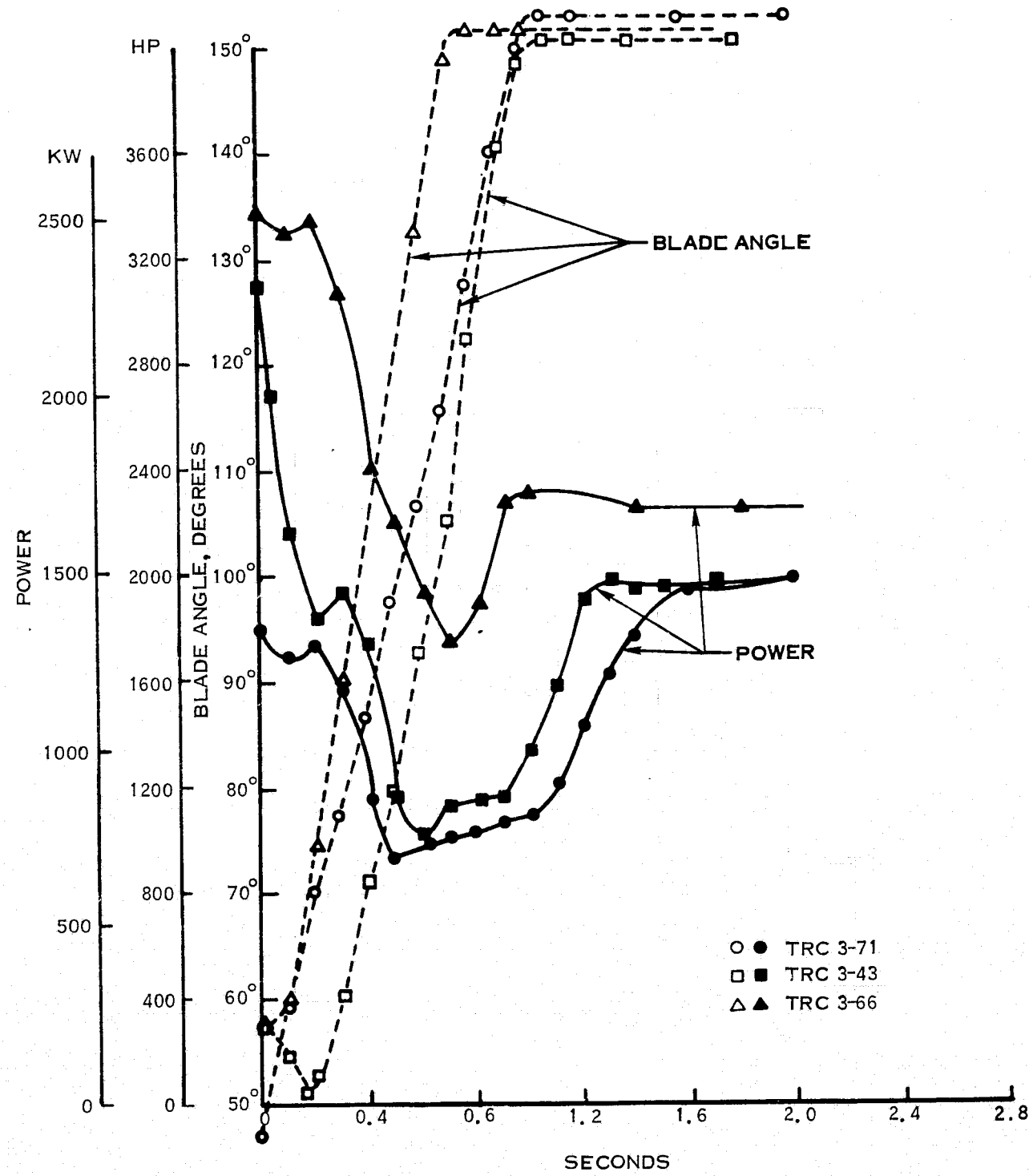

FIGURE 48. Q-FAN DEMONSTRATOR — VARIATION OF POWER AND BLADE ANGLE WITH TIME

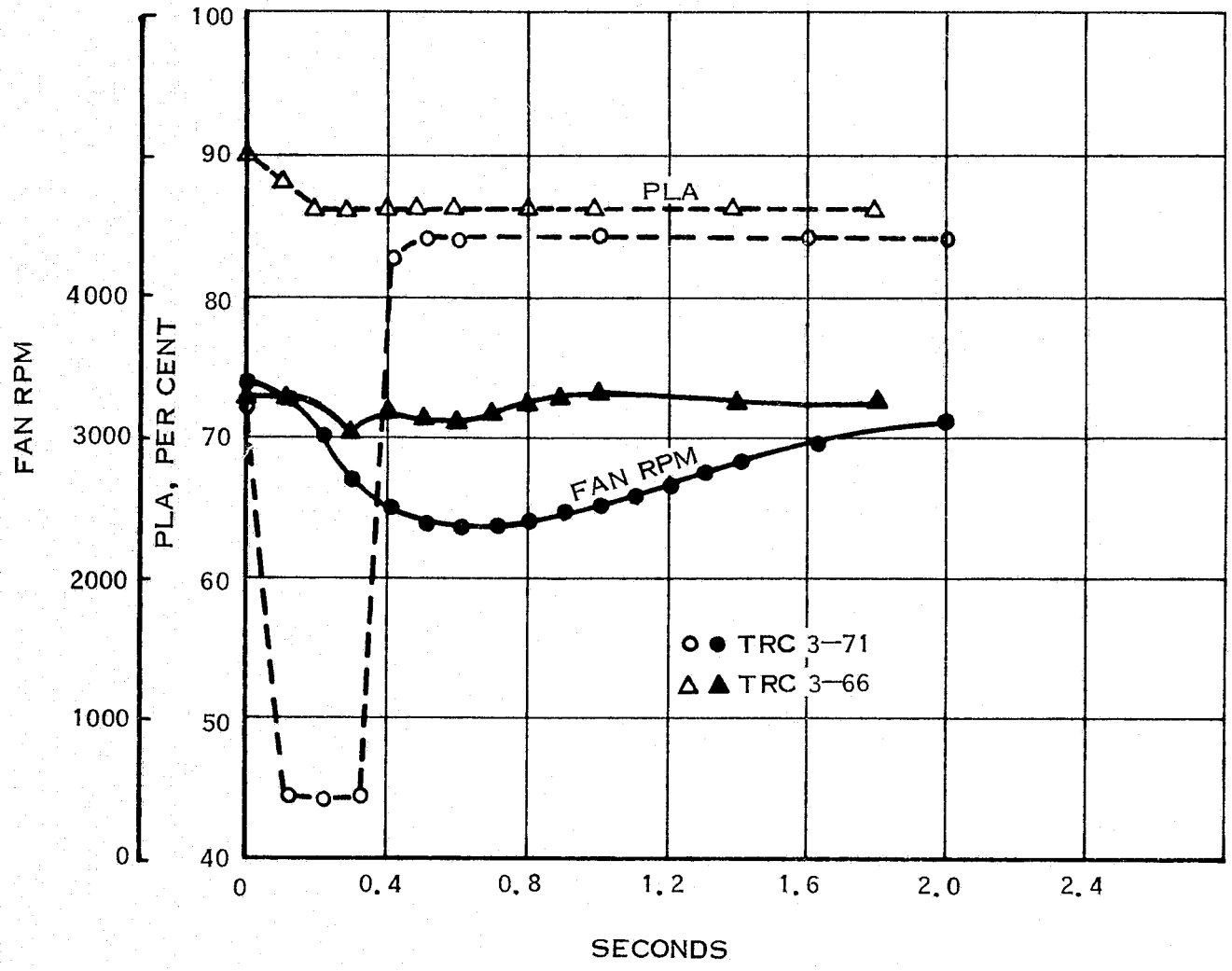

FIGURE 49. Q–FAN DEMONSTRATOR – VARIATION OF FAN RPM AND PLA WITH TIME

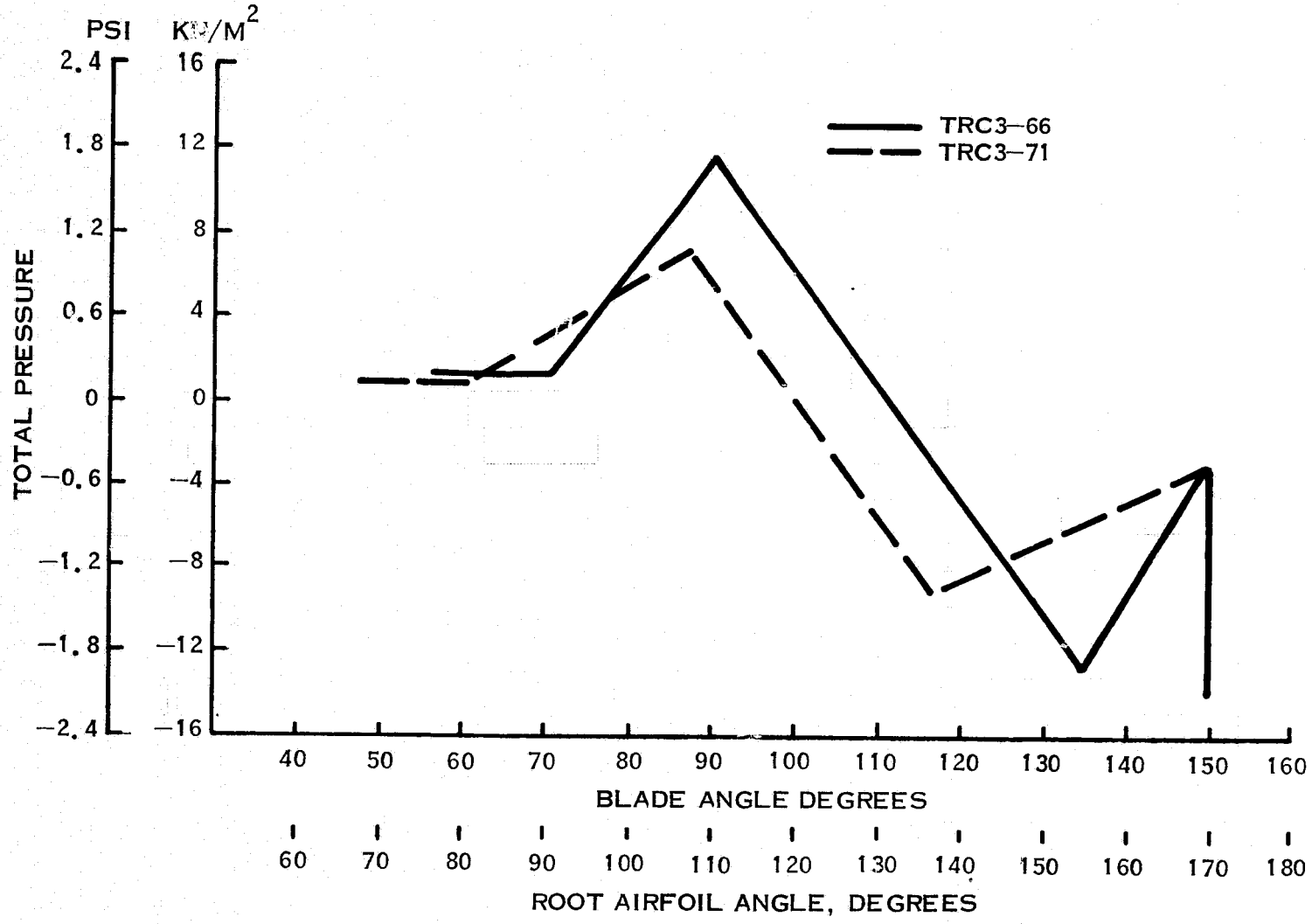

FIGURE 50. Q−FAN DEMONSTRATOR VARIATION OF PRESSURE WITH BLADE ANGLE

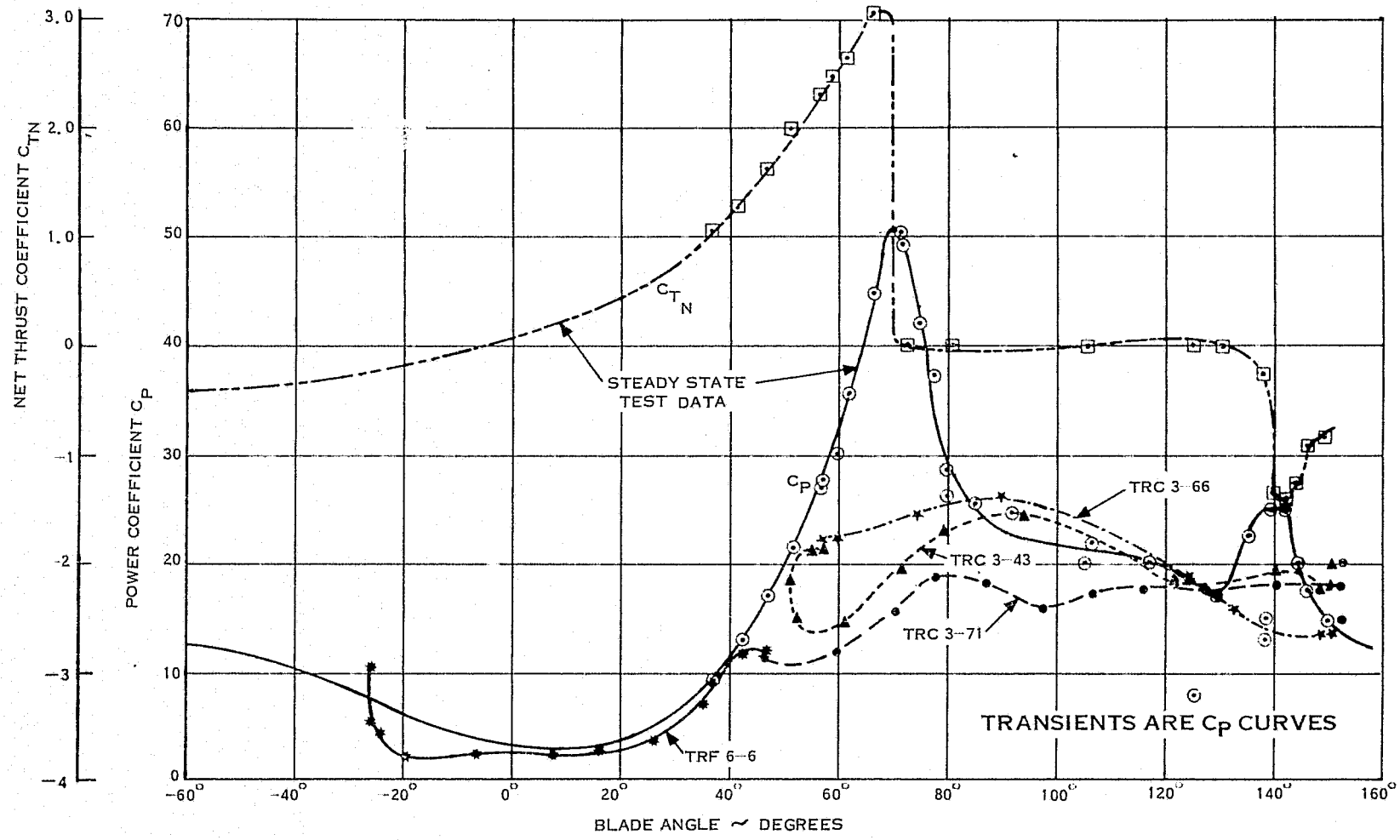

FIGURE 51. Q-FAN DEMONSTRATOR - COMPARISON OF STEADY STATE AND TRANSIENT PERFORMANCE DATA

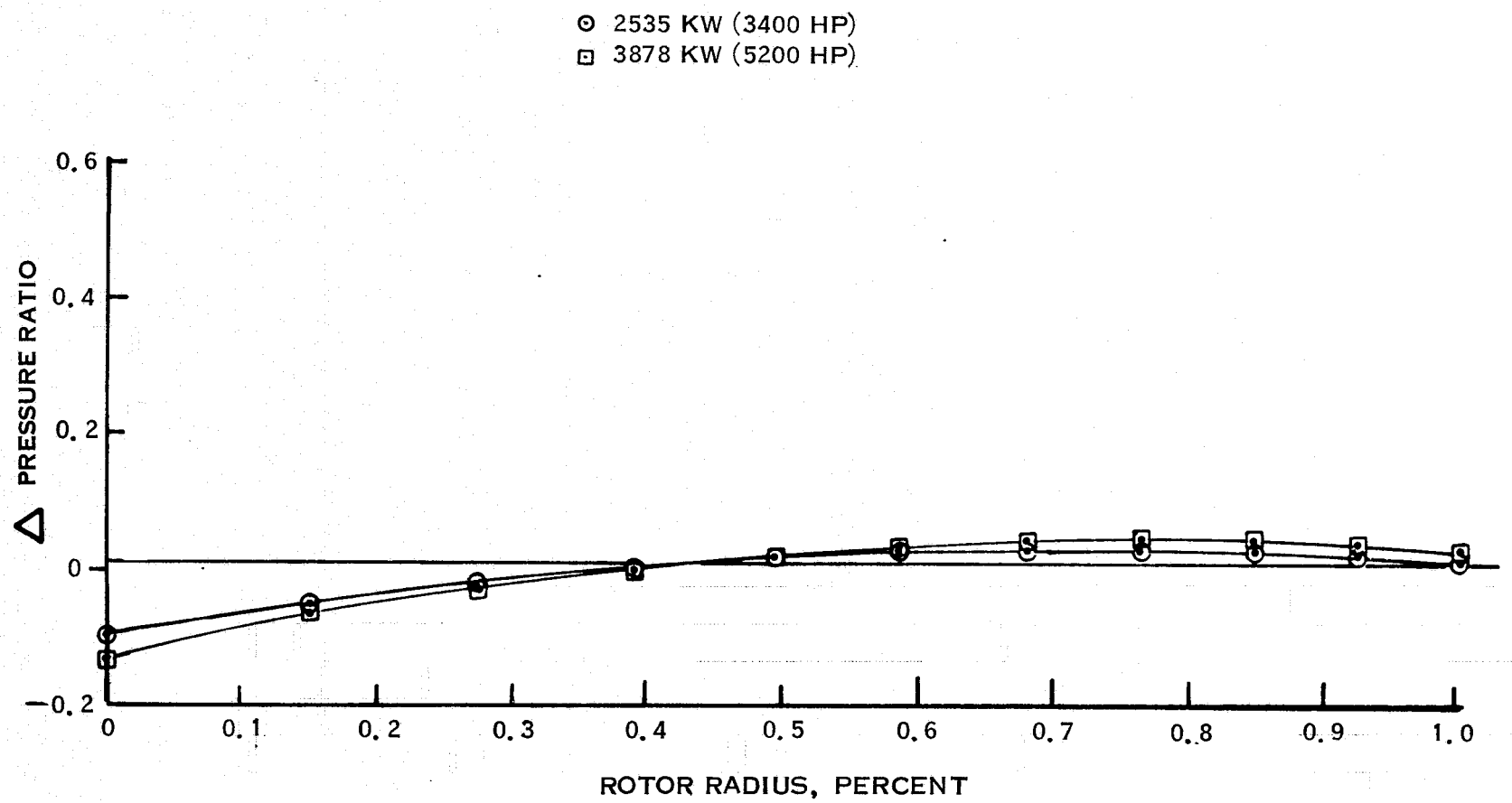

FIGURE 52. Q-FAN DEMONSTRATOR – DISTRIBUTION OF PRESSURE RATIO WITH BLADE RADIUS

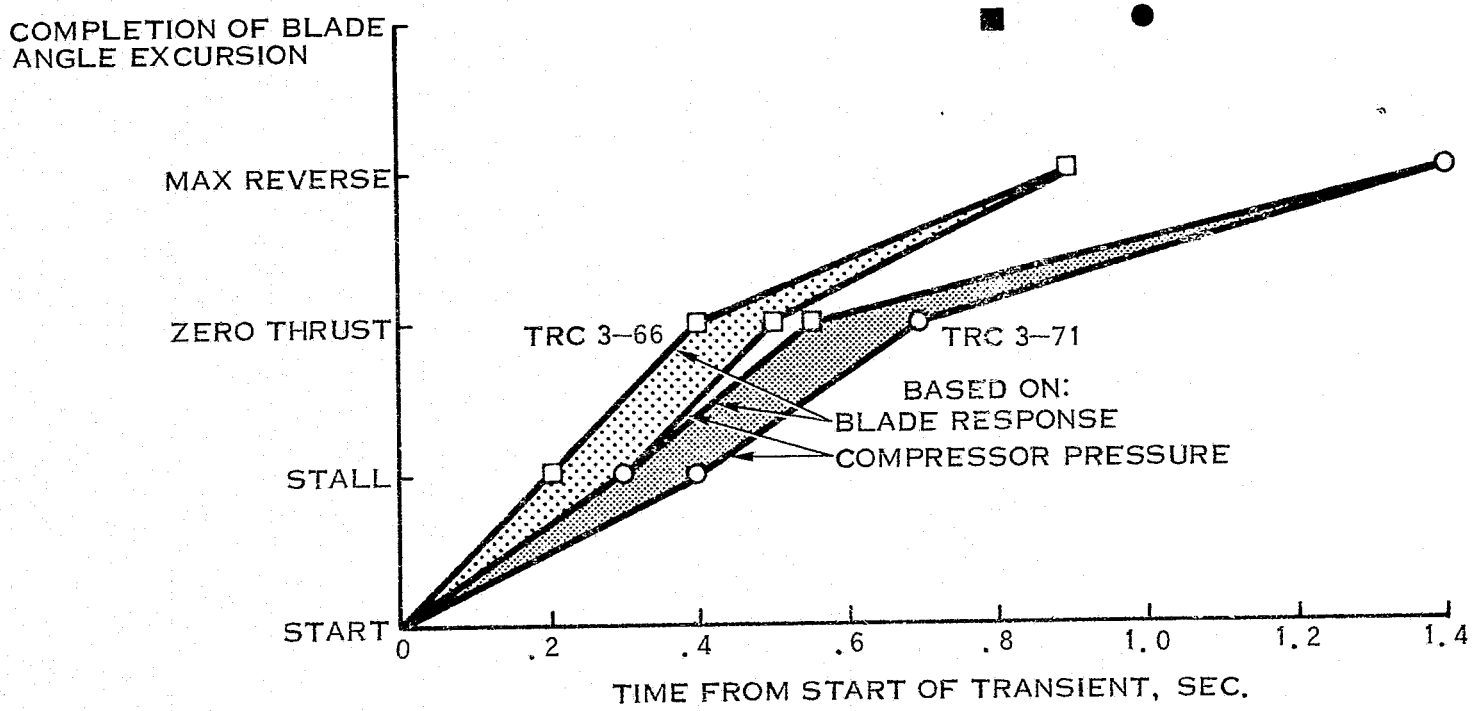

FIGURE 53. Q–FAN DEMONSTRATOR TIME REQUIRED FOR TRANSIENT

REVERSE THRU FEATHER TRANSIENTS

RESPONSE IS TIME FROM FORWARD TO REVERSE THRUST
THRUST SETTING LEVER 70% TO 0%

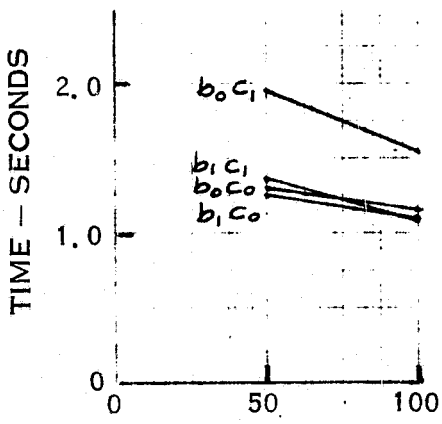

FACTOR A
BLADE ANGLE RATE
BELOW 72° – DEG/SEC

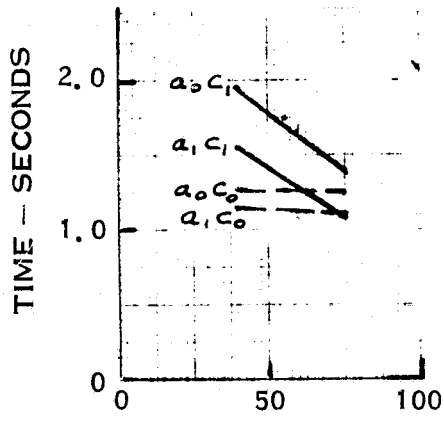

FACTOR B
PLA RESET ANGLE –
DEGREES

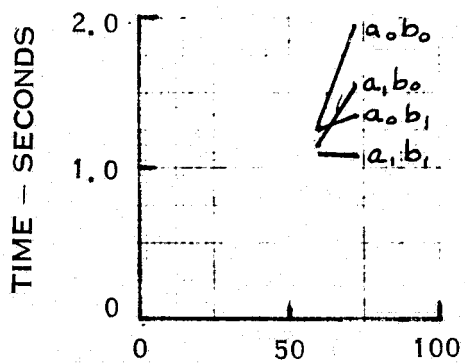

FACTOR C
BLADE ANGLE FOR
COMPLETION OF PLA
RESET – DEGREES

FIGURE 56. Q–FAN DEMONSTRATOR TIME RESPONSE – SCHEDULE 1

REVERSE THRU FEATHER TRANSIENTS

RESPONSE IS TIME FROM FORWARD TO REVERSE THRUST
THRUST SETTING LEVER 70% TO 0%

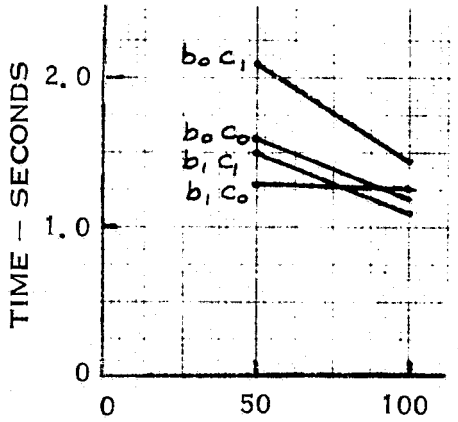

FACTOR A
BLADE ANGLE RATE
BELOW 72° – DEG/SEC

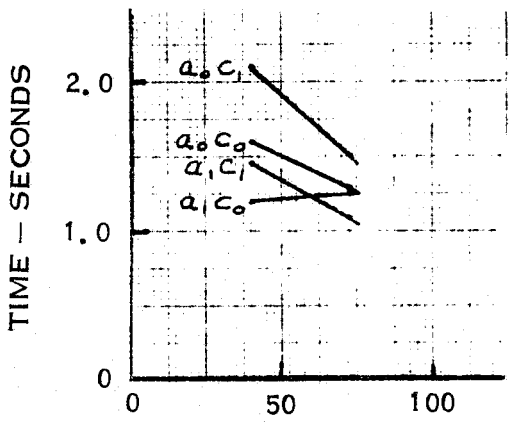

FACTOR B
PLA RESET ANGLE –
DEGREES

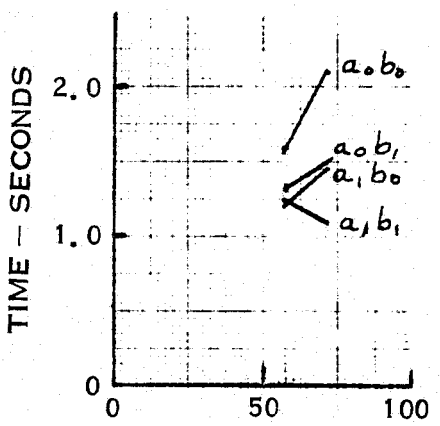

FACTOR C
BLADE ANGLE FOR
COMPLETION OF PLA
RESET – DEGREES

FIGURE 57. Q–FAN DEMONSTRATOR TIME RESPONSE – SCHEDULE 2

REVERSE THRU FEATHER TRANSIENTS

RESPONSE IS TIME FROM FORWARD TO REVERSE THRUST
THRUST SETTING LEVER 70% TO 0%

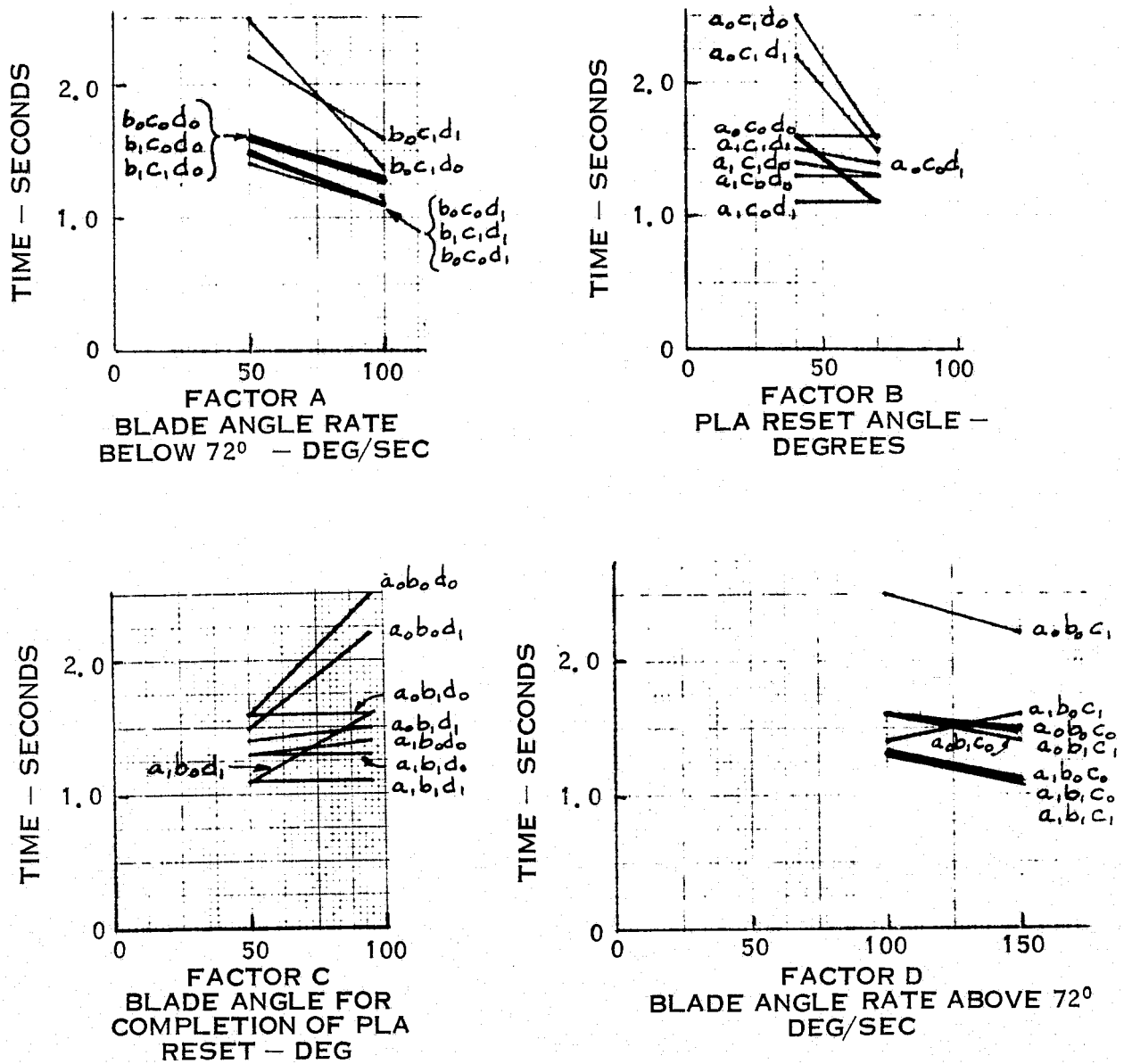

FIGURE 58. Q–FAN DEMONSTRATOR TIME RESPONSE – SCHEDULE 3.
TSL RANGE 70% TO 0%

REVERSE THRU FEATHER TRANSIENTS

RESPONSE IS TIME FROM FORWARD TO REVERSE THRUST
THRUST SETTING LEVER 90% TO 0%

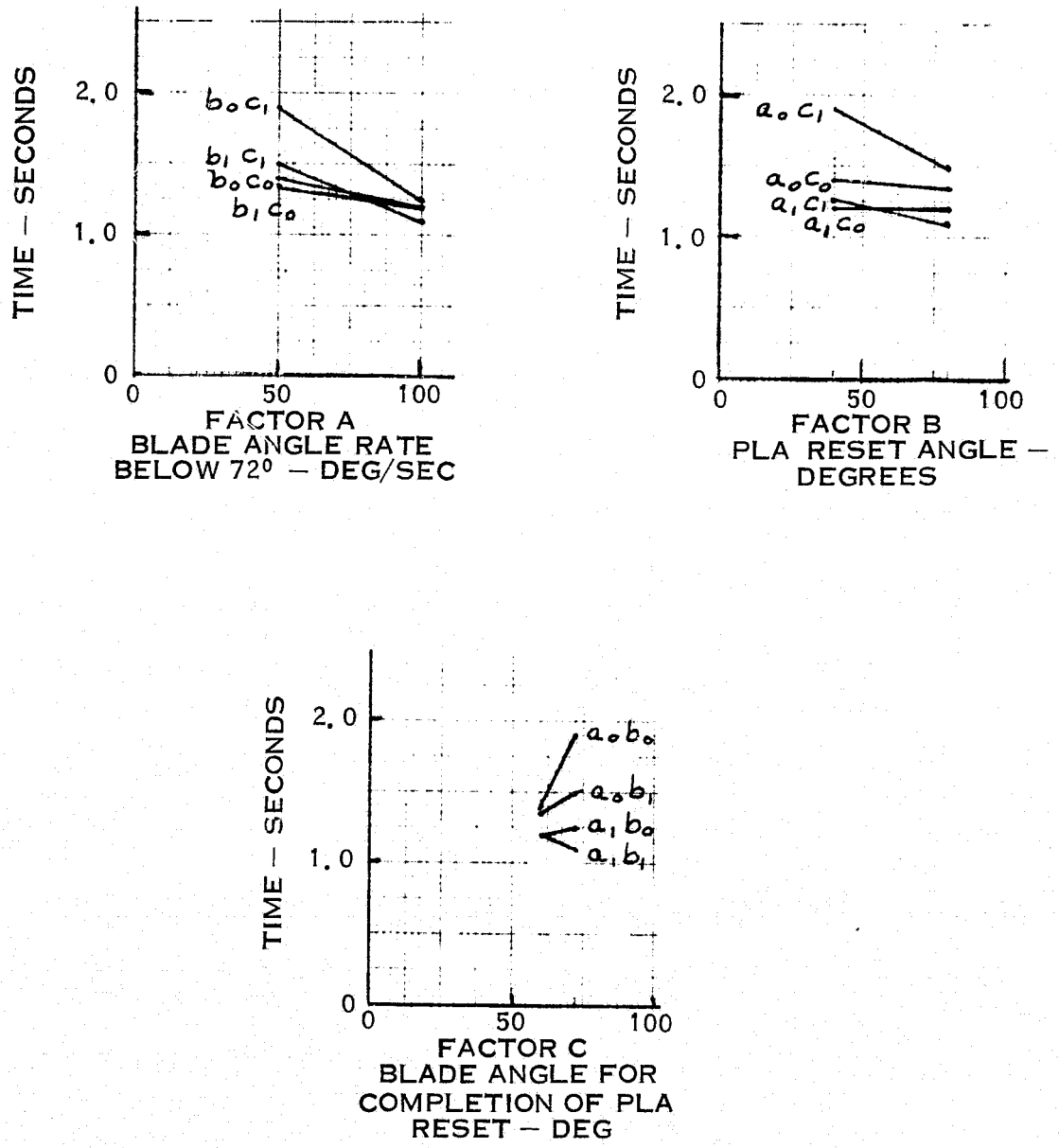

FIGURE 59. Q–FAN DEMONSTRATOR TIME RESPONSE – SCHEDULE 3, TSL RANGE 90% TO 0%

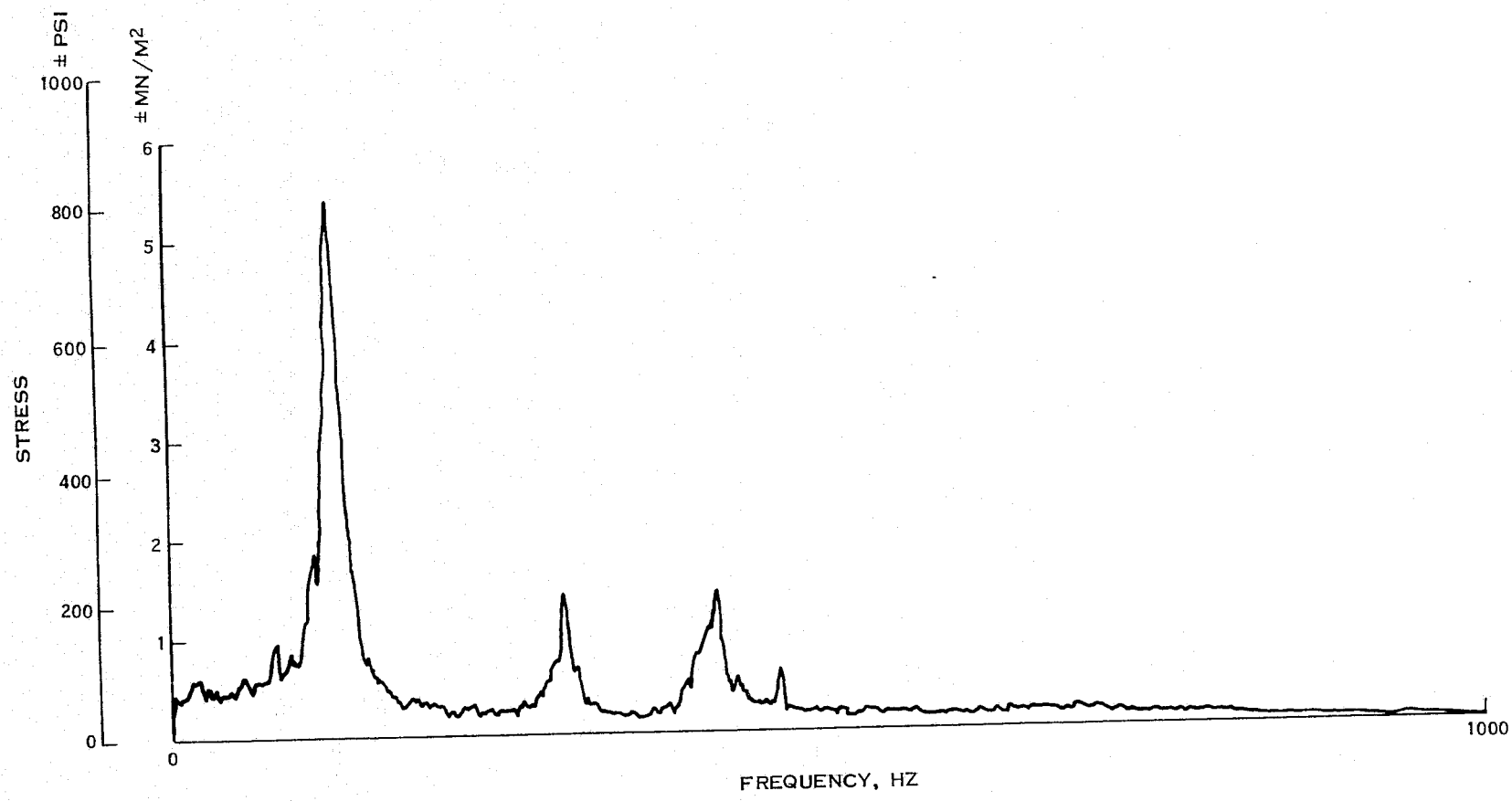

FIGURE 60. Q-FAN DEMONSTRATOR, TYPICAL SPECTRAL PLOT, CHANNEL 3-4.

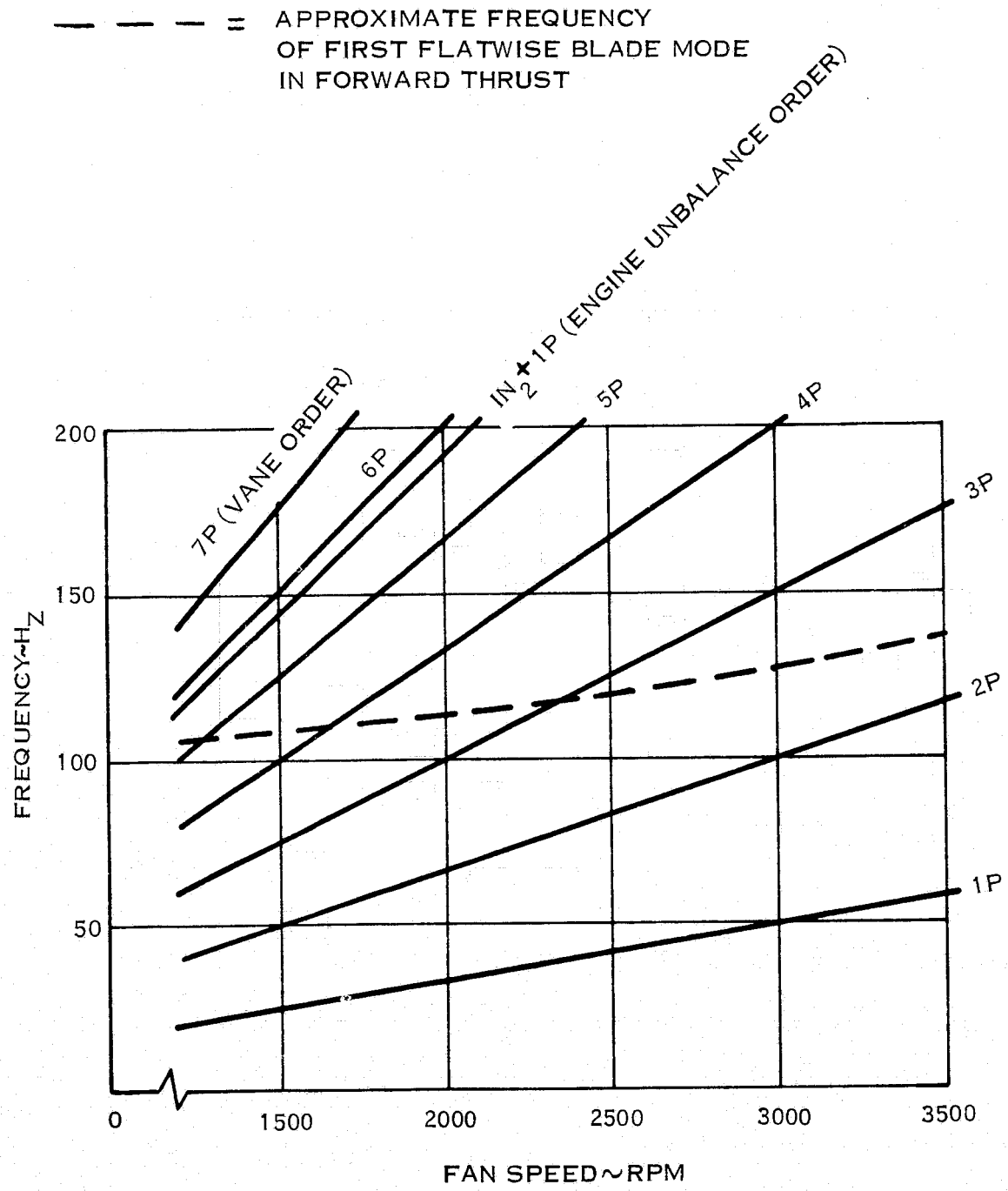

FIGURE 61. Q-FAN DEMONSTRATOR-CRITICAL SPEED DIAGRAM

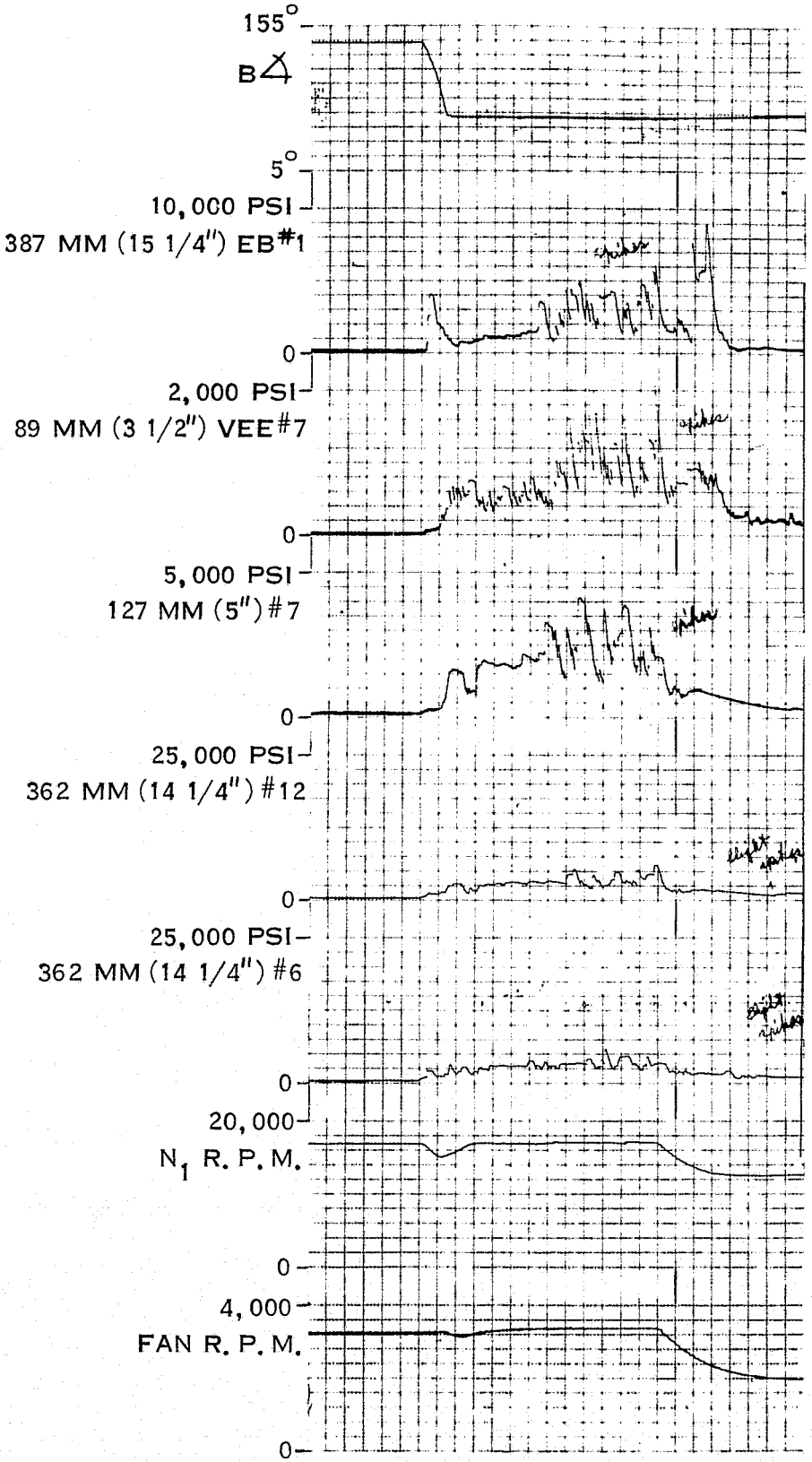

FIGURE 62. Q–FAN DEMONSTRATOR–SANBORN TRACE, TEST POINT TRF 6-3

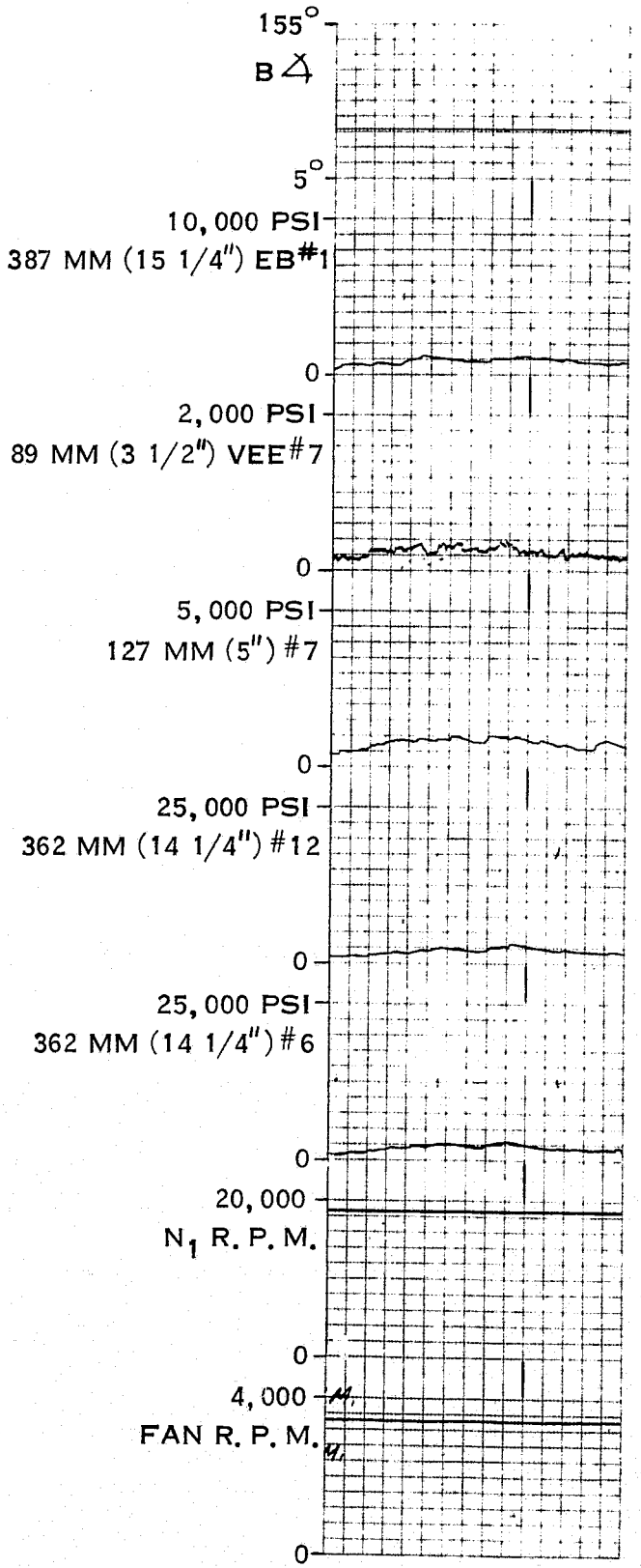

FIGURE 63. Q-FAN DEMONSTRATOR-SANBORN TRACE, TEST POINT TRC3-5.3

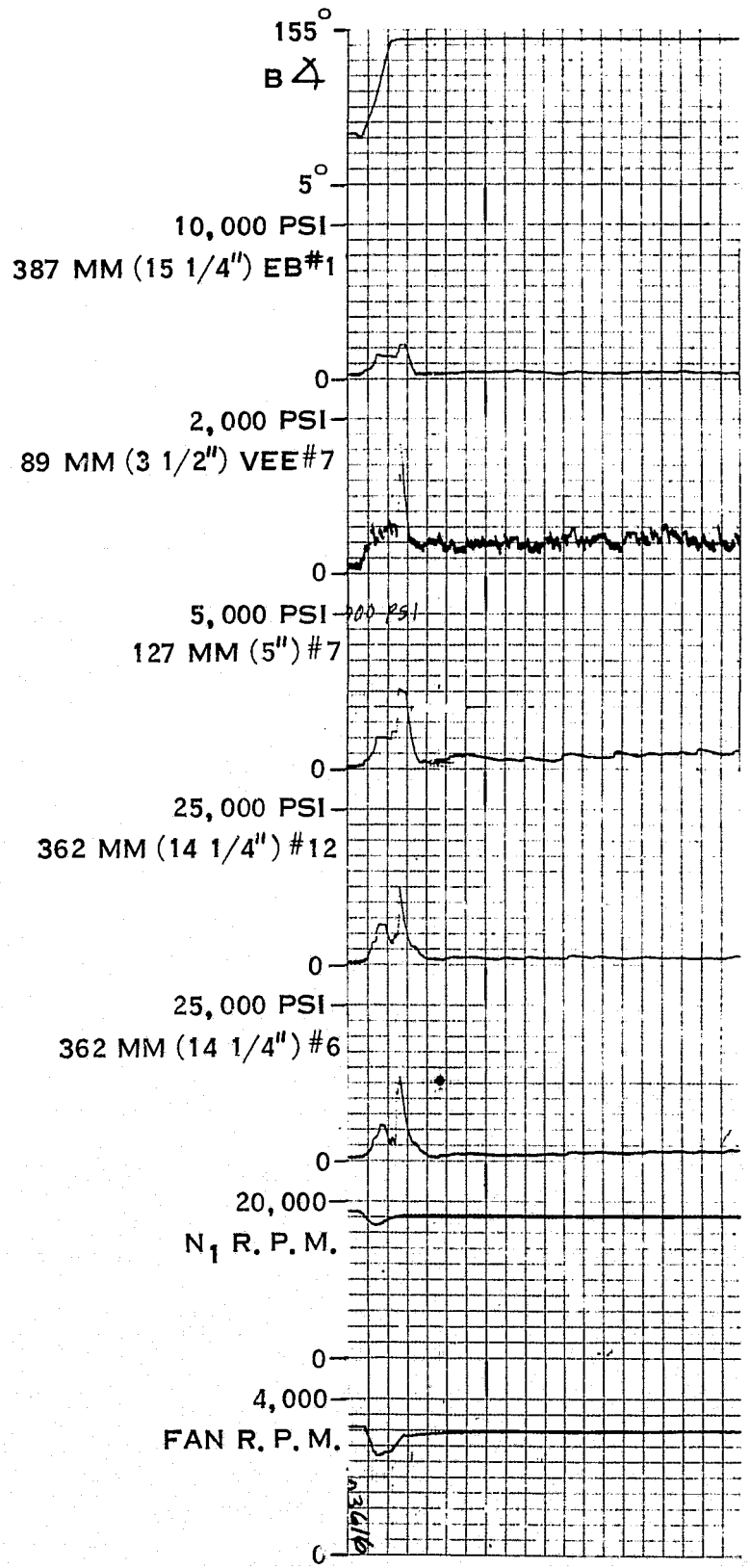

FIGURE 64. Q–FAN DEMONSTRATOR–SANBORN TRACE, TEST POINT TRC3–46

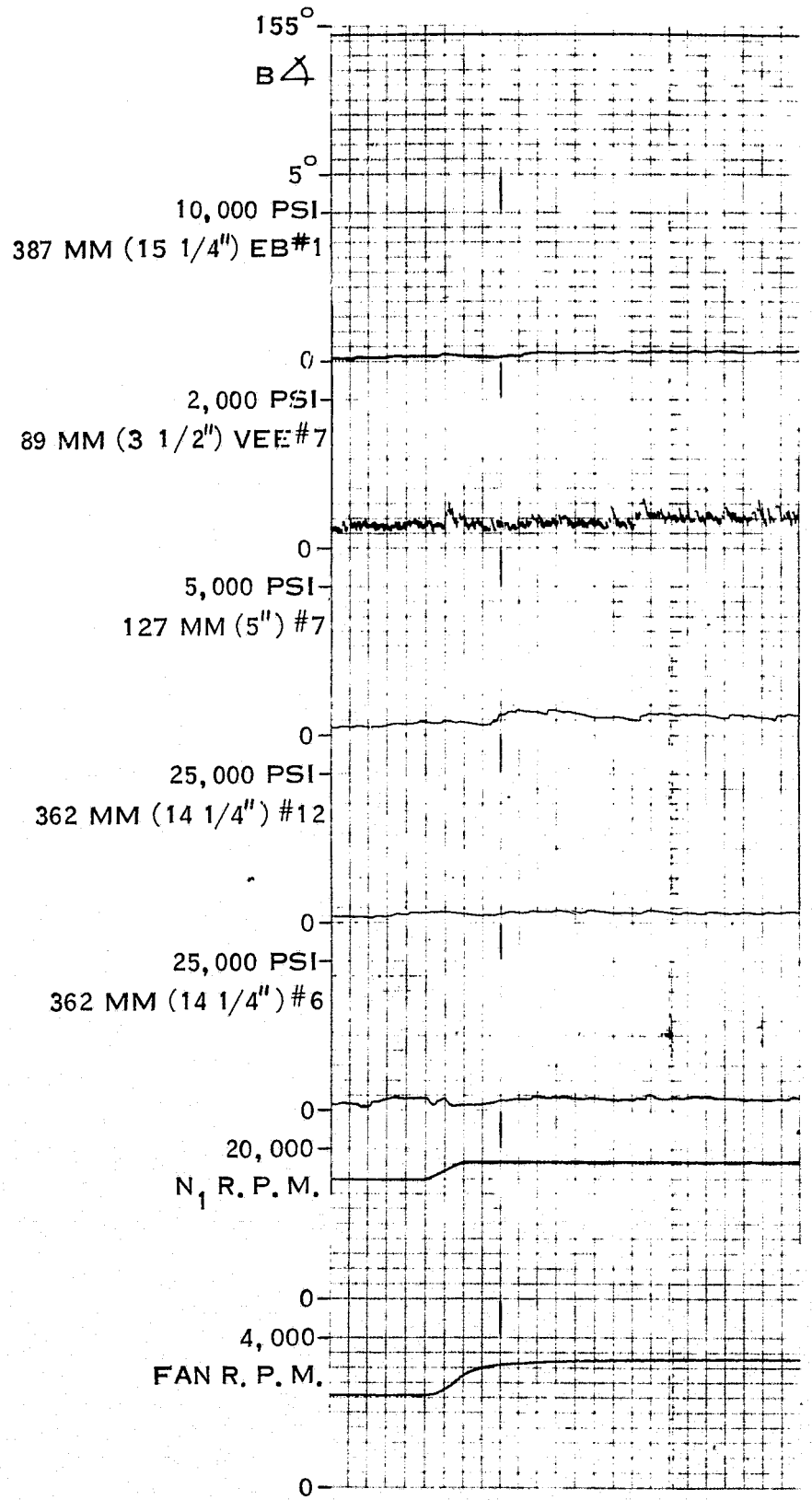

FIGURE 65. Q–FAN DEMONSTRATOR–SANBORN TRACE, TEST POINT TRRC3–1

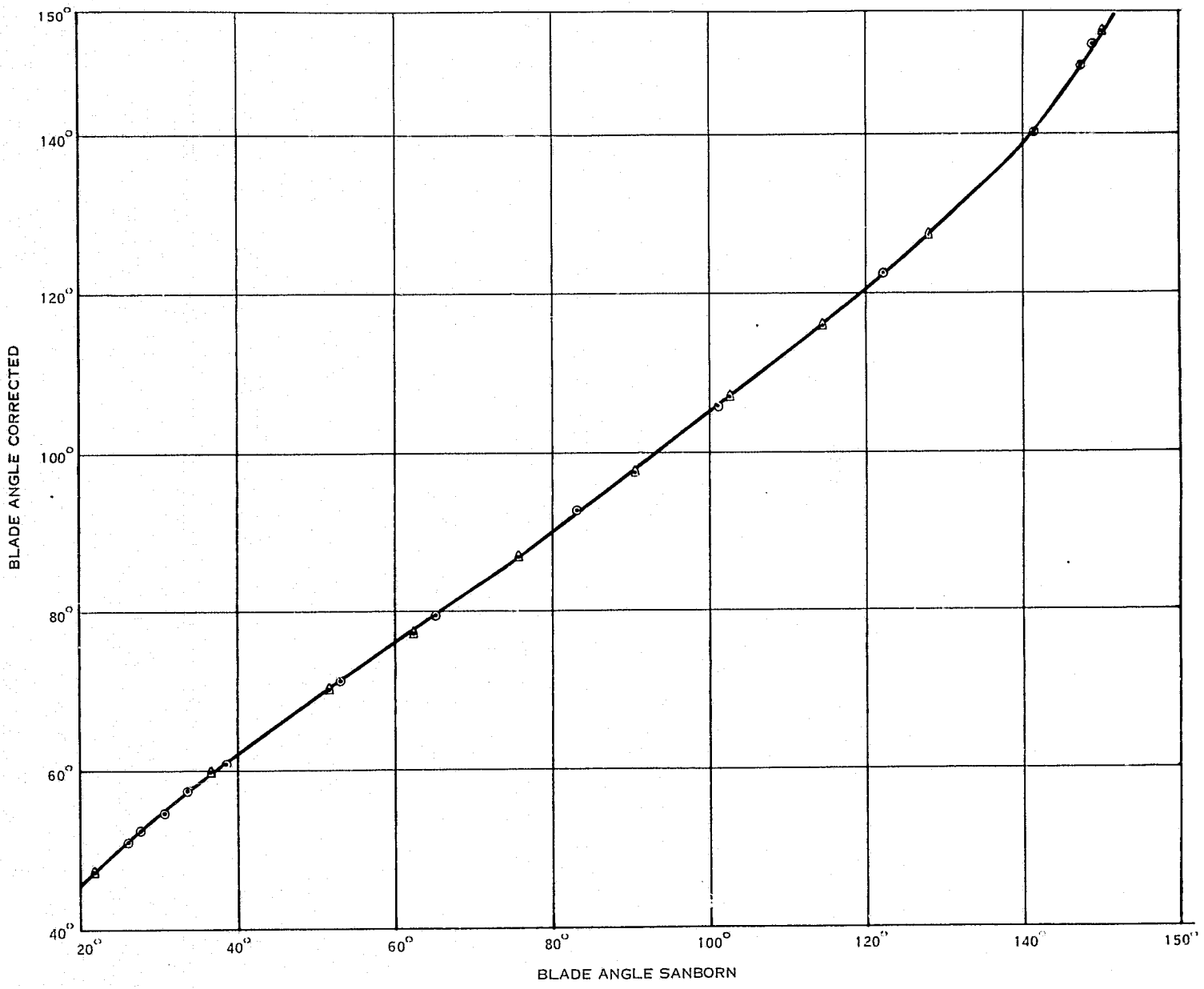

FIGURE 66. Q-FAN DEMONSTRATOR – BLADE ANGLE CALIBRATION

REVERSE THRU FEATHER TRANSIENTS

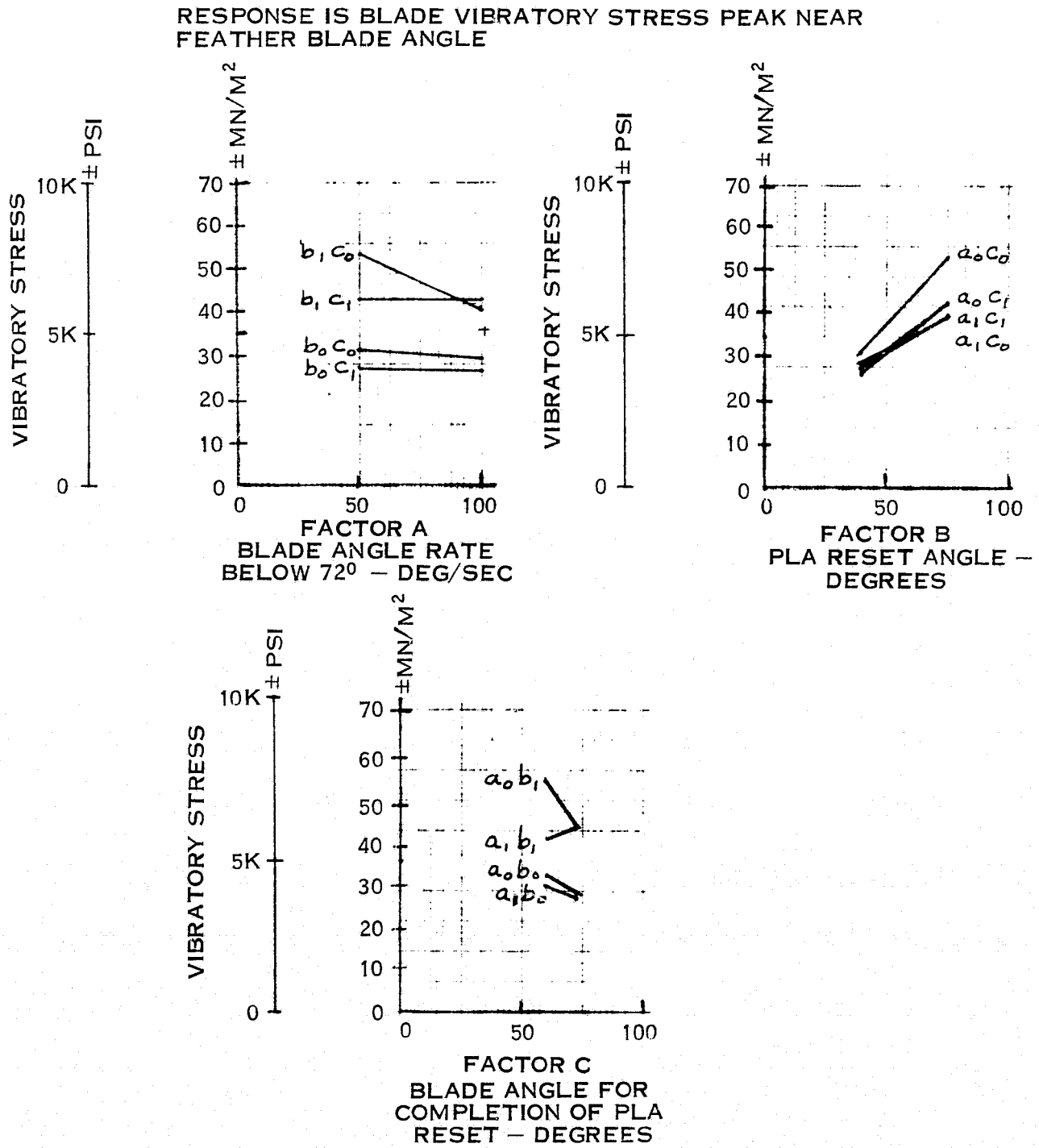

FIGURE 67. Q–FAN DEMONSTRATOR PEAK BLADE STRESS RESPONSE NEAR FEATHER – SCHEDULE 1

REVERSE THRU FEATHER TRANSIENTS

RESPONSE IS AVERAGE BLADE VIBRATORY STRESS NEAR FEATHER BLADE ANGLE

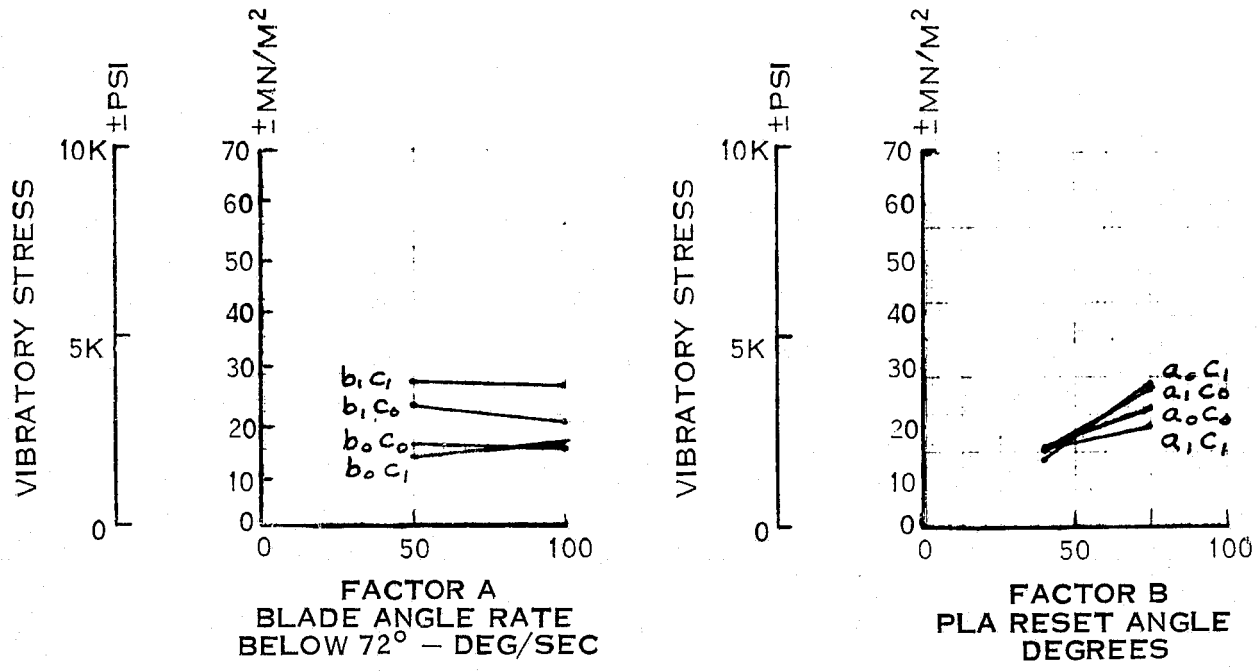

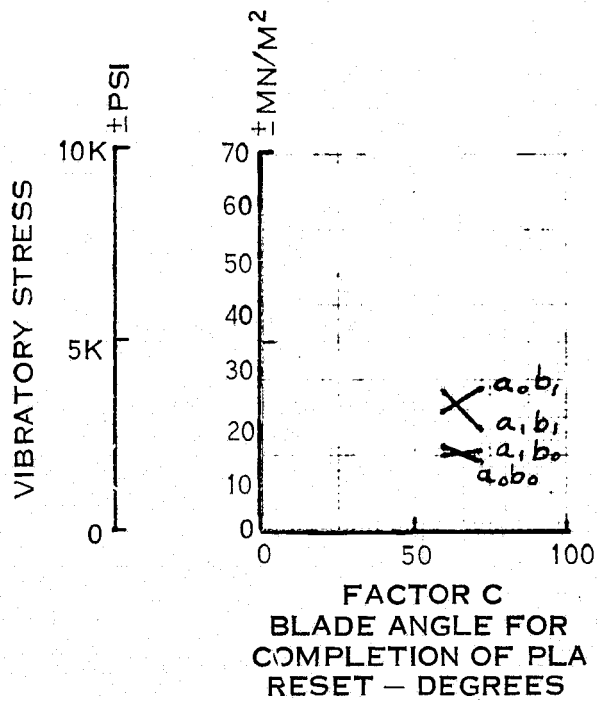

FIGURE 68. Q–FAN DEMONSTRATOR AVERAGE BLADE STRESS RESPONSE NEAR FEATHER – SCHEDULE 1

REVERSE THRU FEATHER TRANSIENTS

RESPONSE IS BLADE VIBRATORY STRESS PEAK NEAR FEATHER BLADE ANGLE

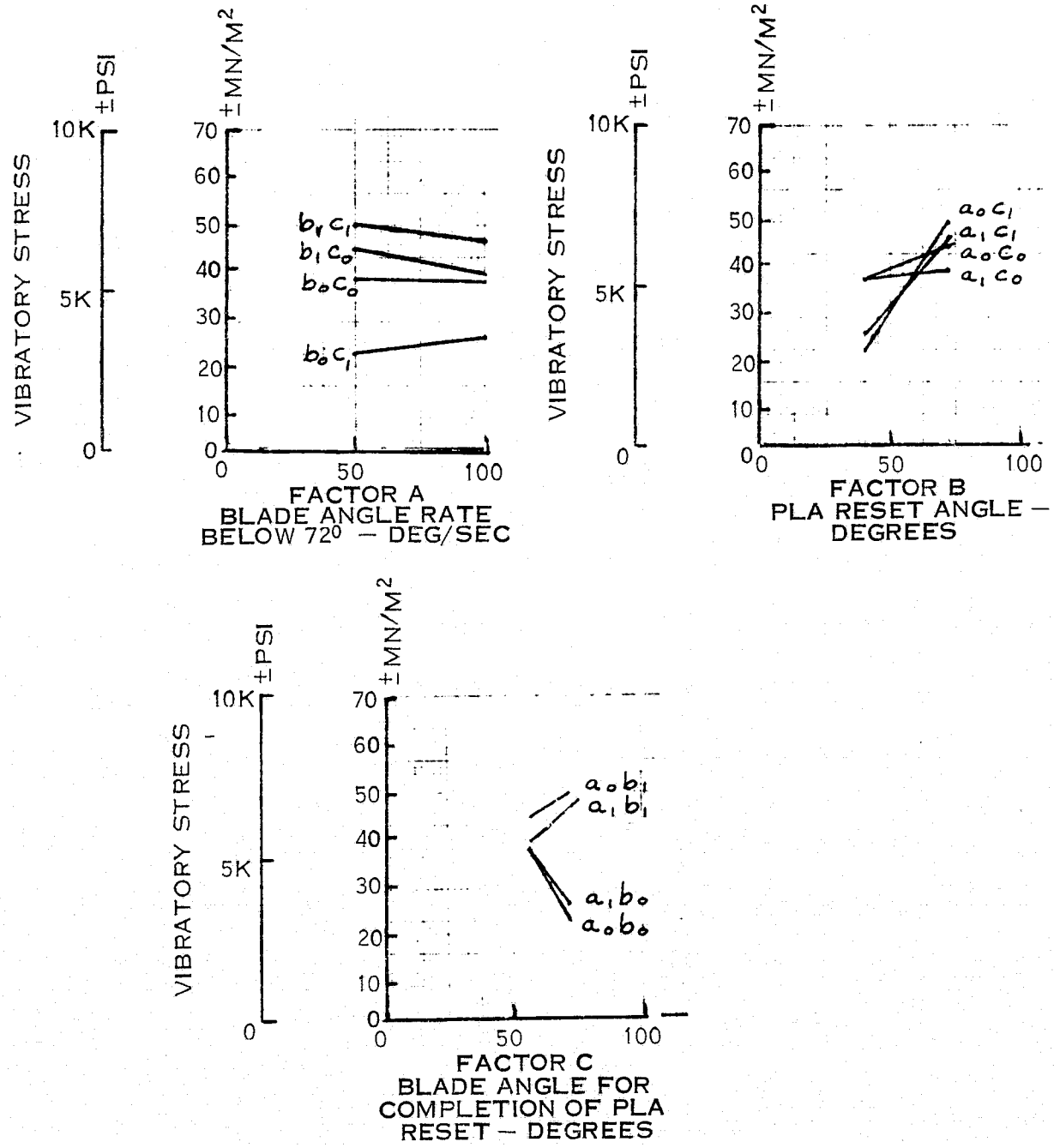

FIGURE 69. Q-FAN DEMONSTRATOR BLADE STRESS RESPONSE NEAR FEATHER — SCHEDULE 2

REVERSE THRU FEATHER TRANSIENTS

RESPONSE IS BLADE VIBRATORY STRESS PEAK NEAR FEATHER BLADE ANGLE

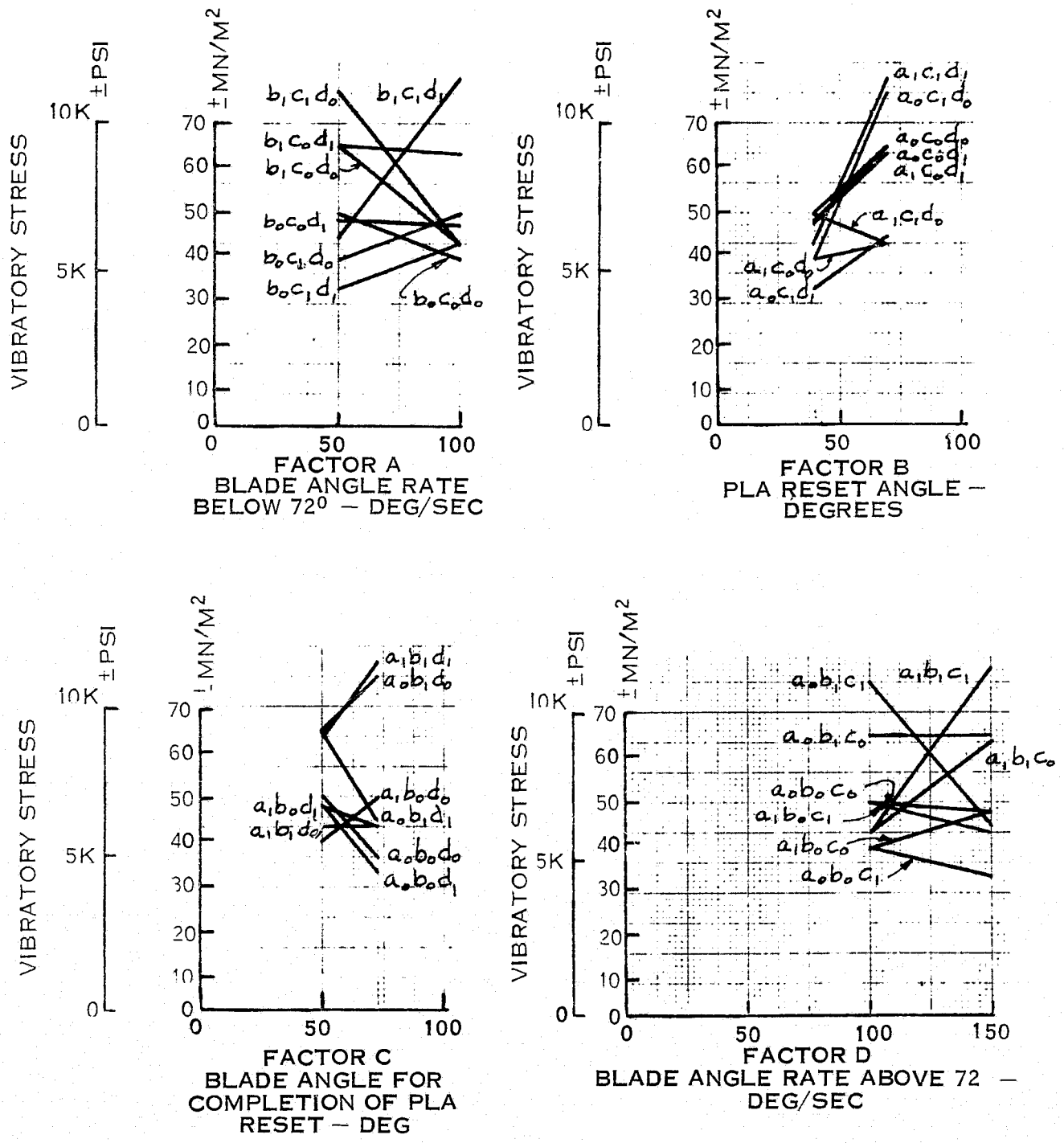

FIGURE 70. Q—FAN DEMONSTRATOR BLADE STRESS RESPONSE NEAR FEATHER — SCHEDULE 3, TSL RANGE 70% TO 0%

REVERSE THRU FEATHER TRANSIENTS

RESPONSE IS BLADE VIBRATORY STRESS PEAK NEAR FEATHER BLADE ANGLE

THRUST SETTING LEVER 90% TO 0%

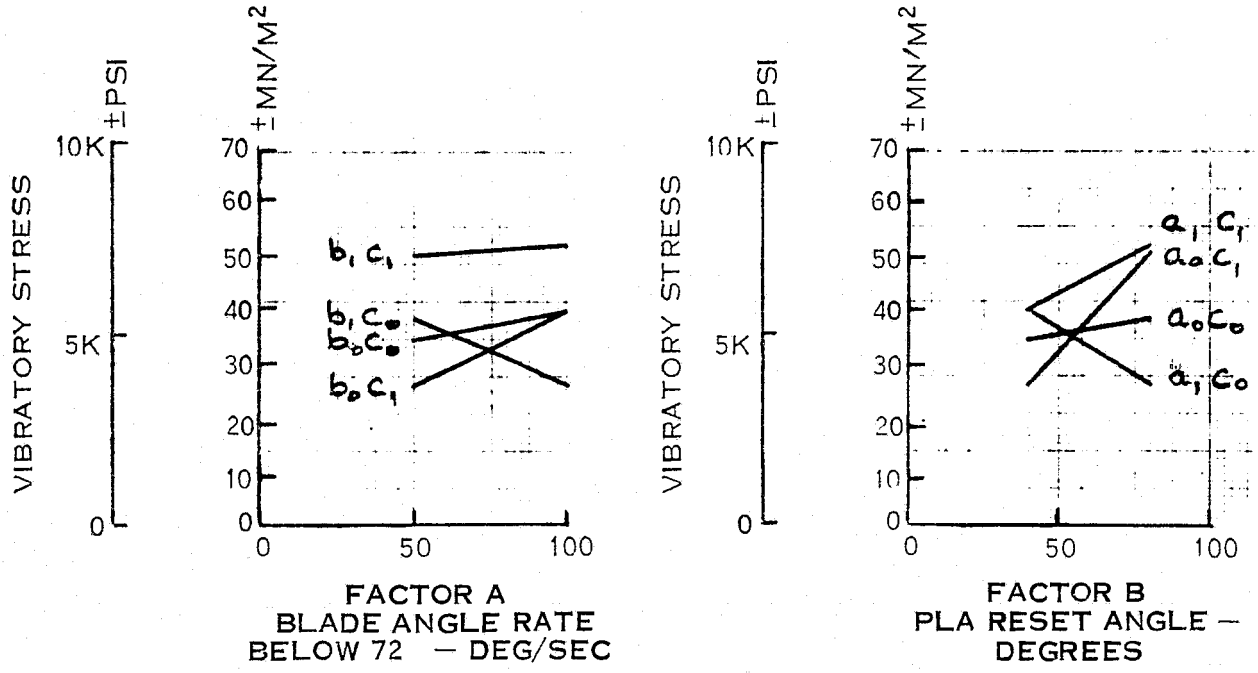

FACTOR A
BLADE ANGLE RATE BELOW 72 — DEG/SEC

FACTOR B
PLA RESET ANGLE — DEGREES

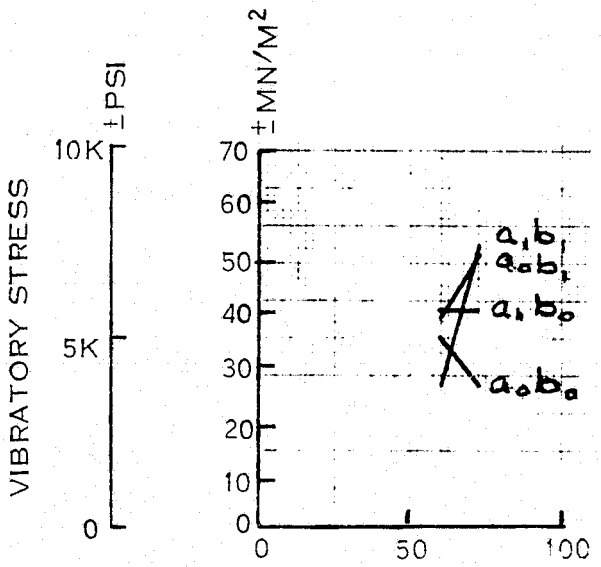

FACTOR C
BLADE ANGLE FOR COMPLETION OF PLA RESET — DEG

FIGURE 71. Q—FAN DEMONSTRATOR BLADE STRESS RESPONSE NEAR FEATHER — SCHEDULE 3, TSL RANGE 90% TO 0%

REVERSE THRU FEATHER TRANSIENTS

RESPONSE IS BLADE VIBRATORY STRESS PEAK NEAR REVERSE BLADE ANGLE

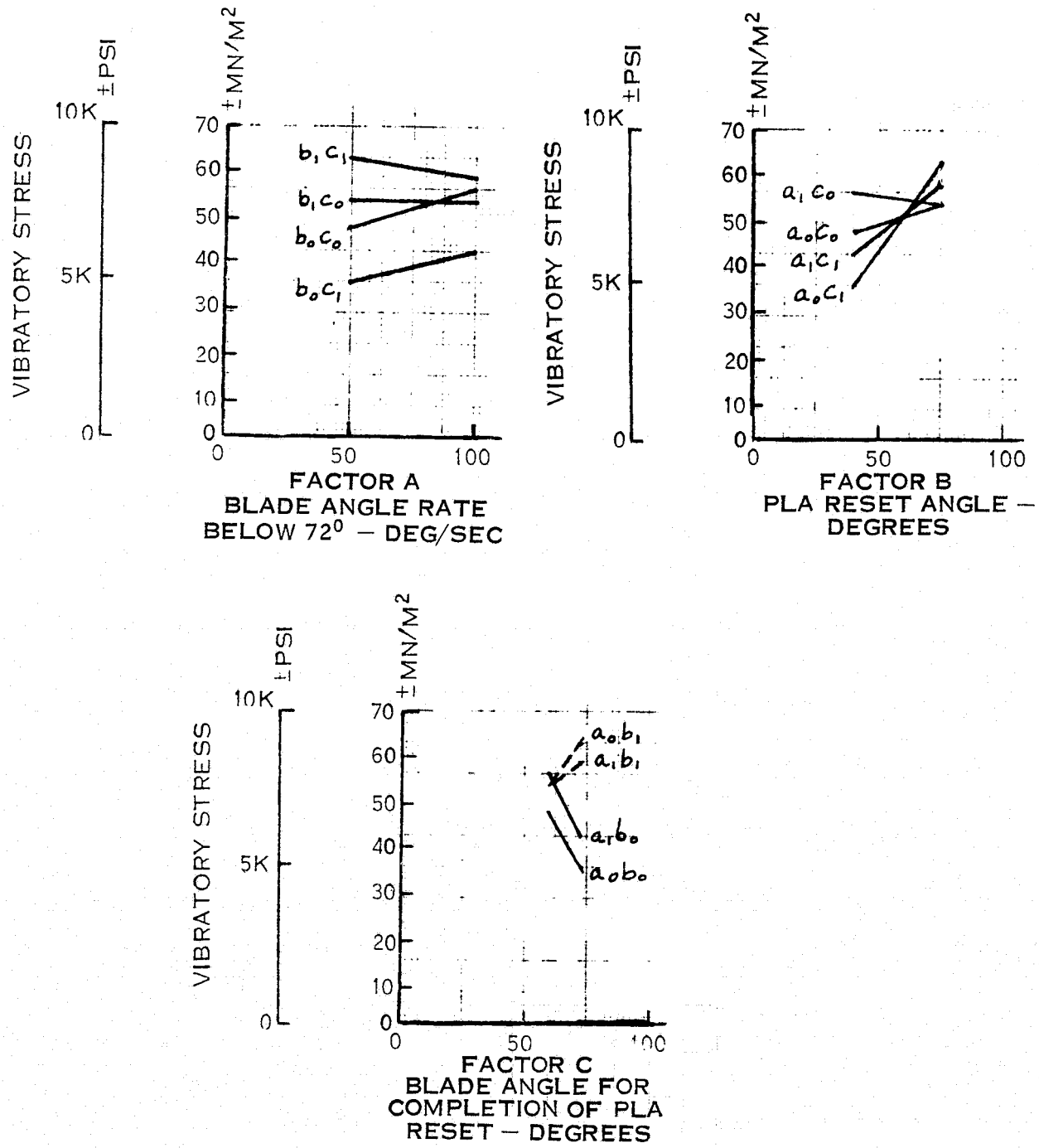

FIGURE 72. Q-FAN DEMONSTRATOR BLADE STRESS RESPONSE NEAR REVERSE — SCHEDULE 1

REVERSE THRU FEATHER TRANSIENTS

RESPONSE IS BLADE VIBRATORY STRESS PEAK NEAR REVERSE BLADE ANGLE

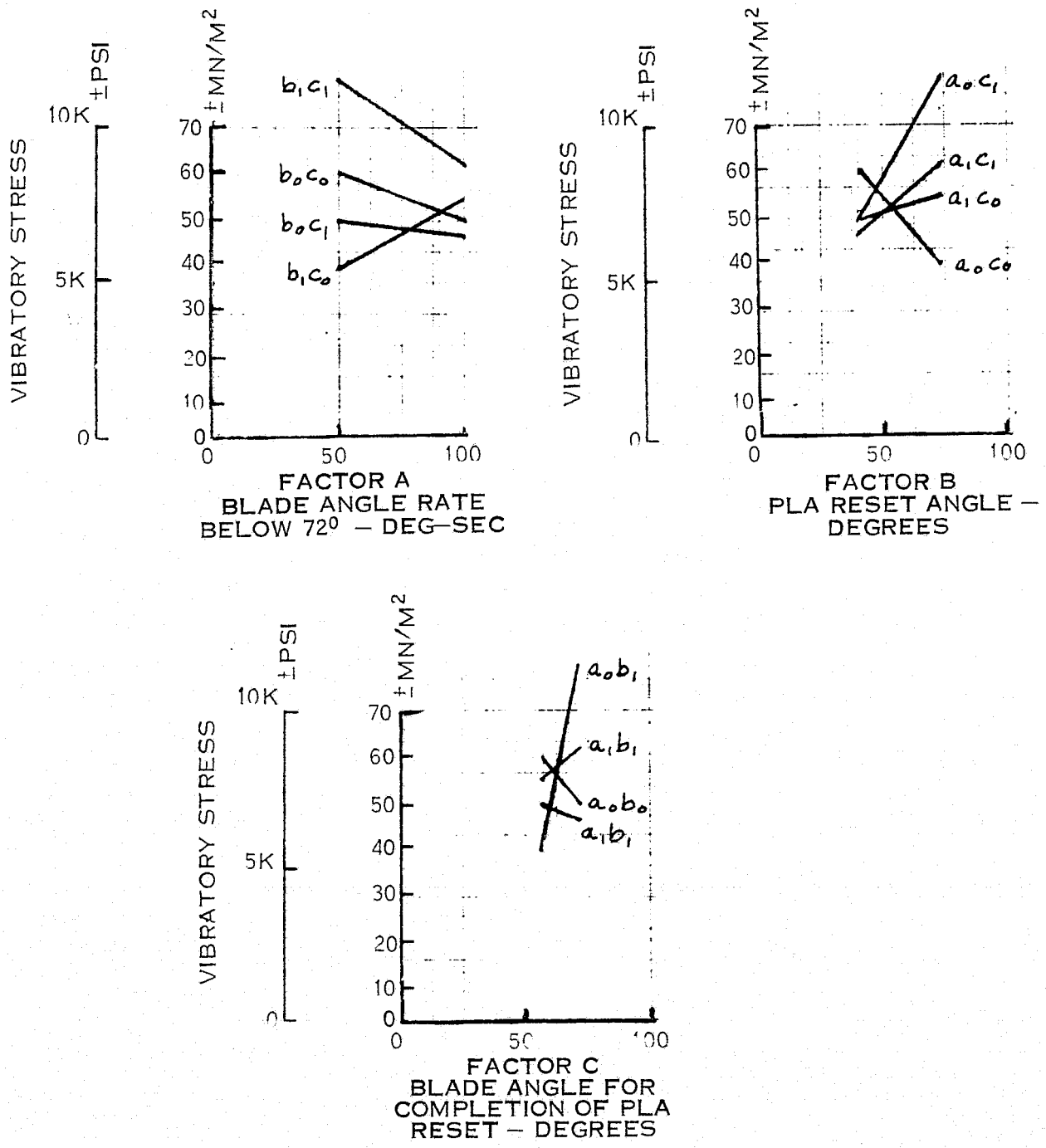

FIGURE 73. Q—FAN DEMONSTRATOR BLADE STRESS RESPONSE NEAR REVERSE — SCHEDULE 2

REVERSE THRU FEATHER TRANSIENTS

RESPONSE IS BLADE VIBRATORY STRESS PEAK NEAR REVERSE BLADE ANGLE

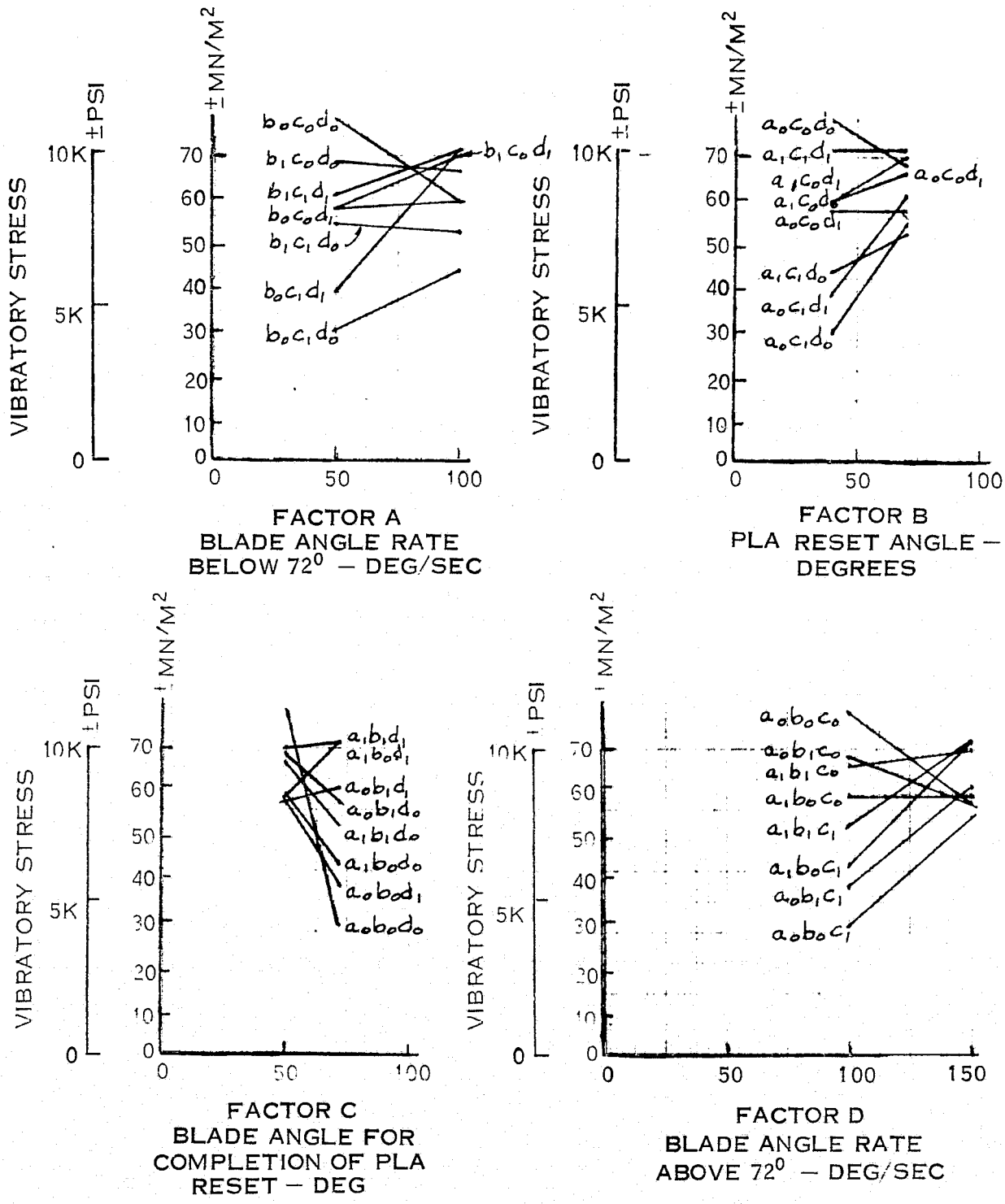

FIGURE 74. Q-FAN DEMONSTRATOR BLADE STRESS RESPONSE NEAR REVERSE — SCHEDULE 3, TSL RANGE 70% TO 0%

REVERSE THRU FEATHER TRANSIENTS

RESPONSE IS BLADE VIBRATORY STRESS PEAK NEAR
REVERSE BLADE ANGLE THRUST SETTING LEVER 90% TO 0%

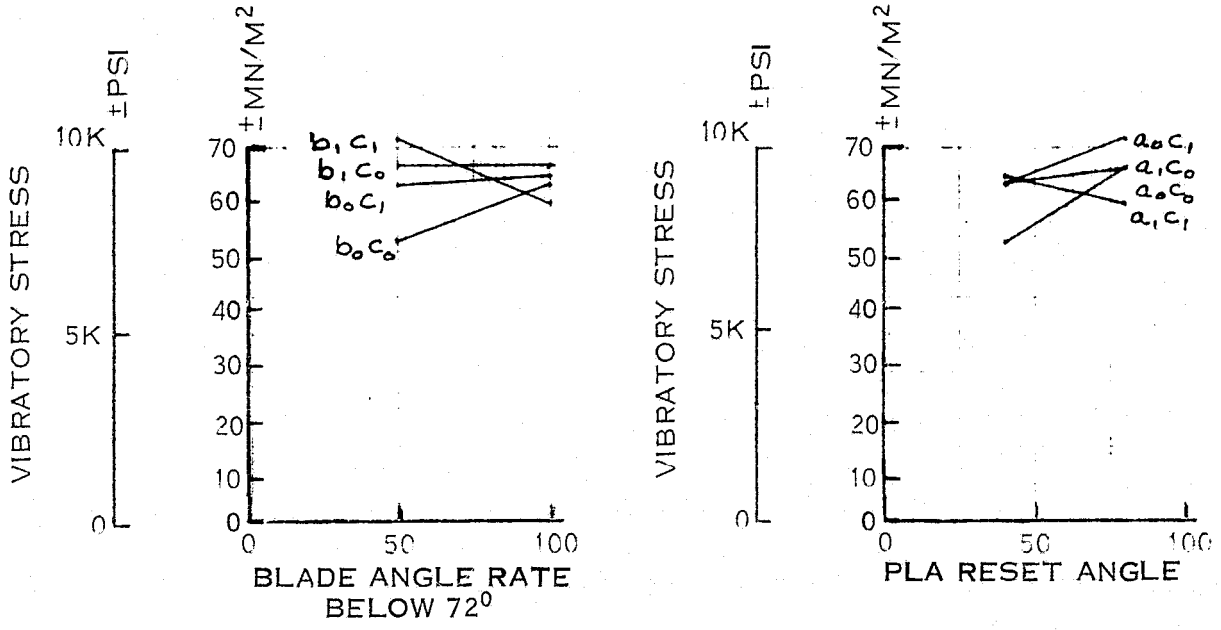

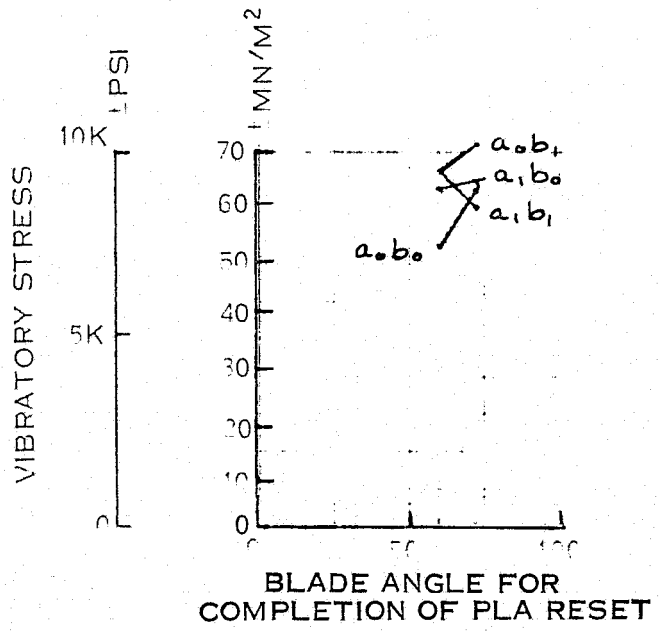

FIGURE 75. Q-FAN DEMONSTRATOR BLADE STRESS RESPONSE NEAR REVERSE – SCHEDULE 3, TSL RANGE 90% TO 0%

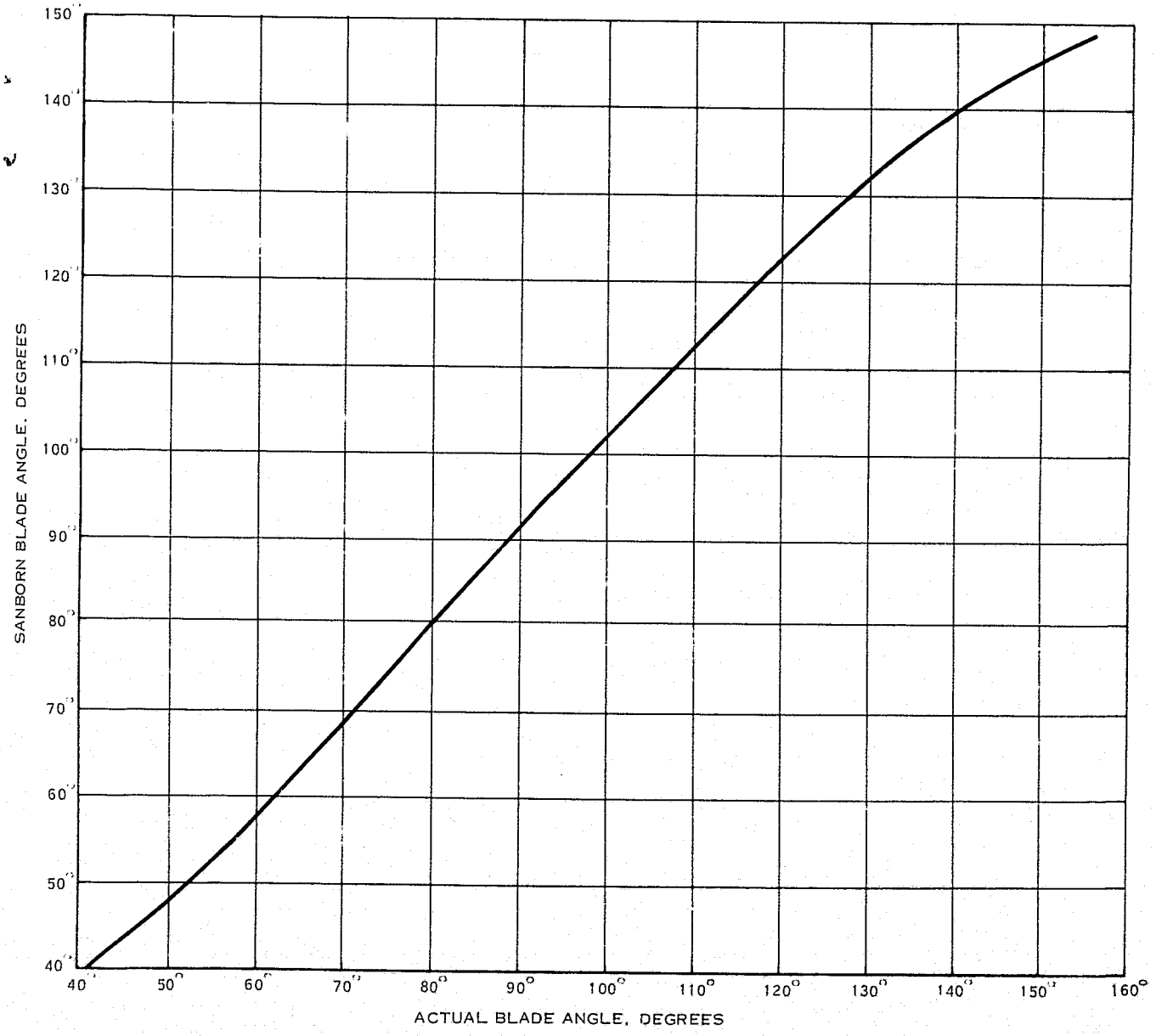

FIGURE 76. Q-FAN DEMONSTRATOR
BLADE ANGLE CALIBRATION CURVE TO BE USED IN SECTION 7, APPENDIX F

6.0 CONCLUSIONS

6.1 Performance - Based on the steady state reverse thrust testing with a take-off nozzle, it has been established that the fan can be operated in this mode. The thrust at a blade angle of 144° and a tip speed of 246 m/s (760 fps) is reduced to 1/3 of the value measured with the reverse nozzle. Compressor face distortion is increased by 74 percent at this test condition.

During transient operation, it was verified that changing the fan blade angle is a practical method of obtaining rapid reverse thrust response. Fan-engine compatibility is good and coordination of the fan blade angle/engine power can be easily achieved.

Transients from forward to reverse thrust through feather can be achieved is less than one second. For the statistically designed experiments the fastest time was achieved with a combination of control variables which included a fast pitch change rate, a small reset in power level, and a short duration of power reset.

6.2 Structural - During the steady state reverse thrust testing with a take-off nozzle, the peak vibratory stress levels at the same blade angle and tip speed were increased by almost seven-fold for some operating conditions as compared to some conditions with the reverse nozzle.

Forward thrust, reverse thrust, and reverse through flat pitch transients can be performed with no significant stress variations.

Blade vibratory stresses vary from blade to blade an average of $\pm$ 1200 psi during a test run and an average of $\pm$ 2000 psi from run to run.

Reverse through feather transients will result in two distinct stress peaks as the blades go through stall and prior to the thrust build up in reverse. Generally the stress peak at reverse is substantially higher than the peak near stall. These stresses have not limited the test program. When simulating a normal landing transient from forward to reverse thrust, the blade vibratory stress level can be reduced up to 40% by reducing the engine power as the blades go through stall. None of the control variables effect the blade vibratory stress levels when the transient is initiated from a high forward thrust.

SECTION 7.0

APPENDICES

APPENDIX A

TEST INSTRUMENTATION

Type of Measurement	Location	Transducer/Readout	Accuracy
Oil Pressure	Engine	Bendix Indicator	±3 psi
Oil Temperature	Engine	Bulb Type (MS28034-1)	±5° F
Oil Level	Engine	Electric Type	-
Turbine Inlet Temperature (T_{T7})	Engine	Thermocouple	-
Fuel Pressure	Engine	Bendix Indicator	±3 psi
Compressor RPM (N_1)	Engine	Hewlett Packard Model 5214L	±1 count
Turbine RPM (N_2)	Engine	Hewlett Packard Model 5214L	±1 count
Torque	Engine	Electric Type	-
Oil Pressure	Q-Fan Gearbox	Bendix Indicator	±3 psi
Oil Temperature	Q-Fan Gearbox	(DS-300-T3-M-T301) Doric Digital Indicator	±5° F
Oil Flow	Q-Fan Gearbox	Hewlett Packard Model 5214L	±1 count
Chip Detector	Q-Fan Gearbox	Tedeco - Type A-54	-
Chip Detector	Engine Gearbox	Magnetic Type	-
Wind Velocity	Test Stand Area	Beckman and Whitney Wind Indicator	±4% F.S.

TABLE 1. TEST STAND ITEMS

Type of Measurement	Location	Transducer/Readout	Accuracy
Wind Direction	Test Stand Area	Measurement System Type A	±3% F.S.
Pitch Change Actuator Pressures	Engine Mount	Pressure Gauge and Pressure Transducers	±3% F.S.

TABLE 1 (continued). TEST STAND ITEMS

Type of Measurement	Location	Transducer	Accuracy
Flatwise Bending	Blade 1; 14.25; F.T.	Strain gauge (half bridge)	±4.2% RMS of full scale
Edgewise Bending	Blade 1; 15.25" F.T.	Strain gauge (half bridge)	±4.2% RMS of full scale
Flatwise Bending	Blade 6; 14.25" F.T.	Strain gauge (half bridge)	±4.2% RMS of full scale
Shear (Camber)	Blade 7; 3.5" F.T. At C.L.	Strain gauge (half bridge)	±4.2% RMS of full scale
Bending (Camber)	Blade 7; 5.0" F.T. At C.L.	Strain gauge (single bridge)	±4.2% RMS of full scale
Flatwise Bending	Blade 7; 14.25" F.T.	Strain gauge (half bridge)	±4.2% RMS of full scale
Flatwise Bending	Blade 12; 14.25" F.T.	Strain gauge (half bridge)	±4.2% RMS of full scale
Stress - 2	Disc-Blade Arm 4	Strain gauge (single bridge)	±4.2% RMS of full scale
Stress - 5	Disc-Blade Arm 4	Strain gauge (single bridge)	±4.2% RMS of full scale
Stress - 6	Disc-Blade Arm 4	Strain gauge (single bridge)	±4.2% RMS of full scale
Inner Root Bending	Exit Guide Vanes 1&4	Strain gauge (single bridge)	±3% RMS of full scale
Dynamic Pressure	Compressor Front Frame (3)	Semiconductor Strain gauge (full bridge)	±2.0% of full scale
Vibration (2)	Fan Gearbox	HS 11 x 1844	±10

TABLE II

STRUCTURAL INSTRUMENTATION

Type of Measurement	Location	Transducer	Accuracy
Vibration (2)	Fan Duct	HS 11 x 1844	±10%
Vibration (3)	Engine	HS 11 x 1844	±10%
IF Speed-Phase Pip	Aft of Rotor	Magnetic Pickup	±2°

NOTES: F.T. - From Tip

C.L. - Centerline

TABLE II (continued)
STRUCTURAL INSTRUMENTATION

Type of Measurement	Location	Transducer/Readout	Accuracy
Total Air Pressure (2)	Fan Duct Exit	Rake / Manometer	±0.1 in.
Total Air Pressure (10)	Upstream of Fan Rotor	Rake / Manometer	±0.1 in.
Static Air Pressure (8)	Upstream of Fan Rotor	Taps / Manometer	±0.1 in.
Total Air Pressure (5)	Entrance to Compressor Inlet Duct	Rake / Manometer	±0.1 in.
Static Air Pressure (2)	Entrance to Compressor Inlet Duct	Rake / Manometer	±0.1 in.
Air Temperature (1)	Compressor Inlet Duct	Doric Digital Ind. (DS-300-T3)	±3° F
Total Air Pressure (45)	Compressor Front Frame	Rake / Manometer	±0.1 in.
Static Air Pressure (8)	Compressor Front Frame	Rake / Manometer	±0.1 in.
Total Air Pressure (3)*	Compressor Front Frame	Kulite Press Transducers	±1%

*Only Performance Instrumentation Used During Transient Testing

TABLE III

PERFORMANCE INSTRUMENTATION

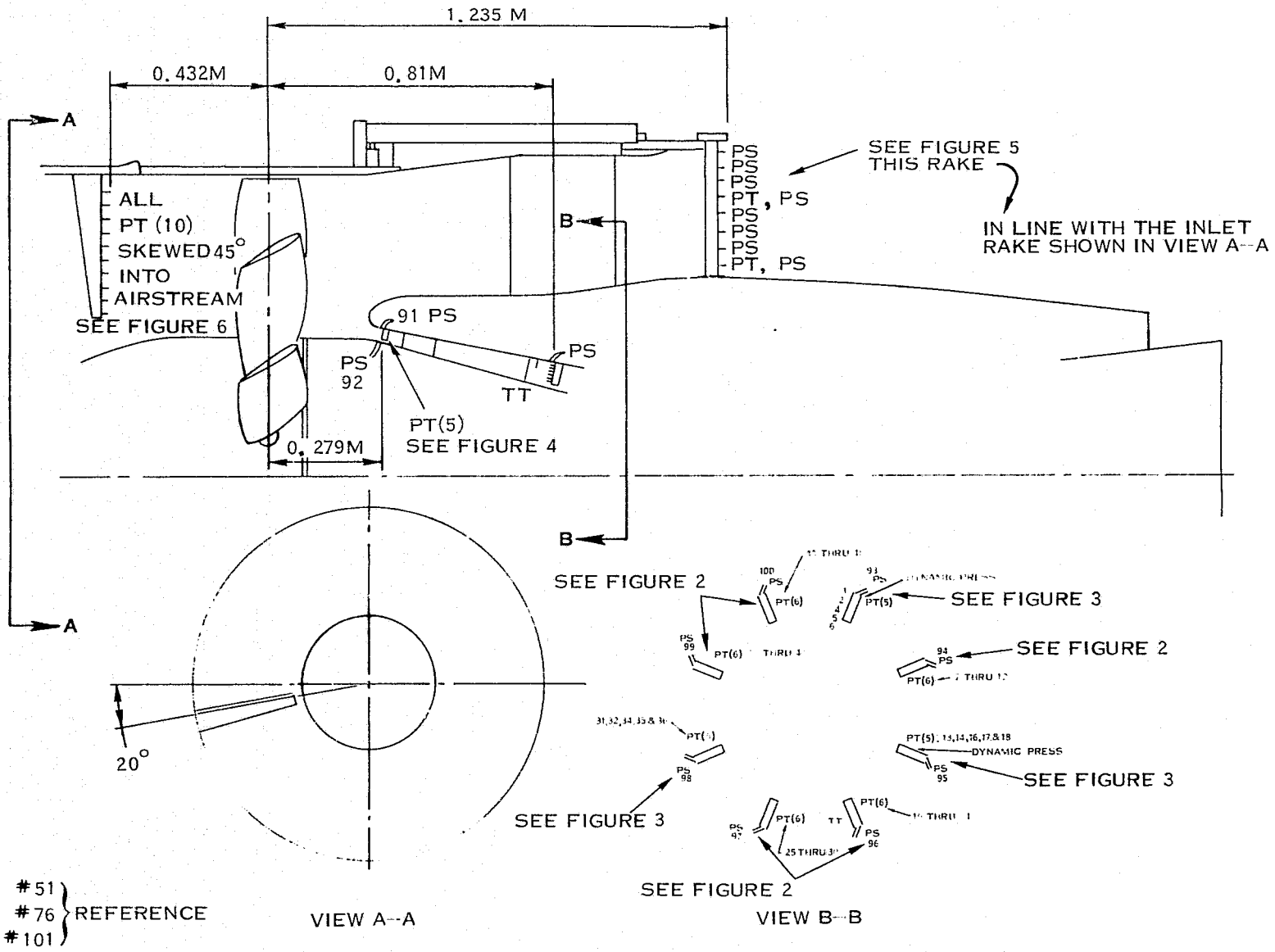

FIGURE 1 STEADY STATE REVERSE PERFORMANCE INSTRUMENTATION

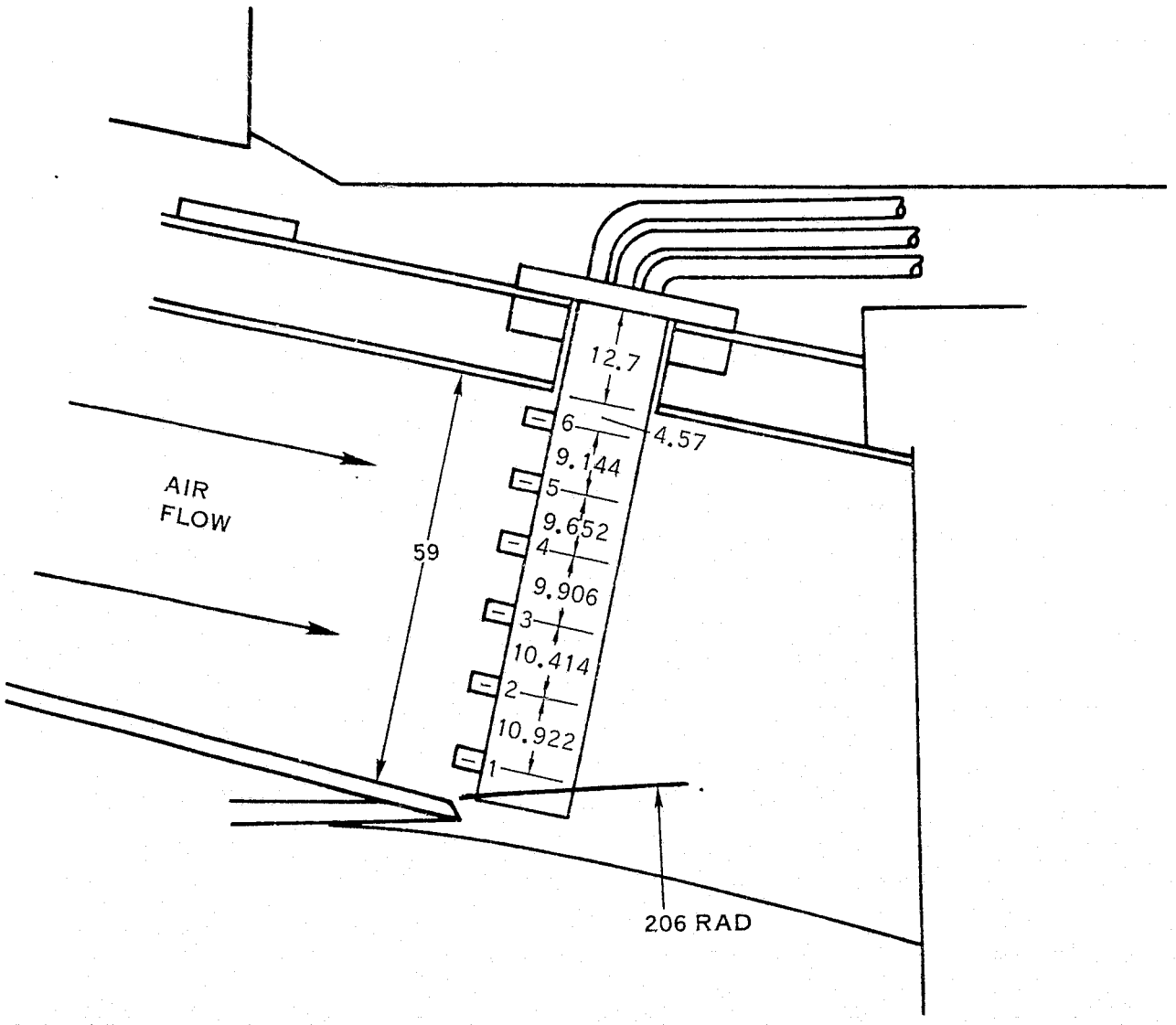

NOTES:
1. ALL DIMS IN MM
2. SEE FIGURE 1 FOR EXACT LOCATION OF THESE RAKES
3. 5 REQUIRED

FIGURE 2.- TOTAL PRESSURE RAKES POSITIONED AT COMPRESSOR FRONT FRAME

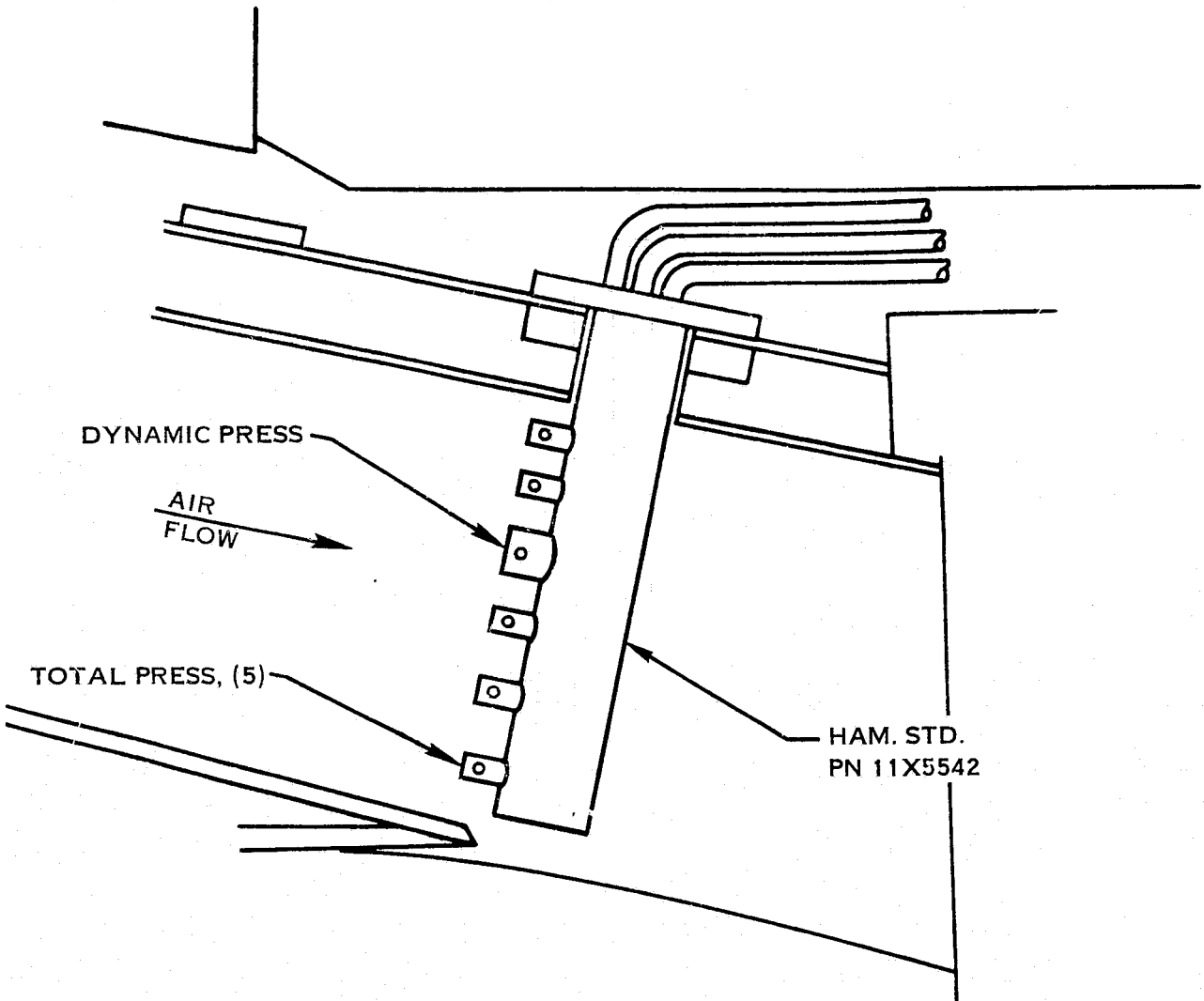

FIGURE 3. TOTAL/DYNAMIC PRESSURE RAKES POSITIONED AT COMPRESSOR FRONT FRAME

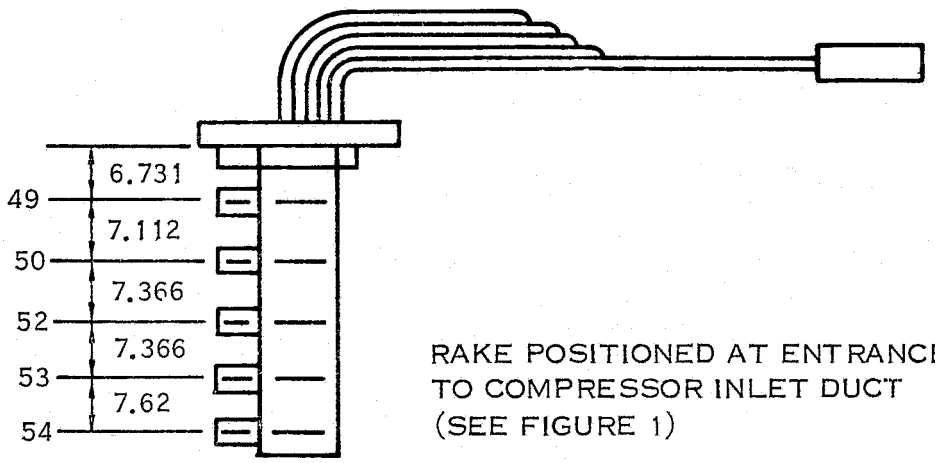

RAKE POSITIONED AT ENTRANCE
TO COMPRESSOR INLET DUCT
(SEE FIGURE 1)

1 RAKE REQUIRED

NOTE: ALL DIMS IN MM

FIGURE 4. PRESSURE RAKE WITH 5 TOTAL PRESSURE PROBES

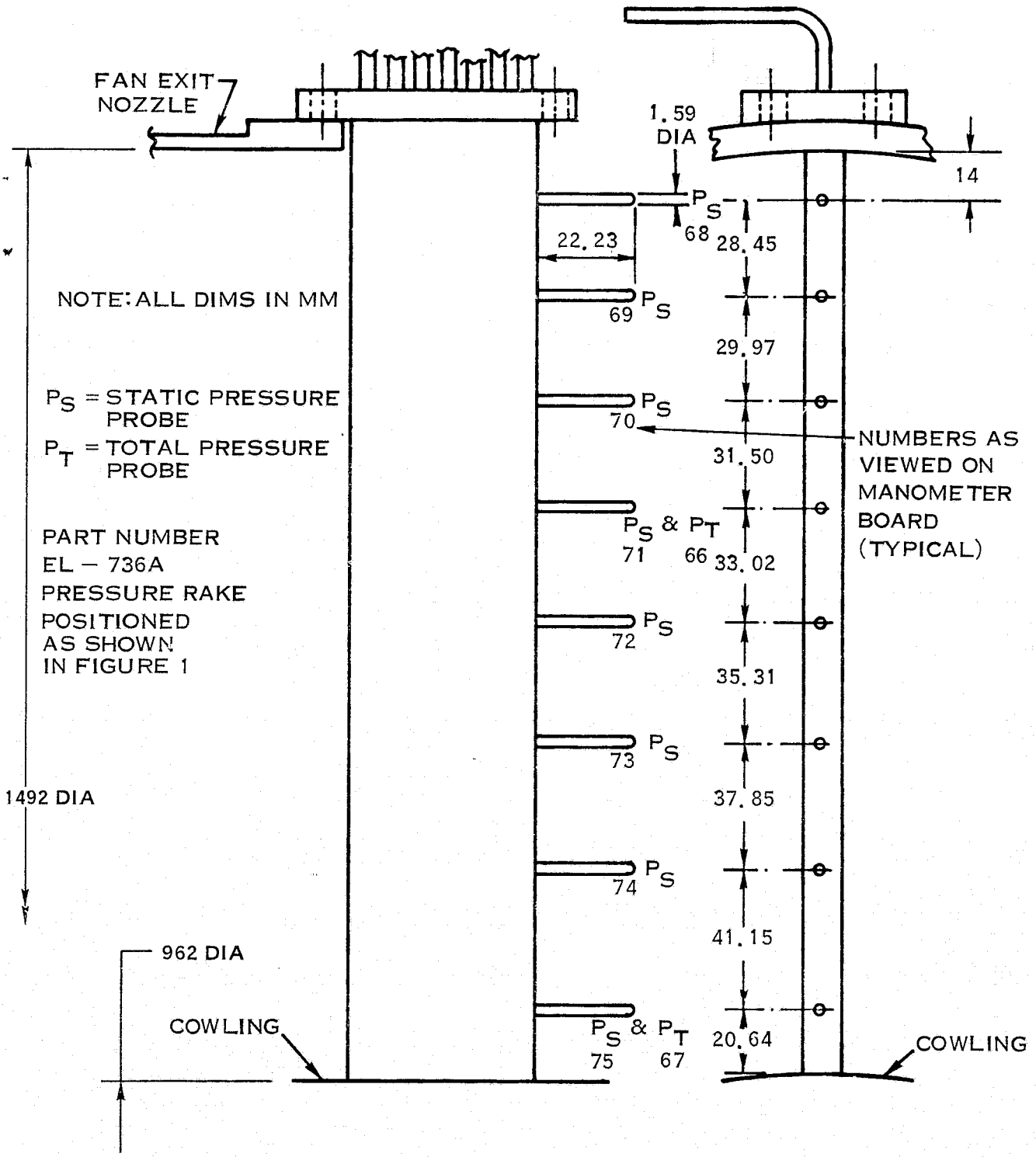

FIGURE 5. RAKE POSITIONED AT EXIT NOZZLE

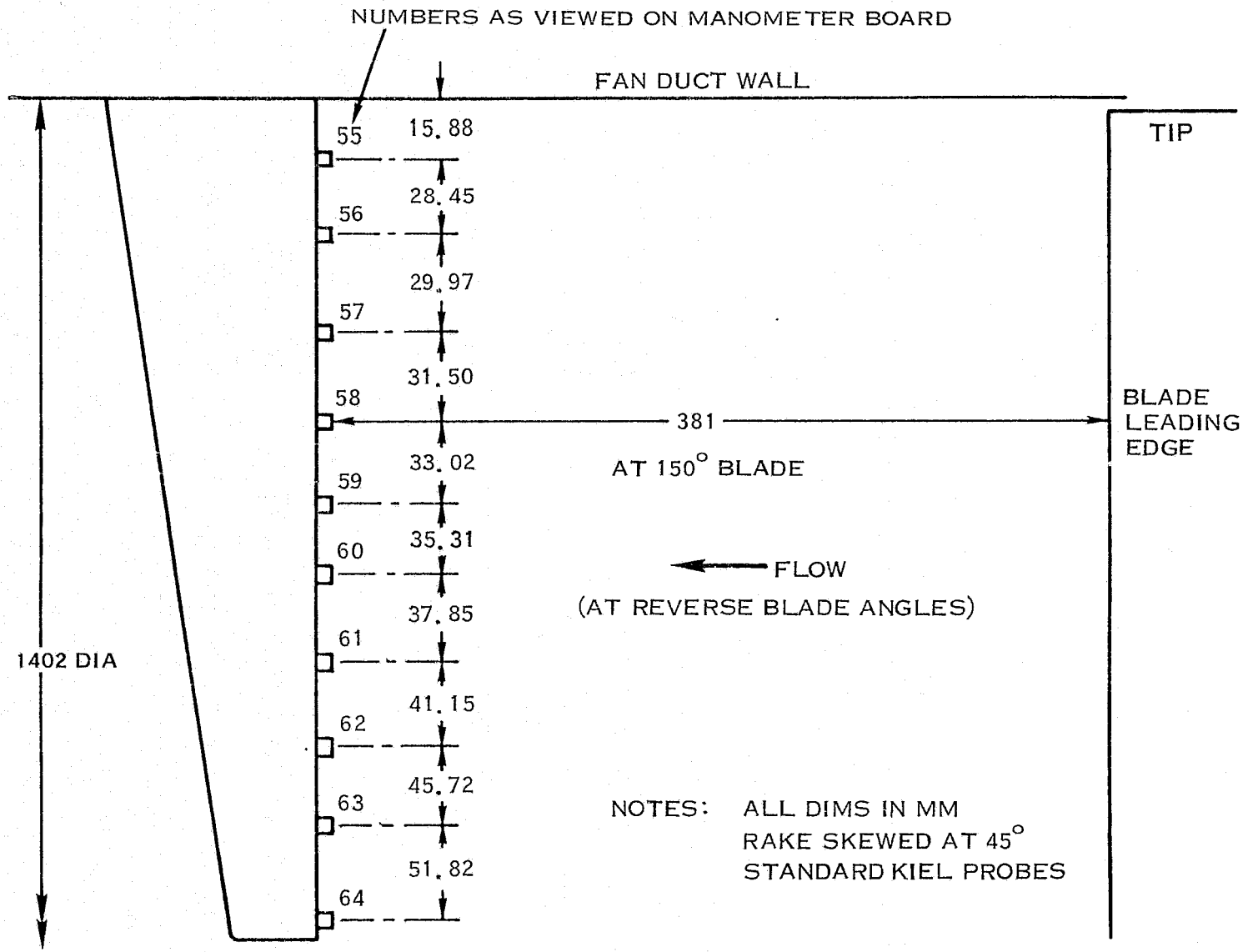

FIGURE 6. EXIT RAKE – REVERSE TESTING

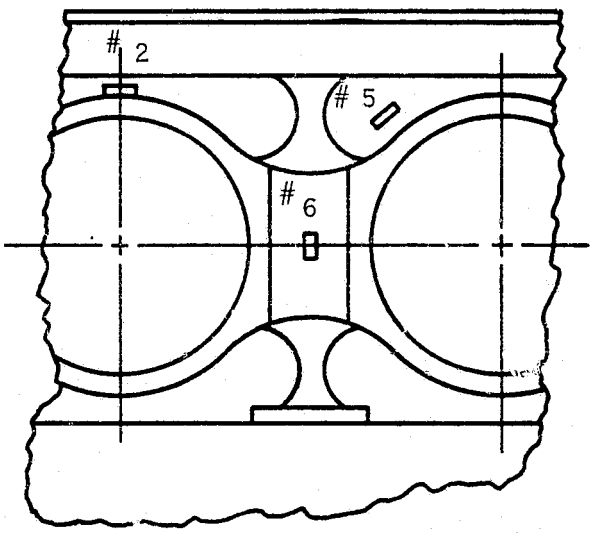

FIGURE 7. DISC GAUGE LOCATIONS

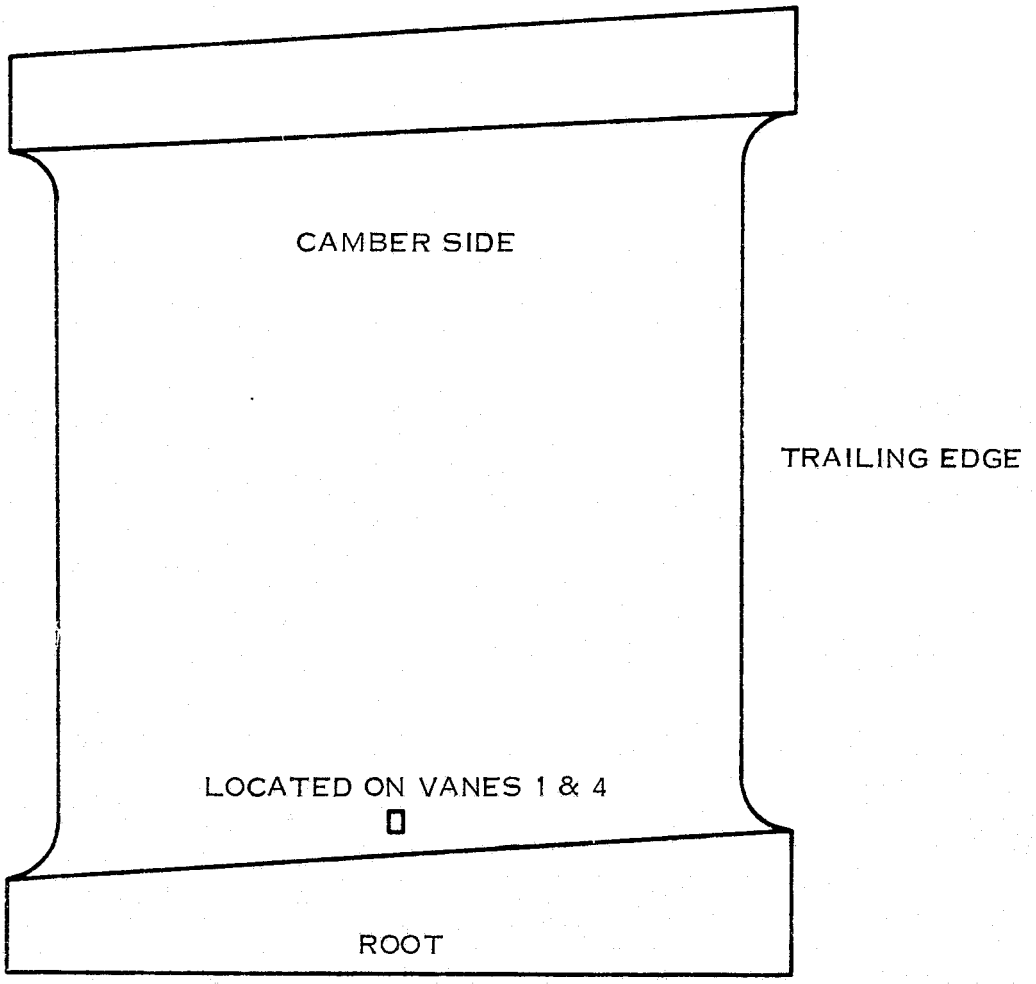

FIGURE 8. VANE GAUGE LOCATIONS

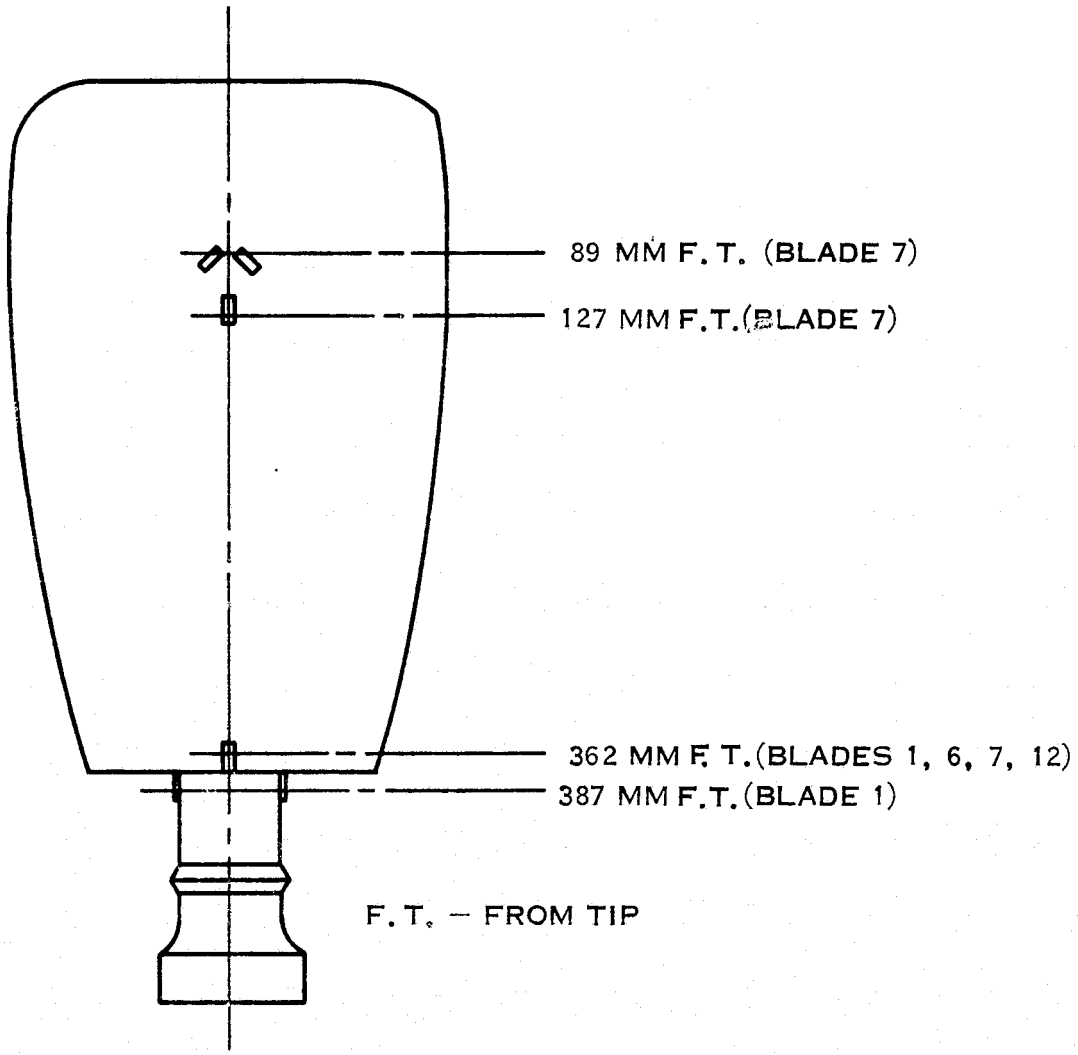

FIGURE 9. BLADE LAYOUT SHOWING VARIOUS GAUGE LOCATIONS

APPENDIX B

LIST OF SYMBOLS

Symbol	Definition	Units
A	Annulus Area	m^2
A	Blade Angle Rate, below 72°β	deg/sec
β	Blade Angle, 3/4 Radius with respect to plane of rotation	Degrees
B	PLA Reset Level	Degrees
C	Blade Angle at Completion of PLA Reset	Degrees
C_x	Axial velocity	m/s
D	Blade Angle Rate, above 72°β	deg/sec
Dist	Distortion, $\frac{Ptmax-Ptmin}{Ptave}$	-
γ	Air Density	Kg/m^3
H_o	Reference Total Pressure	N/M^2
HP	Engine Power	w
M_N	Mach Number	-
N_1	Engine Gas Producer Speed	(revolution)-1
N_2	Engine Power Turbine Speed	(revolution)-1
PLA	Power Lever Angle	Degrees
P_R	Pressure Ratio, P_{T_e}/P_{T_∞}	-
P_T	Total Pressure	N/M^2
P_{Te}	Area Averaged Exit Total Pressure	N/M^2
P_{Tcore}	Core Total Pressure	N/M^2
P_{T_∞}	Ambient Total Pressure	N/M^2
Q	Engine torque	NM

APPENDIX B

LIST OF SYMBOLS (Continued)

Symbol	Definition	Units
R	Local Radius	m
T	Thrust	N
T_e	Thrust of engine	N
T_o	Ambient Total Temperature	°F
Tamb	Ambient Temperature	°F
TSL	Thrust Setting Lever	%
U	Corrected Fan Tip Speed	m/s
V_e	Engine Exit Velocity	m/s
W air	Engine air flow	Kg/sec
W fuel	Engine fuel flow	Kg/hr
W_T	Total Weight Flow	-
W	Total Air Flow	Kg/sec
δ	P/Po Pressure Ratio	-
σ	T/To Temperature Ratio	-

APPENDIX C

Chronological History of Test

Testing of the Q-Fan Demonstrator in fulfillment of NAS3-18513 contract requirements started on July 23, 1974, and the HS test phase was completed on December 10, 1974. During this time period, 40 hours and 17 minutes of test time were accumulated and 213 transients were performed.

The operating experience with the Q-Fan was generally very good during this test program. One incident occurred following reindexing of the blades for reverse through flat pitch testing. A planet carrier bolt failed in fatigue and parts of it and its retaining nut were lodged in the power gear train. The bolts were strengthened and all affected parts were replaced and/or repaired. The remainder of the test program was completed without incident.

Operational reliability of the core engine in this installation was very good. Prior to this test program, some difficulty was encountered where the power turbine accessory drive system interfaces with the engine output shaft. It was theorized that the output shaft was deflecting thus driving the gears into a tight mesh condition. The tooth space width in the accessory gear was increased and the increased backlash apparently eliminated the gear tooth stressing situation.

The analog controller and digital computer control system was entirely adequate and offered sufficient flexibility for this test program.

The following tabulation provides a chronological history of the entire NASA Dynamic Pitch Change Test Program performed at Hamilton STandard.

CHRONOLOGICAL HISTORY OF TEST

Date	Event	Test Time (HR.:Min)	Accum Test Time (Hr.:Min)
Test time previously accumulated			97:13
July 23, 1974	Check Runs	0:09	97:22
July 24, 1974	Check Runs	0:42	98:04
July 25, 1974	Check Runs	0:57	99:01
Aug. 1, 1974	Check Runs	0:14	99:15
Aug. 2, 1974	Test Points R21, 22, 24, 26, 28, 29, 30	1:12	100:27
Aug. 8, 1974	Check Runs	1:53	102:20
Aug. 9, 1974	Check Runs	0:11	102:31
Aug. 13, 1974	Check Runs	0:28	102 59
Aug. 14, 1974	Check Runs	1:17	104:16
Aug. 15, 1974	Check Runs	0:40	104:56
Aug. 16, 1974	Check Runs	0:38	105:34
Aug. 19, 1974	Check Runs	0:09	105:43
Aug. 20, 1974	Check Runs	0:34	106:17
Aug. 21, 1974	Check Runs	0:39	106:56
Aug. 23, 1974	Test Points TFC1-1.1 Thru TFC1-4.1	0:44	107:40
Aug. 26, 1974	Test Points TFC2-1.1 Thru TFC2-3.1 and TFC3-1.2 Thru TFC3-11.2	1:47	109:34
Aug. 27, 1974	Check Runs	0:23	109:57
Sept. 11, 1974	Check Runs	1:38	111:35
Sept. 14, 1974	Check Runs	2:05	113:40
Sept. 16, 1974	Check Runs	0:41	114:21
Sept. 17, 1974	Test Points TFC1-1.2 Thru TFC1-4.2, TRC1-1 Thru TRC1-10, and TFC3-1.3 Thru TFC3-11.3	3:56	118:17

CHRONOLOGICAL HISTORY OF TEST (Cont'd.)

Date	Event	Test Time	Accum Test Time
Sept. 18, 1974	Test Points TRC3-1 Thru TRC3-10, TRC3-41 Thru TRC3-50, TFC2-1.2 Thru TFC2-3.2 and TRC2-1 Thru TRC2-10	3:18	121:35
Sept. 19, 1974	Test Points TRC3-31 Thru TRC3-40	0:54	122:29
Sept. 26, 1974	Test Points TRC3-11 Thru TRC3-30, TRC3-51 Thru TRC3-80, TRRC3-1 Thru TRRC3-4	3:55	126:24
Sept. 27, 1974	Test Points TRC1-11 Thru TRC1-28	0:55	127:19
Oct. 2, 1974	Check Runs - Gearbox Bolt Fracture	0:33	127:52
Nov. 25, 1974	Check Runs	0:14	128:06
Nov. 27, 1974	Check Runs	1:05	129:11
Dec. 3, 1974	Check Runs	1:12	130:23
Dec. 4, 1974	Check Runs	1:32	131:55
Dec. 5, 1974	Check Runs	1:23	133:18
Dec. 6, 1974	Test Points TRF6-1 Thru TRF6-20	2:50	136:08
Dec. 9, 1974	Test Points TRF4-1 Thru TRF4-10	0:44	136:52
Dec. 10, 1974	Balance Runs	0:38	137:30

DISASSEMBLED FOR SHIPMENT TO NASA LeRC FOR ADDITIONAL TESTING

APPENDIX D

REFERENCES

1. W. J. Demers, F. B. Metzger, L. W. Smith, and H. S. Wainauski: Final Report - Testing of the Hamilton Standard Q-FAN^{R} Demonstrator, NASA CR-121265 (HSER 6163), March 1973.

2. G. W. Lewis, Jr., R. D. Moore, and G. Kovich: Performance of a 1.20 Pressure Ratio STOL Fan Stage at Three Rotor Blade Setting Angles, NASA TMX-2837, July 1973.

3. F. W. Glaser, J. A. Wazyniak, and R. Friedman: Noise Data from Tests of a 1.83-Meter (6-ft) Diameter Variable-Pitch 1.2-Pressure-Ratio Fan (QF-9), NASA TMX-3187, March 1975.

4. Bryer and Pankhurst: Pressure Probe Methods for Determining Wind Speed and Flow Direction, National Physical Laboratory; London, Her Majesty's Stationery Office, 1971.

5. Conference: Aeronautical Propulsion NASA Lewis Research Center, 1975. NASA SP-381